

## DFT study of the self-aggregation of asphaltene model compounds

Kassem K. Nege<sup>a</sup>(IC), Mateus R. Lage<sup>b</sup>(PQ), Stanislav R. Stoyanov<sup>c,d</sup>(PQ), José W. de M. Carneiro<sup>a</sup>(PQ)

<sup>a</sup>Instituto de Química, UFF, Outeiro de São João Batista s/n, Centro, Niterói, RJ, 24020-141, Brazil

<sup>b</sup>Universidade Federal do Maranhão, Campus Balsas, Rua José Leão, 484, Centro, Balsas, MA, 65800-000, Brazil

<sup>c</sup> Natural Resources Canada, Canmet ENERGY-Devon, 1 Oil Patch Drive, Devon, Alberta T9G 1A8, Canada

<sup>d</sup> Department of Chemical and Materials Engineering, University of Alberta, Edmonton, Alberta T6G 2 V4, Canada

**Abstract:** Asphaltenes are compounds found in the heavier fractions of the oil as a supramolecular aggregates [1]. The chemical complexity of these fractions of oil creates difficulties for their understanding and the prediction of their behavior. However, many authors have performed studies related to their chemical structure and properties, proposing molecules as asphaltene models, mainly based on data obtained by nuclear magnetic resonance (NMR), elemental analysis and molecular weight [2]. Asphaltenes can cause serious problems in oil exploration, triggered mainly to their deposition that is due to the level of molecular aggregation. The problems caused by the deposition of asphaltenes are present from the exploration to the refining of the petroleum. Thus, it is extremely important to know the mechanisms of aggregation of asphaltenes.

In this work, we performed a theoretical study of the homodimerization and self-aggregation of asphaltene model compounds A and B (Figure 1). These model compounds contain fused aromatic rings and heterocyclic fragments representative of asphaltenes tethered with butyl linkers to represent archipelago asphaltenes [3]. The ability of the DFT functional  $\omega$ B97X-D and 6-31+G (d, p) basis set to predict the optimized geometry and the thermochemistry of aggregation was evaluated [4,5].

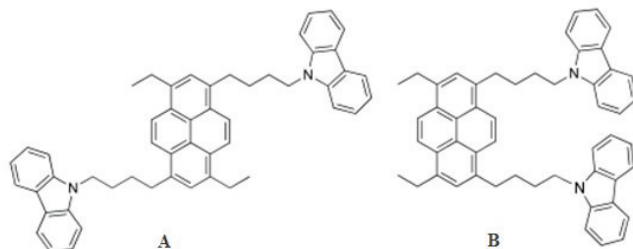


**Figure 1.** Chemical structures of the asphaltene model compounds A and B.



Through the optimized structures A and B, two self-aggregation arrangements, called "Hamburger" and "Self-aggregation" were proposed (Figure 2). The aggregation free energies, given relative to the free energy of the optimized asphaltene structure without self-aggregation (open structure), are listed in Table 1.

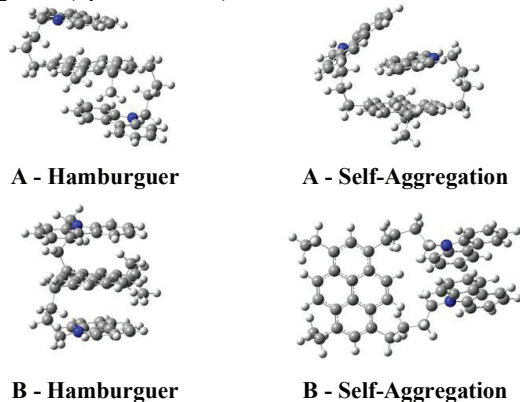


**Figure 2.** Self-aggregation structures of the asphaltene model compounds (A and B).

**Table 1.** Values of the free energy difference of the asphaltenes structures.

Model Compound	Hamburger	Self-aggregation
A	-9.83	-8.54
B	-16.15	-13.86

Therefore, as observed for both cases, the proposed structure of self-aggregation "hamburger" has substantially lower free energy and would be the most probable conformation of these asphaltene model compounds.

**Keywords:** asphaltenes, aggregation, DFT, free energy.

**Support:** KKN and JWMC acknowledges CNPq and MRL acknowledges CAPES for research grants. The research at UFF was supported by FAPERJ.

**References:**

- [1] M. R. Gray, R. R. Tykwinski, J. M. Stryker and X. Tan, *Energy Fuels*, 25, 3125 (2011).
- [2] H. Groezin, O. Mullins. *Energy Fuels*, 14, 677 (2000).
- [3] A. Scherer, F. Hampel, M. R. Gray, J. M. Stryker and R. R. Tykwinski, *J. Phys. Org. Chem.*, 25, 597 (2012).
- [4] L. M. da Costa; S. R. Stoyanov, S. Gusarov, P. R. Seidl, J. W. de M. Carneiro, A. Kovalenko. *J. Phys. Chem. A*, 118, 896 (2014).
- [5] L. M. Costa, S. Hayaki, S. R. Stoyanov, S. Gusarov, X. Tan, M. R. Gray, J. M. Stryker, R. Tykwinsky, J. W. M. Carneiro, H. Sato, P. R. Seidl, A. Kovalenko, *Phys. Chem. Chem. Phys.*, 14, 3922 (2012).



## Multi-Electronic-State Approach of Tetranitrogen

M. X. Silva<sup>a</sup>, B. R. L. Galvão<sup>b</sup>, J. P. Braga<sup>a</sup>, J. C. Belchior<sup>a</sup>

<sup>a</sup>*Departamento de Química – ICEx, Universidade Federal de Minas Gerais, Av. Antônio Carlos 6627, Pampulha, Belo Horizonte, Minas Gerais, Brazil*

<sup>b</sup>*Departamento de Química, Centro Federal de Educação Tecnológica de Minas Gerais, Av. Amazonas 5253, Nova Suíça, Belo Horizonte, Minas Gerais, Brazil*

**Abstract:** There is a rising interest nowadays in employing nanoscale materials as new possible types of fuels. To be considered an efficient fuel, the candidate material must be sufficiently unstable in order to react with another system and then release a considerable amount of energy. On the other hand, it must be stable enough to be synthesized and stored without spontaneously decomposing itself [1]. To accomplish the goal of being considered “green” these materials must not only generate reasonably less toxic products than the current widely spread fuels do, but also demonstrate higher performances while being technically as well as economically attractive [2]. In this context, polinitrogen systems have been studied due to their potential use as high-energy density materials (HEDM), since their dissociation into inert N<sub>2</sub> molecules may release huge amounts of energy [1,3]. Therefore, studies of the photochemistry of polinitrogen systems can be considered important theoretical prototypes. It is relevant either for supporting the detection of their existence through spectroscopic analysis and/or understanding their chemical behavior in Earth’s atmosphere, other astronomical environments or yet as possible fuels [4]. This subject has already been intensively studied for the nitrogen gas [5,6], while quantum chemical calculations are responsible for most of the information on larger polinitrogen systems [7,8]. The formation of linear N<sub>3</sub> from the reaction between two N<sub>2</sub> molecules, for instance, is expected to occur upon photoexcitation and to present a linear N<sub>4</sub> species as transition state [4]. While several calculations involving various polinitrogen isomers indicate high potential energies when compared to molecular nitrogen, only some of them exhibit an essential HEDM feature: high dissociation barrier [3]. Within this perspective, the scientific community has been giving great attention to isomers of tetranitrogen (N<sub>4</sub>), in particular to the tetrahedral form (N<sub>4</sub> – T<sub>d</sub>) [8,9]. In fact, the good understanding of atomic aggregates or clusters in general relies, foremost, on the capacity of generation of plausible structures for those compositions whose available information is scarce. At the same time, approaching systems with typical cluster dimensions requires taking into consideration the effects arising from the quantum behavior of matter, and the applicability of analytical or empirical potentials becomes questionable [10]. In this context, we have employed and upgraded a previously developed genetic algorithm coupled with electronic structure methods [11], namely QGA, tested to survey the potential energy surface of the tetranitrogen system. The QGA approach presented good cost-effectiveness ratio when it comes to the computational effort associated with electronic structure calculations. It is well-suited to assess the potential energy surface of atomic clusters, mainly in cases where no previous information about the structural



arrangement of the system is available. The QGA provided structures in good agreement with coupled cluster results, even though it started from structures generated completely randomly. Theoretical investigations of the electronic potential energy curves associated with the dissociation of the  $N_4$  ( $T_d$ ) into two  $N_2$  molecules were also performed for the electronic ground state and the first excited states using CASSCF(12,12) level of theory implemented in MOLPRO package [12]. The graphs containing the dissociation paths studied involved singlet and triplet states, where it was possible to observe both conical intersections and intersystem crossings. Possible alternative dissociation channels for the  $N_4$  ( $T_d$ ) were then inferred from these crossings and photoexcitation of this species. Coupled cluster (CCSD(T)-F12) calculations were also performed on specific structures to generate benchmark results, which were then compared to results provided by density functional theory (DFT) calculations with several different exchange-correlation functionals in order to find the best match. The tetrazete  $T_d$  and planar  $D_{2h}$  isomers were approached by higher level of theory (CCSD(T)-F12/cc-pCVTZ-F12) than already reported until the present date. The  $N_4$  ( $T_d$ ) was predicted to be  $182 \text{ kcal.mol}^{-1}$  above  $2N_2$  in energy, and  $1 \text{ kcal.mol}^{-1}$  above the  $D_{2h}$  isomer. The unraveling of a possible reaction mechanism involving the abstraction of a nitrogen atom from a  $N_2$  molecule in an excited electronic state, by another excited  $N_2$  molecule, to produce linear  $N_3$  is also currently in progress.

**Key-words:** polinitrogen, aggregates, cluster, photochemistry

**Support:** This work has been supported by Conselho Nacional de Desenvolvimento Científico e Tecnológico (CNPq), Fundação de Amparo à Pesquisa do Estado de Minas Gerais (FAPEMIG) and Coordenação de Aperfeiçoamento de Pessoal de Nível Superior (CAPES).

**References:**

- [1] K. M. Dunn, K. Morokuma, *J. Chem. Phys.*, 102, 4904 (1995).
- [2] T. Brinck, M. Rahm, "Theoretical Design of Green Energetic Materials: Predicting Stability, Detection, Synthesis and Performance, in *Green Energetic Materials*" (2014), John Wiley & Sons, Chichester, United Kingdom.
- [3] P. C. Samartzis, A. M. Wodtke, *Int. Rev. Phys. Chem.*, 25, 527 (2006).
- [4] S. L. Chou, J. I. Lo, M. Y. Lin, Y. C. Peng, H. C. Lu, B. M. Cheng, *Angew. Chem. Ind. Ed.*, 53, 738 (2014).
- [5] A. Lofthus, P. H. Krupenie, *J. Phys. Chem. Ref. Data*, 6, 113 (1977).
- [6] H. Okabe, "Photochemistry of Small Molecules" (1978), John Wiley & Sons, New York.
- [7] M. J. Greshner *et al.*, *J. Phys. Chem. A*, 120, 2920, (2016).
- [8] M. Bittererová, H. Östmark, T. Brinck, *J. Chem. Phys.*, 116, 9740, (2002).
- [9] T. J. Lee, J. E. Rice, *J. Chem. Phys.*, 94, 1215, (1991).
- [10] M. X. Silva, B. R. L. Galvão, J. C. Belchior, *Phys. Chem. Chem. Phys.*, 16, 8895, (2014).
- [11] F. T. Silva *et al.*, *Chem. Phys. Lett.*, 639, 135, (2015).
- [12] H. -J. Werner, P. J. Knowles, G. Knizia, F. R. Manby, M. Schütz, *WIREs Comput. Mol. Sci.*, 2, 242, (2012).



## Multi-Electronic-State Approach of Tetranitrogen

M. X. Silva<sup>a</sup>, B. R. L. Galvão<sup>b</sup>, J. P. Braga<sup>a</sup>, J. C. Belchior<sup>a</sup>

<sup>a</sup>*Departamento de Química – ICEX, Universidade Federal de Minas Gerais, Av. Antônio Carlos 6627, Pampulha, Belo Horizonte, Minas Gerais, Brazil*

<sup>b</sup>*Departamento de Química, Centro Federal de Educação Tecnológica de Minas Gerais, Av. Amazonas 5253, Nova Suíça, Belo Horizonte, Minas Gerais, Brazil*

**Abstract:** There is a rising interest nowadays in employing nanoscale materials as new possible types of fuels. To be considered an efficient fuel, the candidate material must be sufficiently unstable in order to react with another system and then release a considerable amount of energy. On the other hand, it must be stable enough to be synthesized and stored without spontaneously decomposing itself [1]. To accomplish the goal of being considered “green” these materials must not only generate reasonably less toxic products than the current widely spread fuels do, but also demonstrate higher performances while being technically as well as economically attractive [2]. In this context, polinitrogen systems have been studied due to their potential use as high-energy density materials (HEDM), since their dissociation into inert N<sub>2</sub> molecules may release huge amounts of energy [1,3]. Therefore, studies of the photochemistry of polinitrogen systems can be considered important theoretical prototypes. It is relevant either for supporting the detection of their existence through spectroscopic analysis and/or understanding their chemical behavior in Earth’s atmosphere, other astronomical environments or yet as possible fuels [4]. This subject has already been intensively studied for the nitrogen gas [5,6], while quantum chemical calculations are responsible for most of the information on larger polinitrogen systems [7,8]. The formation of linear N<sub>3</sub> from the reaction between two N<sub>2</sub> molecules, for instance, is expected to occur upon photoexcitation and to present a linear N<sub>4</sub> species as transition state [4]. While several calculations involving various polinitrogen isomers indicate high potential energies when compared to molecular nitrogen, only some of them exhibit an essential HEDM feature: high dissociation barrier [3]. Within this perspective, the scientific community has been giving great attention to isomers of tetranitrogen (N<sub>4</sub>), in particular to the tetrahedral form (N<sub>4</sub> – T<sub>d</sub>) [8,9]. In fact, the good understanding of atomic aggregates or clusters in general relies, foremost, on the capacity of generation of plausible structures for those compositions whose available information is scarce. At the same time, approaching systems with typical cluster dimensions requires taking into consideration the effects arising from the quantum behavior of matter, and the applicability of analytical or empirical potentials becomes questionable [10]. In this context, we have employed and upgraded a previously developed genetic algorithm coupled with electronic structure methods [11], namely QGA, tested to survey the potential energy surface of the tetranitrogen system. The QGA approach presented good cost-effectiveness ratio when it comes to the computational effort associated with electronic structure calculations. It is well-suited to assess the potential energy surface of atomic



clusters, mainly in cases where no previous information about the structural arrangement of the system is available. The QGA provided structures in good agreement with coupled cluster results, even though it started from structures generated completely randomly. Theoretical investigations of the electronic potential energy curves associated with the dissociation of the  $N_4$  ( $T_d$ ) into two  $N_2$  molecules were also performed for the electronic ground state and the first excited states using CASSCF(12,12) level of theory implemented in MOLPRO package [12]. The graphs containing the dissociation paths studied involved singlet and triplet states, where it was possible to observe both conical intersections and intersystem crossings. Possible alternative dissociation channels for the  $N_4$  ( $T_d$ ) were then inferred from these crossings and photoexcitation of this species. Coupled cluster (CCSD(T)-F12) calculations were also performed on specific structures to generate benchmark results, which were then compared to results provided by density functional theory (DFT) calculations with several different exchange-correlation functionals in order to find the best match. The tetrazete  $T_d$  and planar  $D_{2h}$  isomers were approached by higher level of theory (CCSD(T)-F12/cc-pCVTZ-F12) than already reported until the present date. The  $N_4$  ( $T_d$ ) was predicted to be  $182 \text{ kcal.mol}^{-1}$  above  $2N_2$  in energy, and  $1 \text{ kcal.mol}^{-1}$  above the  $D_{2h}$  isomer. The unraveling of a possible reaction mechanism involving the abstraction of a nitrogen atom from a  $N_2$  molecule in an excited electronic state, by another excited  $N_2$  molecule, to produce linear  $N_3$  is also currently in progress.

**Key-words:** polinitrogen, aggregates, cluster, photochemistry

**Support:** This work has been supported by Conselho Nacional de Desenvolvimento Científico e Tecnológico (CNPq), Fundação de Amparo à Pesquisa do Estado de Minas Gerais (FAPEMIG) and Coordenação de Aperfeiçoamento de Pessoal de Nível Superior (CAPES).

#### References:

- [1] K. M. Dunn, K. Morokuma, *J. Chem. Phys.*, 102, 4904 (1995).
- [2] T. Brinck, M. Rahm, "Theoretical Design of Green Energetic Materials: Predicting Stability, Detection, Synthesis and Performance, in *Green Energetic Materials*" (2014), John Wiley & Sons, Chichester, United Kingdom.
- [3] P. C. Samartzis, A. M. Wodtke, *Int. Rev. Phys. Chem.*, 25, 527 (2006).
- [4] S. L. Chou, J. I. Lo, M. Y. Lin, Y. C. Peng, H. C. Lu, B. M. Cheng, *Angew. Chem. Ind. Ed.*, 53, 738 (2014).
- [5] A. Lofthus, P. H. Krupenie, *J. Phys. Chem. Ref. Data*, 6, 113 (1977).
- [6] H. Okabe, "Photochemistry of Small Molecules" (1978), John Wiley & Sons, New York.
- [7] M. J. Greshner *et al.*, *J. Phys. Chem. A*, 120, 2920, (2016).
- [8] M. Bittererová, H. Östmark, T. Brinck, *J. Chem. Phys.*, 116, 9740, (2002).
- [9] T. J. Lee, J. E. Rice, *J. Chem. Phys.*, 94, 1215, (1991).
- [10] M. X. Silva, B. R. L. Galvão, J. C. Belchior, *Phys. Chem. Chem. Phys.*, 16, 8895, (2014).
- [11] F. T. Silva *et al.*, *Chem. Phys. Lett.*, 639, 135, (2015).
- [12] H. -J. Werner, P. J. Knowles, G. Knizia, F. R. Manby, M. Schütz, *WIREs Comput. Mol. Sci.*, 2, 242, (2012).



## Computer Simulations to Study the Efficiency of Solvents in the Synthesis of Benzilidenethiazolidinedione in Micro-reactor

Matheus J. Lazarotto and Kaline Coutinho

*Physics institute of University of São Paulo - (IFUSP)*

**Abstract:** In the synthesis of pharmacological substances, batch process is largely used due to its capacity of high increment of size production. However, this method requires analysis of the system before its enlargement (called “scale-up”) that can be complex and longstanding. An alternative way of production is by continuous flow, when the reagents are put together with a solvent in small tubes (usually in micro-reactors) and submitted to high temperatures and pressures. This environment enhances the rate production due to high heat and mass transfer, due to a large surface area through a long extension of the tubes. The continuous flow method does not require scale-up process and results in high quality products (homogeneous mixtures, small reaction time etc.) with ease size production choice [1].

In this context, thiazolidinedione (TZD) derivatives that are used in diabetes treatment can be produced via continuous flow method with benzaldehyde and TZD as reagents. To evaluate the best efficiency production, different configurations of productions were analyzed. Three different solvents were used (Methanol, Ethanol and Propanol) in three temperatures: 98, 120 and 140°C [1]. The experimental data shows that, as temperature rises, ethanol becomes the solvent with best profit, followed by methanol and propanol.

In this work we performed theoretical studies using molecular simulation to try to understand the interactions between the reactants and the solvent in specific thermodynamic conditions used in the micro-reactors. Initially we performed quantum mechanical calculation of the reagents properties (geometry, dipole moment, hydrogen bonds formation; all calculated with the Gaussian09 software[2]). Electronic structure is also calculated separately for the different solvents.

As a first insight, it was found two configurations with hydrogen bond that could enable the reaction between the TZD and benzaldehyde. These two configurations were then used in the initial configuration to simulate the system in solution using Monte Carlo method (with the DICE software [3]), in the correspondent pressure and temperature used in the experimental arrangement. Then, we analyzed the binding energy and the radial distribution functions between the reagents in the presence of the solvent. Our results indicate a small interaction between the reagents. They were separated most of the configurations generated in the simulation. Our result is still not conclusive because we have few configurations to analyze the interactions. Now, we are



performing longer simulations to perform the analysis and try to understand the reactants interactions in the different solvents and the specific thermodynamic conditions.

**Key-words:** Synthesis, Continuous flow, Computational Simulation, Monte Carlo, Solvents, Efficiency.

**Support:** This work has been supported by CAPES

### References:

- [1] Silva, R. R. O; Reação da 2,4-Tiazolidinadiona com o Benzaldeído em Batelada e Microrreator Capilar – 2016. Master's thesis submitted on School of pharmacological sciences of University of São Paulo.
- [2] Gaussian 09, Revision D.01, M. J. Frisch, G. W. Trucks, H. B. Schlegel, G. E. Scuseria, M. A. Robb, J. R. Cheeseman, G. Scalmani, V. Barone, B. Mennucci, G. A. Petersson, H. Nakatsuji, M. Caricato, X. Li, H. P. Hratchian, A. F. Izmaylov, J. Bloino, G. Zheng, J. L. Sonnenberg, M. Hada, M. Ehara, K. Toyota, R. Fukuda, J. Hasegawa, M. Ishida, T. Nakajima, Y. Honda, O. Kitao, H. Nakai, T. Vreven, J. A. Montgomery, Jr., J. E. Peralta, F. Ogliaro, M. Bearpark, J. J. Heyd, E. Brothers, K. N. Kudin, V. N. Staroverov, T. Keith, R. Kobayashi, J. Normand, K. Raghavachari, A. Rendell, J. C. Burant, S. S. Iyengar, J. Tomasi, M. Cossi, N. Rega, J. M. Millam, M. Klene, J. E. Knox, J. B. Cross, V. Bakken, C. Adamo, J. Jaramillo, R. Gomperts, R. E. Stratmann, O. Yazyev, A. J. Austin, R. Cammi, C. Pomelli, J. W. Ochterski, R. L. Martin, K. Morokuma, V. G. Zakrzewski, G. A. Voth, P. Salvador, J. J. Dannenberg, S. Dapprich, A. D. Daniels, O. Farkas, J. B. Foresman, J. V. Ortiz, J. Cioslowski, and D. J. Fox, Gaussian, Inc., Wallingford CT, 2013.
- [3] H. M. Cezar, S. Canuto and K. Coutinho; DICE(v3.0beta) A Monte Carlo program for molecular liquid simulation; University of São Paulo, Brazil (2017).



## Study of new Azo Dyes for DSSCs using DFT

Matheus R. M. Signorelli (PG), Marcus V. J. Rocha (PQ), Luana S. M. Forezi (PQ),  
 Vitor F. Ferreira (PQ), Luciano T. Costa (PQ)  
*Instituto de Química, Universidade Federal Fluminense,  
 CEP 24020-141, Niterói-RJ, Brazil*

**Abstract:** The world panorama consumption increasingly migrates to the clean and easy energy production. Some alternatives to the usual sources are proved by the historically environmental degradation combined to the impact on the life quality of people. In this context, solar energy has emerged as a potential alternative with an open field for research and development.

This project aims precisely at deepening about the technology and operation of the components of the Dye Sensitized Solar Cells (DSSC) [1] with focus to the production of organic azo dyes in order to generate clean energy applying the green chemistry principles. The azo dyes are given special attention, since they are widely used in the paint industry [2], but little reported in the literature of DSSCs. A schematic diagram of DSSC work system is shown in Figure. 1.

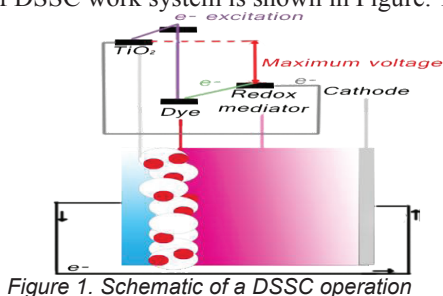


Figure 1. Schematic of a DSSC operation

The two azo compounds chosen for this work have been proposed to be synthesized based originally on the methodology described on [3] with some modifications and additional steps. They are illustrated in Figure. 2:

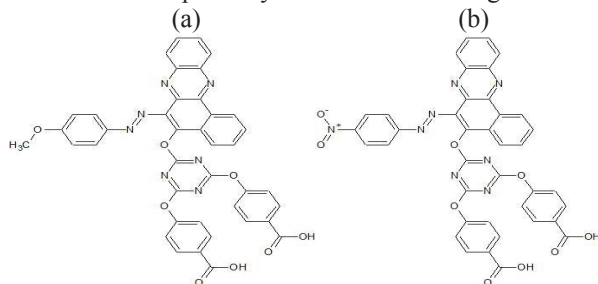
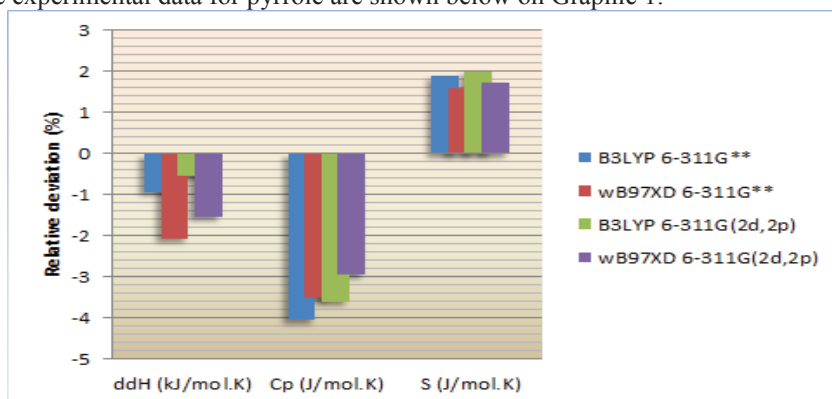


Figure 2. Azo Dyes. (a) Azo 1 (b) Azo 2



DSSC's dyes have been already investigated with DFT method to understand orbitals energy levels [4]. In order to validate the computational methodology, some calculations were performed with the pyrrole due to the similar structure and constituent atoms. From the pyrrole calculations was observed that the functionals B3LYP and wB97XD using 6-311G\*\* or 6-311G(2d,2p) basis set have good agreement with the experimental data shown on [5] (about less than 2% of deviation for enthalpy content and entropy and about less than 4% of deviation for heat capacity – all data collected for 298,15K) and was chosen to be used for the azo dyes calculations. The percentual deviations of thermodynamic properties from the experimental data for pyrrole are shown below on Graphic 1.



Graphic 1: Percentual deviation of thermodynamic values

DFT calculations are being performed for the Azo 1 and Azo 2 and in sequence the electronic and structural properties will be analyzed. The energy levels, thermodynamic parameters and electron population will be used to predict some properties of a dye sensitized solar cell prepared with those organic dyes. Based on that, we expected with the results of this work to validate a solid methodology for predictions of new organic dyes to ensure a lower financial and environmental costs.

**Key-words:** Azo compounds, Organic Dyes, Solar Cells, Dye Sensitized Solar Cells, DSSCs, DFT

**Support:** This work has been supported by CAPES

**References:**

C. Lee et al RSC Adv. 5 (2015) 23810-23825

Labd-Alredha, R. Mhessn et al E-Journal of Chemistry 9 (2012) 465-470

A. I. Francisco, M. D. Vargas, V. F. Ferreira et al J. Braz. Chem. Soc. 21 (2010)

A. Hagfeldt et al Chem. Rev. 110 (2010) 6595-6663

<http://cccbdb.nist.gov/exp2.asp> - NIST, Pyrrole - access in 08/2017



## A study on the reaction of hydroselenenyl (HSe<sup>•</sup>) and selenenic (HSeO<sup>•</sup>) radicals

Mauricio Vega-Tejido, Martina Kieninger, Oscar N. Ventura.

*Computational Chemistry and Biology Group (CCBG), CCBG-DETEMA, Facultad de Química, UdelaR-Isidoro de María 1614 – 11400, Montevideo, Uruguay.  
mauryvg@fq.edu.uy*

**Abstract:** Selenium presents some similarities with de sulfur reactivity and has been described in diverse biological systems. The selenocystein (Sec) residue is the one which characterizes the selenoproteins.<sup>[1]</sup> These proteins has been associated with many cellular mechanisms, for intance, redox signalling and oxydative stress.<sup>[1]</sup> In biology, selenium compounds such as selenocystine (Sec-Sec) were associated with the role of free-radicals scavenger.<sup>[2]</sup>

Selenium species formed in these processes involve neutral and radical intermediaries such hydroselenenyl (HSe<sup>•</sup>) and selenenic (HSeO<sup>•</sup>) moieties. Recently, Borji et al. (2016)<sup>[3]</sup> reported a study of the hydrosulfinyl and mercapto radicals reaction. Here we compare the selenium analogs in order to have an approximation to the behavior of these species in the biological systems.

All the structures were initially optimized by means gaussian 09 program with B3LYP/6-311++G(3df,3pd) using "Ahlichs coulomb fitting" basis set with electronic core potential (ECP) for both Se atoms. Same method was used for the electronic density calculation. After that, the structures were re-optimized using M06-2X, M06-GD3 and B3LYP functionals with 6-311++G(3df,3pd) basis set for all the atoms. The minima in the PES were confirmed by IR frequencies calculations.

In this work is presented a profile of the reaction mechanism of the mentioned Se-radicals showing possible products, intermediates and transition state structures. The process can be described with the initial formation of the CR adduct that derives in INT (through TS2), and then derives in cis-HSeSeOH passing through two possible transition states: TS21 or TS22. The way passing by TS1, that connects directly CR with cis-HSeSeOH, is the one with the highest barrier and positive values in the relative energy. TS31 and TS32 correspond to the cis-trans rotation of the neutral compound HSeSeOH. In figura 1 can be seen the changes in the electronic density that surrounds Se atoms. While CR presents one Se with 1 LP (lone pair) and the other with 2 LP, in INT both presents 2 LP. In INT one of the LP is located between both Se favoring the interaction, in parallel, is observed that the Se-Se bond is shorter in INT (2.2Å) than in CR (2.4Å).



Table of free energies (kcal/mol) relative to the free reactants				
Species	B3LYP	M062x	M06-GD3	$\Delta\Delta G^\ddagger$
HSe+HSeO	0	0	0	0
CR	-31.8	-31.9	-34.9	-
INT	-43.9	-49.0	-45.9	-
Cis-HSeSeOH	-62.3	-67.6	-64.1	-
Trans-HSeSeOH	-62.5	-67.8	-64.3	-
TS1	1.7	2.2	2.1	37.0
TS2	-14.5	-17.6	-17.7	17.2
TS21	-	-4.5	-10.9	34.9
TS22	-	-33.2	-29.2	16.7
TS31	-	-58.2	-54.8	9.2
TS32	-	-59.2	-55.9	8.2

<sup>a</sup> The barriers correspond to the M06-GD3 calculations.

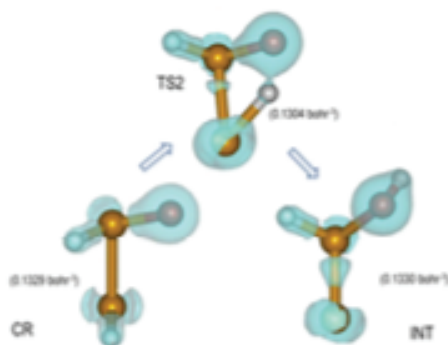


Figure 1.- Electronic density in the conversion of CR in INT [TS2]. Is observed changes in the lone pairs of both Se.

**Key-words:** M06, selenium radicals, electronic density

**Support:** Programa de Desarrollo de Ciencias Básicas (PEDECIBA-Química) and Comisión Sectorial de Investigación Científica (CSIC).

#### References:

- [1] Lovanov A.V., Hatfield D.L., Gladyshev V.N., *Biochimica et Biophysica Acta* 1790 (2009) 1424–1428.
- [2] Kumar, B.S., Kunwar, A., Singh B.G., Ahmad, A., Priyadarsini, K.I., *Biol Trace Elem Res* (2011) 140:127-138.
- [3] Borji S., Vahedpour M., Fazeli S., *Comp. Theor. Chem.* 1086 (2016) 25-35.



## Large amplitude motion affects cleavage reaction barrier in HIV protease

V. De Conto<sup>1</sup>, A.S.K. Braz<sup>1</sup>; L.P.B. Scott<sup>2</sup>; P. Homem-de-Mello<sup>1</sup>, M.D. Coutinho-Neto<sup>1</sup>

<sup>1</sup>*Centro de Ciências Naturais e Humanas, Universidade Federal do ABC, Santo André, São Paulo, Brazil;* <sup>2</sup>*Centro de Matemática, Computação e Cognição, Universidade Federal do ABC, Santo André, São Paulo, Brazil;*

The role of protein flexibility on catalytic activity is a controversial subject. To shed light into this topic we propose the use of configurations generated using normal mode analysis (NMA) and low temperature dynamics [1] of substrate bound HIV protease (HIV-PR) to investigate the cleavage reaction using QM/MM (QM/Molecular Mechanics) methods. HIV-PR is a major drug target used in highly active anti-retroviral therapy (HAART), where protease inhibitors are commonly used. Our aim is to understand how large-scale protein motion can affect HIV-PR catalytic activity, and thus protein function.

Starting from a substrate bound crystal structure of HIV-PR (PDB assertion code 1KJF) we generate a large ensemble of structures using NMA (250 configurations) employing a recently proposed protocol [2]. Emphasis is placed on 20 states with largest displacements. Selected relevant structures were used to investigate the barrier for the substrate cleavage reaction using PM6 (a semi-empirical method). We used for the QM calculations an active site made of 18 amino acids in addition to 5 water molecules.

Our result suggests a strong dependency between the initial configuration selected and the resulting amino acid cleavage barrier. Particularly interesting was the fact that the barrier for a subset of 32 structures was up to 10kcal.mol<sup>-1</sup> lower than the one obtained from the crystal structure configuration, producing results much closer to experiments.

**Key-words:** QM/MM, NMA, HIV-PR, Large amplitude motion, enzymatic reactions.

**Support:** This work has been supported by FAPES, CAPES.

### References:

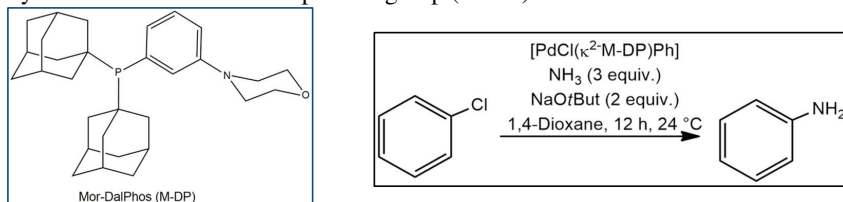
- [1] Exploring Free Energy Landscapes of Large Conformational Changes: Molecular Dynamics with Excited Normal Modes, Mauricio G. S. Costa, Paulo R. Batista, Paulo M. Bisch, and David Perahia, JCTC, 2015, 11 (6), pp 2755–2767.
- [2] Distinct conformational population patterns in the enzymatic activity cycle of the HIV-1 protease as revealed by normal mode analysis, De Conto, V.; Scott, L.P.B.; Perahia, D.; Homem-de-Mello, P.; Coutinho-Neto, M.D. and Braz, A.S.K., Manuscript in preparation.

## A DFT study on Mor-DalPhos ligand in ammonia monoarylation by Buchwald-Hartwig amination

Authors: Maurício P. Franco e Ataulpa A. C. Braga

Address: Instituto de Química, Universidade de São Paulo, São Paulo, São Paulo, Brazil

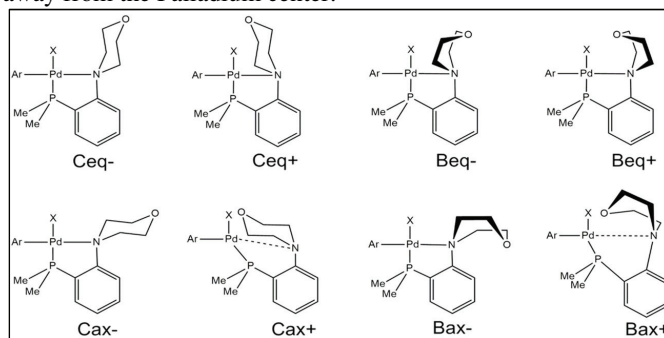
**Abstract:** The use of ancillary ligands with palladium catalysts is very important for the Buchwald-Hartwig amination (BHA). As shown by Stradiotto[1], the use of Mor-DalPhos (Scheme 1) ligand for selective monoarylation of ammonia can achieve excellent yields of aniline at room temperature (Scheme 1) compared to its analogue, which has a dimethyl amine instead of the morpholine group (MorG).



**Scheme 1.** Mor-DalPhos sketch (left) and Ammonia monoarylation reaction equation (right)

To verify the relevance of MorG in BHA, our research group suggested to investigate how the conformation affects intermediates and transition using Density Functional Theory (DFT).

All possible conformation are shown in Scheme 2. The codes *C* or *B* stand for chair or boat conformation, *eq* or *ax* correspond to equatorial or axial position of phenyl group bonded to N of MorG and + or - represents if the oxygen atom of MorG points towards or away from the Palladium center.



**Scheme 2.** Possible conformations and their codes for MorG in the Palladium catalyst.

All optimizations were done under Gaussian09 package with B3LYP/SDD(Pd)/6-31+G(d,p), adding Grimme's dispersion correction "D3" and solvent effect for 1,4-

dioxane were introduced by SMD model. The 1-Adamantyl groups were replaced by methyl groups to simplify the system. All energies reported are Gibbs Free energies at 273.15 K and 1 atm.

Intermediates 1 and 2 have at least two conformations which are almost isoenergetic in Gibbs Free Energy, indicating there isn't a preferential conformation for those intermediates. However in **IM3** and **IM4**, Ceq- conformation is the most stable compared to the others, 1.2 and 4.0 kcal.mol<sup>-1</sup> for **IM3** and **IM4**, respectively.

**Table 1.** Relative Gibbs Free Energy (kcal.mol<sup>-1</sup>) comparing conformations for intermediates 1, 2, 3 and 4

[PdCl(κ <sup>2</sup> -M-DP)Ar] – <b>IM1</b>		[PdNH <sub>3</sub> (κ <sup>2</sup> -M-DP)Ar] <sup>+</sup> – <b>IM2</b>		PdNH <sub>2</sub> (κ <sup>2</sup> -M-DP)Ar – <b>IM3</b>		Pd(κ <sup>1</sup> -P-M-DP) – <b>IM4</b>	
Confor.	ΔG	Confor.	ΔG	Confor.	ΔG	Confor.	ΔG
-	-	-	-	<b>Beq-</b>	13.5	-	-
<b>Beq-</b>	17.0	<b>Ceq+</b>	10.5	<b>Ceq+</b>	8.3	-	-
<b>Ceq+</b>	11.4	<b>Bax-</b>	3.6	<b>Beq+</b>	3.2	<b>Bax-</b>	8.6
<b>Bax-</b>	0.9	<b>Cax-</b>	2.1	<b>Bax-</b>	2.8	<b>Beq-</b>	7.9
<b>Cax-</b>	0.7	<b>Ceq-</b>	0.5	<b>Cax-</b>	1.2	<b>Ceq+</b>	4.0
<b>Ceq-</b>	0	<b>Beq+</b>	0	<b>Ceq-</b>	0	<b>Ceq-</b>	0

Transitions states (**TS**) were found for Chloride Substitution step (**IM1**→**IM2**) and Reductive Elimination step (**IM3**→**IM4**). Both **TSs** shows a clearly preference for **Ceq-** conformations by 3 kcal.mol<sup>-1</sup> than others conformations.

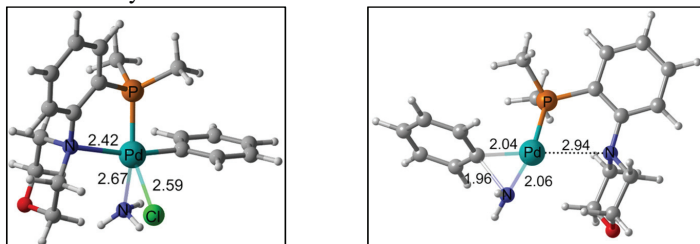


**Figure 1.** Transition state of Chloride Substitution step (left) and Transition State of Reduction Elimination step (right). Both TSs with the most stable conformation.

This work shows that steric hindrance rules over the formation of weak interaction to determine Morpholine Group conformations for the intermediates and transition states calculated so far.

**Key-words:** Buchwald-Hartwig Amination, Transition State, mechanism, Mor-DalPhos

**Support:** This work has been supported by USP, CAPES, Cnpq and FAPESP

**References:**

[1] J; Stradiotto, M. and coworkers, Chem. Eur. J. 2013 , 19 , 2131–2141.

## Estudo teórico de aglomerados moleculares de interesse da indústria petroquímica

Authors: Max Pereira Nunes, Leonardo Baptista

Endereço: *Universidade do Estado do Rio de Janeiro, Faculdade de Tecnologia,  
Departamento de Química e Ambiental,*

**Resumo:** Tendo em vista a necessidade de determinação de propriedades termodinâmicas para fins industriais, equações de estado foram desenvolvidas para obtenção de dados difíceis de se medir experimentalmente. No entanto, tais equações de estado fazem uso de parâmetros de interações intermoleculares que requerem conhecimento detalhado a nível molecular do sistema[1]. Como uso de métodos computacionais mais rigorosos, como cálculo *ab initio* ou dinâmica molecular, são difíceis de se utilizar na rotina das atividades industriais, uma alternativa é o aprimoramento de equações de estado levando em consideração informações obtidas com nível de cálculo mais rigoroso. As equações do método SAFT foram desenvolvidas a partir do uso de informações a nível molecular, de forma que esta metodologia leva resultados precisos para estimativa de parâmetros termodinâmicos[2]. O presente estudo visa a verificação de diversas hipóteses utilizadas para o desenvolvimento do método SAFT utilizando cálculos *ab initio* e métodos DFT. Moléculas isoladas, dímeros e trímeros de compostos aromáticos funcionalizados foram otimizados em nível PBE1PBE, M06-2X e wB97XD com base 6-311G(d,p). Para um cálculo mais preciso da energia de interação, foi utilizado o método composto CBS-QB3 que faz uso de extrapolação ao conjunto de base infinito para obtenção de valores mais precisos de energia. O cálculo da energia de interação de dímeros e trímeros, Tabela 1, foi feito a fim de verificar a hipótese de que a energia de interação para formação de trímeros é igual a energia de interação para formação de dímeros. A análise inicial dos resultados aponta uma diferença maior que 3 kcal mol<sup>-1</sup> para formação dos trímeros de fenol e anilina em relação aos respectivos dímeros. A comparação dos resultados em nível CBS-QB3 e PBE1PBE para formação mostra uma diferença maior que 2 kcal mol<sup>-1</sup> para energia de interação corrigida por ZPE para formação dos dímeros. A Figura 1 apresenta um comparativo entre a estrutura do dímero e trímero de anilina em fase gasosa. No momento se encontra em andamento a análise do mapa de potencial eletrostático de monômeros de modo a verificar a hipótese usada pelo método SAFT de que as moléculas apresentam um ponto de ancoragem bem definido e localizado.



Tabela 1: Valores de  $\Delta E$  em kcal mol<sup>-1</sup> para energia de formação de dímeros e trímeros. Foram consideradas estruturas que fazem ligação de hidrogênio. Os resultados PBE1PBE estão corrigidos para o erro de superposição de base.

	<b>anilina</b>	<b>fenol</b>	<b>nitrobenzeno</b>
		Dímeros - CBS-QB3	
$\Delta E$	-4,526	-7,164	-3,470
$\Delta E(+ZPE)$	-3,624	-6,138	-3,125
		PBE1PBE/6-311G(d,p)	
$\Delta E$	-3,997	-6,097	-5,869
$\Delta E(+ZPE)$	-5,544	-7,385	-6,411
		Trímeros - PBE1PBE/6-311G(d,p)	
$\Delta E$	-8,878	-9,779	
$\Delta E(+ZPE)$	-11,30	-11,81	

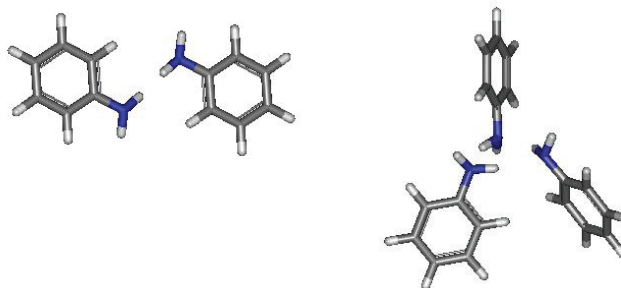


Figura 1: Geometrias otimizadas para o dímero e trímero da anilina. Resultados obtidos em nível PBE1PBE/6-311G(d,p).

**Key-words:** Compostos aromáticos, Ligação de hidrogênio, energia de interação, equações de estado.

**Suporte:** FAPERJ, CNPq e CENAPAD-SP

**Referências:**

[1] Silva-Oliver et al Fluid Phase Equilibria 250 (2006) 37–48.

[2] W.G. Chapman et al Fluid Phase Equil. 52 (1989) 31-38



## Computational study of photosensitizing IR780 and its interaction with transition metals cations

Michele A. Salvador<sup>a</sup>, Andris F. Bakuzis<sup>b</sup>, Ronei Miotto<sup>a</sup>, Paula Homem-de-Mello<sup>a</sup>

<sup>a</sup>*Universidade Federal do ABC – Santo André – Brazil*

<sup>b</sup>*Universidade Federal de Goiás – Goiânia – Brazil*

**Abstract:** Heptamethine dyes are chemical compounds within the indocyanine dye family, and have been explored in photodynamic therapy (PDT)[1], since they are reported to have photosensitizing characteristics. Besides, experimental results indicated that its interaction with magnetic nanoparticles influenced their thermal and spectroscopic properties. In this work we have studied the electronic and thermal properties of IR780 molecule (Figure 1), a lipophilic agent, using Density Functional Theory (DFT) simulations. DFT calculations were performed using B3LYP functional and D3BJ empirical dispersion correction, considering 6-31G(d,p) basis set and def2-TZVP auxiliary basis, as implemented in Orca software. Also, excited state optimization using time-dependent DFT (TD-DFT) methodology was performed in order to compare the infrared spectra in both cases.

In order to understand the role of the interaction with nanoparticles, molecule's bond with transition metals cations  $Mn^{+2}$ ,  $Fe^{+2}$  and  $Co^{+2}$  were investigated, aiming to analyze the changes in dipole moment magnitude and direction, also changes in charge distribution.

Comparing IR780 in ground and excited states, dipole moment decreased substantially, and its direction also changes. In terms of charge distribution the largest differences were in atoms of the central ring. Considering the structures with cations, the larger charge distribution variations were observed in atoms nearer from the cations, as expected. Differences in single point energies of IR780 bonded to metal cations indicate formation of chemical bonds, and the difference increases proportionally with atomic radii.

Although it was not observed significant change in the molecule's geometry between ground and excited states, changes in the infrared spectrum were noticed. In order to clarify these results, further studies are in progress.

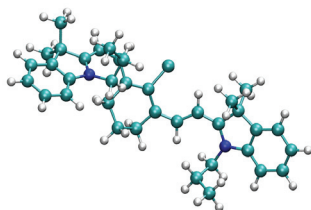


Figure 1: Optimized structure of IR780

Key-words: Density Functional Theory, IR spectrum, excited states, coordinated atoms.

**Support:** This work has been supported by FAPESP and CNPq.

### References:

- [1] X. Tan, S. Luo, D. Wang, Y. Su, T. Cheng, C. Shi, "A NIR heptamethine dye with intrinsic cancer targeting, imaging and photosensitizing properties", *Biomaterials* 33, 2230 (2012).
- [2] Y. Wang, T. Liu, E. Zhang, S. Luo, X. Tan, C. Shi, "Preferential accumulation of the near infrared heptamethine dye IR-780 in the mitochondria of drug-resistant lung cancer cells", *Biomaterials* 35, 4116 (2014).



## Study of Molecular Dynamics, NBO and QTAIM for inhibitors of ALK-5

Michell O. Almeida<sup>a</sup>, Sergio H. D. M. Faria<sup>b,c</sup>, Guelber C. Gomes<sup>d</sup>, Clauber H. S.

Costa<sup>d</sup>, Jerônimo L. Silva<sup>d</sup>, Cláudio N. Alves<sup>d</sup> and Kathia M. Honorio<sup>a,c</sup>

<sup>a</sup>Centro de Ciências e Humanas – UFABC, <sup>b</sup>Instituto de Ciências da Saúde – UNIP,

<sup>c</sup>Instituto de Química – UNICAMP, <sup>d</sup>Laboratório de Planejamento de Fármacos – UFPA, <sup>e</sup>Escola de Artes, Ciências e Humanidades – USP

**Introduction:** TGF- $\beta$  Receptor Type 1 (TGF- $\beta$ 1), also known as activin kinase type 5 (ALK-5), is a biological target related to some types of cancer, such as breast cancer. Inhibition of this target is a strategy that has been studied as a way to treat cancer. In this way, the objective of this work is to use computational chemistry to evaluate the main interactions that occur between the main residues in the active site of ALK-5 (Tyr249, His283 and one structural water) and two inhibitors of this receptor [1, 2].

**Materials and methods:** To evaluate the interactions between the two molecules and the ALK-5 target, the following methodologies were used: molecular docking (GOLD 5.2), molecular dynamics (70 ns, force field ff99SB, AMBER12), QM/MM (ONIOM, B3LYP/cc-PVDZ:UFF, Gaussian 09), analysis of natural bond orbitals (NBO, B3LYP/cc-PVDZ, Gaussian 09) and topological analysis of electronic density of interactions by quantum theory atom in molecules (QTAIM) [3].

**Results and discussion:** Figure 1 shows the results obtained from molecular docking and molecular dynamics simulations.

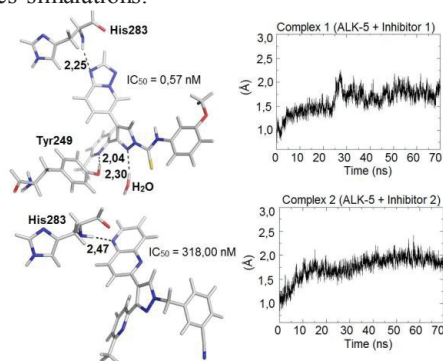


**Figure 1.** Hydrogen bonds between the inhibitors 1 and 2 and the main residues of ALK-5; RMSD values obtained from molecular dynamics to the two complexes.

Figure 1 shows that ALK-5 with the inhibitor 1 (the most active,  $IC_{50} = 0,57$  nM) docked on its active site, as well as hydrogen bonds with the main residues and the structural water. The RMSD values obtained from molecular dynamics simulations

indicate that the complex 1 (ALK-5 + inhibitor 1) presents a greater flexibility. After these analyzes, the conformation of the complexes obtained from the molecular dynamics was used for the QM/MM ONIOM calculations with the objective of evaluating the electronic behavior of the interactions between ALK-5 and the two inhibitor molecules. From the ONIOM results, NBOs were analyzed in order to evaluate the electronic transfer between the ligands and the receptor. Thus, Table 1 shows the results obtained from ONIOM and NBO calculations.

**Table 1.**  $E_{\text{ONIOM}}$  values and interaction intensities obtained from NBO calculations

Interactions - Complex 1			
$(E_{\text{ONIOM}} = -2.732.543,53 \text{ kcal/mol})$	NBO Donor	NBO Aceptor	$\Delta E^2(\text{kcal/mol})$
1 - Inhibitor 1 + H <sub>2</sub> O	LP N	BD*( $\pi$ ) O-H	2,83
2 - Inhibitor 1 + Tyr249	LP N	BD*( $\pi$ ) O-H	11,89
3 - Inhibitor 1 + His283	LP N	BD*( $\pi$ ) N-H	3,82
Interactions - Complex 2			
$(E_{\text{ONIOM}} = -2.56.836,81 \text{ kcal/mol})$	NBO Donor	NBO Aceptor	$\Delta E^2(\text{kcal/mol})$
4 - Inhibitor 2 + His283	LP N	BD*( $\pi$ ) N-H	0,81

Table 1 shows that the complex 1 (the most active) has a lower value of  $E_{\text{ONIOM}}$  and from the NBO analyses, it is possible to notice from the values of  $\Delta E^2$  that the hydrogen bonds that occur between the inhibitor 1 and ALK-5 residues are more intense. Finally, the electron density ( $\rho$ ) and laplacian of electron density ( $\nabla^2\rho$ ) of the bond critical points (BCPs) were analyzed using the QTAIM methodology, and the results obtained can be seen in Table 2.

**Table 2.** Values of electron density and laplacian of electron density

(BCPs)	$\rho$ (u.a.)	$\nabla^2\rho$ (u.a.)
N <sub>27</sub> -H <sub>18</sub> (Inhibitor 1 + Tyr249)	0,025	0,065
N <sub>31</sub> -H <sub>10</sub> (Inhibitor 1 + His283)	0,013	0,040
N <sub>1</sub> -H <sub>54</sub> (Inhibitor 1 + H <sub>2</sub> O)	0,013	0,036
N <sub>15</sub> -H <sub>68</sub> (Inhibitor 2 + His283)	0,010	0,029

The results presented in Table 2 show that  $\rho$  and  $\nabla^2\rho$  for both interactions are positive, confirming the electronic character of a hydrogen bond from the QTAIM theory. Another important finding is that the QTAIM theory corroborates the NBO model, because for both techniques, the interactions with the inhibitor 1 are more intense, and the interaction between the inhibitor 1 and Tyr249 is the most intense.

**Conclusions:** From the obtained results it was possible to analyse the behavior of two inhibitors in the active site of ALK-5, and NBO and QTAIM analyses showed that the inhibitor 1 makes more intense interactions with the biological target, increasing the stability of the complex.

**Key-words:** ALK-5, cancer, inhibitors. ONIOM, NBO, QTAIM.

**Support:** This work has been supported by FAPESP.

#### References:

- [1] D. Kim, *et al.* Bioorg. Med. Chem. Lett. 21, 6049 (2011).
- [2] D. Kim, *et al.* Bioorg. Med. Chem. Lett. 18, 4459 (2010).
- [3] Richard. F. W. Bader, Acc. Chem. Res. 18, 9 (1985).

## Theoretical study of cis and trans structures [Zn(dmsO)<sub>2</sub> (H<sub>2</sub>O) (fum)], where dmsO = dimethylsulfoxide fum = fumaric acid

Authors: Milene Aparecida Rodrigues de Oliveira, Yvonne Primerano Mascarenhas

Address: milene@ifsc.usp.br

**Abstract:** The large number of compounds that may exhibit cis-trans isomerism in inorganic chemistry illustrates, in terms of number of known examples, the progress of synthetic inorganic chemistry. In fact, from the studies conducted by Werner at the beginning of this century to the present day, a huge range of works involving this type of isomers can be found in the literature.<sup>1-7</sup> In the case of isomers in inorganic complexes it is always important to remember that their synthesis, proof of their molecular structures and an evaluation of their properties, provide the decisive arguments for Werner to develop and defend his own theory of coordination<sup>8-13</sup>. The calculations were performed using the Gaussian 98W computational software.<sup>28</sup>

The equilibrium geometry of the studied molecules were calculated using as base set of functions: 6-311 ++ G (3df, 3pd) in the mode DFT B<sub>3</sub>LYP.

The first step of the work consisted in minimizing the molecular energies of the equilibrium geometries for the cis and trans structures, assuming the presence of two water molecules of hydration as observed experimentally in the case of the trans isomer by X-ray diffraction. Such geometries are shown in Fig.1 As expected, due to the presence of water and consequent hydrogen bonds, the "Trans" structure presents a lower energy The most abundant under normal experimental conditions. There is also an unacceptable deformation of the octahedral coordination of Zn in the cis structure due to the van der Waals repulsion between the sulfoxides groups.

The calculated energies with a variation of 2.4 Kcal / mol being a more stable trans structure in the cis structure as binding distances calculated in the Zn-O coordination range from 1.86 to 1.88 Å and the angles calculated in the coordinates range from 104, 96 to 148,85 °, demonstrating a shortening in the bonds, proving a distortion of the octahedral in this conformer. As calculated distances and angles for the trans structure are according to a literature found for the same conformer.

Taking into account these results, we performed calculations of energy minimization of the structures, taking as hydration water the coordination of zinc, for analysis of geometric change related to the position of ligands in cis or trans.

It can be observed that the cis binder generates a tetrahedral geometry with coordinating angles between 108.64 ° and 110.66 °, whereas for the ligands in trans a geometry is presented a planar square where the coordination angle varies between 90.35 ° And 89.75 °.

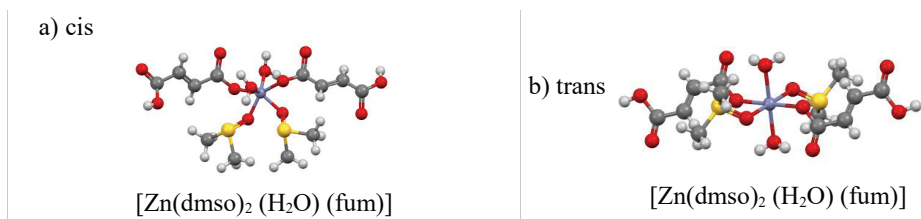


Figure 1. Optimized geometries in the DFT calculation of confounders "Cis" and "Trans"

Already the energy of these structures are closer together varying only 0.1 kcal / mol, where the cis structure has an energy of 2.4 kcal / mol and the trans structure has an energy of 2.3 kcal / mol, thus demonstrating, That the trans structure remains more stable than cis, but the two structures now can coexist.

When calculations were carried out, hydrating the tetracoordinate molecules, both cis and trans structures, resulted in a hexacoordinate structure with octahedral geometry and energy close to an initially isolated structure ( $E = -2.1$  Kcal / Mol).

Analyzing the results obtained by the theoretical calculations, it can be observed that the octahedron of the coordination of the zinc, this distorted in cis, for a good repulsion of spills between the sulfoxides groups. When the coordination of zinc to tetracoordinate is changed, a cis structure has a tetrahedral geometry and a square trans square. As the energies are calculated for the two indicative structures, they can be found, since the energy difference between a cis and trans is small.

But next to the tetracoordinated cis complex a convergent structure for a hexacoordinate transaction with a calculated isolated molecule energy, thus concluding that a hexacoordinated cis structure with 4 ligands and 2 waters is experimentally unlikely.

**Key-words:** Theoretical calculations, geometric isomerism, energy, stability

**Support:** This work has been supported by .....

#### References:

- [1]. Gerber, T. I. A.; Kemp, H.J.; Preez, J. G. H.; *J. Coord. Chem.* 1994, 33, 171.
- [2]. Brickleband, N.; Godfrey, S. M.; McAuliffe, C. A.; Molloy, K. C.; *J. Chem. Soc., Dalton Trans.* 1995, 10, 1593.
- [3]. Nakazawa, H.; Yamaguchi, Y.; Mizuta, T.; Miyoshi, K.; *Organometallics* 1995, 14, 4173.
- [4]. Barnard, C. F. J.; Vollano, J. F.; Chaloner, P. A.; Dewa, S. L.; *Inorg. Chem.* 1996, 35, 3280.
- [5]. Wehman-Ooyevaar, I. C. M.; Drenth, W.; Grove, D. M.; Koten, G.; *Inorg. Chem.* 1993, 32, 3347.
- [6]. Favez, R.; Roulet, R.; Pinkerton, A.; Schwarzenbach, D.; *Inorg. Chem.* 1980, 19, 1356.
- [7]. Al-Najjar, I. M.; Al-Lohedan, H. A.; Issa, Z. A.; *Inorg. Chim. Acta* 1988, 143, 119.
- [8]. Kauffman, G. B.; *Coord. Chem. Rev.* 1973, 11, 161.
- [9]. Springer, C. S.; Sievers, R. E.; *Inorg. Chem.* 1967, 6, 852.
- [10]. Thar, J.; Hovorka, R.; Kirchner, B.; *J. Chem. Theory Comput.* 2007, 3, 1510.



## Averaged electron collision cross sections for thermal mixtures of $\beta$ -Alanine conformers in the gas phase

Milton M. Fujimoto\*<sup>1</sup>, Erik V. R. de Lima<sup>1</sup> e Jonathan Tennyson<sup>2</sup>

*1 Departamento de Física, Universidade Federal do Paraná, 81531-990 Curitiba, PR, Brazil*

*2 Department of Physics & Astronomy, University College London, Gower St., London, WC1E 6BT, UK*

**Abstract:** Beta-alanine (3-aminopropanoic acid,  $\text{NH}_2\text{-CH}_2\text{-CH}_2\text{-COOH}$ ) is the simplest  $\beta$ -amino acid; it is an isomer of  $\alpha$ -alanine in which the amino group is bonded at the  $\beta$  carbon with the respect of carboxylic group ( $-\text{COOH}$ ). Beta-Alanine is a solid at room temperature and found in zwitterionic form in condensed phase. Beta-alanine vaporizes at temperatures near 360 K and it is well-known that in the gas phase it exists as a mixture of charge-neutral conformers. As is often observed for amino acids,  $\beta$ -alanine is a very flexible molecule and it exists as a great variety of spatial stable conformations. In the gas phase, intramolecular interactions are important for stabilizing different spatial arrangements of atoms. In this work, we report a theoretical study comparing elastic cross sections for the 10 lowest-energy conformers of  $\beta$ -alanine in the gas phase for impact energies ranging from 1 to 10 eV. We also present averaged-cross sections which take into account relative populations of different conformers. The R-matrix method used in this work is the UKRMol implementation of the UK molecular R-matrix codes which is describe in details elsewhere Tennyson [1]. The cross sections are calculated in static-exchange-polarization (SEP level) using the same same approach in our previous work in Fujimoto et al [2] which calculations on two alanine conformers were performed. The eigenphase sums, resonance features, differential and integral cross sections are computed for each individual conformer. Resonance positions for the low-energy  $p^*$  shape resonance are found to vary from 2.5 eV to 3.3 eV and the resonance widths from 0.2 eV to 0.5 eV. Averaged cross sections for thermal mixtures of the 10 conformers are presented and a comparison with various temperature-dependent sets of relative populations based on relative Gibbs free energies are shown. A comparison with previous results for the  $\alpha$ -alanine [3] isomer is also done. We believe that these results should be more reliable for comparison with measured data at temperature where the gas phase molecule is experimentally accessible.

**Key-words:** cross sections, amino acids,  $\beta$ -alanine

**Support:** This work has been partially supported by the Brazilian agency Conselho Nacional de Desenvolvimento Científico e Tecnológico (CNPq)

### References:

- [1] J. Tennyson *Phys. Rep.* **491** 29-76 (2010).
- [2] M. M. Fujimoto, S.E. Michelin, J. Tennyson, *Eur. Phys. J. D.* **68** 67 (2014).
- [3] M. M. Fujimoto, E. V. R. de Lima, J. Tennyson, *J. Phys. B: At. Mol. Opt. Phys.* **49**, 215201 (2016).

## Theoretical Study of Cleavage Surfaces and Water Adsorption on B-Nb<sub>2</sub>O<sub>5</sub>

Bastos, M.,<sup>a\*</sup> Duarte, H. A.<sup>a</sup> and De Abreu, H. A.<sup>a</sup>

<sup>a</sup>Universidade Federal de Minas Gerais, Department of Chemistry, Av. Antônio Carlos 6627, 31.270-901, Belo Horizonte – BRAZIL

**Keywords:** Nb<sub>2</sub>O<sub>5</sub>, surface, adsorption, DFT.

**Abstract:** Niobium oxide (Nb<sub>2</sub>O<sub>5</sub>) based systems play an important role in many catalytic processes, mainly when high acidity and water tolerance are needed in the processes. In this report, the structural and energetic results of the B phase cleavage surface study of niobia (B-Nb<sub>2</sub>O<sub>5</sub>) are presented. The cleavage and surface energies have been calculated indicating that the (010)-2 surface is the most favored. The order of stability for the relaxed surfaces is: (010)-2 > (110) > (100) > (010)-1 > (001). The Projected Density of States (PDOS) indicates that the Nb atom is the preferred adsorption site (Lewis acidic sites). Water molecules adsorb molecularly at the surface. However, the dissociative adsorption of water is just slightly higher in energy. Therefore, one can argue that at the surface both mechanisms (molecular and dissociative) may be present.

### 1. Introduction

Nb<sub>2</sub>O<sub>5</sub> is also known as niobia, exists in many polymorphic forms depending on the starting materials, pressure and temperature. According to the phase diagrams of Nb<sub>2</sub>O<sub>5</sub>, their crystallographic phases are classified in three groups: low-temperature (~700 to 900 K), medium-temperature (~900 to 1200 K) and high-temperature (~1223 K).<sup>1</sup> Among the applications of niobia, there is a growing interest in niobium containing materials with potential applications in heterogeneous catalysis, mainly when high acidity and water tolerance are needed in the processes.<sup>2</sup> The phase chosen for the study of water adsorption was B-Nb<sub>2</sub>O<sub>5</sub>,<sup>3,4</sup> a phase of medium-temperature. There is no report concerning the favorable cleavage plane of B-Nb<sub>2</sub>O<sub>5</sub>. In the present work the different cleavage surfaces and the different water adsorption mechanism were investigated. Various geometric configurations were examined for the water adsorption. For the dissociative mechanism for the water adsorption, it was assumed that the dissociated hydrogen atom remains chemisorbed on the surface oxygen atom. All the calculations were carried out by using the Quantum Espresso program package (pWscf).<sup>5</sup> The calculations were performed using PBE XC functional, with an energy cutoff of 60 Ry and at the gamma ( $\Gamma$ ) point. A vacuum layer of 15 Å normal to the surface was used.

### 2. Results and discussion

The proposed cleavage planes were that with low Miller index. The five different surfaces were labeled as: (100), (010)-1, (010)-2, (001), (110) and (111), (Fig.1a). Considerable relaxation occurred on all surfaces (up to 63% reduction in energy). The (010)-2 surface is more likely to cleave (1.37 J m<sup>-2</sup>) among the proposed plans. The



order of stability for the relaxed surfaces is: (010)-2 > (110) > (100) > (010)-1 > (001). Fig.1b shows the (010)-2 optimized surface. The niobium cations are all unsaturated with coordination number equal to five ( $\text{Nb}^{5c}$ ) and oxygen ions have coordination number equal to two forming a bridge with the niobium atoms. In addition there are two types of oxygen atoms, those that are more exposed ( $\text{O}^{\text{up}}$ ) and those that are less exposed ( $\text{O}^{\text{down}}$ ).

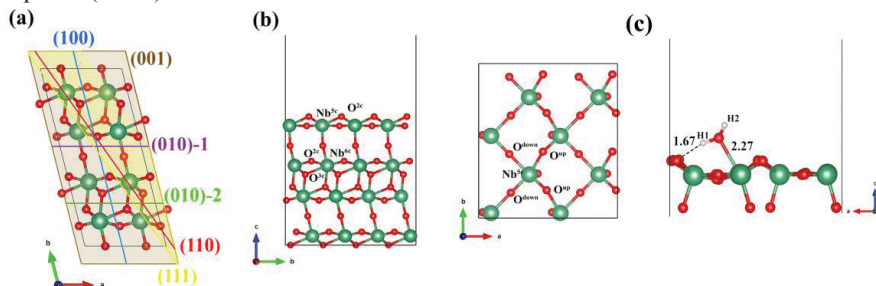


Figure 1: (a) Optimized structure of the B-Nb<sub>2</sub>O<sub>5</sub> bulk, and the six different cleavage planes, (b) optimized structure of B-Nb<sub>2</sub>O<sub>5</sub> (010)-2 surface and (c) water molecule adsorbed on (010)-2 surface.

The calculation of PDOS was performed and showed that the Nb atom is the preferred adsorption site (Lewis acidic sites). The adsorption of a water molecule on the optimized (010)-2 surface was carried out in several configurations. The most favorable adsorption mechanism is molecularly with adsorption energy of 25.6 kcal mol<sup>-1</sup>. The adsorption occurs on the niobium adsorption sites (Fig.2c). In addition, one of the hydrogen of the water molecule (OH1) is pointing toward one oxygen atom, O<sup>up</sup>, forming a hydrogen bond.

### 3. Conclusions

In summary, the cleavage of the B-Nb<sub>2</sub>O<sub>5</sub> along the (010)-2 direction is preferred. The calculations of adsorption energies showed that the molecular adsorption on (010)-2 surface is more favorable than the dissociative. The PDOS of (010)-2 surface showed that the conduction band is composed mainly of *d* orbitals of the niobium atoms. This fact explains the preference for adsorption on the niobium atom, the most electrophilic center. The dissociative mechanism leads to structures that are, at least, 4.4 kcal mol<sup>-1</sup> less favorable than the molecular adsorption. This study suggests that the two states compete in energy and, therefore, the authors believe two configurations are expected to coexist on B-Nb<sub>2</sub>O<sub>5</sub> (010) surface. The effect of the full coverage of water molecules on the surface has been investigated and will be discussed in details.

**Support:** CAPES, FAPEMIG, CNPQ, INCT-ACQUA and UFMG.

#### References:

- [1] I. Nowak, I., Ziolek, M., Chemical Reviews 1999, 99, 3603-3624.
- [2] Tanabe, K., Catalysis Today 2003, 78, 65-77.
- [3] Ercit, T. S., Mineralogy and Petrology 1991, 43, 217-223.
- [4] M. B. Pinto, *et al.* The Journal of Physical Chemistry A 2017, 121, 2399.
- [5] P. Giannozzi, *et al.*, Journal of Physics-Condensed Matter 2009, 21.



## The use of ensemble docking to evaluate the inhibition of the dDat enzyme by the sugar compared with cocaine

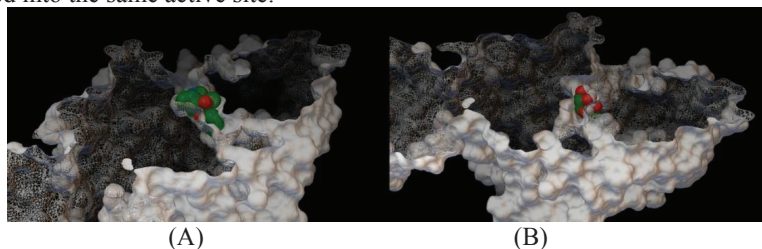
Mírian C. C. Silva (IC)<sup>1</sup>, Pedro H. N. Binda (IC)<sup>1</sup>, Lourival R. de Sousa Neto (PG)<sup>1</sup>, Roberto R. Faria (PG)<sup>1</sup>, Erick G. França (PQ)<sup>2</sup>, Eduardo de F. Franca (PQ)<sup>1</sup>

<sup>1</sup>Universidade Federal de Uberlândia; <sup>2</sup>Instituto Federal de Goiás

**Introduction:** The Dopamine is a very important neurotransmitter responsible for the movement control, motivation, and cognition of the human been in order to stimulate the central nervous system by engaging in the sensations of pleasure and motivation. Thus, dopamine is involved in the dependence processes, from the moment its production is inhibited. Consequently, the use of drugs such as cocaine is responsible for blocking the selective monoamine transporters (dopamine, serotonin, etc.) as well as being an inhibitor of monoamines oxidases. With this, cocaine avoid, in a competitive inhibition, the dopamine to be released in the neural synapse and its returns to the cytosol to be reused for a new process of neurotransmission. Thus, the concentration of dopamine rises in the synapse region, causing one of the effects of the drug. In recent years, the indiscriminate use of sugar has been questioned due to the emergence of diseases such as obesity and diabetes<sup>1</sup>, because glucose consumed in excess can cause the same effects as illicit drugs, such as cocaine and amphetamines<sup>2,3</sup>; however, in a more lenient way.

**Methodology:** In this work we use ensemble docking to dock a single ligand against multiple rigid conformations obtained from molecular dynamics simulation (MD) and compare the bind energies of the glucose (hydrolyzed product of sugar) and cocaine in the dDAT active site. For doing this, the MD of the dDAT enzyme (PDB code: 4xp4 ) was made in explicit water (tip4p model), in NPT ensemble (P = 1 bar e 310K) for 10 ns, using the OPLSAA force-field and the GROMACS 5.06. The ligands (glucose and cocaine) were docked into the dDat active site using the AutoDock 4.2 using Lamarckian Genetic Algorithm (LGA).

**Figure 1** – (A) Cocaine into the dDat active site after molecular docking. (B) Glucose docked into the same active site.





**Results and discussion:** The structural fluctuation of the dDat in water was evaluated by the RMSD and displayed a mean value of 0.36 nm after 1800 ps.

According to the Table 1, the bind energy and the inhibition constant between the glucose and dDat showed that the sugar is capable of inhibit the dopamine transporter enzyme, which confirm the hypothesis that the saccharide can induce some narcotic effect like cocaine. The Figure 1 shows the interaction between the ligands and enzyme. Moreover, RMSD displayed the water effect on enzyme structure and on the bind energy with the ligands (Table 1). Thus, greater structural fluctuations imply in less favorable interactions, suggesting that the solvent decrease the protein activity, according to these simulation setups. It has been expected because the molecular dynamics simulation did not considered the co-factors: Cholesterol Hemiccinate, Cholesterol, Maltose and 1-ethoxy-2-(2-ethoxyethoxy)ethane.

**Table 1** – Molecular Dynamics RMSD and bind energies between dData-cocaine and dDat-glucose resulted from molecular docking made from uncorrelated structures extracted from MD simulation.

Frames (ps)	RMSD	Bind Energy (Kcal)	
		Cocaine	Sugar
0	0	-8.37	-6.18
2000	0.39	-8.49	-7.71
5610	0.27	-8.9	-6.69
7920	0.38	-7.32	-6.89
9780	0.45	-4.16	-2.97

**Conclusion:** The ensemble docking calculations showed that the glucose is capable of inhibit the dopamine transporter enzyme and reinforces the hypothesis that sugar in excess can cause dependence, as cocaine.

**Key-words:** Binding energy, inhibition constant, dopamine, cocaine, sugar, ensemble docking, enzymatic activity.

**Support:** FAPEMIG (CEX-APQ-02176-11) and Rede Mineira de Química (RQ-MG: RED-00010-14)

**References:**

- [1] Bittman, M. "An Inconvenient Truth About Our Food". *The New York Times*. Retrieved Apr 13, 2014.
- [2] O'Sullivan, M. "Fed Up movie review: The sins of sugar". *The Washington Post*. Retrieved Apr 13, 2014.
- [3] Wang, K. H.; Penmatsa, A.; Gouaux, E. *Nature*. **2015**, *521*, 322.





## Painel 245 | PN.245

# Abordagem por métodos de estrutura eletrônica no processo de ESIPT em derivados de 2-(2'-hidroxifenil)benzazóis

Munique R. Pereira(PG), Roiney Beal(PG), Gabriel M. Zanotto(PG), Paulo F. B. Gonçalves(PQ)

muniquerper@gmail.com

Universidade Federal do Rio Grande do Sul, Instituto de Química, Grupo de Química Teórica. Av. Bento Gonçalves, 9500, Porto Alegre-RS

### INTRODUÇÃO

As reações de transferência de próton intra ou intermolecular podem ser consideradas como um dos processos mais fundamentais e importantes em diversas áreas de pesquisa. Dependendo das características estruturais, a transferência do próton pode ocorrer no estado fundamental ou excitado. Entre os processos que ocorrem no estado excitado estão a transferência de próton intramolecular no estado excitado (ESIPT – Excited State Intramolecular Proton Transfer), mostrado na Figura 1.

Além de serem importantes rotas de desativação em sistemas biológicos, as moléculas que apresentam ESIPT são altamente atrativas do ponto de vista sintético e tecnológico, devido as suas características fotoquímicas e fotofísicas únicas que lhe conferem importantes aplicações. Uma das aplicações de interesse é o uso como sondas fluorescentes, que na área de biomedicina permite captar imagens para o estudo e diagnóstico de doenças. Alguns derivados de heterociclos do tipo 2-(2'-hidroxifenil)benzazóis são biologicamente ativos e podem ser usados como sondas fluorescentes na determinação espectrofluorimétrica de enzimas e aminoácidos contidos em amostras biológicas.

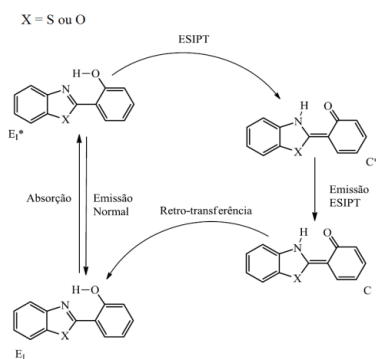


Figura 1: Caminho de reação proposto

### METODOLOGIA

Todos os cálculos foram executados utilizando a metodologia TD-DFT (Time Dependent Density Functional Theory) com o funcional wB97XD e ADC(2). As geometrias das formas Enol e Ceto foram calculadas a nível wB97XD/6-31G(d) e ADC(2)/DZVP enquanto a análises das transições foram feitas com a adição de funções





difusas, nos níveis wB97XD/6-311+G(d,p) e ADC(2)/TZVP. O efeito do solvente foi adicionado através do modelo de solvatação PCM (Polarizable Continuum Model) em conjunto com o TD-DFT e COSMO em conjunto com o ADC(2), com os solventes acetonitrila, etanol e tolueno. Foi assumido que a reação ESIPT ocorre entre os estados  $E^*$  e  $C^*$  relaxados em solvente.

## RESULTADOS E DISCUSSÕES

As análises foram feitas nos derivados do 2-(2'-hidroxifenil)benzazol, benzoxazol ( $X=O$ ) e benzotiazol ( $X=S$ ), partindo-se das geometrias otimizadas dos estados fundamental e excitado, para as formas Enol e Ceto, utilizando os solventes acima citados. O perfil do processo de ESIPT foi traçado de forma a comparar as energias liberadas na transferência do próton.

Considerando os cálculos feitos com TD-DFT, a reação em acetonitrila obteve a maior diferença de energia entre forma Enol\* e forma Ceto\*, sendo a última a mais estável, sendo de 0,30 e 0,35 eV para os derivados benzoxazol e benzotiazol, respectivamente. As reações com os solventes etanol e tolueno obtiveram diferenças de energia entre forma Enol\* e forma Ceto\*, nas faixas de 0,24 a 0,30 eV para o derivado benzoxazol e 0,29 a 0,35 eV para o derivado benzotiazol, seguindo a tendência esperada para a diminuição da constante dielétrica, uma vez que a forma Ceto\* apresenta maior momentum de dipolo que a forma Enol\*. Os resultados obtidos com TD-DFT são comparáveis aos obtidos no nível ADC(2).

## CONCLUSÕES

As reações em acetonitrila e tolueno ocorreram de acordo com as expectativas, sendo em acetonitrila o solvente que mais estabilizou a forma Ceto\*, uma vez que a constante dielétrica é maior que a do tolueno. Entretanto, a reação em etanol não seguiu de acordo com resultados experimentais encontrados na literatura. Isto provavelmente se deve ao fato de que o modelo de solvatação utilizado (PCM) não considera moléculas de solvente explícitas, não descrevendo possíveis ligações de Hidrogênio, explicando o fato de que na literatura a reação não ocorre apenas em etanol. Os resultados obtidos tanto em TD-DFT como em ADC(2) são qualitativamente equivalentes.

**Palavras-chave:** ESIPT, TD-DFT, benzoxazol, benzotiazol

**Suporte:** Este trabalho foi feito com suporte da CAPES e CNPQ.



## Theoretical analysis of IGP-ZnO and IGP-ZnO nanotubes

Authors: Marana, N. L., Fabris, G. S. L., Sambrano, J. R.

Address: Modeling and Molecular Simulations Group, São Paulo State University (Unesp), Campus Bauru, Brazil.

### Abstract:

Porous materials have gained attention in the last few years due to the increase of potential application, in special, on electronic devices. One of the most studied porous materials are the porous graphene (PG) and graphenylene (GP), that differ according to the pore configuration. Recently, Brunetto et al. [1] reported a theoretical study of PG and GP structures using the density functional tight-binding method. They showed that the band gaps of PG and GP are 3.3 and 0.8 eV, respectively, i.e., the bandgap increases with the pore. Yu [2] showed that GP has a promising potential as anode material for lithium-ion batteries and exhibits high storage capabilities; in addition, Song et al. [3] reported that GP, with its well-defined porous network, can be used as molecular sieve for gas separation and storage.

There are several inorganic materials with similar structure (honeycomb) of graphene, such as boron nitride (BN), gallium nitride (GaN) and zinc oxide (ZnO), among others. Based on that and the advantages showed by PG and GP, the inorganic materials were also studied as a porous shape, such as porous boron nitride (PBN), inorganic graphenyleneboron nitride (IGP-BN) and porous ZnO.

In special, porous ZnO [4] was synthesized in different nanoparticles, showing superior photocatalytic activity and high selectivity compared to nonporous ZnO nanoparticles. Therefore, the aim of this work is to analyze the structural and electronic properties of (0001) inorganic graphenyleneZnO (IGP-ZnO) and inorganic graphenylene ZnO nanotube (IGP-ZnONT) (10, 10) and (12, 0) (see Figure 1). The properties were compared with the nonporous (0001) surface and nanotube properties.

The study was conducted by DFT simulations using CRYSTAL14 program [5], with B3LYP hybrid functional and all-electron basis set. From the optimized IGP-ZnO (0001) monolayer surface, the armchair and zigzag nanotubes were obtained and fully re-optimized.

As it occurs with the nonporous ZnO nanotubes (ZnONTs) [6], the IGP-ZnONTs present the same behavior with respect to the geometry and bandgap such as the (0001) IGP-ZnO. Regarding the geometry, the (0001) IGP-ZnO and IGP-ZnONTs present three different Zn-O bonds and, after the optimization, all structures maintain this characteristic, which is 1.82, 1.88 and 1.98 Å. Such behavior is also observed for bond angles, Zn-O-Zn, that also present three different angles due the porous configuration, 90, 120 and 150 degrees. Concerning the nanotube diameter, the zigzag nanotube presents smaller diameter if compared to the armchair nanotube, even though they have the same number of atoms.



In regards to the electronic properties, all analyzed morphologies present indirect bandgap at  $\Gamma$ -X point, which is in disagreement with nonporous morphologies [6], whose bandgaps are direct at  $\Gamma$  point. Besides that, the porous morphologies present bandgaps about 0.9 eV higher than nonporous morphologies, i. e.,  $\sim 5.42$  eV, which show that pores cause the increase of the bandgap, as well as the observed for the PG and GP[1].

Interesting to highlight that regarding the elastic constants, due to the one-dimensional structure of nanotubes, they present only  $c_{11}$  constant and, for the IGP-ZnONT, the  $c_{11}$  constant is seven times higher than the constant for the ZnONTs. In other words, the IGP-ZnONTs is much more rigid and difficult to deform than the ZnONTs. In contrast, the pore breaks the symmetry of the cluster  $[\text{ZnO}_4]$  and, hence, the IGP-ZnO morphologies studied does not present piezoelectric constants.

Therefore, it is concluded that, although the IGP-ZnO morphologies present some characteristics of nonporous ZnO, many of the properties presented here correspond to a new material, with different structure, larger bandgap, more rigid which should be more exploited, mainly, according to their possible applications.

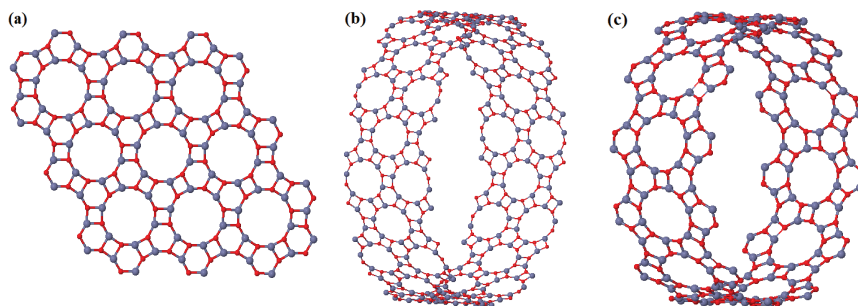


Figure 1: IGP-ZnO morphologies (a) (0001) surface, (b) armchair (10, 10) nanotube and (c) zigzag (12, 0) nanotube

**Key-words:** IGP-ZnO, nanotube, DFT

**Support:** CNPQ (46126-4), CAPES PROCAD (88881068492/2014-01) and FAPESP (2016/07954-8, 2016/07476-9 and 2016/25500-4).

### References:

- [1] G. Brunetto, P. a S. Autreto, L. D. MacHado, B. I. Santos, R. P. B. Dos Santos and D. S. Galvão, *J. Phys. Chem. C*, 116 (2012).
- [2] Y.-X. Yu, *J. Mater. Chem. A*, 1, 13559 (2013).
- [3] Q. Song, B. Wang, K. Deng, X. Feng, M. Wagner, J. D. Gale, K. Müllen, L. Zhi, M. Saleh, X. L. Feng, K. Müllen and R. Fasel, *J. Mater. Chem. C*, 1, 38–41 (2013).
- [4] Marana, N. L., Casassa, S. M., Longo, E., Sambrano, J. R., *J. Phys. Chem. C*, 120, 12, 6814 (2013).
- [5] R. Dovesi, R. Orlando, A. Erba, C. M. Zicovich-Wilson, B. Civalleri, S. Casassa, L. Maschio, M. Ferrabone, M. De La Pierre, P. D'Arco, Y. Noël, M. Causà, M. Rérat nd B. Kirtman, *Int. J. Quantum Chem.*, 114, 1287–1317 (2013).



## Computational investigation of the OH initiated oxidation of C6 unsaturated alcohols

Natália Aparecida Rocha Pinto (GR), Stella Maris Resende (PQ)

*Laboratório de Química Atmosférica Teórica (LAQAT)  
Departamento de Ciências Naturais, Universidade Federal de São João del-Rei (UFSJ)  
São João del-Rei, Minas Gerais, Brazil.*

**Abstract:** An important class of compounds emitted into our atmosphere is the volatile organic compounds (VOCs).[1] The presence of these compounds in the atmosphere has important environmental consequences because their oxidation leads to the formation of organic aerosols, which are involved in the regulation of the planet climate and the physical and chemical properties of the atmosphere.[2] Among oxygenated VOCs, an important group are C6 alcohols, which are emitted when plants are stressed or drying grass.[3] In this work, we investigated the first step of the atmospheric oxidation, initiated by OH radical, of (Z)-hex-3-en-1-ol, (E)-hex-3-en-1-ol, (Z)-hex-4-en-1-ol and (E)-hex-4-en-1-ol alcohols, whose structural aspects have already been determined by us and for which the atmospheric decomposition process has not yet been determined theoretically. Geometry optimizations and harmonic frequencies calculations were conducted at the MP2/cc-pVTZ level of theory. We have considered two possibilities for the first step of the reaction: hydrogen abstraction or OH addition, generating four possible products for each isomer. The values obtained for reaction enthalpy and Gibbs free energy are in Table 1 and in Table 2.

**Table 1.** Reaction enthalpy ( $\Delta H_r$ ) and Gibbs free energy ( $\Delta G_r$ ) for the reaction of OH with (Z)-hex-4-en-1-ol and (E)-hex-4-en-1-ol alcohols, in  $\text{kJ mol}^{-1}$  (298 K and 1 atm).

Compounds	(Z)-hex-4-en-1-ol		(E)-hex-4-en-1-ol	
	$\Delta H_r$	$\Delta G_r$	$\Delta H_r$	$\Delta G_r$
<b>H abstraction in C4</b>	-110.06	-108.62	-115.93	-112.65
<b>H abstraction in C5</b>	-112.00	-110.39	-117.22	-113.83
<b>OH addition in C4</b>	-167.14	-123.46	-179.34	-129.49
<b>OH addition in C5</b>	-168.14	-124.82	-169.22	-126.38



**Table 2.** Reaction enthalpy ( $\Delta H_r$ ) and Gibbs free energy ( $\Delta G_r$ ) for the reaction of OH with (Z)-hex-3-en-1-ol and (E)-hex-3-en-1-ol alcohols, in  $\text{kJ mol}^{-1}$  (298 K and 1 atm).

Compounds	(Z)-hex-3-en-1-ol		(E)-hex-3-en-1-ol	
	$\Delta H_r$	$\Delta G_r$	$\Delta H_r$	$\Delta G_r$
<b>H abstraction in C3</b>	-95.38	-94.29	-91.67	-89.63
<b>H abstraction in C4</b>	-110.47	-110.28	-89.80	-87.85
<b>OH addition in C3</b>	-158.86	-117.95	-165.28	-113.82
<b>OH addition in C4</b>	-167.31	-128.09	-174.66	-130.20

All values obtained for  $\Delta H_r$  and  $\Delta G_r$  are negative, which shows that all reaction possibilities are exothermic and exoergic. In general, hydrogen abstraction and OH addition in (Z)-hex-4-en-1-ol and (E)-hex-4-en-1-ol compounds are more favorable at C5 than C4; in (Z)-hex-3-en-1-ol and (E)-hex-3-en-1-ol, reaction in C4 is more favorable than in C3; OH addition is preferable to the hydrogen abstraction and the reaction with the (E) isomer leads to more favorable products than the reaction with the (Z) isomer. According our knowledge, this is the first determination of these values for this system. Kinetic studies are in progress.

**Key-words:** *ab initio*, thermochemistry, atmospheric chemistry, volatile organic compounds.

**Support:** This work has been support by CNPq, FAPEMIG e Rede Mineira de Quimica (RQ-MG).

#### References:

- [1] A. Guenther, C. N. Hewitt, D. Erickson, R. Fall, C. Geron, T. Graedel, P. Harley, L. Klinger, M. Lerdau, W. A. Mckay, T. Pierce, B. Scholes, R. Steinbrecher, R. Tallamraju, J. Taylor, P. J. Zimmerman, *Geophys. Res. Atmos.* 100, 8873 (1995).
- [2] J. H. Seinfeld, S. N. Pandis, "Atmospheric Chemistry and Physics", 2a ed. (2006), WileyInterscience, New York.
- [3] A. C. Heiden, K. Kobel, C. Langebaterls, G. Schuh-Thomas, J. Whildt, *J. Atmos. Chem.* 45, 143 (2003).



## Development of an empirical binding free energy model for phosphatidylinositol 4-kinase inhibitors

Natalie Mounteer Colodette (PG)<sup>1‡</sup>, Carlos Mauricio R. Sant'Anna (PQ)<sup>1,2</sup>, Eliezer J. Barreiro (PQ)<sup>1\*</sup>

<sup>1</sup>LASSBio - Instituto de Ciências Biomédicas - UFRJ - CCS - Ilha do Fundão, Rio de Janeiro, RJ

<sup>2</sup>Departamento de Química, Instituto de Ciências Exatas, UFRRJ, Rodovia BR465, km 7, 23970-000, Seropédica, RJ

\*nm.colodette@gmail.com

\*ejbarreiro@ccsdecania.ufrj.br

**Abstract:** Kinases are proteins that have the function of transferring a  $\gamma$ -phosphate group of adenosine triphosphate (ATP) to hydroxyl groups of protein or lipid substrates, a process called phosphorylation [1]. One example is fosdatidylinositol 4-kinase (PI4K) responsible for phosphorylation at the 4-position of the inositol ring, thus forming the phosphatidylinositol 4-phosphate (PI4P) which regulates processes such as apoptosis, metabolism, cell growth and proliferation [4]. Due to its importance in physiological processes, PI4K is also related to the development of several diseases such as viral infections, cancers and neurological diseases [4]. Therefore, the search of new ligands for this enzyme may be of great therapeutic value and may also help to better understand the mechanisms of action by which the enzyme works. One of the ways to search for new ligands is to use *in silico* methods, where one can study the aspects involved in ligand-receptor interactions in detail and thus obtain proposed drugs with greater therapeutic advantages.  $K_i$  or  $IC_{50}$  values are constants that relate to the affinity of compounds for enzymes or receptors, and they are related to the free energy of binding ( $\Delta G$ ), which can be evaluated with empirical models by correlation with a series of energy terms theoretically obtained. Calculated parameters can be subjected to a multiple linear regression analysis to generate a model to predict the free energy and, therefore, the affinity of the compounds [6]. Based on the studies of Keaney and coworkers [7] eleven PI4KIII $\beta$ -selective compounds (Figure 1) with  $IC_{50}$  ranging from 4 to 9727 nM were selected. All compounds had the energy minimized by the PM6 semi-empirical method after conformational analysis with the Spartan'16 program. The compounds were docked into the active site of the enzyme (crystallographic structure PDB: 4D0L) through the GOLD v. 5.5 program. The ChemPLP scoring function was used and the runs were made in triplicate, selecting the solutions with the best score. Calculations of the enthalpies of formation ( $\Delta H_f$ ) for complex, empty site and ligand were performed for each of the compounds with the PM7 semi-empirical method of the program MOPAC2016 and these data were used to obtain the interaction enthalpy ( $\Delta H_{interaction}$ ) by the following equation:

$$“\Delta H_{interaction} = \Delta H_f \text{ complex} - (\Delta H_f \text{ protein} + \Delta H_f \text{ ligand})”$$



Other information obtained included: the torsional energy ( $E_{tors.}$ ) with the GOLD program and the solvation energy ( $E_{solv.}$ ) with the Spartan'16 program. These parameters were combined in a multiple linear regression analysis by the OriginPro 2017 Student Version program to obtain a correlation function with the activity data ( $pIC_{50}$ ). It was possible to obtain an optimal correlation with an adjusted  $R^2$  of 0.895:

$$pIC_{50} = -0,05068\Delta H_{int.} + 0,36485E_{tors.} - 2,60214E_{solv.} - 0,04654E_{solv.}^2 + 32,84142$$

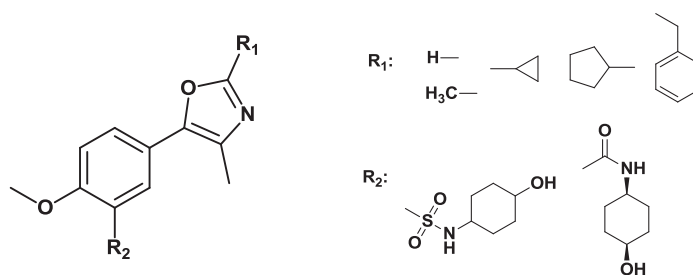


**Figure 1:** General structures of selected compounds

Given the good results obtained for this initial series of PI4KIII $\beta$ -selective compounds, new correlations involving a greater number of compounds and greater structural variability will be explored, seeking to obtain the most general activity prediction equation possible. This model will be useful to identify novel effective enzyme ligands in compound libraries and thus find new proposed PI4KIII $\beta$  inhibitors.

**Key-words:** PI4KIII $\beta$ , *In silico* methods, empirical binding free energy model.

**Support:** This work has been supported by CAPES, CNPq, FAPERJ and INCT-Inofar. The work was carried out in Laboratório de Avaliação e Síntese de Substâncias Bioativas (LASSBio) of the Federal University of Rio de Janeiro (UFRJ).

#### References:

- [1] AVILA, C. M. *et al. Revista Virtual de Química* **2010**, 2(1): 59-82.
- [2] GEHRMANN, T. *et al. European journal of biochemistry* **1998**, 253: 357-370.
- [3] BALLA, A. *et al. TRENDS in cell biology* **2006**, 16(7): 351-361.
- [4] BOURA, E. *et al. Experimental Cell Research* **2015**, 337: 136-145.
- [5] OLIVEIRA, F. G. *et al. Bioorganic & Medicinal Chemistry* **2006**, 14: 6001-601.
- [6] WANG, S. *et al. Journal of Medicinal Chemistry* **1994**, 37: 1326-1338.
- [7] KEANEY *et al. Bioorganic & Medicinal Chemistry Letters* **2014**, 24: 3714-3718.



## Analysis of charge, charge flux and dipole flux contributions for infrared intensities of the OH stretching mode in carboxylic acid dimers

Natieli A. da Silva<sup>a</sup> (PG), Roberto L. A. Haiduke<sup>a</sup> (PQ)

<sup>a</sup> Department of Chemistry and Molecular Physics, São Carlos Institute of Chemistry, USP, São Carlos, SP.  
natieli.iqsc@usp.br

The relevance of hydrogen bonds for chemical and biological systems motivates several experimental or theoretical studies on the nature of this type of interaction which governs not only the integrity of the genetic code of living beings, but also allows a variety of flat polycyclic aromatic molecules to intersect between the nitrogen bases of deoxyribonucleic acid (DNA) [1]. IUPAC defines hydrogen bonding as an "attractive interaction between a hydrogen atom of a molecule or a molecular fragment XH, where X is more electronegative than H, and an atom or group of atoms of the same or different molecules" [2]. This type of interaction can be represented simply by X-H ... Y, where X-H refers to the proton donor monomer and Y is the end of the acceptor unit where the interaction occurs.

The stretching of the X-H bond is usually the mode that shows larger intensity increments in the infrared spectra during the formation of hydrogen bonds when compared to the data of the respective isolated donor monomer. Thus, the partitioning of dipole moment derivatives in contributions of charge, charge flux and dipole flux (CCFDF), [3] from multipoles of the Quantum Theory of Atoms in Molecules (QTAIM), allows a deeper understanding of the reasons for the increase in infrared intensities of certain vibrational bands during the dimerization process of carboxylic acids.

All electronic structure calculations were performed in the *Gaussian 09* program [4] using the B2PLYP hybrid functional with the aug-cc-pVTZ base set. The QTAIM parameters of charge and atomic dipole were obtained with the AIMAll program [5] at the equilibrium positions of the atoms and in structures distorted by individual displacements of  $\pm 0.01$  Å along the three Cartesian axes. Finally, the infrared intensities were estimated by the CCFDF/QTAIM model using dipole moment derivatives in relation to the normal vibration coordinate.

The variations of infrared intensities for the analyzed vibrational modes can be understood in terms of dipole moment derivatives in relation to the normal mode of vibration (Equation 1) [6]. The contributions of charge, charge flux, dipole flux and the cross terms between these quantities can be visualized in Table 1.

$$A = \frac{N\pi}{3c^2} \left[ \left( \frac{\partial \bar{\mu}}{\partial Q_i} \right)_C^2 + \left( \frac{\partial \bar{\mu}}{\partial Q_i} \right)_{CF}^2 + \left( \frac{\partial \bar{\mu}}{\partial Q_i} \right)_{DF}^2 + 2 \left( \frac{\partial \bar{\mu}}{\partial Q_i} \right)_C \left( \frac{\partial \bar{\mu}}{\partial Q_i} \right)_{CF} + 2 \left( \frac{\partial \bar{\mu}}{\partial Q_i} \right)_C \left( \frac{\partial \bar{\mu}}{\partial Q_i} \right)_{DF} + 2 \left( \frac{\partial \bar{\mu}}{\partial Q_i} \right)_{CF} \left( \frac{\partial \bar{\mu}}{\partial Q_i} \right)_{DF} \right] \quad (1)$$

**Table 1:** Variations of charge (C), charge flux (CF), dipole flux (DF) contributions and cross terms for the

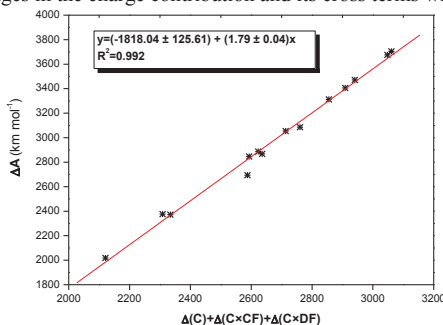
intensity,  $A$ , ( $\text{km mol}^{-1}$ ) of O-H stretching mode during dimerization according to the CCFDF/QTAIM model

System	$\Delta A^C$	$\Delta A^{CF}$	$\Delta A^{DF}$	$\Delta A^{C \times CF}$	$\Delta A^{C \times DF}$	$\Delta A^{CF \times DF}$	$\Delta A^a$
BrCOOH...BrCOOH	126.1	-159.0	59.3	2672.1	249.3	727.9	3675.9
ClCOOH...ClCOOH	127.2	-239.9	65.1	2450.9	276.9	632.6	3312.8
FCOOH...FCOOH	123.8	-405.1	80.3	1834.3	350.5	392.7	2376.6
HCOOH...HCOOH	90.0	-469.1	-32.9	2222.1	-191.3	399.1	2017.8
ClCOOH...BrCOOH	126.7	-207.4	61.9	2551.7	262.1	676.5	3471.4
ClCOOH...FCOOH	125.2	-337.5	74.1	2152.4	315.5	516.8	2846.6
ClCOOH...HCOOH	150.3	-382.1	48.7	2288.8	196.9	565.0	2867.6
BrCOOH...HCOOH	150.2	-344.6	48.5	2416.8	193.3	621.3	3085.4
FCOOH...BrCOOH	124.9	-299.2	69.1	2293.2	294.8	571.3	3054.1
FCOOH...HCOOH	144.8	-458.3	50.6	1972.6	216.7	445.3	2371.8
CH <sub>3</sub> COOH...BrCOOH	145.0	-117.4	37.8	2744.4	171.6	722.8	3704.2
CH <sub>3</sub> COOH...ClCOOH	132.6	-178.1	29.2	2630.3	146.1	646.0	3406.1
CH <sub>3</sub> COOH...FCOOH	144.2	-322.7	44.6	2265.9	212.8	541.5	2886.3
CH <sub>3</sub> COOH...HCOOH	177.6	-417.9	37.2	2361.3	48.7	487.5	2694.5

$$^a \Delta A = \left[ (A_{O-H}(s) + A_{O-H}(as))_{Dimer} - (A_{O-H}(a) + A_{O-H}(b))_{Monomer} \right]$$

The dimerization process results in an expressive increment in infrared intensities of the O-H stretching. The main factor responsible for these changes in intensities after the formation of the two hydrogen bonds is the charge variation of each atom during dimerization along with changes in the cross term between charge and fluxes of charge and atomic dipole (Figure 1).

**Figure 1:** Variations of the infrared intensity of the O-H stretching modes during dimerization as a function of the sum of changes in the charge contribution and its cross terms with charge and dipole fluxes



**Key-words:** hydrogen bonds, carboxylic acids, infrared intensity and CCFDF model.

**Support:** CAPES and FAPESP (2010/18743-1 and 2014/23714-1).

#### References:

- [1] S. Schneider, C. Kern, *J. Am. Chem. Soc.*, 101, 4081 (1978).
- [2] E. Arunan, *et al.*, *Pure App. Chem.*, 83, 1637 (2011).
- [3] R. L. A. Haiduke, R. E. Bruns, *J. Phys. Chem. A*, 109, 2680 (2005).
- [4] M. J. Frisch, *et al.*, *Gaussian 09*, Revision D02, Gaussian Inc. Wallingford CT (2009).
- [5] T. A. Keith, *AIMAll (Version 16.11.09)*, TK Gristmill Software, Overland Park KS, USA (2013), aim.tkgristmill.com.
- [6] A. F. Silva, *et al.* *J. Phys. Chem. A*, 116, 8238 (2012).

## Brønsted Acid Catalyzed O- to N-Alkyl Migratory Rearrangement in Pyridine

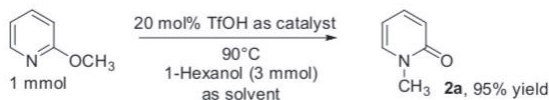
Nelson H. Morgon<sup>a</sup>, Aguinaldo R. de Souza<sup>b</sup>, Abhishek K. Mishra<sup>c</sup>, Srijit Biswas<sup>c</sup>

<sup>a</sup>Universidade Estadual de Campinas, Instituto de Química, Campinas, SP, Brazil

<sup>b</sup>Universidade Estadual Paulista, Departamento de Química, Bauru, SP, Brazil

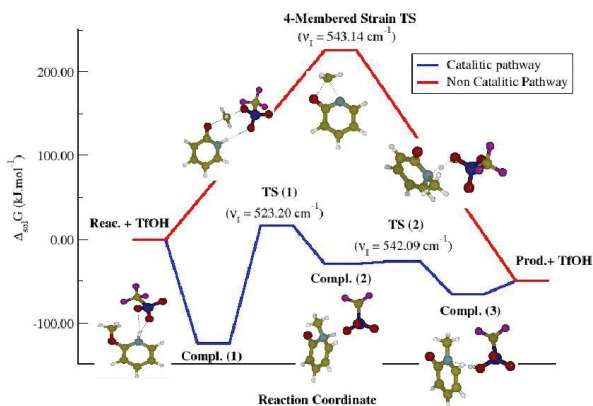
<sup>c</sup>Centre of Biomedical Research (CBMR), SGPGIMS Campus, Raebareli Rd, Lucknow 226014, Uttar Pradesh, India

**Abstract:** The reaction Brønsted acid catalyzed O- to N-alkyl migratory rearrangement in pyridine (Fig. 1) is consistent to the research interest to develop metal and ligand free methods to reduce environmental impact and increase atom efficiency. In this reaction also the generated substituted pyridones are a very important core structures found in various bio-active natural products. It is known Brønsted acid having O=X-OH moiety can act as bifunctional catalyst and can simultaneously activate two reactive centres in a unique way via a cyclic transition state[1].

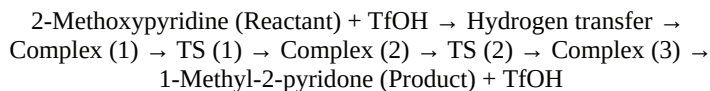


TfOH = Trifluoromethanesulphonic acid

Electronic and molecular structures of compounds originated from the reaction Brønsted acid catalyzed O- to N-alkyl migratory rearrangement in pyridine were theoretically investigated through theoretical calculation. These calculations were performed using DFT employing the hybrid exchange-correlation functional B3LYP. Geometry optimizations and evaluation of harmonic frequencies were performed at the B3LYP/6-311++G(2d,p). The optimized structures were confirmed to be minima by vibrational frequency analysis. The single point energy calculations were carried out at B3LYP/6-311++G(3df,2p) level on corresponding optimized geometries. Solvent effects are included using the SMD Solvation Model. All computations were performed using the Gaussian 09, Revision D.01 package[2]. The non-catalytic is an unfavourable pathway. The reaction may be proceeding through the following mechanism involving two transition states - TS (1) and TS(2) (Fig. 2).



The full mechanism displayed at Fig.2 is:



**Key-words:** 2-Methoxypyridine, 1-Methyl-2-pyridone, B3LYP, SMD

**Support:** The authors gratefully acknowledge financial supports from FAPESP and CNPq (Brazilian Science Funding Agencies) as well as the computational facilities of GridUNESP. SB also acknowledge the financial supports from DST (INSPIRE Faculty Award) for the experimental works.

#### References:

- [1] A. K. Mishra, S. Biswas, J. of Org. Chem. 81(6), 2355 (2016).
- [2] <http://www.gaussian.com>



## Computational Study of Glycine and its Radical Cation and Contributions to the Interstellar Chemistry

Neubi F. Xavier Junior<sup>1</sup>, Leonardo Baptista<sup>2</sup>, Glauco F. Bauerfeldt<sup>1</sup>

<sup>1</sup>*Departamento de Química, Instituto de Ciências Exatas, Universidade Federal Rural do Rio de Janeiro, Rodovia Br km 7, Seropédica, RJ, Brasil*

<sup>2</sup>*Departamento de Química e Ambiental, Faculdade de Tecnologia, Universidade do Estado do Rio de Janeiro, Rodovia Presidente Dutra Km 298 – RJ, Brazil*

**Abstract:** Glycine is mostly present in interstellar medium (ISM) in solid phase, covered by a ice mantle. But, subjected to some high energy phenomena of the hostile ISM, glycine can undergo to gas phase.<sup>1</sup> This hypothesis is corroborated since the fragments associated to this amino acid decomposition are frequently encountered in space, even though molecule itself is hardly found in gas phase.<sup>2</sup> This work aims to the understanding of the chemical behavior of glycine in the ISM. Specifically, a kinetic study of glycine decomposition is undergone in order to bring some answers to its formation and decomposition channels and to the possibility of its survival in the ISM, in its way to Earth. All calculations including geometry optimizations, vibrational frequencies and reaction paths, have been performed at the B3LYP/6-311++G(2d,2p) level and additional single point calculations at the CCSD(T)/6-311++G(2d,2p)//B3LYP/6-311++G(2d,2p) level have been performed in order to improve the electronic energies. A detailed study of the structures and reactivity of glycine as an isolated system is performed. Moreover, considering that glycine can also be ionized due to the impact with high-energy photons and particles, similar work has been performed for the radical cation. A conformational analysis of glycine in its neutral and radical cations forms reveals a spectrum of eight and four conformers of glycine and glycine radical cation, respectively. The conformers were characterized according to the dihedral angles and this nomenclature scheme of the conformers is suggested. The population analysis suggests that the lowest energy conformer prevails over all other conformers (~100% to 75%, neutral form, from 50 to 300 K and ~100% to 95%, radical cation form, from 50 to 300K). An interconversion scheme was proposed and rate coefficients were calculated. The calculated ionization energy, 9.0 eV, is in very good agreement with the experimental determinations (8.8 – 9.3 eV). Saddle points have been located for the deamination and decarboxylation reaction of the neutral form and decarboxylation of the radical cation and reaction paths have been calculated adopting the IRC algorithm. Dissociation reactions have also been explored using modified Morse Potentials. Among dissociations and decomposition reactions, the deamination reaction is the dominant channel for the neutral form, with a barrier height of 44.76 kcal/mol and the dissociation that leads to HOCO and (CH<sub>2</sub>NH<sub>2</sub>)<sup>+</sup> products was the most favored radical cation unimolecular reaction, with a dissociation limit of 53.04 kcal/mol. In this work, it was proposed that high energy phenomena can make solid phase glycine undergo to gas phase glycine in neutral and cation radical form, in



fundamental state and neutral form in excited state. With the data reported in this work and a possible study of glycine in excited state, we can finally understand the role of glycine in the ISM and the possible paths leading to its formation and decomposition in primitive Earth.

**Key-words:** amino acids, astrochemistry, chemical kinetics, glycine, B3LYP, DFT

**Support:** UFRRJ and CAPES

**References:**

- [1] S. Pilling, L. Mendes, V. Bordalo *et al*, *Astrobiology*, 13, 79-91 (2013).
- [2] A. Pernet, J. Pilmé, F. Pauzat *et al*, *Astronomy & Astrophysics*, 552 (2013).



# Variational Transition State Theory Calculations of the Hydrogen Abstraction Reactions $O(^3P) + cis\text{-CH}_3\text{OCHO}$ : Effects of Multidimensional Tunneling on the Rate constants and Branching Ratio

E. F. V. de Carvalho<sup>1</sup>, O. Roberto-Neto<sup>2</sup>

<sup>1</sup>*Departamento de Física, Universidade Federal do Maranhão, São Luís, 65085-580, Maranhão, Brazil*

<sup>2</sup>*Divisão de Aerotermodinâmica e Hipersônica, Instituto de Estudos Avançados, São José dos Campos, 12228-001, São Paulo, Brazil*

**Abstract:** Thermal rate constants and product branching ratio of hydrogen abstraction from *cis*-CH<sub>3</sub>OCHO by O(<sup>3</sup>P) giving as products CH<sub>3</sub>OCO + OH (R1) and CH<sub>2</sub>OCHO + OH (R2) [1] were computed with variational transition state theory including microcanonically optimized multidimensional tunneling. The dynamics calculations include anharmonicity and hindered rotational corrections for the torsion around the C–O bond in methyl formate. Benchmark calculations of barrier heights and the reaction energetic have been carried out by coupled cluster theory with extrapolation to the complete basis set (CBS) limit method [2] using various basis sets. CBS/D-T results for enthalpy of reaction at 0 K for R1 (–3.1 kcal/mol) and R2 (–2.7 kcal/mol) are in good agreement with the values obtained through the Hess' law a 298 K, i.e. –2.61 and –1.81. At 298 K, the calculated value of the rate constant with the CVT/μOMT method is  $8.1 \times 10^{-15} \text{ cm}^3 \text{ molecule}^{-1} \text{ s}^{-1}$  which agrees well with the single-temperature discharge-flow measurement value of  $9.3 \times 10^{-15} \text{ cm}^3 \text{ molecule}^{-1} \text{ s}^{-1}$  [3]. The branching ratio predict by the present work shows that the formation of CH<sub>3</sub>OCO + OH (R1) reaction path is the dominant reaction path from 200 to 1300 K.

**Key-words:** methyl formate; hydrogen abstraction; M06-2X, CCSD(T), rate constants  
**Support:** This work has been supported by FAPEMA, CNPq.

## References:

- [1] S. Dooley, M. P. Burke, M. Chaos, Y. Stein, F. L. Dyer, V. P. Zhukov, O. Finch, J. M. Simmie, H. J. Curran, *Int. J. Chem. Kinet.* 42, 527 (2010).
- [2] J. M. L. Martin, P. R. Taylor, *Chem. Phys. Lett.* 248, 336 (1996).
- [3] S. Mori, *Bull. Inst. Chem. Res.* 59, 116 (1981).

## Theoretical study of hydration free energy of the $C_{60}$ , $Li^+@C_{60}$ , $Na^+@C_{60}$ and $K^+@C_{60}$

Osmair Vital de Oliveira

*Instituto Federal de Educação, Ciência e Tecnologia de São Paulo – câmpus Catanduva*

**Abstract:** Fullerene ( $C_{60}$ ) and endofullerene (a chemical specie trapped into  $C_{60}$ ) are a molecule class largely explored to be used in chemical, medicine, biology, and others. Although the fullerene has been known since 1985, its solvation process in water is not clear in the literature. For example, there is not a consensus if the hydration free energy ( $\Delta G_{\text{hyd}}$ ) of the  $C_{60}$  is less or greater than zero. Therefore, in the present work, molecular dynamics (MD) technique was used to study the solvation process of the  $C_{60}$  and it complexed with the  $Li^+$ ,  $Na^+$  and  $K^+$  ions, with goal to improve its solubility. All simulations were performed in the GROMACS 5.0.7 package [1]. The Lennard-Jones parameter developed by Girifalco [2] was used for  $C_{60}$ , the electrostatic parameters (charge) of the endofullerenes (ions@ $C_{60}$ ) were obtained in previous work [3] using DFT/B3LYP/6-31G(2d,2p), and water solvent was described by the SPC model. The hydration free energies were calculated using the thermodynamic integration (TI) method. The structural analysis along 5 ns of MD simulations show that the ions trapped on  $C_{60}$  does not alters the overall solvation process, and the local structure of water molecules around the solute is preserved. The following  $\Delta G_{\text{hyd}}$  values were obtained:  $C_{60}$  (-32.5) >  $Li^+@C_{60}$  (-132.0) >  $K^+@C_{60}$  (-136.0) >  $Na^+@C_{60}$  (-143.0  $\text{kJ}\cdot\text{mol}^{-1}$ ). Our  $\Delta G_{\text{hyd}}$  value of the  $C_{60}$  agree reasonably with theoretical calculations (-36.6  $\text{kJ}\cdot\text{mol}^{-1}$ ) [4] and with experimental data (-24.45  $\text{kJ}\cdot\text{mol}^{-1}$ ) estimated by Luzhkov [5]. For all endofullerenes, our  $\Delta G_{\text{hyd}}$  values are in agreement with B3LYP/LANL2DZ/PCM calculations [6]. Overall, the present results can contribute to understand the solvation process of  $C_{60}$  and endofullerenes ions@ $C_{60}$ .

**Key-words:** hydration free energy, endofullerene, molecular dynamics simulation

**Support:** This work has been supported by IFSP-Catanduva

### References:

- [1] H.J.C. Berendsen, D. van der Spoel, R. Drunen, *Comp. Phys. Comm.* 91, 43 (1995).
- [2] L.A. Girifalco, *J. Phys. Chem.* 96, 858 (1992).
- [3] O.V. Oliveira, A.S. Gonçalves, *Comp. Chem.* 2, 51 (2014).
- [4] A. Muthukrishnan, M.V. Sangaranarayanan, *Chem. Phys.* 331, 200, (2007).
- [5] V.B. Luzhkov, V.M. Volokhov, G.A. Pokatovich, *Chem. Phys. Lett.* 676, 95 (2017).
- [6] T. Yu. Dolinina, N.S. Rusova, V.B. Luzhkov, *Russ. Chem. Bul.* 3, 400 (2011).

## Theoretical Study of HCO + O Reactions

Patricia R P Barreto<sup>1</sup>, Henrique O Euclides<sup>1</sup>, Ana Claudia PS Cruz<sup>1</sup>,  
Alessandra F Albernaz<sup>2</sup>, Washington B da Silva<sup>3</sup>, Eberth Correa<sup>4</sup>

<sup>1</sup>Laboratório Associado de Plasma, Instituto Nacional de Pesquisas Espaciais, CP515,  
São José dos Campos, SP, CEP 12247-970

<sup>3</sup>Instituto de Física, Universidade Brasília, CP04455, Brasília, DF, CEP 70919-970

<sup>3</sup>Instituto Federal de Brasília, Campus Ceilândia, Ceilândia, DF, CEP 72220-260

<sup>4</sup>Universidade de Brasília, Campus do Gama, Gama, DF, CEP 72444-240, Brasil

**Abstract:** The HCO species is important in combustion, atmospheric chemistry and planetary science, but to our acknowledgments there is not results regards the reaction HCO + O. There is extensively studied by both experimental and theoretical on CO + OH = CO<sub>2</sub> + H [1,2] reaction and few studies of CH + O<sub>2</sub> = CO<sub>2</sub> + H and CH + O<sub>2</sub> = CO + OH, with the O<sub>2</sub> in the triplet ground state [3]. In this work, we present a complete potential energy surface (PES) for reaction HCO + O with different products, as:



and also, for reactions:

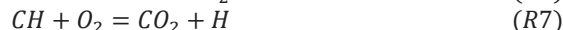


Figure 1 present the complete PES for the HCO+O reaction.

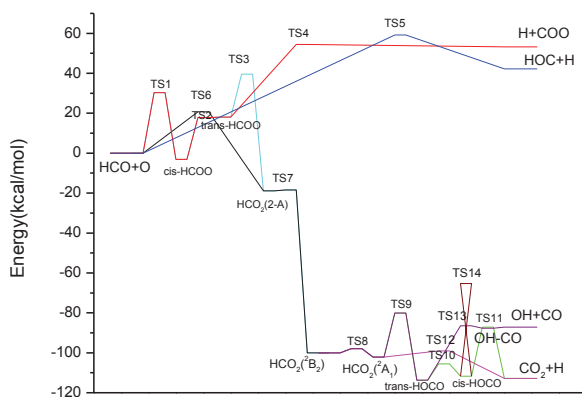


Figure 1: Complete PES for the HCO+O reaction

Figure 2 present the PES for the CO + OH and CH+O<sub>2</sub> reaction.

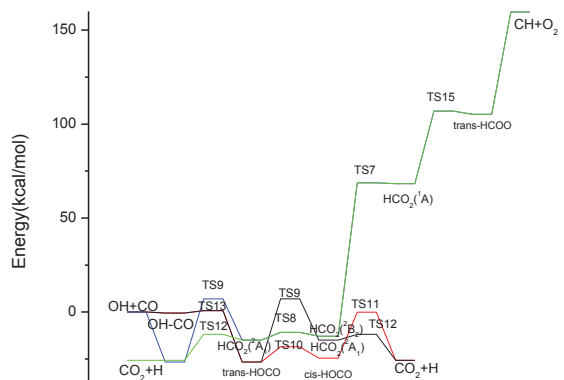


Figure 2: Complete PES for the CO+OH and CH+O<sub>2</sub> reaction

Fifteen transition state were determined and the rate constant were calculated using transition state theory and master equation software package MESMER [4], at low pressure written in the Arrhenius and alternatives forms.

The CBS-QB3 Method, in Gaussian 09 program, was employed to optimize the geometries, vibrational frequencies and energies of the reactant, intermediate complexes, transition states, and products of the H + HCO, CO+OH and CH+O<sub>2</sub> reactive process. To confirm that the transition state really connects to designated intermediates along the reaction path, the intrinsic reaction coordinate (IRC) calculations were performed. Also the IRC calculations were used to confirm the connection between the designated transition states and the reactants or products.

**Key-words:** Mesmer, reaction rate, H+HCO

**Support:** This work has been supported by CAPES and CNPq.

**References:**

- [1] T. L. Nguyen, B.C. Xue, R. E. Weston, Jr., J. R. Barker, J. F. Stanton, J. Phys. Chem. Lett. 3, 1549 (2012).
- [2] X. Song, J. Li, H. Hou, B. Wang, J. Chem. Phys. 125, 094301 (2006).
- [3] M.-B. Huang, B.-Z. Chen, Z.-X. Wang, J. Phys. Chem. A 106, 5490 (2002)..
- [4] D. R. Glowacki, C.-H. Liang, C. Morley, M. J. Pilling, S. H. Robertson, J. Phys. Chem. A 116 (2012) 9545.

## Activation of polar bonds by electric fields: An Electron Localization Perspective

Authors: Paúl Pozo<sup>1</sup>, Luis Rincón<sup>1,2</sup>, F. Javier Torres<sup>1,2</sup>

<sup>1</sup>Universidad San Francisco de Quito (USFQ), Grupo de Química Computacional y Teórica (QCT – USFQ), Dpto. de Ingeniería Química, Quito 17-1200-841, Ecuador.

<sup>2</sup>Universidad San Francisco de Quito, Instituto de Simulación Computacional (ISC-USFQ), Diego de Robles y Vía Interoceánica, Quito 17-1200-841, Ecuador.

**Abstract:** The electron localization induced by an external electric field is evaluated using the information content of the same-spin conditional pair density [1]. In this work we consider the stretching of the C-X (X: halogen) bonds of methyl halide molecules, under the experience of a homogeneous static electric field and a static heterogeneous one, created by a source of point charges. In addition, in order to assess the importance of ionic structures throughout the chemical bond breaking, we project the Generalize Valence Bond (GVB) wave-function in their classical covalent and ionic structures (see for instance [2]). The increase of electric fields, is expected to have a reorganization of the electrons when the bond is subjected under a strong enough field. These general observations are thoroughly explained using a simple Valence Bond model that involve the increment of the resonance energy between the covalent and the ionic structures and the curve crossing between the two structures after some field strength.

**Key-words:** Valence Bond Theory, External Electric Fields, Electron Localization, Methyl Halide Bonds.

**Support:** This work has been performed by employing the resources of the USFQ's High Performance Computing system (HPC-USFQ). The authors would like to thank USFQ's Chancellor Grants and PolyGrants programs for financial support.

**References:**

- [1] A. Urbina, F.J. Torres, L. Rincón, "The electron localization as the information content of the conditional pair density", *J. Chemical Physics*, 144 (2016).
- [2] L. Rincón, J. Mora, F.J. Torres, R. Almeida "On the activation of  $\sigma$ -bonds by electric fields: A Valence Bond perspective", *J. Chemical Physics*, 477 (2016).

## Theoretical Investigation of the Oxidation Reactions of Primary Alcohols to Aldehydes using *o*-iodoxybenzoic acid Reagent.

Paula do Nascimento Goulart, Glauco Favilla Bauerfeldt, Arthur Eugen Kummerle,

Renata Barbosa Lacerda

Rodovia BR 465, Km 07, s/n - Zona Rural, Seropédica - RJ, 23890-000

IBX (*o*-iodoxybenzoic acid) has gained popularity as a soft oxidant for the conversion of alcohols to aldehydes or ketones [1]. According to the literature, IBX promotes the oxidation of certain aliphatic primary alcohols to the corresponding aldehydes with excellent yield, but when this reaction is applied to aromatic alcohols, the oxidation product is a carboxylic acid [2]. Because of these differences, it is desired to study the oxidation reactions of some alcohols, evaluating the effect of the substituent group change in the proposed routes for the reaction mechanism. For this study, the GAUSSIAN software was used with the aid of the GaussView program through the semi-empirical method PM6 for calculations of geometry optimization, obtaining transition states and evaluation of the reaction paths. Therefore, in this work, a mechanism is proposed, considering the electron transfers, in two steps, as shown in figures 1 and 2 below. From the calculated data from theoretical study of this reaction, we expected to comprehend the different yields obtained for these oxidations, as well as to suggest the most probable product. Experiments show that the oxidation reactions of most of the investigated alcohols converts to the corresponding carbonyl compound with yields greater than 90%, besides presenting the product free of impurities and a good insulation. However, exceptions are noted with respect to some aromatic compounds, which showed oxidation to the corresponding carboxylic compound under similar reaction conditions[3]. Table 1 shows that the oxidation reactions of the primary alcohols are thermodynamically allowed taking into account the different radicals proposed.



Figure 1-Mechanism for the first step.

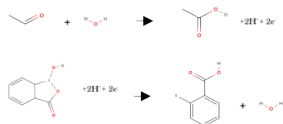


Figure 2- Mechanism for the second step.

Table 1 Variation of the free energy for the reaction of each alcohol being oxidized to its aldehyde, step 1 of the proposed mechanism.

R(-CH <sub>2</sub> OH)	ΔGr <sub>1</sub> (kcal/mol)
benzila	-94,66
Etila(-C <sub>2</sub> H <sub>5</sub> )	-92,62
Metila(-CH <sub>3</sub> )	-92,65
Etilfmoc(-C <sub>2</sub> H <sub>4</sub> O <sub>2</sub> Cl)	-104,82
fenil	-91,46
propfenil	-83,03
ftalimidanitrom	-92,41
ftalimidanitroo	-91,40
ftalimidametoxim	-91,88
ftalimidametoxio	-93,06
ftalimida	-83,86
ftalato	-91,63



It can be observed, for the saddle point of the first stage, that the alcohol oncoming occurs through the interaction between the isolated pair of electrons of oxygen and iodine, making the latter hypervalent. There is also the transfer of a proton to the hydroxyl group of the ibx, causing the departure of a water molecule. An optimized structure was obtained as a pre-barrier intermediate. In this intermediate, the hypervalence of the iodine atom is observed. A transition state was also obtained for the first stage of the mechanism. The chart below, in figure 3, illustrates such results that have been achieved so far.

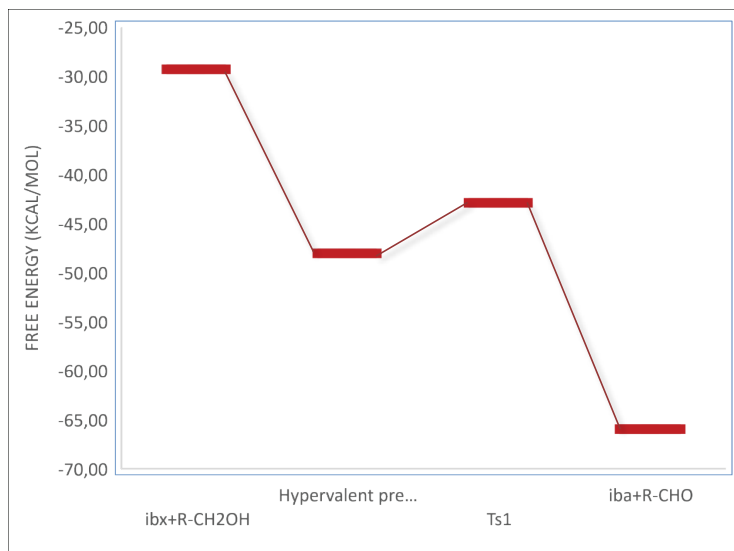


Figure 3-Free energy surface for the first stage of the proposed reaction mechanism.

It is also desired to investigate the transition states obtained from the optimization of structures, considering the assistance of an explicit water molecule in the system studied, since it is suspected that this explicit solvent molecule is important for the system and that, from of it, the reaction progresses towards the proposed mechanism.

**Key-words:** oxidations, ibx, hypervalent, PM6

**Support:** This work has been supported by CAPES

**References:**

- [1] Frigerio, M.; Santagostino, M. *Tetrahedron Lett.* 1994, 35
- [2] Julius T. Su and William A. Goddard III *J. AM. CHEM. SOC.* 2005, 127
- [3] Leonard, N. J.; Carraway, K. L. *J. Heterocycl. Chem.* 1966, 3, 485



## Excited-State Intramolecular Proton Transfer in triphenylimidazolic compounds

Authors: Fabricio Carvalho, Fernando H. Bartoloni, Paula Homem-de-Mello

Address: Universidade Federal do ABC, Santo André, SP

**Abstract:** The excited state intramolecular proton transfer (ESIPT) of compounds derived from triphenylimidazole was investigated based on the density functional theory (DFT). Structural parameters, as bonds and angles in the fundamental and excited states, potential energy surfaces for the proton transfer, as well as, IR and UV-vis spectra and correlated electronic properties have been obtained. For compounds with electron donor substituents character, the intramolecular hydrogen bond is strengthened in the excited state and the opposite effect is observed for compounds that have electron withdrawing substituents. This observation is confirmed by -OH stretching bands in vibrational spectra. From the analysis of the electronic spectra it can be seen that the effects of the substituents clearly affect the electronic density of the compounds in the excited state S1. The analysis of the atomic charges was fundamental to understand how the proton transfer process occurs in the excited state: in the ground state, the oxygen atom is more negative than the imidazole nitrogen atom, while, in the excited state S1, the oxygen atom becomes less negative and the nitrogen atom becomes more negative, which favors the proton transfer. The potential energy surfaces for the proton transfer were calculated for the fundamental and excited states. There is no energy barrier in the excited state for some compounds, and a very low barrier for others. However, for the compounds with withdrawing substituents, the barriers to the proton transfer become larger.

**Key-words:** proton transfer, excited state, DFT, triphenylimidazole.

**Support:** This work has been supported by CAPES, CNPq and FAPESP.

### References:

- [1] Zhao, G.-J.; Han, K.-L. *Biophys. J.* 94, 38 (2008).
- [2] Morales, A. R.; Schafer-Hales, K. J.; Yanez, C. O.; Bondar, M. V.; Przhonska, O. V.; Marcus, A. I.; Belfield, K. D. *ChemPhysChem* 10, 2073 (2009).
- [3] Zhao, G.-J.; Liu, J.-Y.; Zhou, L.-C.; Han, K.-L. *J. Phys. Chem. B* 111, 8940 (2007).

## Core-valence stockholder AIM analysis and its connection to non-adiabatic effects in small molecules [1]

Paulo H. R. Amaral and José R. Mohallem

*Laboratório de Átomos e Moléculas Especiais, Departamento de Física, ICEx,  
Universidade Federal de Minas Gerais,  
Av. Antonio Carlos 6627, Belo Horizonte, Minas Gerais, Brazil*

Non-adiabatic corrections to the rovibrational energy levels of light molecules are essential if we wish to make calculations that account to high resolution spectroscopy [2]. They should be added to the energies obtained from potential energy surfaces generated by highly accurate Born-Oppenheimer calculations, after adding Born-Oppenheimer diagonal corrections and relativistic corrections.

The non-adiabatic corrections are hardly obtained from exact calculations. Instead, they are evaluated as the difference between the energies obtained with the nuclear masses and with effective masses in the nuclear equation. We propose here a model to obtain the  $\mathbf{R}$ -dependent percentage of electrons that moves with the atomic nuclei during molecular vibration. For this, we invoke a previous theory of separation of motions of core and valence fractions of electrons in a molecule [3] and the concept of Atoms-in-Molecules (AIM) in the stockholder scheme [4]. We develop one-electron effective potentials which allow the identification of the parts of the AIM which move along with the nuclei. These electrons are called core electrons. In the nuclear equation, the reduced mass of the nuclei is then replaced by a mass that corresponds to the nucleus mass plus the core electron mass. With this recipe, we calculate the most accurate non-adiabatic corrections to vibrational energy levels so far for the apolar ( $\text{H}_2^+$ ,  $\text{H}_2$ ) and polar ( $\text{HeH}^+$ ,  $\text{LiH}$ ) molecules. This achievement can resume the discussion of the AIM being observable or not.

**Key-words:** Non-adiabatic corrections, AIM, molecular spectroscopy

**Support:** This work has been supported by CNPq and FAPEMIG

### References:

- [1] P. H. R. Amaral and J. R. Mohallem, *J. Chem. Phys.*, **146**, 194103 (2017).
- [2] P. R. Bunker and R. E. Moss, *Mol. Phys.*, **33**.
- [3] J. R. Mohallem, L. G. Diniz and A. S. Dutra, *Chem. Phys. Lett.*, **501**, 575 (2011).
- [4] P. Bultinck, C. Van Alseney, P. W. Ayers and R. Carbó-Dorca, *J. Chem. Phys.*, **126**, 144111 (2007).

## DFT study of water adsorption on (001) $\text{Mn}_3\text{O}_4$ surface

Paulo R. G. Gonçalves Jr, E. C. Santos, H. A. de Abreu, H. A. Duarte

*GPQIT, Departamento de Química □ ICEX, UFMG, 31.270-901, Belo Horizonte - MG*

**Abstract:** Hausmannite ( $\text{Mn}_3\text{O}_4$ ) is a material with normal spinel structure that presents the formula  $\text{A}^{2+}\text{B}_2^{3+}\text{O}_4$  where tetrahedral sites are occupied by the  $\text{Mn}^{2+}$  and the octahedral sites by  $\text{Mn}^{3+}$  cations. This oxide has tetragonal arrangement with space group  $I41/amd$ . In recent years, this material has attracted interest for applications in water treatment[1, 2]. The  $\text{Mn}_3\text{O}_4$  show polar surfaces, formally characterized by an unbalanced electrostatic potential, which gives rise to a dipole moment perpendicular to the surface. However, Kresse and co-workers [3] have shown that this formal instability is an artificial consequence of the simplified ionic model and can be removed by mechanisms involving changes near of the surface such as charge redistribution, reconstruction, and interactions with neighboring atoms. It has been reported that the cleavage of hausmannite[4, 5] leads indistinctly to the oriented plane (001). Nevertheless, a study of the formation of thin films of  $\text{Mn}_3\text{O}_4$  oriented in other crystallographic directions, such as the  $\text{SrTiO}_3$  substrate oriented surface (110) has also been reported[6]. In this sense, based on the optimized bulk structure, we tested several hausmannite slab models (figure 1) to compare the cleavage energies of different planes, and we investigated the adsorption of water molecules on the most stable surface calculated.

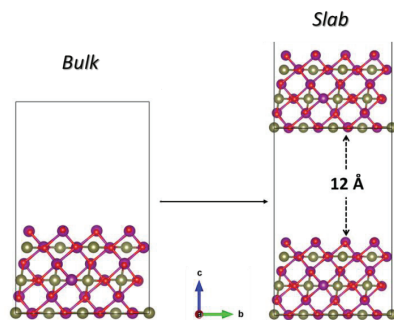


Figure 1. Slab models from the  $\text{Mn}_3\text{O}_4$  bulk.  $\text{Mn}^{2+}$  (green),  $\text{Mn}^{3+}$  (purple) and Oxygen (red).

The calculation of  $\text{Mn}_3\text{O}_4$  surfaces were investigated using DFT/planewaves and GGA/PBE functional as implemented in Quantum-ESPRESSO package. It was used a cutoff energy of 40 Ry,  $3 \times 3 \times 1$   $k$ -point mesh sampling based on the Monkhorst-Pack scheme,  $2 \times 2 \times 1$  supercell and  $12 \text{ \AA}$  vacuum layer were chosen for the slab calculation. After optimization of the surfaces, the values of surface and cleavage energies are presented in table 1.

Table 1. Cleavage and surface energies, surface area and coordination number of the different  $Mn_3O_4$  plane models.

Surfaces	$E_{cleavage}$ ( $J.m^{-2}$ )	$E_{surface}$ ( $J.m^{-2}$ )	Coordination number	
			$Mn^{2+}_{tetrahedral}$	$Mn^{3+}_{octahedral}$
<i>Bulk</i>	-	-	4	6
(001)	2.33	1.40	2	5
(100) = (010)	5.07	1.93	3	3
(101) = (011)	3.38	1.96	4	3, 4
(110)	6.49	1.85	1, 3	3
(111)	3.54	1.68	4	4, 5
(112)	3.14	1.78	4	4

According to our calculations, the surface (001) is the most favorable to cleave in comparison to the other simulated planes, being therefore the most stable surface of  $Mn_3O_4$ . This cleavage exposes the  $Mn^{+2}$ ,  $Mn^{+3}$  and  $O^{-2}$  ions asymmetrically. Based on this estimate, we studied the adsorption of water molecules on the surfaces (001), which presented 3 types: molecular, hydrogen bond interaction, and dissociative. The results indicated that water adsorption occurs dissociatively, with adsorption energy of about -28 kcal mol<sup>-1</sup>.

**Keywords:**  $Mn_3O_4$ , surfaces, DFT, planewaves, adsorption.

**Support:** This work has been supported by IFMA, FAPEMA, FAPEMIG and INCT-ACQUA.

#### References:

- [1] G.C. Silva, V.S.T. Ciminelli, A.M. Ferreira, N.C. Pissolati, P.R.P. Paiva and J.L. López, *Materials Research Bulletin*, 49 (2014) 544.
- [2] K. Babaeiveli, A.P. Khodadoust and D. Bogdan, *Journal of Environmental Science and Health, Part A*, 49 (2014) 1462.
- [3] G. Kresse, O. Dulub and U. Diebold, *Physical Review B*, 68 (2003) 245409.
- [4] V. Bayer, R. Podloucky, C. Franchini, F. Allegretti, B. Xu, G. Parteder, M.G. Ramsey, S. Surnev and F.P. Netzer, *Physical Review B*, 76 (2007) 165428.
- [5] W.Y. Li and Q.L. Chen, *Advanced Materials Research* 2012.
- [6] O.Y. Gorbenko, I.E. Graboy, V.A. Amelichev, A.A. Bosak, A.R. Kaul, B. Güttler, V.L. Svetchnikov and H.W. Zandbergen, *Solid State Communications*, 124 (2002) 15.

## ***Ab initio* Investigation of Layered Double Hydroxides with Intercalated Herbicides**

Pedro Ivo R. Moraes, Sérgio R. Tavares, Viviane S. Vaiss, Alexandre A. Leitão

*Departamento de Química, Universidade Federal de Juiz de Fora, Juiz de Fora, MG  
36036-330, Brazil*

**Abstract:** Layered double hydroxides (LDHs) or hydrotalcite-like compounds exist either as naturally occurring minerals or as synthesized materials by low-cost synthesis methods. LDHs consist of positively charged metal hydroxide layers having the composition  $[M^{2+}_{1-x} M^{3+}_x(OH)_2]^{x+}[A^{m-}_{x/m} \cdot nH_2O]$  where  $M^{2+}$  and  $M^{3+}$  are divalent and trivalent cations, respectively. The value of  $x$  is the molar fraction and can vary between 0.2 and 0.33, and  $A^{m-}$  is the interlayer anion [1]. The contamination of soils and ground water by pesticides is a consequence of their increasing use in modern agriculture. The contamination of ground and surface water reservoirs by acid pesticides is even higher, because their anionic form predominates under the pH conditions of the soil and of the water environments, thus being weakly retained in the soil [2]. All calculations were performed using the codes available in the Quantum-Espresso package [3], which implements the DFT [4] framework using a plane-wave bases set, periodic boundary conditions, and pseudopotentials. We used the generalized gradient approximation, GGA-PW91 [5] for the exchange-correlation (XC) functional, and Vanderbilt ultrasoft pseudopotentials [6] were also used to describe the ion cores. The investigated herbicides are 2,4D (2,4-dichlorophenoxyacetic acid) and MCPA (4-chloro-2-methylphenoxyacetic acid) intercalated in Mg-Al and Zn-Al LDH with  $x = 0.33$  for both. The supercells used for their constructions were  $(2\sqrt{3} \times 2\sqrt{3})R30^\circ$  [7], with each supercell having two intercalated herbicides in their anionic forms. The structures were fully optimized and their basal spacings calculated for [Mg-Al-2,4D], [Mg-Al-MCPA], [Zn-Al-2,4-D] and [Zn-Al-MCPA] were 19.10 Å, 19.20 Å, 19.00 Å and 19.08 Å, respectively. These results present a good agreement with the experimental values [8-9]. The electronic density difference plots were made for the LDHs in order to study the interactions between the layers, the anions, and the hydration water molecules. We can see a strong interaction between the anion carboxyl group and the layer hydroxyl groups, and also with the water molecules. We can also observe the interaction between the layer hydroxyl groups and the water molecules. The interactions between the interlayer anions are weak. The projected density of states (pDOS) shows that, for each structure, the basic site is the intercalated anion. The Bader analysis was also performed to verify the atomic charge distribution in the LDH structure. The anion has the same charge in each structure, while the charge is different in the layer for Mg (1.75  $e$ ) and Zn (1.36  $e$ ). The Bader charges of the layer oxygen atoms were also distinct for the Mg-Al



layer and for the Zn-Al layer, being  $-1.95 e$  and  $-1.82 e$ , respectively. This work is still under development.

**Key-words:** Layered Double Hydroxides, LDH, Herbicide, DFT

**Support:** This work has been supported by the Brazilian agencies CAPES, CNPq and FAPEMIG, Brazilian agencies and the enterprise Petrobras S/A (CENPES). We also thank the CENAPAD-SP computational center for the use of its facilities.

**References:**

- [1] F. Cavani, F. Trifirò, A. Vaccari, *Catalysis Today*, 11, 173 (1991).
- [2] R. Celis, M. C. Hermosín, L. Cox, J. Cornejo, *Environ. Sci. Technol.*, 33, 1200 (1990).
- [3] P. Giannozzi, et al, *J. Phys.: Condens. Matter*, 21, 395502 (2009).
- [4] P. Hohenberg, W. Kohn, *Phys. Rev.*, 136, 864B (1964).
- [5] J. P. Perdew, Y. Wang, *Phys. Rev. B: Condens. Matter Mater. Phys.*, 45, 13244 (1992).
- [6] D. Vanderbilt, *Phys. Rev. B: Condens. Matter Mater. Phys.*, 41, 7892 (1990).
- [7] D. G. Costa, et al, *J. Phys. Chem. C*, 114, 14133 (2010).
- [8] L. P. Cardoso, R. Celis, J. Cornejo, J. V. Valim, *J. Agric. Food Chem.* 54, 5968 (2006).
- [9] M. Lakraimi, et al, *J. Mater. Chem.*, 10, 1007 (2000).



## 2D, 3D and Hybrid QSAR Studies for a Set of 3-Benzyl-(arylmethylene)furan-2(5H)-ones and Their Herbicide Activity

Authors: Pedro Oliveira Mariz de Carvalho, Márcia Miguel Castro Ferreira.

Address: Institute of Chemistry, State University of Campinas, Brazil.

**Abstract:** Agriculture is one of the main sources of food for the population. Pest control is important for high crop efficiency and, nowadays, it is done mainly by the application of synthetic pesticides. However, continuous use of pesticides with the same mechanism of action induces the adaptation of pests, which acquire resistance. Moreover, environmental concern increased over the years, leading to stringent regulation of pesticide use.[1,2] Therefore, the research for novel synthetic pesticides is essential for food production. QSAR study is an important tool on the research of biochemical processes, such as pesticides' action, because it is able to extract valuable information from experimental data. The objective of this work is: to use herbicide activity of a set of 34 nostoclode analogues (Image 1), which act into the photosystem II, to build QSAR

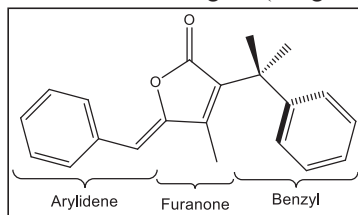


Image 1 – Nostoclode analogue.

models; then, to interpret the obtained models aiming for a better understanding of the ligand-receptor interactions between the photosystem II and these analogues. The substitutions are located on the arylidene group and the herbicide activity used were percentage of inhibition of the photosynthesis process ranging from 5.0 to 57.8% with mean value of 23.9%.[2] The structures were optimized, starting from crystallographic data, using

Gaussian 09 at B3LYP/Def2-TZVPP level. For the 2D-QSAR study, several molecular descriptors (energies, gap, dipole moment, polarizability, charges and molecular coefficients) were calculated using Gaussian 09. The descriptors were selected firstly by excluding those presenting low correlation with the biological activity, then by building PLS models and looking for good statistical results (RMSECV,  $R^2$ ,  $Q^2$ , regression vector etc.) in Pirouette software. For the 3D-QSAR study, the structures were converted to topology files using Topolbuild-1.3 (GAFF force field), and were aligned in a grid. The molecular descriptors were Coulomb and Lennard-Jones potential energies calculated by the  $\text{NH}_3^+$  probe in each grid point (1 Å increment). Variable selection was carried out in three steps: (1) using Comparative Distribution Detection Algorithm (CDDA) in MATLAB; (2) by using OPS algorithm in QSAR Modeling; (3) by building PLS models and looking for good statistical results. For the hybrid QSAR study, the final molecular descriptors from the 2D and 3D QSAR models were merged and a new variable selection was carried out. The number of latent variables in PLS models were determined by leave-one-out cross-validation. One inactive compounds (inhibition lower than 5%) and four



others presented atypical behavior in all models. The statistics produced by all generated models are presented below. They were also validated according to their robustness and chance correlation by using the leave-N-out and y-randomization tests.[1,3]

2D-QSAR: n = 29; descriptors = 6; latent variables: 1 (LV1: 53.8%); RMSEC = 8.8105%;  $R^2 = 0.7353$ ; RMSECV = 9.4110%;  $Q^2 = 0.6756$ .

3D-QSAR: n = 29; descriptors = 7; latent variables: 2 (LV1: 40.5%; LV2: 27.5%); RMSEC = 8.2149%;  $R^2 = 0.7784$ ; RMSECV = 9.3189%;  $Q^2 = 0.6820$ .

Hybrid-QSAR: n=29; descriptors = 7; latent variables: 2 (LV1: 43.3%; LV2: 25.9%); RMSEC = 7.2378%;  $R^2 = 0.8280$ ; RMSECV = 8.0807%;  $Q^2 = 0.7609$ .

A preliminary comparison among the models shows that the 2D and 3D QSAR models were statistically similar (3D slightly better than 2D) and the hybrid-QSAR model presented better correlations and lower errors than the other two.[3] The 2D atomic partial charge descriptors showed the importance of the benzyl ring, even though no substituents are located on it. This observation alongside with the photosystem II active site and the results from literature support the possibility of a ligand-receptor interaction by  $\pi$ -stacking between the benzyl group and a residue's aromatic ring.[4,5] The other 2D descriptors indicated important interactions involving the carbonyl group in the furanone ring, which is a good hydrogen bond acceptor, and the arylidene ring, where the substituents are located. The 3D descriptors showed similar interactions, emphasizing the results indicated by the 2D descriptors. However, the descriptors selected to build the hybrid-QSAR model showed that the 2D descriptors were better to describe the benzyl ring interactions, whilst the 3D descriptors were better to describe the other groups of the nostoclide analogues. Therefore, the 2D and 3D descriptors indicated similar results for the herbicide activity of these analogues, but it was possible to achieve better statistics when using them together, in the hybrid-QSAR model. Furthermore, the analysis of the descriptors used in the QSAR models indicated importance of the interactions involving, mainly, the benzyl aromatic ring and, secondarily, the carbonyl of the furanone ring and the substituents of the arylidene ring.[1]

**Key-words:** 2D-QSAR, 3D-QSAR, Quantum Chemistry, PLS regression, Herbicides.

**Support:** CNPq, FAPESP.

**References:**

- [1] P. O. M. de Carvalho, "Estudo da atividade praguicida de dois conjuntos de compostos com ação no fotossistema II" (Master's dissertation), 2017, Sistema de Bibliotecas da Unicamp, Campinas-SP, Brazil.
- [2] R. R. Teixeira *et al.*, J. Agric. Food Chem., 56, 2321-2329 (2008).
- [3] R. Kiralj, M. M. C. Ferreira, J. Braz. Chem. Soc., 20 (4), 770-787 (2009).
- [4] M. Suga *et al.*, Nature, 517, 99-103 (2015).
- [5] F. Breton *et al.*, "Mimicking the Plastoquinone-Binding Pocket of Photosystem II Using Molecularly Imprinted Polymers" in "Biotechnological Applications of Photosynthetic Proteins: Biochips, Biosensors and Biodevices", M. T. Giardi, E. V. Piletska, Springer US (2006), 155-165.



## Encapsulation process of *p*-Cymene into $\beta$ -Cyclodextrin: A Theoretical Study.

Pollyanna P. Maia (IC) and Clebio S. Nascimento Jr. (PQ)

*LQTC: Laboratório de Química Teórica e Computacional - Departamento de Ciências Naturais, Universidade Federal de São João del-Rei (UFSJ), Campus Dom Bosco, São João del-Rei, MG.*

*pollypmaia@hotmail.com*

**Abstract:** A theoretical study using semi-empirical (PM3) and DFT calculations (B97D) was performed in both gas and aqueous phases, in order to obtain structural and energetic properties for the encapsulation process of *p*-Cymene into  $\beta$ -cyclodextrin. Two modes of inclusion were assumed for the [*p*-Cym... $\beta$ -CD] *host-guest* complex: (i) Mode A, when the guest is placed in the hydrophobic cavity of the CD by the wider rim; (ii) Mode B, when the guest is included by the inner rim. As result, we have shown that Mode A complex is slightly more favorable than the Mode B. This fact can be explained by the inclusion depth of *p*-Cym which favors the rise of dispersive forces inside de host cavity.

**Key-words:** *p*-Cymene,  $\beta$ -cyclodextrin, *host-guest* complexes.

The *host-guest* complexes of bioactive molecules with cyclodextrins (CDs) have been extensively studied and utilized to improve their solubility, dissolution rate, and bioavailability of poorly water-soluble drugs [1]. CDs can increase the aqueous solubility, chemical reactivity, and spectral properties of numerous lipophilic drugs which are used as guest molecules, without changing their intrinsic ability to permeate lipophilic membranes. *p*-Cymene (*p*-Cym) is a naturally-occurring aromatic organic compound also named *p*-isopropyltoluene [2]. It is classified as a hydrocarbon related to a monoterpene and one of the main constituents of the essential oil from species of Protium, with more than 80% of these species found in the Amazon region. Besides, *p*-Cym is an important intermediate used in pharmaceutical industries and for the production of fungicides, pesticides, as flavoring agent. However, due to its lipophilic chemical structure, the *p*-Cym presents low solubility in many polar solvents, as water. In this sense, a new *p*-Cym/CD formulation may provide desirable pharmacokinetic and pharmacodynamics effects such as improvement of drug solubility. The formation of *host-guest* inclusion complexes involving *p*-Cym and CD has been studied experimentally [3]. However, in all of these works, no information about the topology of the complex and thermodynamic properties was provided. In this context, in the present work we carried out a theoretical study of the molecular inclusion process involving the *p*-Cym and  $\beta$ -CD. Our main goal was to understand, at the molecular level, the structural and energetic factors that influence the formation of such complex and its physicochemical properties. Semiempirical (PM3) and DFT (B97D/6-31G(d,p)) calculations were performed in order to obtain reliable structures and thermodynamic properties. Within the quantum



mechanical formalism the solvent effect (water) was taking into account using the polarized continuum model (IEFPCM). Two modes of inclusion were assumed for the [*p*-Cym... $\beta$ -CD] complex: (i) Mode A, when the guest is placed in the hydrophobic cavity of the CD by the wider rim; (ii) Mode B, when the guest is included by the inner rim. The inclusion complexes were studied considering the 1:1 molar ratio in gas and aqueous phases. All theoretical calculations were carried out using the Gaussian 2009 quantum mechanical package. The main results are summarized in Table 1.

**Table 1:** B97D/6-31G(d,p)//PM3 complexation energies ( $\Delta E_{compl}$ ) and Gibbs free energy ( $\Delta G$ ) calculated in gas and aqueous phases for the [*p*-Cym... $\beta$ -CD] inclusion complexes. Values given in kcal.mol<sup>-1</sup>.

Complexes	$\Delta E_{compl(g)}$	$\Delta G(g)$	$\Delta E_{compl(aq)}$	$\Delta G(aq)$
[ <i>p</i> -Cym... $\beta$ -CD] Mode A	-14.71	5.94	-14.17	6.48
[ <i>p</i> -Cym... $\beta$ -CD] Mode B	-12.69	6.99	-11.85	7.82

In Table 1, it is possible observe that the  $\Delta E_{compl}$  and  $\Delta G$ , both in gas (*g*) and aqueous (*aq*) phases are slightly more favorable for the Mode A complex (Figure 1). The more stability observed for Mode A can be associated to the depth of inclusion *p*-Cym which favors the rise of dispersive forces inside de host cavity. This result is quite relevant once it is the first topological study in literature concerning the formation of such inclusion complex involving *p*-Cym and  $\beta$ -CD.

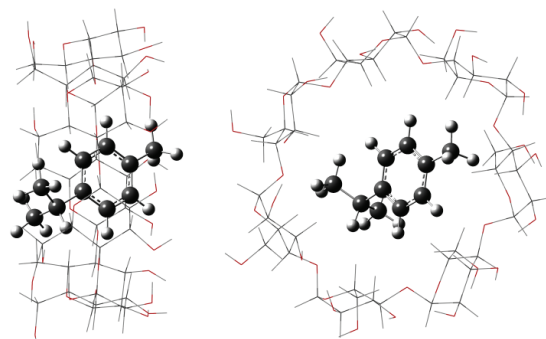


**Figure 1:** Optimized geometry for [*p*-Cym... $\beta$ -CD] Mode A complex in two views.

**Support:** The authors thank CAPES, FAPEMIG and CNPq for the financial support.

#### References:

- [1] T. Loftsson *et al.*, *Expert Opinion on Drug Delivery*, **2** (2005) 335.
- [2] M. F. Santanna *et al.*, *Revista Brasileira Farmacognosia*, **21** (2011) 1138.
- [3] A.Ciobanu *et al.*, *Food Res. Int.* **53** (2013) 110; J. S. S. Quintans *et al.*, *Phytomedicine* **20** (2013) 436; M. R. Serafini *et al.*, *J. Therm. Anal. Calorim.* **109** (2012) 951.



## Study of Excited States of Polycyclic Aromatic Hydrocarbons (PAHs)

Rafael Oliveira Lima, Fernanda Bettanin, Luiz F. A. Ferrão, Francisco B. C. Machado

*Departamento de Química, Instituto Tecnológico de Aeronáutica, São José dos Campos, SP, Brasil*

Polycyclic aromatic hydrocarbons (PAHs) have been used as graphene's model of electronic structure characterization [1]. Since the initial graphene experiments, it has been used in several areas, such as sensors manufactory, organic semiconductors, spintronic and non-linear optics and the study of its electronic structure is very important for these applications [2]. Therefore, the characterization of the fundamental and excited electronic states of PAHs, *n*-acenes (Figure 1a) and periacenes (Figure 1b) is the main goal of this work.

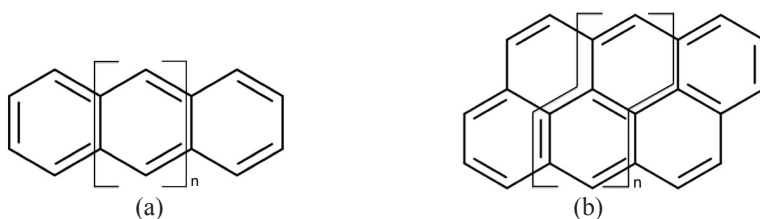


Figure 1. (a) Structure of studied acenes ( $n=0-4$ ) and (b) periacenes ( $n=0-4$ )

Molecular quantum chemistry methods are highly used in PAHs studies. In this work, the Time-Dependent Density Functional Theory (TD-DFT) was employed with M06-2X and WB97-XD functionals and 6-31G\* basis set. The absorption spectra calculations were performed to describe the two lower singlet energy excitations that correspond to the La and Lb bands of acenes (Figure 2) and periacenes (Figure 3). Properties as the character of the transition and the involved orbitals were analyzed. The La band consists in a single HOMO→LUMO excitation while Lb band consists in two single excitations: HOMO-1→LUMO and HOMO→LUMO+1. La band present an ionic character and Lb, covalent character. La band was good described by both tested functionals presenting results close to experimental data. Lb band is harder to be described but both functionals present the same tendency as the experimental data.

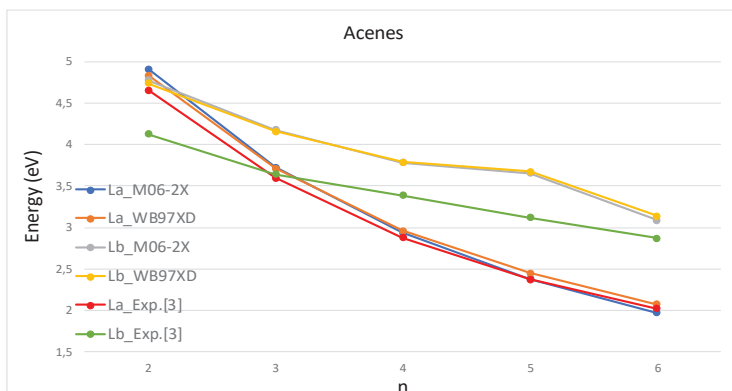


Figure 2. La and Lb band energies for all acenes studied calculated with M06-2X and WB97XD and experimental [3].

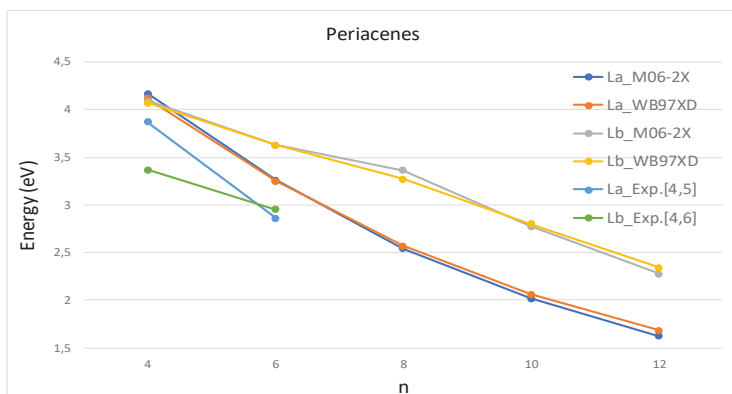


Figure 3. La and Lb band energies for all periacenes studied calculated with M06-2X and WB97XD and experimental [4-6].

**Key-words:** Acenes, periacenes, excited states, TD-DFT.

**Support:** This work has been supported by CNPq, CAPES, FAPESP.

**References:**

- [1] Cioslowski, J.; Weniger, E. J., *J. Comput. Chem.*, **14**, 1468 (1993).
- [2] Bettanin, F.; Ferrão, L. F. A.; Pinheiro, Jr. M.; Aquino, A. J. A.; Lischka, H.; Machado, F. B. C.; Nachtigalova, D., *J. Chem. Theory Comput.* Accepted.
- [3] Biermann, D.; Schmidt, W. Diels-Alder. *J. Am. Chem. Soc.*, **102**, 3163 (1980).
- [4] Bito, Y.; Shilda, N.; Toru, T. *Chem. Phys. Lett.*, **328**, 310 (2000).
- [5] Parac, M.; Grimme, S. *Chem. Phys.*, **292**, 11 (2003).
- [6] Johannesssen, C.; Gorski, A.; Waluk, J.; Spanget-Larsen, J. *Polycycl. Aromat. Compd.*, **25**, 23 (2005).



## Aggregation of Asphaltenes Using a Top-down Molecular Modeling Hierarchical Approach

Raphael S. Alvim, Filipe C. D. A. Lima, Caetano R. Miranda

*Departamento de Física dos Materiais e Mecânica, Instituto de Física, Universidade de São Paulo, 05508-090, São Paulo, SP, Brasil*

**Abstract:** Asphaltenes are a class of high-density molecules obtained from crude oil. The implications of asphaltene stability within the oil matrix production affect the whole oil supply chain production. This reduces the oil recovery because of mobility changes in the reservoir [1]. So far, the experimental and theoretical investigations have not addressed discussions at electronic level regarding a nanoaggregation mechanism influenced by resin molecules. We studied the molecular models already established in the literature for specific types molecules of asphaltene (**A**) with large aromatic island and resin (**R**) rich in heteroatoms [2,3]. From a hierarchical approach, we employed molecular mechanics simulations performed by the LAMMPS software [4] to calculate the potential energy surface to obtain the best conformations for the possible dimers **A-A**, **A-R** and **R-R**, as well as the relevant combinations of trimers **A-R-A**, **A-A-R** and **A-A-A**. After this, the energetically most favorable possibilities of aggregation conformations were further relaxed by the Density-Functional Theory calculations with corrections of dispersion forces implemented in the Quantum ESPRESSO package [5]. Our results show the aggregation mechanism is related to the rearrangement of the charge toward the stability of the  $\pi - \pi$  stacking during the **A + R** interaction taking as reference the aggregates of **A**. The growth of the nanoaggregates was followed up by the changes toward the degeneracy of the electronic states, dipole moment and radius of gyration. It is expected that **R** itself might be inner destabilizers on the aggregation process naturally present in oil. From industrial point of view, the knowledge of the aggregation mechanism may allow the design of new surfactants or compounds with specific functional groups to control the formation and destabilization of the asphaltene nanoaggregates.

**Key-words:** Asphaltenes, nanoaggregates, aggregation mechanism, molecular mechanics, DFT.

**Support:** This work has been supported by PETROBRAS and Brazilian agencies CNPq and FAPESP. Computational time: Blue Gene/Q supercomputer (Rice University), HPC of Universidade de São Paulo, UFABC, CENAPAD-SP and SAMPA group.

### References:

- [1] J. J. Adams, *Energ. Fuels*, 28, 2831 (2014).
- [2] E. S. Boek, D. S. Yakovlev, T. F. Headen, *Energ. Fuels*, 23, 1209 (2009).
- [3] H. K. Al Halwachi, D. S. Yakovlev, E. S. Boek, *Energ. Fuels*, 26, 6177 (2012).
- [4] S. J. Plimpton, *Comput. Phys.*, 117, 1 (1995).
- [5] P. Giannozzi, et al *Phys. Cond. Matter*, 21, 395502 (2009).

## Glycerol adsorption energy onto Pt and PtSn (001) surfaces using density functional theory and vdW corrections

Raquel Costabile Bezerra, Hidembergue Ordozgoith Frota, Kelson Mota Teixeira de Oliveira, Raimundo Ribeiro Passos

*Address: Department of Chemistry, Federal University of Amazonas, 69080-900 Manaus, AM, Brazil*

**Abstract:** Glycerol is a versatile molecule because of its wide applicability, one of them is its use as fuel in fuel cells, since glycerol has a reliable energy density and reversible efficiency [1]. However, the oxidation of alcohols into fuel cells is one of the major challenges of these systems [2-5]. Computational theoretical studies have been carried out for a better understanding of the oxidation of electrochemical process [6]. This work deals with the glycerol adsorption on the surfaces of Pt and PtSn by computational calculations based in Density Functional Theory (DFT) [7,8]. The calculations were performed using Quantum Espresso program [9]. Exchange and correlation energies were determined using Perdew–Burke–Ernzerhof (PBE) [10] form of the generalized gradient approximation (GGA). The energy cutoff for the wave-function is 25 Ry (340 eV). Ultrasoft pseudopotentials [11] and a 6x6x1 Monkhost-Pack k-point mesh were used. A Marzari-Vanderbilt smearing of 0.2 eV was applied. A 2x2x1 slab with three layers was created for each metal surface all of them kept the Pt-bottom layer freeze according to the Pt unit cell lattice parameter. Studies shown that glycerol has several conformers [12], then the three lower energy conformers were used to add it over the surfaces in this work. Van der Waals (vdW) corrections (DFT-D2) [13] were also included to study the effects of long range interactions. The results (see Figure 1 and Table 1) show that for the Pt and PtSn, both in plane 001, the lower energy configurations with van der Waals correction presented lower energy than those without this correction and in both cases, the configuration of the highest energy was the 3d configuration in which only one O atom of glycerol is pointed to the surface and the other two are in the opposite direction. Through the theoretical data, it was observed that the glycerol molecule interacts with the atoms of the surfaces of the metals principally via M-O, as already mentioned in the literature [14-16], since the states of greater contributions coming from the oxygen atoms overlap the *d*-states of the metals. With the exception of conformer 2, the other two conformers presented configurations with the lowest energy coming from the surface with the three oxygen atoms of the glycerol molecule. Thus, this work re-affirms the idea that the molecule adsorb on the surface of transition metals via M-O bonding, besides, changes in the adsorption energy of the glycerol configurations occurred with the addition of Sn in the structure of Pt. The van der Waals correction led to configurations of the lower energy glycerol on both Pt and PtSn surfaces.

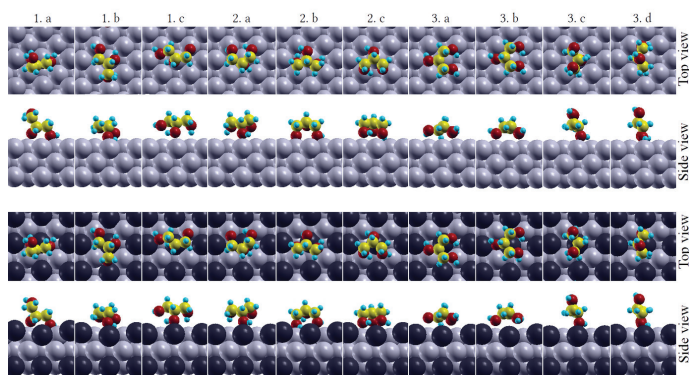


Figure 1: Configurations of glycerol on Pt and PtSn surfaces.

Table 1: Energies of glycerol adsorption for configurations.

Configurações	1a	1b	1c	2a	2b	2c	3a	3b	3c	3d
$E_{-0.01}^{DFT} (eV)$	-0.94	-1.06	-1.66	-1.64	-1.24	-1.16	-1.07	-1.07	-0.31	-0.86
$E_{-0.01}^{DFT+vdW} (eV)$	-1.99	-2.68	-2.48	-2.18	-2.85	-2.32	-2.71	-2.70	-1.32	-1.85
$E_{-0.01}^{DFT} (eV)$ - DFT-D2	-0.68	-1.49	-1.49	-1.82	-1.08	-1.61	-0.74	-1.20	-0.52	-0.58
$E_{-0.01}^{DFT+vdW} (eV)$ - DFT-D2	-2.20	-2.91	-2.45	-2.86	-3.17	-3.09	-2.24	-2.36	-1.27	-1.80

**Key-words:** DFT, glycerol, Pt and PtSn, van der Waals corrections

**Support:** This work has been supported by CNPq.

**References:**

- [1] B. Katryniok, et al. Green Chem., 13, 1960 (2011).
- [2] Z. Zhang, et al. J. Hydrogen Energy, 37, 9393 (2012).
- [3] A. Falase, et al. Electrochim. Acta, 66, 295 (2012).
- [4] P. S. Fernández, et al. Electrochim. Acta, 66, 180 (2012).
- [5] J. F. Gomes, G. Tremiliosi-Filho. Electrocatal., 2, 96 (2011).
- [6] B. Braunschweig, et al. Catal. Today, 202, 197 (2013).
- [7] P. Hohenberg, W. Kohn. Phys. Rev., 136, B864 (1964).
- [8] P. Giannozzi, et al. J. Phys.: Condens. Matter, 21, 395502 (2009).
- [9] W. Kohn, L. J. Sham. Phys. Rev., 140, A1133 (1965).
- [10] J. P. Perdew, et al. Phys. Rev. Letters, 77, 18, 3865 (1996).
- [11] A. M. Rappe, et al. Phys. Rev. B, 41, 1227 (1990).
- [12] C. S. Callam, et al. J. Am. Chem. Soc., 58, 11743 (2001).
- [13] S. Grimme. J. Comput. Chem., 27, 1787 (2006).
- [14] B. Liu, J. Greeley. Phys. Chem. Chem. Phys., 15, 6475 (2013).
- [15] B. Liu, J. Greeley. J. Phys. Chem. C, 115, 19702 (2011).
- [16] P. Tereshchuk et al. J. Phys. Chem. C., 118, 15251 (2014).



## Theoretical Calculations on Diels-Alder Reactions: Case Study of Cyclopentadiene and Alkyl Acrylate

Régis Casimiro Leal,<sup>a,b</sup> and Rogério Custodio<sup>a</sup>

<sup>a</sup> Instituto de Química, Universidade Estadual de Campinas (UNICAMP), 13084-970, Campinas, São Paulo - SP, Brasil

<sup>b</sup> Instituto Federal de Educação, Ciência e Tecnologia do Rio Grande do Norte (IFRN), 59215-000, Nova Cruz, Rio Grande do Norte - RN, Brasil

**Abstract:** Diels-Alder reactions are more complex than the simple interaction between the reactants suggests and no justification can be generalized in an attempt to explain the selectivity of a given product. Therefore these reactions continue to be a challenge for high-accuracy calculations [1]. An interesting case that may exemplify the nature of this type of mechanism is the reaction between cyclopentadiene and alkyl acrylate, R = H and R = CH<sub>3</sub> (Figure 1) [2-5]. The simple substitution of hydrogen by a methyl group in the dienophile is responsible by the opposite predominance of the product formed.

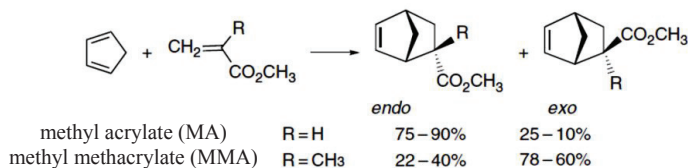


**Figure 1.** Scheme of the reaction between cyclopentadiene and alkyl acrylate.

Ruiz-López et al. [3] by using the SCRF model and ab initio calculations suggest that the polarity of the medium influences the selectivity of these particular reactions. Hondrogiannis et al. [4] say that the ratio of endo to exo products is strongly dependent on the activity of the alumina. Stefaniak et al. [5] showed that a higher stereoselectivity to the endo isomer was found in the majority of cases involving cyclopentadiene and alkyl acrylates in the presence of pyrrolidinium ionic liquids.

In this work, calculations were performed with the Gaussian 09 program, initially at the B3LYP/6-31G(d) level followed by QCISD(T) single point calculations using the same basis set. The results showed a small energy difference of  $\sim 0.5$  kcal mol<sup>-1</sup> between the barriers and stereoisomers formed by the reaction between Cp and MA, with both levels of theory tested. This is not enough argument to explain the experimental yield for this reaction. The transition state (TS) were characterized by a single imaginary frequency.

For the Cp and MMA reaction, it is observed a difference between barriers of 1.3 kcal mol<sup>-1</sup> in favor of the path leading to the exo product. This difference decreases to 0.8 kcal mol<sup>-1</sup> with QCISD(T). Finally, the TSs were submitted to the Intrinsic Reaction Coordinate (IRC) procedure at the B3LYP/6-31G(d) level of theory and the results can be seen in Figure 2.

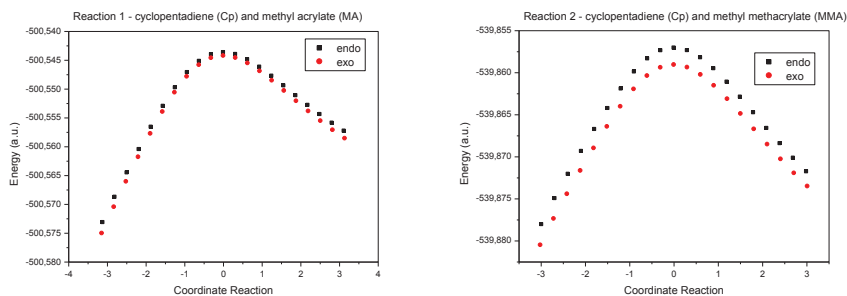


**Figure 2.** IRCs for the reactions between the Cp + MA (left) and Cp + MMA (right).

The energy differences below  $1 \text{ kcal mol}^{-1}$  between both barriers or products are not sufficient to justify the experimental yield of the reaction between Cp and MA. The lower barrier of the reaction between Cp and MMA for the exo path shows that the factors controlling the endo:exo selectivity changes according to specific cases, such as the reactions treated in this work where steric effects prevail. More accurate calculations are being carried out and will be presented in the meeting.

**Key-words:** Diels-Alder reaction, steric effects, endo/exo selectivity.

**Support:** This work has been supported by CAPES, FAPESP (Center for Computational Engineering and Sciences, Grant 2013/08293-7), CNPq, FAEPEX-UNICAMP.

### References:

- [1] R. C. Leal, D. H. Pereira, R. Custodio, *Rev. Proc. Quím. - Edição Especial XVIII SBQT*, 18, 190, (2015).
- [2] J. A. Berson, Z. Hamlet, W. A. Mueller, *J. Am. Chem. Soc.*, 84, 297 (1962).
- [3] M. F. Ruiz-López, X. Assfeld, J. I. García, J. A. Mayoral, L. Salvatella, *J. Am. Chem. Soc.*, 115, 8780 (1993).
- [4] G. Hondrogianis, R. M. Pagni, G. W. Kabalka, P. Anosike, R. Kurt, *Tetrah. Lett.*, 31, 5433, (1990).
- [5] W. Stefaniak, E. Janus, E. Milchert, *Catal. Lett.*, 141, 742–747 (2011).



## Relativistic effects on the noble gas chemistry: A study of the $\text{HNgF} \rightarrow \text{Ng} + \text{HF}$ ( $\text{Ng} = \text{Ar}, \text{Kr}, \text{Xe}$ and $\text{Rn}$ ) decomposition reaction

Régis T. Santiago, Roberto L. A. Haiduke

*Instituto de Química de São Carlos, Universidade de São Paulo, CP 780, 13560-970, São Carlos, SP, Brasil.*

Actually, there is a growing interest in chemical reactions involving noble gases. The experimental evidence of molecules like HArF promoted a renewed interest on the noble gas research field [1-2]. However, some aspects are still unknown [2]. One of them is the importance of relativistic effects in reaction mechanism calculations by quantum chemistry methods. Decomposition pathways for HArF and HKrF were previously investigated by the Relativistic Effective Core Potential (RECP) method [3]. Thus, we performed a new study including Xe and Rn compounds along with more advanced relativistic treatments. Our objective is to analyze the relativistic effects for the decomposition pathway of HNgF ( $\text{Ng} = \text{Ar}, \text{Kr}, \text{Xe}$  and  $\text{Rn}$ ) compounds into HF and a noble gas atom.

All the optimization, vibrational frequencies and Intrinsic Reaction Coordinate (IRC) calculations were done with the Gaussian 09 package [4]. We used the Density Functional Theory (B3LYP functional), aug-cc-pVTZ basis set for H, F, Ar and Kr and aug-cc-pVTZ-PP basis set for Xe and Rn atoms. The IRC calculations connected the reactants to the products of each investigated reaction. Next, the previously optimized structures were used in the DIRAC 16 program [5], by means of Coupled Cluster calculations with single and double iterative excitations along with perturbative triple substitutions (CCSD-T) and RPF-4Z basis sets [6]. Hence, we determined electronic energies in the non-relativistic (NR) and relativistic treatments, Dirac Coulomb (DC) and DC-SF (spin-free).

The electronic energies of activation ( $E_{\text{act}}$ ) and energies changes ( $\Delta E$ ) for reactions with HArF and HKrF are in nice agreement with a previous study [2]. Table 1 shows our results ( $\text{kcal mol}^{-1}$ ).

Table 1: Electronic energies of activation ( $E_{\text{act}}$ ) and energies changes ( $\Delta E$ ) obtained with NR, DC-SF and DC treatments for each decomposition reaction ( $\text{kcal mol}^{-1}$ ).

Reaction	$E_{\text{act}}$			$\Delta E$		
	NR	DC-SF	DC	NR	DC-SF	DC
HArF $\rightarrow$ Ar + HF	25.62	25.88	25.88	-135.32	-134.91	-134.91
HKrF $\rightarrow$ Kr + HF	34.26	34.85	34.83	-115.64	-114.99	-114.91
HXeF $\rightarrow$ Xe + HF	40.50	41.00	40.81	-91.19	-92.08	-91.70
HRnF $\rightarrow$ Rn + HF	39.65	41.56	40.05	-80.31	-84.31	-80.96



Firstly, analyzing the activation energies, we can notice that scalar relativistic effects increase  $E_{\text{act}}$  between 1.0 and 4.6%. On the other hand, spin orbit coupling corrections decrease this activation energy by as much as 3.8% (HRnF). Moreover, analyzing the energy differences between products and reactant, we can notice the same trend. Hence, there is a significant cancellation between scalar relativistic effects and spin-orbit coupling for compounds with the heaviest noble gases (Xe and Rn). Overall, the high barriers obtained indicate that all HNgF compounds are kinetically stable.

In summary, we conclude that relativistic effects can change significantly the energetics ( $E_{\text{act}}$  and  $\Delta E$ ) of these decomposition reactions. As expected, the HRnF compound showed the highest relativistic correction. Moreover, this investigation reveals a surprising cancellation between scalar relativistic affects and spin orbit coupling terms.

**Key-words:** relativistic effects, decomposition reaction, noble gas chemistry

**Support:** This work has been supported by CNPq (305366/2015-7) and FAPESP (2010/18743-1 and 2014/23714-1)

**References:**

- [1] Christe, K. O. *Angew. Chem. Int. Ed.* 40, 1419 (2001).
- [2] Chaban, G. M.; Lundell, J.; Gerber, R. B. *Chem. Phys. Lett.*, 364, 628 (2002).
- [3] Chen, Y. L.; Hu, W. P. *J. Phys. Chem. A* 108, 4449. (2004).
- [4] Gaussian 09, Revision D.01, Gaussian, Inc., Wallingford CT, 2016.
- [5] DIRAC, A Relativistic ab initio Electronic Structure Program, Release DIRAC16 (2016).
- [6] Teodoro, T. Q.; da Silva, A. B. F.; Haiduke, R. L. A. *J. Chem. Theory Comput.*, 10, 3800 (2014).



## Parâmetros Estruturais e Eletrônicos para o Cálculo da Temperatura Crítica de Supercondutores do tipo $A_2BC_{60}$ (A e B: Na, K, Rb e Cs)

Renato C. da Silva<sup>1</sup>, Cristiano C. Bastos<sup>2</sup>, e Antonio C. Pavão<sup>1</sup>

<sup>1</sup>Universidade Federal de Pernambuco, Departamento de Química Fundamental

<sup>2</sup>Universidade Federal Rural de Pernambuco, Departamento de Química

**Resumo:** Variados parâmetros estruturais e eletrônicos ajudam na compreensão da supercondutividade [1-5]. Em particular, sistemas do tipo  $A_2BC_{60}$  (A e B: Na, K, Rb, Cs) demonstram relações quantitativas entre a energia de ionização e afinidade eletrônica com a temperatura crítica ( $T_c$ ) [1,2]. É possível encontrar na literatura diferentes ligantes A e B, como  $Na(NH_3)_4$  no lugar do sódio no  $Na_2CsC_{60}$ , elevando a  $T_c$  de 12K para 29K [3]. Considerando a possibilidade de extensões da teoria BCS [4,5], a fórmula  $T_c = 120e^{-1/\rho}$  e a análise estatística de QSAR, foi possível obter uma expressão  $\rho$  para os sistemas  $A_2BC_{60}$  em função de propriedades dos metais, a diferença de energia dos orbitais de fronteira, eletronegatividade, potencial de ionização, raio iônico, e relativo aos cristais, o parâmetro de rede. Para isso, foi utilizado um conjunto treino:  $Na_2KC_{60}$ ,  $Na_2RbC_{60}$ ,  $Na_2Rb_{0.5}Cs_{0.5}C_{60}$ ,  $Na_2CsC_{60}$ ,  $K_3C_{60}$ ,  $K_2RbC_{60}$ ,  $K_{1.5}Rb_{1.5}C_{60}$ ,  $Rb_2KC_{60}$ ,  $K_2CsC_{60}$ ,  $Rb_3C_{60}$ ,  $Rb_2CsC_{60}$ ,  $Cs_2RbC_{60}$  e  $Cs_3C_{60}$ .

$$\rho = 2.3001 - 0.2168 \sum I - \frac{1.2136}{a} \left( \frac{\sum \Delta HL}{\sum r} \right)^2 + 0.0191 (\sum \chi)^2$$

Com esta expressão, prevemos corretamente 26.3K para o  $(NH_3)_4NaC_{60}$  ( $T_c$  experimental = 29.6K), segundo a Tabela 1. Uma fórmula da literatura prevê  $T_c = 61.8K$  para  $(NH_3)_4Na_2CsC_{60}$ , praticamente o dobro do valor correto [2]. Considerando esta análise robusta o suficiente, propomos novos ligantes que podem elevar a  $T_c$ .

**Tabela 1.**  $T_c$  experimental e calculada para alguns dos supercondutores utilizados

Supercondutor	$T_c$ experimental (K)	$T_c$ teórica (K)	$T_c$ Hetfleisch et al [3]
$K_3C_{60}$	19.0	17.6	21.3
$Rb_3C_{60}$	29.0	28.4	26.9
$Rb_2CsC_{60}$	31.0	30.9	30.1
$Cs_3C_{60}$	35.0	35.3	36.5
$(NH_3)_4Na_2CsC_{60}$	29.6	26.3	61.8
$(N_2H_4)_4Cs_2NaC_{60}$	---	55.7	108.5
$(CH_3OH)_4Na_2CsC_{60}$	---	62.1	122.2
$(N_2H_4)_4Na_3C_{60}$	---	77.5	165.6



Estes ligantes seguem o critério de analogia isoglobal [6], mantendo ligantes tetraédricos e uma base de Lewis:  $\text{Na}[(\text{CH}_3)_2\text{N}]_4$ ,  $\text{Na}(\text{CH}_3\text{OH})_4$ ,  $\text{Na}[(\text{CH}_3)_2\text{O}]_4$ ,  $\text{Na}[\text{CH}_3\text{NH}_2]_4$ ,  $\text{Na}[\text{N}_2\text{H}_4]_4$  e  $\text{Cs}[\text{N}_2\text{H}_4]_4$ . Segundo nossa análise, a temperatura crítica pode ser elevada acima de 70K.

**Palavras-chave:** supercondutividade, BCS e QSAR, temperatura crítica, propriedades estruturais e eletrônicas

**Apoio:** Este trabalho tem apoio da CAPES e CENAPAD-SP

### Referências:

- [1] S. Larsson, J Supercond Nov Magn 28, 315 (2015).
- [2] F. Hetfleisch, Marco Stepper, H.-P. Roeser, A. Bohr, J. S. Lopez, M. Mashmool, S. Roth, Physica C 513, 1 (2015).
- [3] Y. Iwasa, H. Shimoda, Y. Miyamoto, T. Mitani, Y. Maniwa, O. Zhou, T.T.T Palstra, J. Phys. Chem Solids 58, 1697 (1997).
- [4] W. L. Mc Millan, Physical Review 167, 331 (1968).
- [5] G.W. Webb, F. Marsiglio, J.E. Hirsch, Physica C 514, 17 (2015). Chuck-Hou Yee, Turan Birol and Gabriel Kotliar, Europhysics Letters 111, 17002(2015).
- [6] R. Hoffmann, Angew. Chem. Ont. Ed. Eng. 21, 711(1982).



## Title: Pentacyclic Triterpenes isomers $^{13}\text{C}$ NMR Chemical Shift Prediction Using GIAO- mPW1PW91/3-21G//PM7 Level of Theory

Authors: Rênica Alves de Moraes Rocha,<sup>a</sup> Thais Forest Giacomello,<sup>a</sup> Gunar Vingre da Silva Mota,<sup>a</sup> Antonio Maia de Jesus Chaves Neto,<sup>b</sup> Fabio Luiz Paranhos Costa,<sup>\*a</sup>

Address: <sup>a</sup>Department of Chemistry, Federal University of Goiás, REJ Jataí 75801-615, Brasil.

<sup>b</sup>Natural Science Faculty, Federal University of Pará, ICEN UFPA Belém 66075-110, Brasil

**Abstract:** Triterpenes are a class of natural products with great importance due to their biological and pharmacological activities [1]. These molecules may have complex structures, which makes their structural characterization through routine analytical techniques a difficult task. Despite the recent advances in spectroscopic techniques, cases of revision of erroneously established natural product structures are still to be found in the literature [2]. Therefore, it is necessary to develop quantum calculation protocols aimed in the structural determination of these compounds. In order to spread its applicability to different time-demanding tasks, a protocol should have the bigger cost-effectiveness ratio as possible. In this work we intend to test the robustness of a scaling factor based on GIAO//semi-empirical (mPW1PW91/3-21G//PM7) [3] calculations to determine the  $^{13}\text{C}$  NMR chemical shifts ( $\delta$ ) of 6 pentacyclic triterpenes [4] (2 pairs of regioisomers), i.e.,  $\alpha$ -amyrin (**I**) –  $\beta$ -amyrin (**II**) and  $\alpha$ -amyrin acetate (**III**) –  $\beta$ -amyrin acetate (**IV**), glutinol (**V**) and glutinol acetate (**VI**), see figure 1. It's worth to note that, the compounds **I**, **II** and **V** are diastereoisomers ( $\text{C}_{30}\text{H}_{50}\text{O}$ ) as well as the compounds **III**, **IV** and **VI** ( $\text{C}_{32}\text{H}_{52}\text{O}_2$ ). The  $\delta$  are obtained as  $\delta_{\text{calc}} = \sigma_{\text{TMS}} - \sigma$ , where  $\sigma_{\text{TMS}}$  is the isotropic shielding constant of the reference compound, tetramethylsilane (TMS), calculate at the same level of theory. The scaled  $\delta$  ( $\delta_{\text{scal}}$ ) were obtained u the equation:  $\delta_{\text{scal}} = 1.14 \cdot \delta_{\text{calc}} - 4.70$  (**1**).

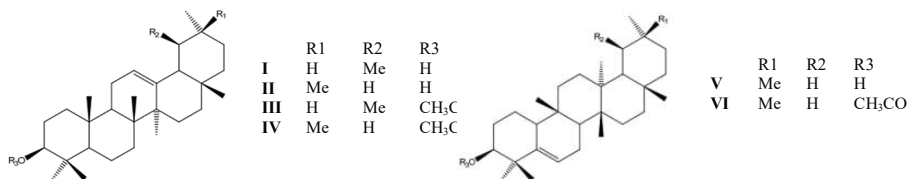


Figure 1. pentacyclic triterpenes:  $\alpha$ -amyrin (**I**),  $\beta$ -amyrin (**II**),  $\alpha$ -amyrin acetate (**III**),  $\beta$ -amyrin acetate (**IV**), glutinol (**V**) and glutinol acetate (**VI**).



The 6 triterpenes were submitted to randomized conformational searches using Monte Carlo method and MMFF force field, as implemented in SPARTAN08 [5]. For complete conformational analysis and the conformer's selection protocol, see Giacomello *et alli* [6]. All DFT quantum mechanical calculations were performed in gas phase, using Gaussian 09 software package [7], PM7 calculations were performed using MOPAC2012 [8]. Table 1 shows for the 6 pentacyclic triterpenes, the Mean Absolute Deviation (MAD) and the Root Mean Square Deviation (RMSD), in ppm, before and after (in parenthesis) the application of the equation 1.

Table 1. Statistics parameters MAD and RMS, in ppm, for the 6 triterpenes.

Statistics/Molecules	(I)	(II)	(III)	(IV)	(V)	(VI)
MAD <sub>calc</sub> (MAD <sub>scal</sub> )	2.65 (1.11)	2.97 (1.66)	3.10 (1.25)	3.25 (1.33)	2.51 (1.56)	3.25 (1.89)
RMS <sub>calc</sub> (RMS <sub>scal</sub> )	3.75 (1.34)	4.73 (3.11)	4.93 (1.43)	4.96 (1.56)	3.78 (1.92)	4.99 (2.33)

The results showed that at the mPW1PW91/3-21G//PM7 level of theory it was able to reproduce the experimental data with small errors. After the application of the scaling factor (which intend to cancel systematic errors), the MAD and RMD errors became significantly smaller (almost 50% for all molecules). This means that even low-levels of theory can be used to cancel systematic errors. Thus, we conclude that the level of theory GIAO-mPW1PW91/3-21G together with the use of the scaling factor represented by the linear equation  $\delta_{scal} = 1.14 \cdot \delta_{calc} - 4.7$  shows an efficient and low cost tool for the calculation of  $^{13}\text{C}$  NMR chemical shifts and triterpenes.

**Key-words:** Triterpenos; Ressonância Magnética Nuclear  $^{13}\text{C}$ ; Modelagem Molecular.

**Support:** This work has been supported by FAPEG.

**References:**

- [1] P. Dzuback. M. Hajduch. D. Vydra. A. Hustova. M. Kvasnica. D. Biedermann. Pharmacological activities of natural triterpenoids and their therapeutic implications. *Nat. Prod. Rep.*, 23, 394-411 (2011).
- [2] K. C. Nicolaou; S. A. Snyder, *Ang. Chem. Int. Ed.*, 44, 1012 (2005).
- [3] F. L. P. Costa; T. F. Giacomello; R. A. de M. Rocha; A. M. de J. C. Neto; G. V. da S. Mota, *Adv. Sci. Eng. Med.* 9, 254, (2017).
- [4] C. E. Fingolo; T. de S. Santos; M. D. M. Vianna Filho; M. A. C. Kaplan, *Molecules*, 18, 4248 (2013).
- [5] Spartan'08, Wavefunction Inc., Irvine California, USA, 2010.
- [6] T. F. Giacomello; R. A. de M. Rocha; A. M. de J. C. N.; G. V. Da S. Mota; F. L. P. Costa, *Adv. Sci. Eng. Med.* 9, x, (2017), accepted.
- [7] A. E. Frisch; M. J. Frisch; G. Trucks, *Gaussian 09, Revision D.01* (2009).
- [8] J. J. P. Stewart. *Journal of Molecular Modeling*, 19, 1 (2013).



## Combination of Electronic Structure Calculations and Rovibrational Spectroscopic Constants for Enhancement of Lennard-Jones Potential in the Description of Molecules Involving Gas-Nobles

Rhuiago Mendes de Oliveira<sup>a,c</sup>, Yuri Alves de Oliveira<sup>c</sup>, Luiz Guirheme de Macedo<sup>b</sup> e Ricardo Gargano<sup>c</sup>.

<sup>a</sup> Instituto Federal do Maranhão (IFMA), Buriticupu, MA 65393-000, Brazil

<sup>b</sup> Faculdade de Biotecnologia, Instituto de Ciências Biológicas, Universidade Federal do Pará (UFPA), Belém, PA 66075-110, Brazil

<sup>c</sup> Instituto de Física, Universidade de Brasília (UnB), PO Box 04455, Brasília, DF 70919-970, Brazil.

**Abstract:** The properties of noble gases are of great interest for the development of Modeling techniques and as standard values for experimental studies. The diatomic molecules of noble gases in their fundamental electronic states represent ideal prototypes of van der Waals type molecules, their spectroscopic and thermodynamic properties have been extensively studied both theoretically [1, 2] and experimentally [3,4]. These molecules are of special interest in the field of metrology [1]. Since to determine the properties of thermophysical fluid, it is necessary to know the potential energy curve between two noble gas atoms. In this work, we first determined the electronic energies for the ground state via the coupled[5] cluster method - CCSD(t) for the following molecular systems: He-He, He-Ne, He-Ar, He-Kr, He-Xe, Ne-Ar, Ne-Kr, Ne-Xe, Ar-Ar, Ar-Kr, Ar-Xe, Kr-Kr, Kr-Xe and Xe-Xe. These energies were calculated for three different basis sets; aug-cc-pVTZ, aug-cc-pVQZ and aug-cc-pV5Z. These energies were then carefully adjusted using the analytical form named Improved Lennard Jones (ILJ) in order to obtain the additional parameter beta of each molecular system. This parameter accounts for the hardness/softness of the two involved partners. In particular, we can observe that the aug-cc-pV5Z basis set with the corrected BSSE [6] provided (for all studied systems) beta parameter values very close to 9 (Experimental value). The quality of the ILJ analytical form (using the adjusted parameter beta) was tested through the rovibrational spectroscopic constant calculations. The ILJ obtained results agree very well with the experimental data [4] and theoretical [7] results available for in the literature.

**Key-words:** Gas nobles, Electronic energies, Improved Lennard Jones and Rovibrational spectroscopic constants .

**Support:** The authors thank CNPq and FAPDF for financial supports.



### References:

- [1] KOVÁCS, Attila et al. Benchmarking density functionals in conjunction with Grimme's dispersion correction for noble gas dimers (Ne<sub>2</sub>, Ar<sub>2</sub>, Kr<sub>2</sub>, Xe<sub>2</sub>, Rn<sub>2</sub>). *International Journal of Quantum Chemistry*, v. 117, n. 9, 2017.
- [2] KULLIE, Ossama; SAUE, Trond. Range-separated density functional theory: a 4-component relativistic study of the rare gas dimers He<sub>2</sub>, Ne<sub>2</sub>, Ar<sub>2</sub>, Kr<sub>2</sub>, Xe<sub>2</sub>, Rn<sub>2</sub> and Uuo<sub>2</sub>. *Chemical Physics*, v. 395, p. 54-62, 2012.
- [3] KOPERSKI, Jarosław. Study of diatomic van der Waals complexes in supersonic beams. *Physics Reports*, v. 369, n. 3, p. 177-326, 2002.
- [4] OGILVIE, J. F.; WANG, Frank YH. Potential-energy functions of diatomic molecules of the noble gases I. Like nuclear species. *Journal of molecular structure*, v. 273, p. 277-290, 1992.
- [5] MORGON, Nelson H.; COUTINHO, Kaline. *Métodos de química teórica e modelagem molecular*. Editora Livraria da Física, 2007.
- [6] BOYS, S. F; BERNARDI, Fiorenza de. The calculation of small molecular interactions by the differences of separate total energies. Some procedures with reduced errors. *Molecular Physics*, v. 19, n. 4, p. 553-566, 1970.
- [7] GOLL, Erich; WERNER, Hans-Joachim; STOLL, Hermann. A short-range gradient-corrected density functional in long-range coupled-cluster calculations for rare gas dimers. *Physical Chemistry Chemical Physics*, v. 7, n. 23, p. 3917-3923, 2005.



## The influence of dopants elements at the electronic properties of Pd<sub>12</sub>M Clusters: A DFT study

Ricardo de Almeida<sup>1,PG\*</sup>, Samara F. B. da Fonseca<sup>1,IC</sup>, Leonardo Baptista<sup>2,PQ</sup>,  
Maurício T. de M. Cruz<sup>1,PQ</sup>,

<sup>1</sup>*Departamento de Química Geral e Inorgânica, Instituto de Química, Universidade do Estado do Rio de Janeiro (UERJ), Campus Maracanã, Rio de Janeiro (RJ), Brasil.*

*\*rialmeida1975@gmail.com, cruzmtm@uerj.br*

<sup>2</sup>*Departamento de Química Ambiental, Faculdade de Tecnologia, Universidade do Estado do Rio de Janeiro (UERJ), Rod Pres Dutra Km 298, Rio de Janeiro (RJ), Brasil.*

**Introduction:** The catalysis industries had received great importance since the industrial revolution.<sup>[1]</sup> The clusters of palladium has been widely used to the process of oxidation of CO,<sup>[2-3]</sup> reduction of nitric oxide<sup>[4]</sup> and unburned hydrocarbons in automotive converter.<sup>[1]</sup> Furthermore, palladium is a promising catalyst due to its various applications,<sup>[5-6]</sup> and good thermal stability.<sup>[1]</sup> Due to these factors, the study of palladium catalyst has been substantially increased.<sup>[5-6]</sup> In this work, we performed DFT/BP86/Lanl2dz/6-311+G(d) calculations to study the adsorption of NO in the prototype catalyst Pd<sub>13</sub> and Pd<sub>12</sub>M (M = Fe, Co, Ni) clusters. The scope of this study is to provide information about possible structural and electronic changes in a Pd<sub>13</sub> cuboctahedron cluster when doped with Fe, Co, Ni, face to adsorption of a single NO molecule.

**Key-words:** palladium cluster, DFT, electronic properties, NO adsorption

**Methodology:** In this work, palladium clusters containing 13 atoms in cuboctahedron arrangement (Pd<sub>12</sub>M) were doped at the center position with Fe, Co and Ni. In all Pd<sub>12</sub>M clusters, several electronic spin states were optimized. As a second step, a single NO molecule was optimized in different positions on the Pd<sub>12</sub>M cluster, where Pd–Pd and Pd–M distance were kept fixed in 2.751 Å.<sup>[7]</sup> In all calculations, the lowest energy states were obtained and stability test of wave functions were performed. The calculation of adsorption energy (E<sub>ad</sub>) NO/Pd<sub>12</sub>M (M = Fe,Co,Ni) was performed. The DFT/BP86 methodology was employed using Gaussian 03 program. The electrons of the NO molecule were described by 6-311+G(d) basis sets. For the palladium clusters, the valence and core electrons were described by DV95 and the LANL2DZ pseudopotential, respectively. All computed energies were corrected by the basis set superposition error (BSSE), calculated by the counterpoise method. The equilibrium geometries were full optimized since no symmetry constraint has been imposed (Fig.1).



**Results and discussion:** The analysis of the adsorption energy of NO on Pd<sub>12</sub>M, when Pd–Pd and Pd–M are kept fixed in 2.751 Å, shows that the NO molecule adsorbs preferentially in *hollow*, followed by the *bridge* and *atop* modes, for both pure and doped Pd<sub>13</sub> cluster (see Tab. 1). When the palladium agglomerate is relaxed, the NO molecule keeps on the *hollow* site preferentially, except on Pd<sub>12</sub>Fe cluster, changing to the *bridge* mode (Fig. 1).

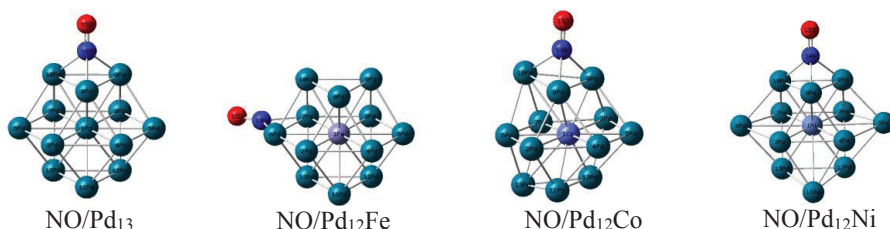


**Figure 1.** Preferential NO adsorption on Pd<sub>12</sub>M clusters optimized with BP86/Lan12dz

**Table 1.** NO Adsorption Energy (kcal.mol<sup>-1</sup>).

Clusters	NO/Pd <sub>12</sub> M (Pd–Pd = 2.751Å)			NO/Pd <sub>12</sub> M (opt)		
	<i>atop</i>	<i>bridge</i>	<i>hollow</i>	<i>atop</i>	<i>bridge</i>	<i>hollow</i>
Fe	-36.85	-49.31	-54.38	-40.44	-54.32	-53.32
Co	-44.59	-52.21	-58.43	-36.18	(*)	-46.69
Ni	-47.03	-55.45	-61.30	-44.60	-41.02	-47.54
Pd	-45.87	-60.74	-63.02	-43.34	-49.64	-50.96

(\*) changed to *hollow*.

**Conclusion:** By using density functional calculations, we theoretically investigated NO adsorption on Pd<sub>13</sub> and Pd<sub>12</sub>M clusters. The preferential adsorption mode for the NO molecule is *hollow*, regardless whether the clustering is pure or doped by the metals studied. The NBO analysis reveals that the Pd→NO back-donation is stronger than the donation in both Pd<sub>13</sub> and Pd<sub>12</sub>M clusters, in all adsorption modes obtained.

**Support:** The authors would like to thank CAPES and FAPERJ for the financial support.

#### References:

- [1] R.C. Deka et al., Int. J. Quantum. Chem., 115, 837 (2015).
- [2] O.O. Neria et al., J. Mol. Model. C, 21, 279 (2015).
- [3] D. Palagin, P. k. Doya, Phys. Chem. Chem. Phys, 17, 28010 (2015).
- [4] R.A.V. Santen, I. Tranca, E.J.M. Hansen, Catal. Today, 244, 63-64(2014).
- [5] X. Wu et al., RSC Adv.,5, 51142 (2015).
- [6] R.L. Johnston et al., Nanoscale., 6, 11777 (2015).
- [7] Z.M. Yang et al., J. Phys. Chem. Lett, 658, 7 (2016).



## Electronic and structural properties of supercritical fluids. Evaluation of force fields for the description of the absorption spectrum of paranitroanilina in supercritical CO<sub>2</sub>

Ricardo de Lima e Sylvio Canuto

*Instituto de Física, Universidade de São Paulo, CP 66318, São Paulo, São Paulo  
05315-970, Brazil*

**Abstract:** In this work we study the structural and electronic properties of supercritical CO<sub>2</sub> starting with the evaluation of force fields based on previous ab initio Born-Oppenheimer molecular dynamics (BOMD) [1]. The main application is the description of the absorption spectrum of paranitroanilina (pNA) [2,3] in supercritical CO<sub>2</sub>. The supercritical CO<sub>2</sub> is considered a "green alternative" to conventional organic solvents and the search for safer solvents, along with the increasing awareness of environmental issues has led to the interest in "green chemistry" [4,5], seeking sustainable solutions. At first we studied three traditional force fields for CO<sub>2</sub>, applied in the supercritical region. These force fields can be validated by first principles simulation. We considered the supercritical condition for CO<sub>2</sub> as T=315K,  $\rho=0.81\text{g/cm}^3$  and the classical force field of Zhang and Duan [6]. We also did an analysis consisting of a change of the atomic point charges and the geometry of CO<sub>2</sub>, including a non-linear case in which an angle (O-C-O)=176° was considered [1]. The study of the solvatochromism of pNA in supercritical CO<sub>2</sub> was made considering all these situations, evaluating the theoretical outcome and the experimental results. The simulation generates structures using Monte Carlo and are used in quantum mechanics calculations using DFT (CAM-B3LYP [7]). To verify the importance of a proper description of the structural property, we considered another geometry for the pNA geometry different from that we used initially in the simulations with supercritical CO<sub>2</sub>. This "modified geometry" of pNA was obtained from a previous Born-Oppenheimer simulation [1] and was used in a Monte Carlo simulation with the nonlinear CO<sub>2</sub> for the supercritical condition. The results of all simulations indicated that the changes of atomic charges and thus in the polarization due to the solvent, has no great significance in the absorption spectrum of the pNA. When considering the nonlinear CO<sub>2</sub>, we obtained slightly better results. But the most significant results are obtained for the situation in which we use the modified geometry of pNA. Part of the shift in the absorption spectrum of the pNA comes with the electrostatic contribution of solute-solvent interaction and the other part comes from the structural change.

**Key-words:** S-QM/MM, solvatochromism, absorption spectrum, supercritical fluids.



### References:

- [1] B. J. C. Cabral, R. Rivelino, K. Coutinho and S. Canuto, *J. Chem. Phys.* 142, 024504 (2015).
- [2] Y. Marcus, *J. Phys. Org. Chem.* 18, 373 (2005).
- [3] S. Kim and K. P. Johnston, *Ind. Eng. Chem. Res.* 26, 1206 (1987).
- [4] C. Reichardt, *Solvents and Solvent Effects in Organic Chemistry*, 4th Ed. Wiley-VCH (2010).
- [5] P. Jessop and W. Leitner, *Handbook of Green Chemistry, Volume 4: Supercritical Solvents*. W. Leitner and W. Jessop (Eds.) Wiley-VCH, 1-30 (2010).
- [6] Z. Zhang and Z. Duan, *J. Chem. Phys.* 122, 214507 (2005).
- [7] T. Yanai, D. P. Tew and N. C. Handy, *Chem. Phys. Lett.* 393, 51-57 (2004).



## Inhibitors of Salicylic Acid Binding Protein 2 (SABP2) Design by Docking and Molecular Dynamics

Ricardo Fagundes da Rocha, Vanessa Petry do Canto, Gustavo Pozza Silveira & Paulo Augusto Netz

*Instituto de Química, Universidade Federal do Rio Grande do Sul (UFRGS), Avenida Bento Gonçalves, 9500, Bairro Agronomia, CEP 91501-970, Porto Alegre, Rio Grande do Sul, Brasil.*

**Abstract:** Since plants are susceptible to biotic and abiotic attacking, they present short and long-term defense mechanisms that are mediated by several signaling molecules, such as salicylic acid (SA) [1]. However, the signal to distal plant regions is not driven by SA, but through methyl salicylate (MeSA) molecule. The MeSA is generated in a reaction catalyzed by SABP2 (catalytic site formed by Ser81, Asp210 and His238), which converts SA into MeSA at the damage site, and then allows the stress message to be carried to distant spots, where MeSA is converted back to SA [2]. The briefly described mechanism related to SA, MeSA and SABP2 plays a central role on plants physiology and SABP2's inhibitors development can be an interesting strategy on molecular design for agriculture and biotechnology applications, for instance for the improvement of *Vitis vinifera L.* plantations. Therefore, the aim of this present study is to describe and to compare the interactions of different SA analogues with SABP2. The structures for 58 SA analogues molecules were built with Gauss View [3], the protonation degree was determined with Marvin Sketch [4], and the optimization step was conducted with Gaussian 09 by using *ab initio*, Hartree-Fock 6-31G (d,p) calculations [5]. Protein (SABP2) structure, PDB-ID 1Y7I, was obtained from Protein Data Bank, <https://www.rcsb.org/pdb/home/home.do>, and its protonation pattern checked with online software PROPKA, <http://propka.org/> [6]. Docking analysis was done through AutoDockVina (grid of 20 x 20 x 20 Å) [7], while molecular dynamics has been performed with Gromacs package (TIP3P water model, Amber force field, pH = 7,00 and temperatures of 278 K, 288 K and 298 K) [8]. The protonation degree analysis of the 58 molecules generated 100 relevant species to be tested. Docking analysis pointed 31 species with favorable scores (when the energy for interaction between SA analogue and SABP2 is more negative than that for SA and SABP2) and positioned at enzyme active site. The best score was found for 1-(1H-Tetrazol-5-yl)-2-chlorobenzene, - 8.6 kcal.mol<sup>-1</sup>, while that for SA is - 6.7 kcal.mol<sup>-1</sup>. However, this molecule is halogenated, being not a good choice because its environmental effects. Hence, for molecular dynamics the selected SA analogue was the second best 2-(1H-Tetrazol-5-yl)phenol, which presented a score of - 7.8 kcal.mol<sup>-1</sup>. Currently, the molecular dynamics tests are under way. A brief analysis of root mean square



fluctuation (RMSF) at active site residues for 10 ns showed an increase for Ser81 and a decrease for Asp210. Additionally, it was possible to observe an elevated number of hydrogen bonds at active site region for 10 ns.

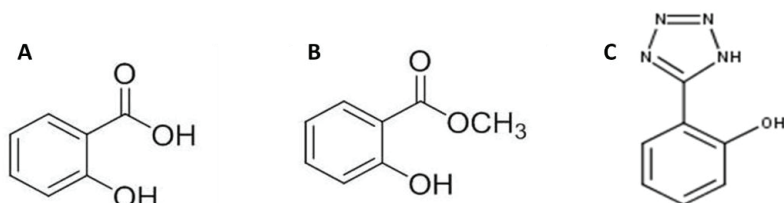


Figure 1. A. Salicylic acid. B. Methyl salicylate. C. 2-(1H-tetrazol-5-yl)phenol.

**Key-words:** Docking. Molecular dynamics. SABP2. Salicylic acid.

**Support:** This work has been supported by Centro Nacional de Supercomputação (CESUP), Conselho Nacional de Desenvolvimento Científico e Tecnológico (CNPq), Coordenação de Aperfeiçoamento de Pessoal de Nível Superior (CAPES) and Programa de Pós-Graduação em Química/UFRGS.

**References:**

- [1] Chen Z. et al., *Plant Signaling & Behavior* 4:6, 493-496 (2009).
- [2] Forouhar F. et al, *Proc. Natl. Acad. Sci.* 102, 5: 1773-1778 (2005).
- [3] Dennington R. et al, *GaussView, Version 4.1.* Shawnee Mission, KS: Semichem Inc. 11. (2007).
- [4] Marvin 5.12.3 EvaluationMode ChemAxon ([www.chemaxon.com/marvin/sketch/index.php](http://www.chemaxon.com/marvin/sketch/index.php)) (2013).
- [5] Frisch M.J. et al, *Gaussian 09, Revision A.1.* Wallingford, CT: Gaussian, Inc. 12. (2009)
- [6] Hendrickson W. A. J. *Synchrotron Rad.* 6, 845-851 (1999).
- [7] Trott O. & Olson A.J.J., *Auto-DockVina: improving the speed and accuracy of docking with a new scoring function, efficient optimization, and multithreading.* *Comput Chem.* 31:455-461 (2010).
- [8] Van Der Spoel D. et al, *GROMACS molecule & liquid database.* *Bioinformatics.* 28:752-753 (2012)



## H-S... $\pi$ interactions

Rabeshe Pereira Quintino (IC), Ricardo Gargano (PQ), João B. L. Martins (PQ)

*Address: Centered and Italic, Font: Tomes Roman 12pt*

**Abstract:** The hydrogen sulfide gas has an intense relationship with environmental chemistry and astrophysics. The alteration of the composition of atmosphere has as main factor from the human activities, by the increase of the concentration of some of its components and by the inclusion of other chemical species. These aspects make this gas of interest to various areas of science. [1] H<sub>2</sub>S events can be found in the oil and natural gas deposits, in the extraction of salt (sodium chloride), in groundwater, in sanitary sewers, and others. In industries, H<sub>2</sub>S comes from acid gas removal processes, effluent treatment, and also fermentation. The effects of this atmospheric pollution on the environment are observed in several regions of the Earth and, therefore, it is a subject of global relevance [2]. Therefore, it is extremely important to carry out studies of interaction processes between the chemical species that can be found in the atmosphere involving H<sub>2</sub>S.

To verify the interactions between dimers, especially the hydrogen bonding, computational calculations was carried out. More specifically, we studied the interactions of type HS ...  $\pi$ , and HS ... X, among which, H<sub>2</sub>S ... H<sub>2</sub>S, H<sub>2</sub>S ... NO, H<sub>2</sub>S ... CO, H<sub>2</sub>S ... CO<sub>2</sub>, H<sub>2</sub>S ... Benzene, H<sub>2</sub>S ... Phenol, H<sub>2</sub>S ... Chlorobenzene, H<sub>2</sub>S ... Nitrobenzene, H<sub>2</sub>S ... C<sub>2</sub>H<sub>2</sub> and H<sub>2</sub>S ... C<sub>2</sub>H<sub>4</sub>. For this purpose, the electronic structure program GAUSSIAN09 was used. Calculations were performed using the Density Functional Theory (DFT), using the B3PW91 functional, and the second-order Møller-Plesset perturbation theory (MP2). Allied to each method, we used the aug-cc-pVTZ basis function, and will be verified the influence of the base function when in the analysis of the hydrogen bond and other cooperative interactions. The Discrete Variable Representation (DVR) method was used to find the spectroscopic constants using the systems rovibrational energies.

### Results and Discussion

In order to investigate and understand how the interaction of the dimers occurs, their interaction energies were calculated at DFT and MP2 level. With this, the energies found showed a good correlation between the density functional B3PW91 and the MP2 reference. In addition, one of the significant properties in characterizing the formation of a hydrogen bond relates to the changing of the frequency of the vibrational stretching mode. The frequency calculation of the MP2 method obtained higher stretching frequencies, symmetrical and asymmetrical, when compared to the frequencies of the same complexes calculated with DFT. Different analyzes were used for the interaction energy, including basis size superposition error (BSSE) and zero point energy (ZPE). The highest interaction energy was found for the H<sub>2</sub>S-H<sub>2</sub>S dimer, with both methods.

### Final Remarks



It was concluded that the calculations of interaction energies of different complexes involving  $\text{H}_2\text{S}$  showed that the most stable is  $\text{H}_2\text{S}-\text{H}_2\text{S}$  dimer and that the B3PW91 density functional, in general, showed a good correlation with the MP2 reference. As for the spectroscopic constants, the DVR method calculations are not yet complete.

**Key-words:**  $\text{H}_2\text{S}$ , ab initio, dimers.

**Support:** This work has been supported by UnB, FAPDF, CNPq and CAPES.

**References:**

- [1] L. Remuzgo, G. Truelba, J. M. Sarabia, *Physica A*, 2016, 444, 146-157.
- [2] F. D. Meylan, V. Moreau, S. Erkman, *J. CO2 Utilization*, 2015, 12, 101-108



## Effect of counterion on the self-assembly of N-hydroxy alkyl ammonium surfactants

José Renan da Silva (IC), William D. A. B. da Silva (IC), Roberta P. Dias (PQ)

*Núcleo Interdisciplinar de Ciências Exatas e Inovação Tecnológica (NICIT), Centro Acadêmico do Agreste, UFPE, CEP: 55002-970 Caruaru, PE.*

**Abstract:** Surfactants are amphiphilic molecules and find application in almost every chemical industry, like as detergents, paints, cosmetics, pharmaceuticals and used for environmental protection [1]. This lack of applications is due their physicochemical properties that gives them the ability to promote aggregation and interaction with different interfaces [2,3]. Our goal is understanding how the nature of counterion change the properties of aggregation. In this study, we investigate how this important property of aggregation varies for cationic surfactants molecules of N,N-dimethyl-N-alkyl-N-(hydroxyethyl) ammonium salt (HEA<sup>+</sup>) with different counterions as fluoride, chloride, bromide and iodide using molecular dynamics (MD) simulations in explicit solvent. We also investigate the influence of head-group size, using HEA<sup>+</sup>, HBA<sup>+</sup>, HPA<sup>+</sup> The twelve systems were simulated for 200ns each. Computational simulations were performed using GROMOS 54a7 [3] force field and GROMACS program [4]. The results show that formation of the molecular aggregates is depend of the chemical nature of counterions, as can be seen in figure 1. Also, was observed that head-group size affect the shape of micelle. Details about protocols and others structural results will be presented and discussed during the conference.

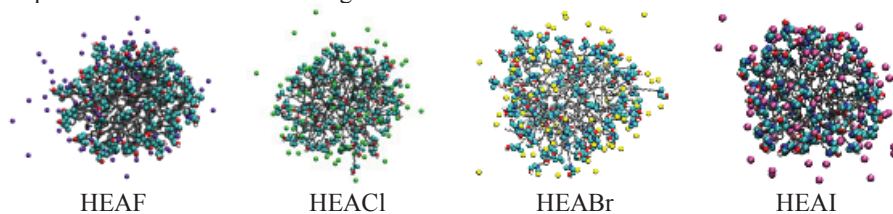


Figure 1: Structures of micelles after 200ns .

**Key-words:** Surfactants, Counterions, Molecular Dynamics.....

**Support:** This work has been supported by CNPq and FACEPE

**References:**

- [1] T. F. Tadros "Applied Surfactans" (2005), Wiley-VCH, Weinheim, Germany.
- [2] M. G. A. Da Silva, M. R. Meneghetti, A. Denicourt-Nowick, A. Roucoux, *RSC Adv.* **2014**, 4, 25875-25879.
- [3] J. A. Da Silva, R. P. Dias, G. C. A. Da Hora, T. A. Soares, M. R. Meneghetti. *J. Braz. Chem. Soc.* **2017** in press
- [4] Schmid, N.; Eichenberger, A. P.; Choutko, A.; Riniker, S.; Winger, M.; Mark, A. E.;



- Gunsteren, W. F. *Eur. Biophys. J.* **2011**, *40* (7), 843–856
- [5] Pronk, S.; Páll, S.; Schulz, R.; Larsson, P.; Bjelkmar, P.; Apostolov, R.; Shirts, M. R.; Smith, J. C.; Kasson, P. M.; van der Spoel, D.; Hess, B.; Lindahl, E. *Bioinforma.* **2013**, *29* (7), 845–854



## Energy and rovibrational spectroscopic constants for fullerenes dimers $(C_{20})_2$ , $(C_{24})_2$ , $(C_{36})_2$ , $(C_{60})_2$ , $(C_{70})_2$ and $(C_{84})_2$

Rodrigo A. L. Silva<sup>1</sup>, Daniel F. S. Machado<sup>2</sup>, Valter H. Carvalho-Silva<sup>1</sup>, Luciano Ribeiro<sup>1</sup>, Heibbe C. B. de Oliveira<sup>2</sup>, Demétrio Antônio da Silva Filho<sup>3</sup>

*Laboratório de Química Teórica e Estrutural de Anápolis, Universidade Estadual de Goiás, Anápolis, Brazil<sup>1</sup>*

*Laboratório de Estrutura Eletrônica e Dinâmica Molecular, Instituto de Química, Universidade de Brasília, Brasília, Brazil<sup>2</sup>*

*Instituto de Física, Universidade de Brasília, Brasília, Brazil<sup>3</sup>*

**Abstract:** Fullerenes have been studied both experimentally and theoretically for the last years. Several applications have been done, such as: in material science area [1], in the production or transportation of drugs [2], and to build up solar cells [3]. Nevertheless, there are only some small works reporting spectroscopic data of fullerenes dimers. The main goal of this work is to calculate the rovibrational energies and spectroscopic constants of fullerenes dimers  $(C_{20})_2$ ,  $(C_{24})_2$ ,  $(C_{36})_2$ ,  $(C_{60})_2$ ,  $(C_{70})_2$  and  $(C_{84})_2$ . To achieve this goal, we built up potential energies curves for the related systems and employed the Rydberg analytic function [4]. The spectroscopic constants were obtained employing the Dunham's [5] and the Discrete Variable Representation (DVR) methods [6]. The results found to the dissociation energy values  $D_e$  indicate that, in overall, these values increase as the carbon atoms number increase. Analysis by employing the Quantum Theory of Atoms in Molecules (QTAIM) [7] allowed us to verify that the fullerenes studied here, were stabilized by a non-covalent interaction.

**Key-words:** Fullerene dimers, Spectroscopic properties, QTAIM

**Support:** This work has been supported by CAPES.

### References:

- [1] S. Arshadi and F. Anisheh, *J. Sulfur Chem.* 0, 1 (2017).
- [2] I. Nierengarten and J. F. Nierengarten, *Chem. - An Asian J.* 9, 1436 (2014).
- [3] G. J. Zhao, Y. J. He, and Y. Li, *Adv. Mater.* 22, 4355 (2010).
- [4] William F. Sheehan, *J. Chem. Inf. Model.* 53, 1689 (1965).
- [5] J. L. Dunham, *Phys. Rev.* 41, 721 (1932).
- [6] J. J. S. Neto and L. S. Costa, *Brazilian J. Phys.* 28, 1 (1998).
- [7] R. F. W. Bader, *Chem. Rev.* 91, 893 (1991).

## Probing the antioxidant potential of phloretin and phlorizin through a computational investigation

Rodrigo A. Mendes<sup>1,2</sup>, Bruno L. S. Silva<sup>1</sup>, Renato G. Freitas<sup>1</sup>, and Gabriel L. C. de Souza

<sup>1</sup>*Departamento de Química, Universidade Federal de Mato Grosso, 78060-900 Cuiabá, Brazil*

<sup>2</sup>*Instituto de Química de São Carlos, Universidade de São Paulo, 13566-590 São Carlos, Brazil*

**Abstract:** Dihydrochalcones (DHCs) are a class of polyphenols that attract considerable attention for being used in the human diet as functional foods due to their pharmacological activity, including antioxidant, antibacterial, anti-inflammatory, antitumor, and antiviral properties [1]. In terms of antioxidant activity, it is well known that the potential of a given substance can be probed through its capability to scavenge free radicals by (mainly) the mechanisms of hydrogen-atom transfer (HAT) and single electron transfer (SET) [2,3]. In HAT, where an H-atom is transferred to a free radical, there is a strong dependence on the O-H bond dissociation enthalpy (BDE), since there will be higher antioxidant activity when there is a weaker O-H bond. The BDE (i.e., energy to break the O-H bond) is computed as the difference in the heat of formation between the neutral molecule (ArOH) and corresponding radical (ArO\*). On the other hand, in SET, a single electron is transferred from the molecule (ArOH) to the free radical. Clearly, the smaller the ionization potential (IP) for ArOH, the lower the energetic cost to abstract an electron.

Very recently, our group performed a computational study on two flavonols that were isolated from Loranthaceae family plant extracts: *kaempferol 3-O- $\alpha$ -L-arabinofuranosyl-(1 $\rightarrow$ 3)- $\alpha$ -L-rhamnoside* and *quercetin 3-O- $\alpha$ -L-arabinofuranosyl-(1 $\rightarrow$ 3)- $\alpha$ -L-rhamnoside* [4], which are glycosylated versions of kaempferol and quercetin, respectively. One of the goals of the previous study was to probe how much the presence of the sugar group would affect the values of BDEs and IPs. In the present work, we extend this idea to examining phloretin and its glycoside phlorizin (see Figure 1 for chemical structures).

In this work, the structures and energetics of phloretin and phlorizin were examined with density functional theory, using the B3LYP [5,6], M06-2X [7], and LC- $\omega$ PBE [8] functionals with both the 6-311G(d,p) and 6-311+G(d,p) basis sets [9]. Properties connected to antioxidant activity, i.e, bond dissociation enthalpies (BDEs) for OH groups and ionization potentials (IPs), were computed in a variety of environments including the gas-phase, *n*-hexane, ethanol, methanol, and water. All the computations were performed using the Gaussian 09 software suite [10].

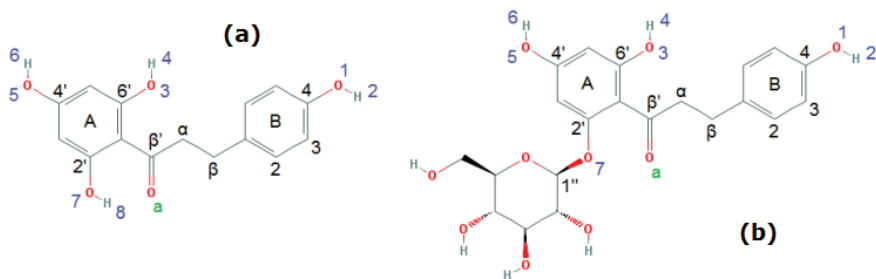


**Figure 1.** Representation of chemical structures, along with atom numbering for (a) phloretin and (b) phlorizin.

The smallest BDEs among the four OH groups for phloretin (three for phlorizin) were determined (using B3LYP/6-311+G(d,p) in water, for instance) to be 79.36 kcal/mol for phloretin and 79.98 kcal/mol for phlorizin while the IPs (at the same level of theory) were obtained as 139.48 and 138.98 kcal/mol, respectively. By comparing with known antioxidants, these values for the BDEs indicate both phloretin and phlorizin show promise for antioxidant activity. In addition, the presence of the sugar moiety has a moderate (0-6 kcal/mol depending on functional) effect on the BDEs for all OH groups. Interestingly, the BDEs suggest that (depending on the functional chosen) the sugar moiety can lead to an increase, decrease, or no change in the antioxidant activity. Therefore, further experimental tests are encouraged to understand the substituent effect on the BDEs for phloretin and to help determine the most appropriate functional to probe BDEs for DHCs. Additional results will be presented and discussed during the Conference.

**Key-words:** Antioxidant activity, dihydrochalcones, bond dissociation energy, ionization potential, density functional theory

**Support:** This work has been supported by CNPq.

#### References:

- [1] I. Fernandez-Pastor *et al.*, *J. Nat. Prod.* 79, 1737 (2016).
- [2] J. S. Wright *et al.*, *J. Am. Chem. Soc.* 123, 1173 (2001)
- [3] M. Leopoldini *et al.*, *J. Phys. Chem. A* 108, 4916 (2004).
- [4] G. L. C. de Souza *et al.*, *J. Mol. Model.* 22, 100 (2016).
- [5] A. D. Becke, *J. Chem. Phys.* 98, 5648 (1993).
- [6] C. Lee, W. Yang, and R. G. Parr, *Phys. Rev. B* 37, 785 (1988).
- [7] Y. Zhao and D. G. Truhlar, *Theor. Chem. Account.* 120, 215 (2006).
- [8] O. A. Vydrov and G. E. Scuseria, *J. Chem. Phys.* 125, 234109 (2006).
- [9] M. J. Frisch, J. A. Pople and J. S. Binkley, *J. Chem. Phys.* 80, 3265 (1984).
- [10] M. J. Frisch *et al.*, Gaussian Inc., Wallingford CT, G09, Revision D.01 (2009).

## Basis Functions Search for the Electronic Spectra Simulations of Polypyridyl Ruthenium Sensitizers Applied on DSSCs

Rodrigo Fraga de Almeida<sup>1</sup>, André Sarto Polo<sup>2</sup>, Luiz Antônio Sodré Costa<sup>1</sup>

<sup>1</sup>NEQC – Núcleo de Estudos em Química Computacional, UFJF – Universidade Federal de Juiz de Fora, Rua José Lourenço Kelmer, s/n, 36036-900, Juiz de Fora – MG, Brazil.

<sup>2</sup>POLO GROUP, UFABC - Universidade Federal do ABC, Avenida dos Estados, 5001, 09210-580, Santo André – SP, Brazil.

**Abstract:** Nowadays there is a great demand for clean energy once the fossil fuels reserves are limited and the use of these fuels pollute the atmosphere bringing negative effects to the planet. The dye-sensitized solar cells (DSSCs) appear to be a solution to this problem because of its low cost and high efficiency when compared to traditional silicon cells [1,2]. Many kinds of molecules may be used as dye or sensitizer in DSSCs, but from all kinds, the most investigated are the ruthenium(II) complexes. They show high chemical stability, intense absorption in a large interval of visible and extending to near infrared electromagnetic spectrum. The use of sensitizers having such characteristics result in DSSCs that exhibit high efficiency and favorable photo-electrochemical properties [3]. The ruthenium complexes studied here are the *cis*-[Ru(R<sub>2</sub>-phen)(dcbpy)(NCS)<sub>2</sub>], where dcbpy is 2,2'-bipyridine-4,4'-dicarboxylic acid and R<sub>2</sub>-phen is 1,10-phenanthroline with R substituents at the positions 4 and 7 [4, 5], an example is shown in figure 1a. Different substituents in these and other positions at the phenanthroline, change the complexes' photo-electrochemical properties, making them better or worse to be used in DSSCs [4, 5]. One of the properties of importance to apply a molecule as a dye in a DSSC, is the absorption of incident electromagnetic radiation with wavelength lower than 920 nm [6]. In this work is presented a computational study based on DFT using B3LYP functional and the basis functions developed by Barros *et al.* for ruthenium [7], only the basis set used for the ligands were changed, among them are 6-31G(d) and 6-31+G(d). These were tested intending to find a good methodology for UV-Vis spectrum simulation of the *cis*-[Ru(R<sub>2</sub>-phen)(dcbpy)(NCS)<sub>2</sub>] complexes, for R = H, CH<sub>3</sub>, Ph, cbz (carbazole). Figure 1b shows the experimental and simulated spectra (using 6-31G(d)) for the Ph substituent. The geometries were optimized in the gas phase and the TD-DFT calculation were done in

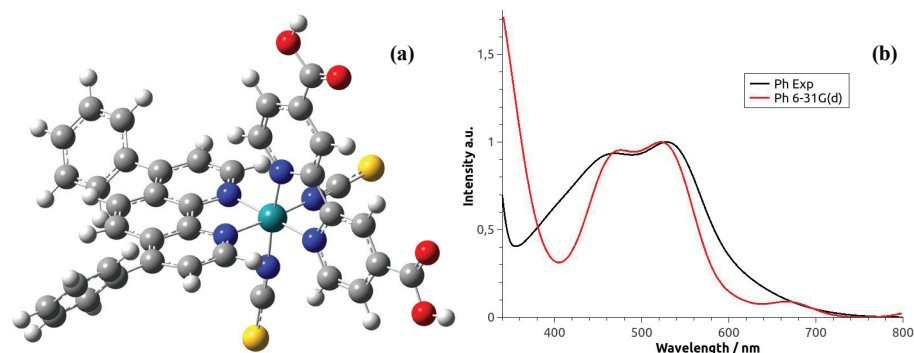


**Figure 1.** (a) DFT optimized structure of  $cis\text{-[Ru(Ph}_2\text{-phen)(dcbpy)(NCS)}_2\text{]}$ . (b) Comparison between experimental (black) and calculated (red) UV-Vis spectra.

**Key-words:** DSSCs, ruthenium(II) sensitizers, DFT, electronic spectra.

**Support:** FAPEMIG, FAPESP, CNPq

**References:**

- [1] B. O'Regan; M. Grätzel, *Nature*, 353, 737 (1991).
- [2] M. Grätzel, *Letters to Nature*, 414, 338 (2001).
- [3] A.M.M. Al-Alwani, *et al. Renewable and Sustainable Energy Reviews*, 65, 183 (2016).
- [4] A.V. Müller, *et al. RCS Advances*, 6, 46487 (2016).
- [5] R.N. Sampaio, *et al. ACS Applied Materials & Interfaces*, (2017).
- [6] M. Grätzel, *Journal of Photochemistry and Photobiology*, 4, 145 (2003).
- [7] C.L. Barros *et al. Molecular Physics*, 108, 1965 (2010).

## Theoretical study of the adsorption of alcohols on H-ZSM-5 zeolite

Authors: Rogério J. Costa<sup>1</sup> (PG), José R. S. Politi<sup>1</sup> (PQ), Elton A. S. Castro<sup>2</sup> (PQ), João B. L. Martins<sup>1</sup> (PQ)

Address: <sup>1</sup>Universidade de Brasília (UnB)  
<sup>2</sup>Universidade Estadual de Goiás (UEG)

Demand for energy and raw materials derived from non-renewable sources of energy such as coal, oil and natural gas has increased rapidly in recent years and has been fueling the search for alternatives to renewable sources [1]. Plastic, gasoline, rubber, paints and other materials can be produced from the catalytic alcohols dehydration on surfaces of adsorbents formed by oxides or aluminosilicates [1,2,3]. The main objective of this work is the theoretical study of the adsorption of methanol, ethanol, propanol and n-butanol in a specific pore of zeolite H-ZSM-5 (Figure 1 a-c). The calculations were performed with the Gaussian09 package using classical, semi-empirical and DFT methods in combinations with two different layers of theory through the ONIOM hybrid method.

**Key-words:** Adsorption, H-ZSM-5, alcohols, ONIOM

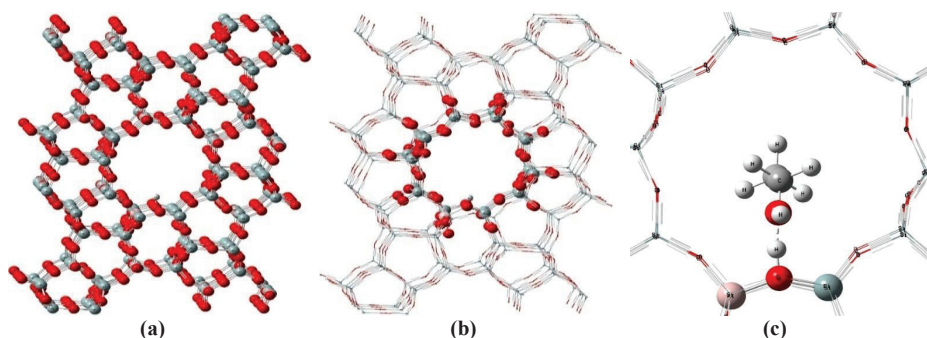


Figure 1. (a) H-ZSM-5 zeolite model, (b) specific pore e (c) Complex model of H-ZSM-5/alcohol.

The adsorbent and adsorbate models were optimized separately and together (cluster) for energy analysis. The results showed bond energy variation with the relaxation of the central pore tetrahedron of H-ZSM-5. The effect was more accentuated with the heavier alcohols for both the hybrid methods: ONIOM2-PM6/UFF and ONIOM2-DFT/UFF, as shown in Figure 2 (a) e (b), indicating that the the adsorption with the zeolite is dependent on the size of the alcohols.

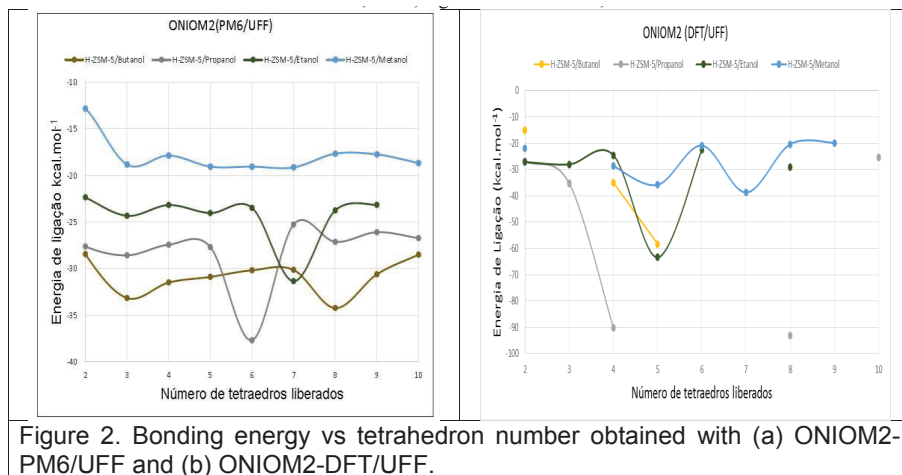


Figure 2. Bonding energy vs tetrahedron number obtained with (a) ONIOM2-PM6/UFF and (b) ONIOM2-DFT/UFF.

**Support:** This work has been supported by CNPq, CAPES, FAPDF

### References:

- [1] F. F. Madeira.; K. B. Tayeb.; L. Pinard.; H. Vezin.; S. Maurv. Applied Catalysis A, 443-444, (2012).
- [2] T. Maihom.; M. Probst.; J. Limtrakul. American Chemical Society. 118, 18564-18572, (2014).
- [3] M. J. Spencer. Prog. Mater. Sci. 57, 437-486, 2012.

## The role of hydrogen bonds and solvent effects on mechanical behavior of mortar coatings applied on the facades of structural masonry buildings

Rogério V. A. Jr (IC)<sup>1</sup>, Marcia K. D. L. Belarmino (PG)<sup>1</sup>, Nathan B. Lima (PG)<sup>2</sup>,  
Romilde A. Oliveira (PQ)<sup>2</sup>, Renan U. F. Ioras (PQ)<sup>3</sup>, and Nathalia B. D. Lima (PQ)<sup>1</sup>

<sup>1</sup> *Departamento de Química Fundamental, Universidade Federal de Pernambuco, 50740-540, Recife (PE), Brasil.*

<sup>2</sup> *Escola Politécnica, Universidade de Pernambuco, 50720-001, Recife (PE), Brasil.*

<sup>3</sup> *Fábrica BR Ind Pré-Moldados, 54490-130, Jaboatão dos Guararapes (PE), Brasil.*

**Abstract:** Mortar coatings applied on the facades of structural masonry buildings play an important role in the performance of vertical fences, and contribute to the waterproofing and protection of the external agents[1,2]. Routinely, the plastering mortar is employed for this purpose. It is also often employed a layer of roughcast mortar on the structural masonry before the use of the plastering mortar. In this sense, the main goal of our study was evaluated the role of the hydrogen bonds and the effect of the water as solvent to the mechanical behavior, experimentally measured, of the two strategies to apply the layer of plastering mortar on the structural masonry buildings: (i) with, and (ii) without an addition of the roughcast layer. The theoretical/computational methodology was the use of PM7 semiempirical method[3], which is available at quantum chemical software MOPAC 2016[4]. We considered the PM7 values of enthalpy of reaction,  $\Delta_rH$ , calculated both in the gas phase, and water solvent phase. The water solvent effects on the  $\Delta_rH$  property were calculated by the COSMO model[5]. The mechanical behavior experiments were based on tensile strength tests of two walls, each one with the mortar coatings proposed in this work. Both walls evaluated in this study were performed by using concrete blocks with compressive strength of 4 MPa. Experimental results indicate that in the two cases studied, the tensile strength tests were 0.56 MPa for the case with roughcast layer, and 0.57 MPa for case without roughcast layer, i. e., the roughcast layer, seemingly, not affect the tensile strength of the material. The mechanical behavior verified can be associated with the hydrogen bonds between components of the two types of mortar employed: calcium hydroxide and silicon dioxide. Our PM7 results indicating that energy of hydrogen bonds between  $\text{Ca}(\text{HO})_2$  and water are more pronounced than the energy of hydrogen bonds between the  $\text{SiO}_2$  and water. On average, the  $\Delta_rH$  PM7 value, in the gas phase, for the possibilities of hydrogen bonded complexes  $[(\text{calcium hydroxide})\cdots(\text{H}_2\text{O})_n]$ ,  $n=1$  or  $2$ , is  $-31$  kJ/mol. For the corresponding possibilities of hydrogen bonded complexes  $[(\text{silicon dioxide})\cdots(\text{H}_2\text{O})_n]$  this value is  $-20$  kJ/mol. When the solvent effect is considered, the  $\Delta_rH$  PM7 of  $[(\text{calcium hydroxide})\cdots(\text{H}_2\text{O})_n]$  hydrogen bonded complexes, in average, is  $-17$  kJ/mol, where the corresponding value of  $[(\text{silicon dioxide})\cdots(\text{H}_2\text{O})_n]$  hydrogen bonded



complexes is only -5 kJ/mol. In conclusion, being the calcium hydroxide the mainly component of plastering mortar, the enthalpy of the formation of hydrogen bonds, as well as the water effect in this property, seemingly, are associated with the mechanical behavior of tensile strength of this mortar when applied in the facades of structural masonry buildings.

**Key-words:** hydrogen bonds; semiempirical; mortar; roughcast; tensile strength.

**Support:** This work has been supported by CAPES, CNPq, and FACEPE(PRONEX).

**References:**

- [1] A. Corradi, Marco, Borri, Antonio and Vignoli, Experimental Evaluation of In-plane Shear Behaviour of Masonry Walls Retrofitted Using Conventional and Innovative Methods, *J. Br. Mason. Soc.* 21, 29–41 (2008).
- [2] A.I.N. Press, An assessment of facade coatings against colonisation by aerial algae and cyanobacteria, 42, 2555–2561 (2007).
- [3] J.J.P. Stewart, Optimization of parameters for semiempirical methods VI: more modifications to the NDDO approximations and re-optimization of parameters, *J. Mol. Model.* 19, 1–32 (2013).
- [4] J.J.P. Stewart, MOPAC2016 (Molecular Orbital PACKage). <http://openmopac.net/MOPAC2016.html> (accessed July 29, 2017).
- [5] A. Klamt, G. Schüürmann, COSMO: a new approach to dielectric screening in solvents with explicit expressions for the screening energy and its gradient, *J. Chem. Soc., Perkin Trans. 2*, 799–805 (1993).





# Painel 287 | PN.287

## Estudo da Fotólise da Acetanilida por métodos multiconfiguracionais

Roiney Beal(PG), Josene M. Toldo(PQ), Paulo F. B. Gonçalves(PQ)

nei\_beal@hotmail.com

Universidade Federal do Rio Grande do Sul, Instituto de Química, Grupo de Química Teórica. Av. Bento Gonçalves, 9500, Porto Alegre - RS

### Introdução

A acetanilida é uma importante molécula que serve como protótipo para o estudo da fotólise de toda uma classe de moléculas a qual pertence o paracetamol. Um fator que tornou a pesquisa da molécula tão interessante é a possibilidade de ocorrer um rearranjo Photo-Fries. O rearranjo de Photo-Fries (PFR – Photo-Fries Rearrangement) - uma conversão fotoquímica de ésteres e amidas em orto e para-hidroxi-fenonas - é um passo-chave na síntese de um grande número de compostos.

Estudos teóricos já realizados, conforme o modelo proposto por Toldo,<sup>1</sup> mostram que a PFR ocorre em um modelo de três estados, um estado de absorção com caráter  $1\pi\pi^*$ , um estado ré-dissociativo com caráter  $1n\pi^*$  e um estado dissociativo com caráter  $1\pi\sigma^*$ . No caso aqui estudado, a clivagem homolítica da ligação OC–N dá origem a um par de radicais carboxila e fenoxila. A recombinação subsequente conduz a amida de partida e a ciclo-hexadienona intermediária, que se tautomeriza para produzir os produtos rearranjados. O passo final é um deslocamento do hidrogênio, que pode prosseguir via tunelamento ou por rearranjo do solvente.

Através de métodos multiconfiguracionais, este estudo visa elucidar o mecanismo de dissociação da molécula.

### Metodologia

Os cálculos teóricos foram realizados utilizando o protocolo MS-CASPT2 // CASSCF, no qual as energias foram calculadas com *multi-state complete active space second-order perturbation theory* (MS-CASPT2) em estruturas otimizadas com *complete active space self-consistent field level* (CASSCF). Os pontos críticos (mínimos, estados de transição e interseção cônica) e as coordenadas de reação foram otimizados com um espaço ativo incluindo 14 elétrons em 12 orbitais e uma média de estados em três estados (SA3-CASSCF (14,12)). Os cálculos foram realizados utilizando o programa MOLCAS 8.

### RESULTADOS E DISCUSSÃO

A análise das coordenadas de reação relaxadas nos estados excitados calculados com MS-CASPT2 // CASSCF mostra que após a fotoexcitação, a dissociação ocorre

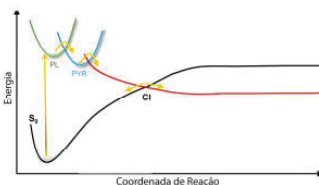




através do estado S1 envolvendo três estados. Um perfil de energia potencial esquemático que resume este modelo de três estados é mostrado na Figura 1. Ao longo das linhas contínuas, a distância de ligação OC-N é a principal coordenada de reação.

Durante a otimização de S1, foram encontrados dois mínimos. O primeiro (S1-PL) possui uma conformação planar da porção acetil, esse estado foi definido com estado de absorção. O segundo mínimo (S1-PYR) tem uma piramidalização significativa do átomo de carbono na porção acetil, deslocando o oxigênio para fora do plano molecular. Possui um estado definido com pré-dissociativo. O mínimo S1-PYR é 0,27 eV abaixo do mínimo S1-PL.

Conforme mostrado na figura ao lado, após o acesso a um estado de absorção, a molécula passa para um estado pré-dissociativo. Seguindo a coordenada de reação (em conformidade com outro estudo nesta área<sup>1</sup>) o sistema posteriormente acessa um estado dissociativo.



Uma intersecção cônica (IC) entre as superfícies dissociativas e S0 é encontrada próximo de 2 Å. Este cruzamento é uma característica já conhecida para essa classe de moléculas. Após a IC, os caminhos de reação são de duas maneiras, com um ramo retornando ao S0 e o outro ramo que segue a superfície dissociativa.

Ambos os estados pré-dissociativo e dissociativo foram investigados como ponto de partida para a quebra de ligação OC-N. Os perfis de energia potencial S1-relaxados mostram que a dissociação só é possível após o acesso ao estado pré-dissociativo.

## CONCLUSÃO

É possível concluir que a clivagem da ligação ocorre devido a uma interação de três estados eletrônicos: um  $1\pi\pi^*$  aromático, que absorve a radiação, um estado pré-dissociativo que transfere a energia eletrônica do anel aromático para a região dissociativa, e por último, um dissociativo, responsável pela clivagem homolítica. A transferência de  $1\pi\pi^*$  para pré-dissociativo é impedida por uma grande barreira de energia. Depois de acessado o estado dissociativo e atingindo uma interseção cônica, a molécula pode retornar a sua conformação original, dissociar ou formar intermediários que são precursores para PFR. Assim, estes três estados sempre controlarão a absorção, transferência de energia e os intermediários de dissociação no PFR.

**Keywords:** CASSCF, CASPT2, ACETANILIDA

**Suporte:** CAPES e CNPQ.

<sup>1</sup>Josene M. Toldo, Mario Barbatti, and Paulo F. B. Gonçalves, *A three-state model for the Photo-Fries rearrangement*, Phys. Chem. Chem. Phys. **2017** Jul 26; 19(29):19103-19108



## Title: Theoretical investigations of nonlinear optical properties of two heterocyclic chalcones.

Authors: Rosemberg Fortes Nunes Rodrigues, Ricardo Rodrigues Ternavisk, Adailton Neres De Castro, Márcio José Dias, Clodoaldo Valverde.

Address: *Campus de Ciências Exatas e Tecnológicas, Universidade Estadual de Goiás, BR 153, km 98, 75.132-903 Anápolis, GO, Brazil.*

**Abstract:** The emergence of the Optoelectronics together with the discovery in the decade of 60 of a new area of research named Molecular Modeling, stimulated the development of new materials whose properties provide its employment in the context of the Optoelectronics. We studied properties of the structure geometry, molecular electrostatic behavior and the nonlinear optical properties of the centrosymmetric heterocyclic chalcones (E)-1-(5-methylfuran-2-yl)-3-(5-methylthiophen-2-yl)prop-2-en-1-one (3) and the noncentrosymmetric heterocyclic chalcone (E)-1-(5-Chlorothiophen-2-yl)-3-(thiophen-2-yl)-2-propen-1-one (7), to provide insights of their linear and nonlinear optical properties in the static and dynamic cases. A new approach treating the supermolecule is employed in combination with an interactive electrostatic system in which the atoms of neighboring molecules are considered as point charges. The ab initio computational results of (hyper) polarizabilities are derived from an iterative process and confirm these crystals as good candidates for photonic devices, such as optical switches, modulators, pyrazoline derivatives and optical energy applications.

**Key-words:** Electrical Properties, Electrostatic iteration, Supermolecule approach.

**Support:** The authors would like to thank the following Brazilian agencies for financial support: Conselho Nacional de Desenvolvimento Científico e Tecnológico (CNPq), Coordenação de Aperfeiçoamento Pessoal de Nível Superior (CAPES) and Fundação de Apoio à Pesquisa do Estado de Goiás (FAPEG).

### References:

- [1] A. N. Castro, F.A.P. Osório, R.R. Ternavisk, H.B. Napolitano, C. Valverde, B. Baseia, *Chem. Phys. Lett.* 681, 110 (2017).
- [2] SPACKMAN, M. A.; MUNSHI, P.; JAYATILAKA, D. The use of dipole lattice sums to estimate electric fields and dipole moment enhancement in molecular crystals. *Chemical physics letters*, Elsevier, v. 443, n. 1, p. 87-91, 2007.
- [3] C. Valverde, R.F.N. Rodrigues, D.F.S. Machado, B. Baseia, H.C.B. de Oliveira, J. *Mol. Model.* 23, 122 (2017).
- [4] RODRIGUES, R. F. et al. Solid state characterization and theoretical study of nonlinear optical properties of a uoro-n-acylhydrazide derivative. *PloS one*, Public Library of Science, v. 12, n. 4, p. e0175859, 2017.



[5] Liew Suk Ming , Jozaizulfazli Jamalis, Helmi Mohammed Al-Maqtari, Mohd Mustaqim Rosli , Murugesan Sankaranarayanan , Subhash Chander , Hoong-Kun Fun , Syn-thesis, Characterization, Antifungal Activities and Crystal Structure of Thiophene-based Heterocyclic Chalcones, Chemical Data Collections (2017).



## Title: Adsorption of CO<sub>2</sub>-C<sub>3</sub>H<sub>8</sub> mixtures on Na-ZSM-5: a molecular simulation study

Authors: Sarah Arvelos, Thalles S. Diógenes, Lucienne L. Romanielo

Address: Av. João Naves de Ávila, 2121, Bloco 1K, Faculdade de Engenharia Química, Universidade Federal de Uberlândia, Faculdade de Engenharia Química, Bloco K, CEP 38408-144, Uberlândia, MG, Brazil.

**Abstract:** Zeolite crystals with cations present, such as Na-ZSM-5, are widely used for gas sequestration, and separation process. One possible application is as an adsorbent to separate CO<sub>2</sub> from propane (C<sub>3</sub>H<sub>8</sub>) in petrochemical industry. This separation by zeolites is a defying research topic, because there are size and polarizability differences between the molecules. In literature, it is reported experimentally inverse shape selectivity in adsorption of this mixture on Na-ZSM-5 [1].

In this work, molecular simulations (GCMC) were performed to evaluate the equilibrium of adsorption of CO<sub>2</sub>/C<sub>3</sub>H<sub>8</sub> pure and binary mixtures on Na-ZSM-5 zeolite.

The crystalline structure of Na-ZSM-5 was built by replacing Si atoms with Al atoms (obeying Lowenstein's rule) starting from an all-silica zeolite structure (silicalite-1) obtained in the literature [2]. The Si/Al ratios desired were 15 and 60. The cations Na<sup>+</sup> were inserted on the structure by canonic (NVT) simulations. The parameters used to represent the oxygen on the rigid framework was found on the work of June, Bell and Theodorou [3] and Makrodimitris et al.[4] and the parameters associated to the Na<sup>+</sup> were based on Calero work [5].

In order to carry out the simulations, we identified in the literature suitable models for describing the gases in the bulk phase. CO<sub>2</sub> molecule was treated by a three site rigid model (TraPPE[6]) that account the intrinsic quadrupole moment using partial charges. For the C<sub>3</sub>H<sub>8</sub>, the TraPPE model [7] already was select, in which the molecules are treated by a discharged united atom representation.

The potential energies associate with different sites were tuned aiming to represent experimental equilibrium isotherms.

Non-bonded interactions  $U(r_{ij})$  are modeled using pairwise-additive potentials consisting of Lennard-Jones (LJ) 12-6 and Coulomb's law [8]:

$$U(r_{ij}) = 4\epsilon_{ij} \left[ \left( \frac{\sigma_{ij}}{r_{ij}} \right)^{12} - \left( \frac{\sigma_{ij}}{r_{ij}} \right)^6 \right] + \frac{1}{4\pi\epsilon_0} \frac{q_i q_j}{r_{ij}}$$

During the development of the work, we tested the influence of partial charges of the extraframework cations on the correct representation of experimental data. Comparing the adsorption of CO<sub>2</sub> on silicalite-1 and Na-ZSM-5 (both zeolites have MFI framework), it is clear the electric field created by the sodium cation distribution strongly increase the adsorption of the CO<sub>2</sub>.



Our results showed that the force field presented depicts well the isotherms studied. The magnitude of the potential energies associated with different sites on cationic zeolite suggest there are a polarization effect on propane when these molecules are in mixtures with CO<sub>2</sub> on Na-ZSM-5.

**Key-words:** Adsorption, GCMC, separation, ZSM-5

**Support:** This work has been supported by FAPEMIG. We thank the funding agency for their financial assistance.

### References:

- [1] G. Calleja, J. Pau, J.A. Calles, S. Al, *J. Chem. Eng. Data.* 43, 994 (1998).
- [2] D.H. Olson, G.T. Kokotailo, S.L. Lawton, W.M. Meier, *J. Phys. Chem.* 85, 2238 (1981).
- [3] R.L. June, A.T. Bell, D.N. Theodorou, *J. Phys. Chem.* 94, 1508 (1990).
- [4] K. Makrodimitris, G.K. Papadopoulos, D.N. Theodorou, *Macromolecules.* 105, 777 (2001).
- [5] E. García-Pérez, I.M. Torrén, S. Lago, D. Dubbeldam, T.J.H. Vlught, T.L.M. Maesen, B. Smit, R. Krishna, S. Calero, *Appl. Surf. Sci.* 252, 716 (2005).
- [6] J.J. Potoff, J.I. Siepmann, *AIChE J.* 47, 1676 (2001).
- [7] M.G. Martin, J.I. Siepmann, *J. Phys. Chem. B.* 102, 2569 (1998).
- [8] D. Frenkel, B. Smit, "Understanding molecular simulation: from algorithms to applications"(2002), Academic-Press, San Diego-CA, USA.



## Probing the effect of sugar substitution on the antioxidant-related properties of flavonols

Shawan K. C. Aldeida<sup>1</sup>, Rodrigo A. Mendes<sup>1</sup>, and Gabriel L. C. de Souza<sup>1</sup>

<sup>1</sup>*Departamento de Química, Universidade Federal de Mato Grosso, 78060-900 Cuiabá, Brazil*

**Abstract:** In the recent past, our group did accomplish a computational investigation on two flavonols that were isolated from Loranthaceae family plant extracts: *kaempferol 3-O- $\alpha$ -L-arabinofuranosyl-(1 $\rightarrow$ 3)- $\alpha$ -L-rhamnoside* and *quercetin 3-O- $\alpha$ -L-arabinofuranosyl-(1 $\rightarrow$ 3)- $\alpha$ -L-rhamnoside* [1], which are glycosylated versions of kaempferol and quercetin, respectively. Among the goals of the referred study was to probe how much the presence of the sugar group would affect the values of bond dissociation enthalpies (BDEs) and ionization potential (IPs) when in comparison with the parent molecules. The BDEs and IPs are important energetic properties in order to investigate the antioxidant potential of a given compound, since they are connected to the hydrogen-atom transfer (HAT) and to the single electron transfer (SET) mechanisms, respectively [2,3]. In the present work, the ideas initiated in de Souza *et al.* [1] were taken further and an investigation on the antioxidant-related properties of *myricetin 3,4'-di-O- $\alpha$ -L-rhamnopyranoside* (which is a *myricetin* doubly substituted with the *rhamnopyranoside* moiety) was performed. The structures of the *myricetin 3,4'-di-O- $\alpha$ -L-rhamnopyranoside* and its parent molecule is shown in Figure 1.

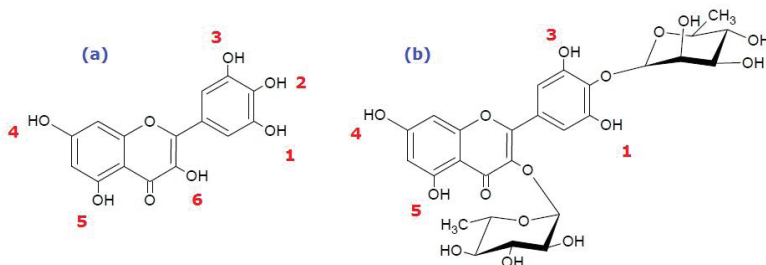


**Figure 1.** Representation of the chemical structures: (a) *myricetin* and (b) *myricetin 3,4'-di-O- $\alpha$ -L-rhamnopyranoside*. OH group numbering is given in red.

The geometries of the neutral molecules and their radicals were optimized (using default convergence criteria) using density functional theory (DFT) with the B3LYP exchange-correlation functional [4,5]. All optimizations were carried out without the inclusion of symmetry constraints. Computations for open-shell species were undertaken with the unrestricted formalism UB3LYP. The 6-311+G(d,p) basis set [6] was utilized. Vibrational frequencies were computed to characterize the conformations as minima, to evaluate the zero-point energy corrections, and to determine

thermodynamic quantities (at 298 K). Solvent effects were included using the integral equation formalism polarizable continuum model for *n*-hexane, methanol, ethanol, and water. All computations were performed with the Gaussian 09 software suite [7].

The BDEs and IPs determined in the gas phase and water are presented in Table 1.

OH group	<i>myricetin</i>				<i>myricetin 3,4-di-O-alpha-L-rhamnopyranoside</i>			
	BDE		IP		BDE		IP	
	gas phase	water	gas phase	water	gas phase	water	gas phase	water
<b>1</b>	74.99	72.93	162.04	146.58	83.41	81.31	161.11	135.99
<b>2</b>	66.52	64.29			---	---		
<b>3</b>	74.92	72.83			79.50	80.84		
<b>4</b>	86.60	87.18			87.06	86.84		
<b>5</b>	90.49	95.06			97.38	91.95		
<b>6</b>	78.12	82.21			---	---		

**Table 2.** BDE and IP (given in kcal.mol<sup>-1</sup>) for *myricetin* and *myricetin 3,4-di-O-alpha-L-rhamnopyranoside* computed at the B3LYP/6-311+G(d,p) level of theory.

The computed BDEs for *myricetin* have OH group **2** as the smallest followed by groups **3**, **1**, **6**, **4**, and **5**, respectively, indicating that the hydroxyl **2** would be primarily responsible for its antioxidant activity. In the *myricetin 3,4-di-O-alpha-L-rhamnopyranoside* compound, there are no hydroxyl groups **2** and **6** available due to the substitution; for this compound, BDEs order are **3** < **1** < **4** < **5**. This behavior can be observed for results determined in both gas phase and water. The presence of the substituent leads to an increase in all the BDEs values (except to the groups **4** and **5** computed in water). Hence, the antioxidant activity would be decreased with the inclusion of the *rhamnopyranoside* moiety.

The IPs values present a decrease (more pronounced in water) when the *myricetin* is substituted. However, the IPs are approximately double the BDEs and, thus, the antioxidant activity through the SET mechanism is unlikely to happen. The complete set of results will be presented in the Conference.

**Key-words:** Antioxidant activity, substituent effect, bond dissociation energy, ionization potential, density functional theory

**Support:** This work has been supported by CNPq.

#### References:

- [1] G. L. C. de Souza *et al.*, J. Mol. Model. 22, 100 (2016).
- [2] J. S. Wright *et al.*, J. Am. Chem. Soc. 123, 1173 (2001).
- [3] M. Leopoldini *et al.*, J. Phys. Chem. A 108, 4916 (2004).
- [4] A. D. Becke, J. Chem. Phys. 98, 5648 (1993).
- [5] C. Lee, W. Yang, and R. G. Parr, Phys. Rev. B 37, 785 (1988).
- [6] M. J. Frisch, J. A. Pople and J. S. Binkley, J. Chem. Phys. 80, 3265 (1984).
- [7] M. J. Frisch *et al.*, Gaussian Inc., Wallingford CT, G09, Revision D.01 (2009).

## Theoretical study of the molecular fragmentation mechanism of the hybrid $\delta$ -FeOOH/PMMA

Authors: Silviana Corrêa<sup>1</sup>, Telles C. Silva<sup>1</sup>, Máira S. Pires<sup>1</sup>, Livia C. T. Lacerda<sup>1</sup>, Elaine F. F. da Cunha<sup>1</sup>, Teodorico C. Ramalho<sup>1</sup>

Address: <sup>1</sup>Laboratory of Molecular Modeling, Chemistry Department, Federal University of Lavras, Lavras/MG

**Abstract:** The organic-inorganic hybrid materials are synthesized using an organic phase comprised of polymers and an inorganic phase which may be a variety of materials, such as metal nanoparticles, oxide nanoparticles, nanotubes or clays. The synthesis of these materials with optimized properties constitutes an area in constant expansion, with potential application in the area of catalysis and chemical sensors [1,2]. The use of magnetic materials, to synthesize inorganic organic hybrids with polymer matrix and developed to explore as physical and chemical properties. The polymers may be shaped to allow inorganic particles to be incorporated. Hybrids based on poly(methylmethacrylate) - PMMA and iron oxides have been studied in recent years, especially with magnetic iron oxides. The magnetic properties are guaranteed only if they are found in a maximum dispersion of iron oxide in the polymer matrix, PMMA is considered a good dispersant of magnetite nanoparticles. Among iron oxide oxides, feroxyhyte ( $\delta$ -FeOOH) attracted particular attention to its stability in biochemical media. Due to its superparamagnetic properties, it is a potentially interesting material to be used in modern medicine. Despite its great importance, detailed computational and experimental work on this subject soon appeared [1,3]. Thus, this work aims to propose and understand the mechanism of molecular fragmentation of the hybrid  $\delta$ -FeOOH/PMMA using theoretical calculations. The theoretical study used the ADF package with the DFT method, the functional density PBE. The set of functions of the Slater type TZP. The computations performed for the fragmentation mechanism of the  $\delta$ -FeOOH/PMMA hybrid are described in Figure 1. According to the experimental data using the PMMA-maghemite hybrid, the order of loss intensity of the fragments is:  $\text{COH}^+ > \text{CH}_3^+ > \text{CO}_2\text{CH}_3^+$ . However the order of stability found by theoretical calculations was  $\text{CH}_3^+ > \text{COH}^+ > \text{CO}_2\text{CH}_3^+$ . The activation energy ( $\Delta E$ ) for  $\text{COH}^+$  was  $56 \text{ kcal.mol}^{-1}$  higher than that of  $\text{CH}_3^+$ . In comparison to  $\text{CO}_2\text{CH}_3^+$ , the difference of  $\Delta E$  is  $119 \text{ kcal.mol}^{-1}$  and  $175.29 \text{ kcal.mol}^{-1}$ , respectively. The order of theoretical stability found showed good agreement with previously published experimental studies. Thus, the kinetic control can occur in the process of  $\delta$ -FeOOH/PMMA fragmentation.

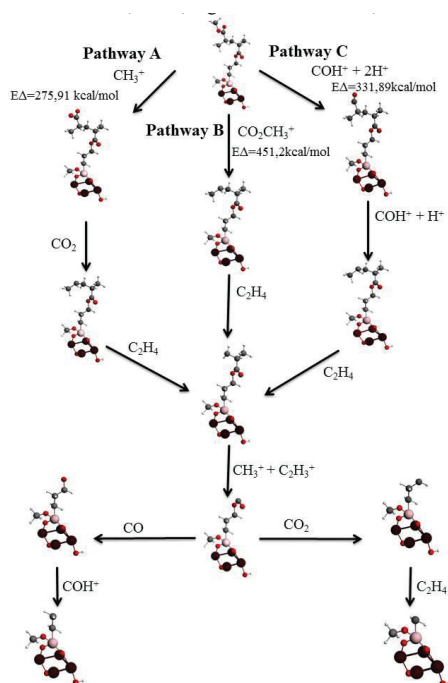


Figure 1: Fragmentation mechanism of  $\delta$ -FeOOH/PMMA hybrid.

Through the theoretical calculations it was possible to predict and propose a mechanism of fragmentation for the material. Allowing to discuss the best pathways of formation of the fragments and the chemical factors that influence the losses.

**Key-words:** DFT, PMMA, Feroxyhyte, fragmentation mechanism

**Support:** This work has been supported by CAPES, CNPq and UFLA.

#### References:

- [1] S. Corrêa et al. J. Nanomaterials, 2016, 2462135 (2016).
- [2] J.C. Colmenares, E. Kuna. Molecules, 22, 790 (2017).
- [3] M. V. J. Rocha et al. Spectrochim. Acta - Part A Mol. Biomol. Spectrosc., 117, 276–283 (2014).



## Molecular Dynamics Simulations of a new family of Glycoside Hydrolase (GH-X)

Authors:

Sinkler Tormet G.<sup>a</sup>, Erica T. Prates<sup>a</sup>, Fabrício Bracht<sup>a</sup>, Pedro Avellar Costa<sup>b</sup>, Camila Ramos dos Santos<sup>b</sup>, Murakami Mario T.<sup>b</sup>, Munir S. Skaf<sup>a</sup>

<sup>a</sup> *Institute of Chemistry, University of Campinas # UNICAMP, Cx.P. 6154, Campinas, SP 13083-970, Brazil*

<sup>b</sup> *Laboratorio Nacional de Biociências, Centro Nacional de Pesquisas em Energia e Materiais, Campinas, SP, Brazil*

### Abstract:

Glycoside Hydrolases (GH) are enzymes that play important roles in the hydrolysis of glycosidic bonds during the degradation of biomass in complex sugars such as cellulose, hemicellulose and amylases [1]. Consequently, the structural characterization of these enzymes is considered highly valuable for the second generation ethanol processes due to the close relationship with the sugar degradation process [2]. The use of molecular dynamics techniques to study the properties of the substrate and the catalytic residues have been essential to determine enzymatic properties that cannot be easily or impossible to study from in vivo or in vitro experimental methodologies [3]. In this study, molecular dynamics simulations were performed in order to obtain trajectories and evolution of the residues that form the catalytic side of a new glycoside hydrolase family (GH-X).

**Key-words:** Molecular Dynamics, Glycoside Hydrolases, Trajectories.

**Support:** This work has been supported by CAPES 330030, FAPESP: 20173/08293-7.

### References:

- [1] A. A. Shvartsburg, M. F. Jarrold, *Chem. Phys. Lett.*, 261, 86 (1996).
- [2] Chundawat, S. P. S., Beckham, G. T., Himmel, M. E. & Dale, B. E. *Annu. Rev. Chem. Biomol. Eng.* 2, 121-45 (2011)
- [3] Sandgren M., Stahlberg J., Mitchinson C. "Structural and biochemical studies of GH family 12 cellulases: improved thermal stability and ligand complexes". *Prog. Biophys. Mol. Biol.* 89: 246-291 (2005)

## Ruthenium(II) Polypyridine Complexes: Photophysics and Electrochemistry

Taís Christofani, Willian R. Rocha

*LQC-MM (Laboratório de Química Computacional e Modelagem Molecular)  
Departamento de Química, ICEX, Universidade Federal de Minas Gerais, Belo Horizonte 31270-901, MG, Brazil*

**Abstract:** Since the report in 1972 by Gafney and Adamson [1] of the electron-transfer quenching of the triplet charge-transfer excited state of  $[\text{Ru}(\text{bpy})_3]^{2+}$ , the interest in the study of the photochemistry of ruthenium polypyridine complexes has increased. Luminescent properties of Ru(II) polypyridine complexes are related to their lowest excited states energy, as well as the orbital nature of these states. The energy of the excited states depends on the field-strength of the ligands, the redox properties of the metal and the ligands, and other intrinsic properties of the ligands [2]. Thus, luminescent characteristics of the complexes can be controlled by choice of the ligands. In the present work, the effect of different ligands on the structural, electronic and spectroscopic properties of  $[\text{Ru}(\text{bpy})_2\text{L}]^{2+}$  complexes (where L = phen: 1,10-phenanthroline, hat: 1,4,5,8,9,12-hexaazatriphenylene, dppz: dipyrido[3,2-a:2',3'-c]phenazine, bpz: 2,2'-bipyrazine, and tap: 1,4,5,8-tetraazaphenathrene) in gas phase and water solvent have been investigated by means of combined DFT/TD-DFT calculations. CDA and EDA analysis showed the complexes with L = bpy, phen and dppz are the ones with a stronger Ru-L bond and also the ligands that present stronger  $\pi$ -acceptor character, while the others are stronger  $\sigma$ -donors. The absorption spectra of the complexes were obtained and they all exhibit MLCT absorption bands between 350-450 nm and LC transitions in the ultraviolet region. However, the MLCT bands in the complexes with L = bpy, phen and dppz are red-shifted in comparison with the other ones and, in general, water also induces a red-shift of the spectral bands. Characterization of the first excited states of the complexes is in progress, as well as their emission spectra.

**Key-words:** ruthenium, polypyridine, photophysics, photochemistry, luminescence.

**Support:** This work has been supported by CNPq, Capes, INCT Catalise and FAPEMIG.

### References:

- [1] Gafney, H. D.; Adamson, A. W. J. Am. Chem. Soc. 1972, 94 (23), 8238–8239.
- [2] Juris, A.; Balzani, V.; Barigelletti, F.; Campagna, S.; Belser, P.; von Zelewsky, A. Coord. Chem. Rev. 1988, 84, 85–277.

## Optimally Tuned Functional Methods as a Way of Improvement in the Description of Optical and Electronic Properties of Phthalocyanines Complexes

Authors: Tamires Lima Pereira, Luciano Almeida Leal, Luiz Antônio Ribeiro Junior, Demétrio Antônio da Silva Filho

*Address: University of Brasilia, Institute of Physics, 70.919-970, Brasilia, Brazil*

**Abstract:** Organic compounds, such as metallophthalocyanines (MePc) have emerged as important candidates to be used as active materials in numerous applications. Several studies have addressed the impact of the position of the central metal atom relative to the organic cage of the phthalocyanine (Pc) and the possibility of exploiting it in numerous applications. We have employed the Density Functional Theory (DFT) to examine the structural, electronic and optical properties of MePc. Due to issues associated with multi-electron self-interaction errors of the conventional functionals, we use long-range corrected functionals, where the range separation parameter is tuned for each structure and the characteristic lengths ( $1/\omega$ ) depend on the chemical nature and size of the system [1]. We analyze the first absorbing excited state energy for the various molecules investigated in this study. We can conclude that the energy of this state in both the molecules have values next comparing the values obtained with X-Ray geometries and the optimized geometry. We show the orbital energies of the highest three occupied orbitals and lowest three unoccupied molecular orbitals, both using the X-Ray and optimized geometries [2]. The HOMO→LUMO energy are very comparable in all the molecules studied. Another important result that this work presents is the optimization of  $\omega$  parameter. Implementing the optimized  $\omega$  on DFT methodologies, the results are improved on this job.

**Key-words:** Long Range Correction optimization, DFT, X-Ray geometries, Phthalocyanines

**Support:** This work has been supported by University of Brasilia, FAP-DF, CNPq and CAPES.

**References:**

- [1] J-D. Chai, H-Gordon, *The Journal of Chemical Physics* 128 (2008) 84106.
- [2] The Cambridge Crystallographic Data Centre (CCDC).

# THE ROLE OF CHARGE TRANSFER IN THE TWO-PHOTON ABSORPTION CROSS SECTION

Tárcius N. Ramos<sup>1</sup>, Daniel L. Silva<sup>2</sup>, Sylvio Canuto<sup>1</sup>

<sup>1</sup>*Instituto de Física da USP*

<sup>2</sup>*Departamento de Ciências da Natureza, Matemática e Educação da UFSCAR-Araras*

**Abstract:** The two-photon absorption process is often more efficient when the transition shows higher charge transfer during the electronic excitation [1]. The interactions with different environments can tune the two-photon absorption cross section (TPACS) related with an electronic transition [2]. The aim of this work is to obtain insights of the effects of charge transfer transitions in the TPACS and to evaluate the efficiency of the two-level model (TLM) compared with the quadratic response theory (RES). Quantify the amount of charge transfer is possible using ground and excited electronic densities [3]. To control the amount of charge transfer in an electronic transition we use a static electric field. Changing the intensity of the field is possible to mimic the electrostatic effects of solvents with different polarities [4]. The TPACS and the charge transfer of the pyridinium-N-phenolate organic molecule is studied in this work. To compute the structural effects, the minimum energy geometry is obtained for the isolated molecule and in the presence of the electric field. Our results show that intense fields induce large charge transfer and large TPACS. These results are more evident when the structure is re-optimized in the presence of the field, showing twice more charge transfer and four times larger TPACS than the results obtained without any field. The TPACS obtained with the TLM shows better agreement with the RES results when larger amount of charge transfer is observed. For an amount of 0.35e of charge transfer, the TLM obtains 41% of the RES value and for 0.8e, the TLM value is 60% of the RES value. The knowledge of the relation between the amount of the charge transfer and the TLM efficiency is important to perform theoretical predictions with lower computational costs.

**Key-words:** two-photon absorption, charge transfer, solvent effects, betaine

**Support:** This work has been supported by grant 2015/14189-3 from São Paulo Research Foundation (FAPESP), CNPq, CAPES and INCT-FCx.

**References:**

- [1] X. He, B. Xu, Y. Liu, Y. Yang and W. Tian. *J. Appl. Phys.*, 111, 53516 (2012).
- [2] M. Johnsen and P. R. Ogilby, *J. Phys. Chem. A*, 112, 7831 (2008).
- [3] T. Le Bahers, C. Adamo and I. Ciofini, *J. Chem. Theory Comput.*, 7, 2498 (2011).
- [4] I. D. L. Albert, T. J. Marks and M. A. Ratner, *J. Phys. Chem.*, 100, 9714 (1996).

## Theoretical Investigation of the Biginelli Reaction Mechanism: When Knoevenagel is a Possible Mechanism Pathway

Tatiane Nicola Tejero, Arthur Eugen Kümmerle, Glauco F. Bauerfeldt

*Departamento de Química, Instituto de Ciências Exatas, Universidade Federal Rural do Rio de Janeiro, Rodovia Br km 7, Seropédica, RJ, Brasil*

**Abstract:** Multicomponent reactions (MCR) have received great attention in organic synthesis and medicinal chemistry, since they allow the design of new molecules and pharmaceuticals, in special, with great structural complexity and excellent yields. [1] In the Biginelli reaction, the reactants are an aldehyde, a  $\beta$ -ketoester and urea or thiourea leading to a myriad of dihydropyrimidinones/thiones. From the possible combinations of the reactants, three reaction pathways can be expected: the Knoevenagel pathway, the iminium ion pathway and the enamine pathway, being the second pointed out, from both experimental and theoretical works with common aromatic and aliphatic  $\beta$ -ketoesters, as the most probable initiation route. [2] However, if a coumarin  $\beta$ -ketoester derivative is used, the Knoevenagel pathway seems to prevail. [3] In order to understand the differences between these reaction pathways, this work has been proposed aiming to the calculations of the possible reaction paths in the coumarin  $\beta$ -ketoester + benzaldehyde + urea MCR and to the understanding of the contribution of the coumarin nucleus in the  $\beta$ -ketoester moiety for the changes in the reaction mechanism. Calculations have been performed at different theoretical levels. First, the semiempirical PM6 method has been adopted and stationary points, including saddle points and several proposed intermediates, have been located. Geometry optimizations have been then performed at the Density Functional Theory (DFT) level, adopting the M06-2X, B3LYP and BHandHLYP functionals and the 6-31+G(d,p) basis set. The former has been chosen, since literature points out this functional as the most suitable for describing reaction thermochemistry and kinetics of organic species, [4] whereas the B3LYP and BHandHLYP functionals have been chosen for comparison (B3LYP is still the most used functional worldwide and the BHandHLYP functional is similar, differing in the coefficients of the exchange terms). Based on the initial guess, provided from the PM6 calculations, stationary points have been located for the three reaction channels at the different DFT levels. From our calculations, the stationary points with lower relative energies belong to the Knoevenagel reaction path. All reaction pathways are initiated with the formation of an ion-dipole pre-barrier complex, stabilized by 27 – 35 kcal mol<sup>-1</sup> (relative to the isolated protonated reactants). The calculated barrier height for the reaction between the coumarin  $\beta$ -ketoester + benzaldehyde (which initiates the Knoevenagel channel) is -18.10 kcal mol<sup>-1</sup> (relative to the isolated protonated reactants). For the enamine and iminium ion pathways, barrier heights are 6.21 kcal mol<sup>-1</sup> and -16.27 kcal mol<sup>-1</sup>, respectively (the enamine pathway is initiated from the coumarin  $\beta$ -



ketoester + urea reaction and the iminium ion is initiated from the urea + benzaldehyde reaction). Therefore, the barrier height of the first step in the Knoevenagel pathway is *ca.* 24 and 2 kcal mol<sup>-1</sup> lower than the barrier heights of the first step in the enamine and iminium ion pathways, respectively. The reaction product in the Knoevenagel pathway is also the most stabilized (30.63 kcal mol<sup>-1</sup> below the isolated protonated reactants, while the products in the enamine and iminium ion pathways are located, with respect to the isolated reactants, at 5.85 and -25.04 kcal mol<sup>-1</sup>, respectively). The second step in all pathways is the dehydration, and barrier heights and reaction energy differences are -12.36 and -20.46, 23.93 and 3.10 and -2.77 and -12.21 kcal mol<sup>-1</sup> (Knoevenagel, enamine and iminium ion, respectively). The final steps concern the addition of the third reactant, and the intermediates and transition states belonging to the Knoevenagel pathway remain the lowest energy structures. Thus the Knoevenagel pathway is finally attributed as the lowest energy pathway in this complex mechanism for the coumarin  $\beta$ -ketoester + benzaldehyde + urea MCR. No great differences in these trends or conclusions have been observed by changing the theoretical level. The Knoevenagel intermediate has been experimentally detected, [3] and such previous observation can be justified from our theoretical calculations. As compared to other intermediates, the Knoevenagel intermediate is the most stabilized, being *ca.* 25 and 10 kcal mol<sup>-1</sup> below the enamine and iminium ion intermediates, respectively. Similar calculations have been performed for the  $\beta$ -ketoester + benzaldehyde + urea MCR, where the  $\beta$ -ketoester nucleus is either a methyl, a phenyl or a 4-OH-phenyl group. For all these reactions, the iminium ion channel has been shown to prevail from all other channels, as previously described in the literature, indicating that the coumarin group plays a distinct role. These results satisfactorily compare to the experimental observations and demonstrate that the coumarin nucleus in the  $\beta$ -ketoester moiety promotes the change of the mechanism initiation from the iminium ion to the Knoevenagel pathway.

**Key-words:** Multicomponent Reaction, Biginelli Reaction, Knoevenagel intermediate

**Support:** FAPERJ and CAPES

**References:**

- [1] M. V. Marques, *et al.* Química Nova 35, 8, 1696 (2011)
- [2] R. O. M. A. de Souza, *et al.* Chem. Eur. J. 15, 9799 – 9804 (2009)
- [3] F. Vitória, *et al.* New J. Chem. 39, 2323-2332 (2015)
- [4] N. Chéron, *et al.* Phys. Chem. Chem. Phys. 14, 7170-7175 (2012)



## ***De novo* design of novel *Mycobacterium tuberculosis* pantothenate synthetase inhibitors**

Taylane da Silva Araújo<sup>1</sup>, Manoelito Coelho S. Junior<sup>1</sup>, Raquel G. Benevides<sup>1</sup>.  
<sup>1</sup>Programa de Pós-Graduação em Biotecnologia, Universidade Estadual de Feira de Santana. *Laboratório de Modelagem Molecular, Av. Transnordestina, s/n - Novo Horizonte, Feira de Santana - Bahia, 44036-900.*  
[araujotaylane@gmail.com](mailto:araujotaylane@gmail.com)

Tuberculosis is infectious disease with 10.4 millions new cases reported per year [1]. The major concern of this disease are the multidrug resistant (MDR) and extensively resistant (XDR) strains, modifying the treatment, last up to 20 months and have 60-75% efficacy [2]. Therefore there is a need to identify new drugs for the tuberculosis treatment [3], in this scenario the enzyme pantothenate synthetase (PS) is an excellent therapeutic target for *Mycobacterium tuberculosis*, since the importance of the enzyme (which is related to the virulence and persistence of the pathogen) has already been proven by the knockout of the panC gene [4]. In order to identify possible inhibitors for PS, an in silico ligand- structure-based *de novo* design. The theoretical molecules was design by two different methods using the web serve E-Lead3D [5] and LigBuilder2.0 software [6] (Figure1). For the E-Lead3D, besides information related to structure, 11 inhibitors were extracted for the ChEMBL and used as template molecule (Tanimoto Coefficient > 0.8). With this method 550 molecules were design. LigBuilder2.0 uses the active site cavity properties (hydrophobic access, HBond donor and HBond acceptors, surface and volume) for the design of the molecules. This method generated 6,282 molecules. Then, all the theoretical molecules created were together submitted to alignment in the screening using pharmacophore model, using the model constructed on other assay of our working group [7]. This model has 9 pharmacophore features, a hydrogen donor center, three acceptor centers and five hydrophobic centers. 458 molecules filtered by pharmacophore model ( $4.49 < QFIT < 40.4$ ) were submitted to molecular docking using DOCK 6.8 software. The protein (PDB ID 4MUH) was prepared in the CHIMERA 10.1, the docking parameters was analyzed by redocking (RMSD value) from the crystallographic ligand. The RMSD = 1,63 Å indicates docking success in repositioning the ligand in protein active site. The molecules were order by number according to Grid Score function. The top ranked molecule is show in Figure 2A, similarity analysis in ZINC15 database (TC<0.9) showed no correspondence match. This molecule forms hydrogen bond observed between carbonyl groups of the ligand and residues Gln69, Gln161 and Ser193. In addition, another hydrogen interaction occurs between the ether group of the molecule and the N-terminal portion of Met37; Hydrophobic interactions between the aliphatic portions of the ligand and the side chains of the residues Pro35, Val139, Phe70 and Leu143, and between the aryl ring of the molecule and the Lys57 side chain; Two salt bridges are observed with one of the carbonyls of the ligand and residues Arg195 and Lys157;  $\pi$ -stacking T-shaped

interaction at the His41 also between the ring aryl. The techniques *de novo* design used in this study show promising because this molecule has inhibitory properties against PS and no similar results have been found in the ZINC15 database, suggesting to be an unpublished molecule.

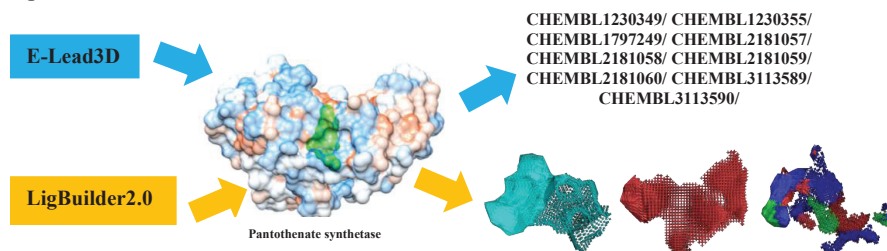


Figure 1: Construction strategy of E-Lead3D tools, using 11 inhibitors (ChEMBL code) as template and LigBuilder2.0 using surface (blue), volume (red) and donor centers HBond (blue), HBond acceptor (red) and hydrophobic (green) of the active site.

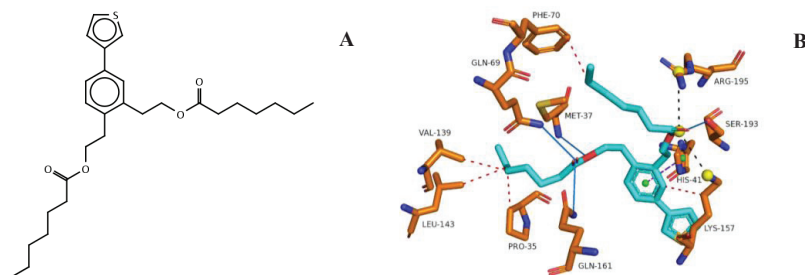


Figure 2: (A) Top ranked molecule by molecular docking. (B) Map of the intermolecular interactions between the top ranked molecule (cyan) and the active site residues of the enzyme (orange). Blue lines - hydrogen bond; Pink dashed lines - hydrophobic interactions; Black dashed lines - salt bridge and Lilac dashed line -  $\pi$ -stacking T-shaped interactions.

**Key-words:** Tuberculosis, pantothenate synthetase, *de novo* design, pharmacophoric modeling, docking.

**Support:** PPGBiotech/UEFS and CAPES was financial support this work.

#### References:

- [1]WHO- World Health Organization, Global tuberculosis report 2016. WHO Report 2016.
- [2]K.D. Green, S. Garneau-tsodikova. *Front. in microb.*, 4, 1(2013).
- [3]C. Lienhardt et al. *J. of Infec. Dis.*, 205, 241(2012).
- [4]V. K. Sambandamurthy et al. *Nat. Med.*, 8, 1171(2002).
- [5]D Douguet. *Nuc. Ac. Res.*, 38, 615 (2010).
- [6]Y. Yuan,J. Pei, L. Lai. *J. of Chem. Inf. and Mod.*, 51, 1083 (2011).
- [7]T. R. S. Carvalho. *Anais XX SEMIC UEFS* (2016).

## Oxidative insertion and activation of the C-H bond of methane by niobium oxides $\text{NbO}_m^{n+}$ ( $m=1, 2$ ; $n=0, 1, 2$ )

Authors: Telles Cardoso Silva<sup>1</sup> (PG), Silviana Corrêa (PG), Máira dos Santos Pires<sup>1</sup> (PG), Livia Clara Tavares Lacerda<sup>1</sup> (PG), Alexandre Alves de Castro<sup>1</sup> (PG), Teodorico de Castro Ramalho<sup>1</sup> (PQ).

*Department of Chemistry, Federal University of Lavras, 37.200-000, Lavras - MG - Brazil*

**Abstract:** Transition metal oxides are considered as prototype models of reactions involving oxidative processes [1]. In this way, the detailed understanding of their electronic and molecular structure is of great interest in the prediction of their catalytic behavior and chemical reactivity toward inert organic molecules which are of industrial interest. In particular, it is possible to highlight the selective oxidation of methane to methanol by transition metal oxides in the gas phase [2]. Therefore, the present computational study intends to evaluate the efficiency of niobium oxides in the methane activation process. Optimization and frequencies calculations were performed using relativistic effective pseudopotentials (ECPs) for transition metals at B3LYP and CCSD (T) levels. For the oxygen and carbon atoms, an extended polarized basis set of 6-311++G(d, p) type was employed. Binding analyzes were performed using the Bader's Theory of Atoms in Molecules (AIM) and Natural Bond Orbitals (NBO) calculations. All calculations were performed in the Gaussian 09 program, with the exception of the AIM calculations that were performed in the AIM2000 program. Posteriorly, the oxidative insertion mechanism of the niobium oxides for the methane binding was investigated; analyzing all the possibilities of molecular precursors, transition state and reaction products. The reaction intermediates and transition states were characterized by vibrational frequency calculations. According to our results, there is a decrease in bonding lengths over the series of monoxides and dioxides. The calculated vibrational frequencies are in good agreement with the experimental values for the Niobium oxides [3]. According to the NBO calculations, a greater contribution is observed for the 4d orbital in the chemical bonds of the monoxide and 5s for the dioxide. According to the AIM calculations, the Bond Critical Point (BCP) is located at the center of the niobium oxides binding; the AIM parameters found point to an ionic and partial covalent character of the bonds of these oxides. The initial electrostatic interaction between methane and niobium oxides based on binding energy values is favored by the increase of oxo-coordinated ligands at the metal center and by the increase of their charge. The oxidative insertion energies of the niobium oxides at the C-H bond of methane are shown in Table 1.

**Table 1.** Activation barriers ( $\Delta E_{\text{act}}$ ) and reaction energies ( $\Delta E_{\text{reaction}}$ ) in kcal/mol for the oxidative insertion of niobium oxides at the C-H bond of methane.

Species	$\Delta E_{\text{act}}$		$\Delta E_{\text{reaction}}$	
	B3LYP	CCSD(T)	B3LYP	CCSD(T)
NbO	23.68	25.81	-28.12	-27.41
NbO <sup>+</sup>	37.86	40.55	-15.62	-17.76
NbO <sup>2+</sup>	50.20	50.61	-10.11	-13.27
NbO <sub>2</sub>	31.80	33.01	-29.85	-32.62
NbO <sub>2</sub> <sup>+</sup>	49.96	51.13	-21.68	-22.98
NbO <sub>2</sub> <sup>2+</sup>	63.96	65.18	-13.59	-15.01

The activation barrier results indicate that the increase in the number of oxo-coordinated ligands at the metal center does not favor the kinetics of the methane activation. As regards the thermodynamics of the reaction, it can be observed that the reaction of niobium oxides with methane is exothermic. The theoretical results indicate that the kinetics of the methane activation processes is not favored due to the increase of oxo-coordinated ligands to the metal. Among the oxides investigated, NbO<sup>2+</sup> shows better thermodynamic and kinetic conditions to react with methane in the gas phase.

**Key-words:** Niobium Oxides, Methane, Theoretical Calculations, Catalytic Effects

**Support:** This work has been supported by DQI-UFLA, CAPES

#### References:

- [1] J. Roithova, D. Schoder, Chem. Rev. 110, 1170 (2010).
- [2] H. Schwarz, K. Eller, Chem. Rev. 91, 1121 (1991).
- [3] G. Ang, S. Lai, M. Chen, J. Phys. Chem. A. 109, 9514 (2005).

## The Quantum Description of Halogen Bonds *via* a Generalized Empirical Potential

Lucas A. Santos, Daniela R. Silva, Elaine, F. F. da Cunha and Teodorico C. Ramalho  
*Department of Chemistry, Federal University of Lavras, Campus Universitário, Lavras-MG, Brazil*

**Abstract:** The Halogen Bonds are crucial to understand phenomena in several fields of science [1]. Recent works have shown strong evidences that non-classical interactions overcome simple electrostatic interactions supported by the  $\sigma$ -hole model [2,3]. Despite of an accurate description of the electronic effects in Halogen Bonds be needed, large systems are still a great challenge to electronic structure methods. In this perspective, we have proposed a new empirical potential designed to perceive the real nature of the Halogen Bonds under subtly modifications in the traditional empirical potentials [3,4].

The models in Figure 1 were used as training set to parameterize the new empirical potential. Our findings have shown that the orbital interactions are, in fact, predominant to minimize the steric repulsion [3]. Furthermore, we have shown that even with electrostatic repulsion, the interaction energies can be stronger in contrast to the  $\sigma$ -hole model predictions [3].

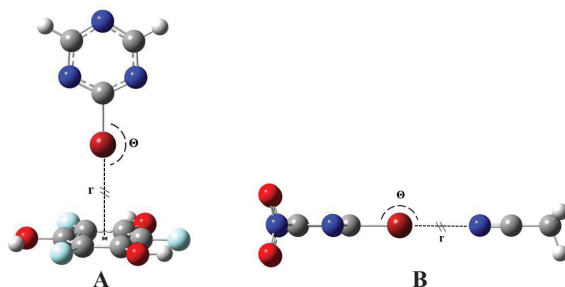


**Figure 1.** Structural models of  $2\text{-XY}\cdots\text{ArZW}$  and  $2\text{-XY}\cdots\text{NC}_2\text{H}_3$  interactions:  $2\text{-Br\_ArF}_3(\text{OH})_3$  (A) and  $2\text{-BrNO}_2\text{-NC}_2\text{H}_3$  (B).  $\Theta$  is the interaction angle and  $r$  is the interaction distance. X = Br, Cl and F; Y =  $\text{NO}_2$ ,  $\text{NH}_2$  and H; W and Z = OH, F and H.

In the current work, a new empirical potential has been developed to describe Halogen Bonds, considering the F, Cl and Br atoms, in function of the quantum parameters  $\delta$  and  $\gamma$ , as showed in equation (1) [3]. A crucial factor to design  $E_{mod}$  was to show the straight relationship between the maximum ESP value on  $\sigma$ -Hole ( $V_{max}$ ) and the energies of LUMOs that contains the  $\sigma^*_{\text{C-X}}$  orbital. This feature has allowed us to build parameters in function of  $V_{max}$  to describe the orbital interactions (eq. 2 and 3), that were the main responsible to lead the Halogen Bonds [3]. In (2),  $\beta$  is an empirical constant depending on the halogen bond acceptor and  $\alpha$  is the van der Waals radii of the halogen.

$$E_{mod} = \varepsilon \left\{ \left( \frac{r_e + \delta \cos \theta / 6}{r} \right)^{10} - 2 \left( \frac{r_e}{r + \gamma} \right)^6 \right\} \quad (1)$$

$$\delta = \frac{\beta V_{max}}{4\pi\alpha^3} \quad (2)$$

$$\gamma = \left[ \frac{2^{2-\delta}(1-\delta)}{25r} \right] \quad (3)$$

The new empirical potential  $E_{mod}$  have also demonstrated a great performance to describe systems in and out of the training set [3]. The traditional force fields have bad predictions on the equilibrium distances and interaction energies, mainly at low range situations (Figure 2). The PES showed in Figure 2 prints the  $E_{mod}$  behavior in contrast to the whole UFF and QM plots. In this scenario, we believe this study will be helpful to improve the force fields description of large systems containing Halogen Bond.

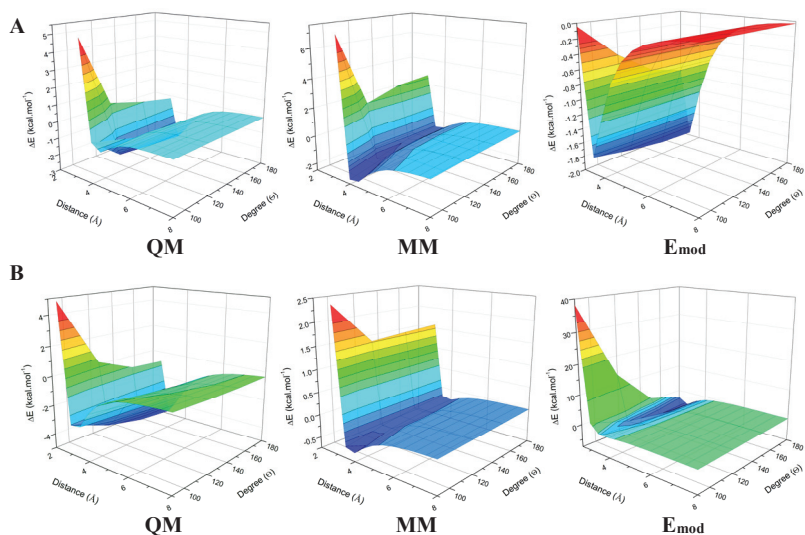


**Figure 2.** Potential Energy Surfaces of 2-Br...Ar (A) and 2-BrNO<sub>2</sub>...NC<sub>2</sub>H<sub>3</sub> (B) interactions calculated by B3LYP-D3BJ/aug-cc-pVTZ (QM), UFF (MM) and  $E_{mod}$  (eq. 1).

**Key-words:** Halogen Bonds, Force Fields, Empirical Potentials.

**Support:** This work has been supported by FAPEMIG, CAPES and CNPq.

**References:**

- [1] G. Cavallo, P. Metrangolo, R. Milani, T. Pilati, A. Priimagi, G. Resnati, G. Terraneo, *Chem. Rev.*, 116, 2478 (2016).
- [2] L. P. Wolters, P. Schyman, M. J. Pavan, W. L. Jorgensen, F. M. Bickelhaupt, *Wiley Interdiscip Rev Comput Mol Sci*, 4, 523 (2014).
- [3] L. A. Santos, E. F. F. da Cunha, T. C. Ramalho, *J. Phys. Chem. A*, 121, 2442 (2017).
- [4] L. A. Santos, E. F. F. da Cunha, M. P. Freitas, T. C. Ramalho, *J. Phys. Chem. A*, 118, 5808 (2014).

## Structural determination of polyphenols by quantum mechanical calculations of $^{13}\text{C}$ NMR chemical shifts: development of a parameterized protocol using a set of chalcones

Authors: Thaís Forest Giacomello,<sup>a</sup> Rênica Alves de Moraes Rocha,<sup>a</sup> Antonio Maia de Jesus Chaves Neto,<sup>b</sup> Gunar Vingre da Silva Mota<sup>b</sup> Fabio Luiz Paranhos Costa,<sup>\*a</sup>

1. Address: <sup>a</sup>Departament of Chemistry, Federal University of Goiás, REJ Jataí 75801-615, Brasil.
2. <sup>b</sup>Natural Science Faculty, Federal University of Pará, ICEN UFPA Belém 66075-110, Brasil

**Abstract:** Polyphenols are one of the most important and certainly the most numerous among the groups of phytochemicals present in the plant kingdom, e.g., chalcones, curcumines, phenolic acids, stilbenoids etc [1]. Chalcone derivatives are found widespread in natural products [2]. This class of compounds is considered as key precursors for flavonoid and isoflavonoid syntheses [2]. They have several biological activities including anti-inflammatory, anti-leishmania, antimetabolic and antiviral are some few examples of their broad range of action etc [2]. Herein, we present the development of a protocol for determination of polyphenols structures, using a set of 13 chalcones (totaling more than 200 chemical shifts,  $\delta$ ) with different substitution pattern, whose structures have been reliably elucidated in literature [3-5]. This protocol consists of GIAO-DFT calculations of  $\delta$  (mPW1PW91/6-31G\*\*//mPW1PW91/6-31G\*) and application of a scaling factor based on a linear regression. The  $\delta$  are obtained as  $\delta_{\text{calc}} = \sigma_{\text{TMS}} - \sigma$ , where  $\sigma_{\text{TMS}}$  is the isotropic shielding constant of the reference compound, tetramethylsilane (TMS), calculate at the same level of theory. The scaling factor was generated by plotting calculated ( $\delta_{\text{calc}}$ ) against experimental chemical shifts of the set of chalcones. Thus, slope (a) and intercept (b) values obtained from this linear regression can be used to generate scaled chemical shifts ( $\delta_{\text{scal}}$ ), using the expression  $\delta_{\text{scal}} = a \cdot \delta_{\text{calc}} \pm b$  (1). Thus, using a set of 13 chalcones the following equation was generated:  $\delta_{\text{scal}} = 1.051 \cdot \delta_{\text{calc}} - 0.870$ ,  $r^2 = 0.989$ . Due to their great conformational flexibility, the set of 13 chalcones as well as 2',6'-dihydroxy-4',4'-dimethoxy-dihydrochalcone [5] and 2-[3-(1,3-benzodioxol-5-yl)propyl]-5-methoxyphenol [6], i.e. the test molecules, were submitted to randomized conformational searches using Monte Carlo method and MMFF force field. For complete conformational analysis and the conformers selection protocol see Giacomello *et al.* [7]. All quantum mechanical calculations were performed in gas phase, using Gaussian 09 software package [8]. For the chalcone set, the Mean Absolute Deviation (MAD) and the Root Mean Square Deviation (RMSD), in ppm, before and after (in parenthesis) the application of the equation (1) are: MAD = 5.84 (2.71) and RMS = 6.61 (3.86). Finally, the robustness of the new protocol and its applicability to others



polyphenols class were evaluated by the calculation of the  $\delta$  for 2 natural compounds with synthesis, biological and therapeutic interest: 2',6'-dihydroxy-4,4'-dimethoxy-dihydrochalcone (dihydrochalcone) (**I**) and 2-[3-(1,3-benzodioxol-5-yl)propyl]-5-methoxyphenol (diarylpropane) (**II**), figure 1. For these molecules the MAD and the RMSD, in ppm, before and after (in parenthesis) the application of the equation (1) are: (**I**) MAD = 4.66 (1.14); RMS = 5.21 (1.81) and (**II**) MAD = 4.94 (1.65); RMS = 5.44 (2.38). Considering a set of 13 chalcones with different substitution pattern, we developed a parameterized protocol for the calculation of  $^{13}\text{C}$  NMR chemical shifts of polyphenols. This protocol, consisted of GIAO-DFT calculations and a linear scaling factor, was able to yield calculated chemical shifts with satisfactory accuracy. Therefore, the calculation protocol developed in this work is a very attractive tool as an alternative to more computationally demanding approaches for the calculation of polyphenols, such as dihydrochalcones and diarylpropanoids.

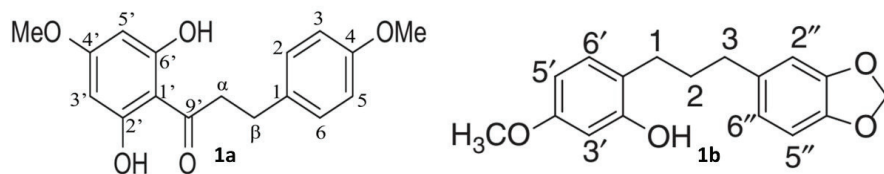


Figure 1. 2',6'-dihydroxy-4,4'-dimethoxy-dihydrochalcone (**1a**) and 2-[3-(1,3-benzodioxol-5-yl)propyl]-5-methoxyphenol (**1b**) molecules.

**Key-words:** GIAO-mPW1PW91/6-31G\*/mPW1PW91/6-31G\*, NMR, polyphenols, chalcones.

**Support:** This work has been supported by Fundação de Amparo à Pesquisa do Estado de Goiás.

**References:**

1. N. R. Perron; J. L. Brumaghim, *Cell Biochem. Biophys.* 53, 75 (2009).
2. P. Singh; A. Anand; V. Kumar, *Eur. J. Med. Chem.* 85, 758 (2014).
3. F. L. P. Costa, P. F. Gomes; A. K. Silva; L. M. Lião, *J. Braz. Chem. Soc.* 00, 1-6 (doi:10.21577/0103-5053.20170062) (2017).
4. C. Díaz-Tielas; E. Graña; M. J. Reigosa; A. M. Sánchez-Moreiras *Planta Daninha*, 34, 607 (2016).
5. P. K. Agrawal, "Carbon-13 NMR of Flavonoids. Studies in Organic Chemistry, v. 34" (1989), Elsevier, Amsterdam. The Netherlands.
6. K. S. Francis; E. Suresh; M. S. Nair, *Nat. Prod. Res.*, 28, 1664 (2014).
7. T. F. Giacomello; R. A. de M. Rocha; A. M. de J. C. N.; G. V. Da S. Mota; F. L. P. Costa, *Adv. Sci. Eng. Med.* 9, x, (2017), accepted.
8. A. E. Frisch; M. J. Frisch; G. Trucks, *Gaussian 09, Revision D.01, User's Reference*, Gaussian Inc., Pittsburgh, USA (2009).



## Estudo teórico do estado iônico da molécula do HCFC-133a

Thayana Maria Lopes de Lima, Railton Barbosa de Andrade, Elizete Ventura do Monte, Silmar Andrade do Monte

[thayana\\_jp@hotmail.com](mailto:thayana_jp@hotmail.com)

**Abstract:** Um dos grandes problemas ambientais é o fenômeno do buraco na camada de ozônio, o qual está relacionado a inúmeras causas, dentre elas os gases nocivos emitidos na atmosfera, como exemplo os CFCs, que mais tarde foram substituídos pelos HCFCs, de acordo com o Protocolo de Montreal. Tais substâncias podem ser uma das fontes de cloro atômico na alta atmosfera, que em um processo catalítico interfere no ciclo natural do ozônio, provocando a destruição deste gás [1,2]. Compreender a fotodissociação dos HCFCs é relevante para o entendimento de seu comportamento na atmosfera superior, mais precisamente na camada de ozônio, que é a responsável por proteger a vida na Terra. Estudo recente sobre a fotodissociação do 2-cloro-1,1,1-trifluoroetano (HCFC-133a) indica a existência de uma provável estrutura de mínimo na curva do 3° estado excitado referente à saída do cloro [3]. Para a molécula  $\text{CH}_3\text{Cl}$  foi comprovada a existência de uma

estrutura estável no 3° estado excitado, a qual apresenta como característica um ligação de hidrogênio  $\text{H}\cdots\text{Cl}$ , responsável pela formação do íon cloreto como fotoproduto da dissociação da ligação  $\text{C}-\text{Cl}$  [4]. Diante do que foi exposto, este trabalho consiste em caracterizar a estrutura que representa o estado iônico da molécula HCFC-133a. Para a caracterização deste estado iônico foram realizados cálculos single point a nível MCSCF, MR-CISD e MR-CISD+Q, juntamente com a otimização de geometria e cálculos de frequência nos dois primeiros níveis, com a base aug-cc-pVDZ e o programa COLUMBUS [5]. Os orbitais representados na Figura 1 foram utilizados na realização dos cálculos. Analisando o comprimento de ligação  $\text{C}-\text{H}$  próxima do cloro, constatou-se que para o método MR-CISD (1,213 Å) houve um aumento comparado ao método MCSCF (1,168 Å). Já para a ligação  $\text{H}\cdots\text{Cl}$  houve uma diminuição, de 1,786 Å (MCSCF) para 1,737 Å (MR-CISD). Foi comprovada a existência de uma estrutura de mínimo em ambos os métodos a partir dos cálculos de frequência. Parte da caracterização pode ser compreendida analisando os dados elencados na Tabela 1, a qual contém os valores da energia de excitação vertical obtida com os métodos MCSCF e MR-CISD e com a base aug-cc-pVDZ. Os pesos das principais configurações foram

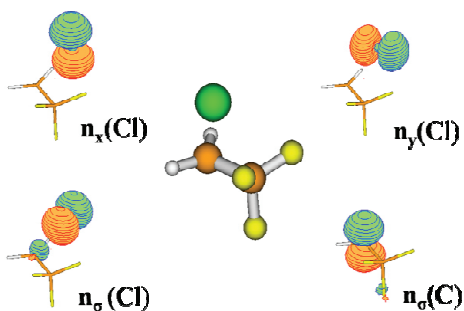


Figura 1: Estrutura do complexo intermediário e orbitais.



maiores que 0,73 (ver Tabela 1). Os estados  $S_1$  e  $S_2$  possuem configurações em que os elétrons apenas se reagrupam nos orbitais  $n_x(\text{Cl})$ ,  $n_y(\text{Cl})$  e  $n_z(\text{Cl})$ . Para o estado  $S_3$ , em que ocorreu uma transição eletrônica entre os orbitais  $n_\sigma(\text{C})$  e o  $n_\sigma(\text{Cl})$ , observamos uma variação considerável (de 0,79 eV) quando comparamos os valores de energia de excitação vertical obtidas com os métodos MCSCF e MR-CISD. A correção de Davidson provocou uma diminuição adicional na energia de excitação vertical de 0,42 eV para  $S_3$ . Esses resultados foram observados tanto na geometria obtida com MCSCF quanto com a geometria MR-CISD. Logo, os efeitos de correlação dinâmica e de extensividade são bem maiores para  $S_3$  do que para os outros estados.

Tabela 1: Energias de excitação vertical (eV) na geometria do estado iônico, juntamente com os pesos das principais configurações (entre parênteses).

Estado	Configurações	Geometria MCSCF/aug-cc-pVDZ			Geometria MR-CISD/aug-cc-pVDZ		
		MCSCF	MRCISD	MRCISD+Q	MCSCF	MRCISD	MRCISD+Q
$S_0$	$(n_x(\text{Cl})^2 + (n_y(\text{Cl})^2 + (n_z(\text{Cl})^2 + (n_\sigma(\text{Cl})^1 + (n_\sigma(\text{C})^1$	0,00 <sup>a</sup> (0,99)	0,00 <sup>b</sup> (0,99)	0,00 <sup>c</sup>	0,00 <sup>d</sup> (0,99)	0,00 <sup>e</sup> (0,84)	0,00 <sup>f</sup>
$S_1$	$(n_x(\text{Cl})^2 + (n_y(\text{Cl})^1 + (n_z(\text{Cl})^2 + (n_\sigma(\text{Cl})^2 + (n_\sigma(\text{C})^1$	0,08 (0,95)	0,06 (0,94)	0,05	0,09 (0,94)	0,06 (0,77)	0,04
$S_2$	$(n_x(\text{Cl})^1 + (n_y(\text{Cl})^2 + (n_z(\text{Cl})^2 + (n_\sigma(\text{Cl})^2 + (n_\sigma(\text{C})^1$	0,19 (0,99)	0,20 (0,99)	0,22	0,21 (0,99)	0,23 (0,84)	0,24
$S_3$	$(n_x(\text{Cl})^2 + (n_y(\text{Cl})^2 + (n_z(\text{Cl})^2 + (n_\sigma(\text{Cl})^2 + (n_\sigma(\text{C})^0$	2,68 (0,95)	1,89 (0,95)	1,47	2,48 (0,94)	1,69 (0,76)	1,27

Energias referentes ao estado fundamental (em hartrees): -834,6442<sup>a</sup>; -835,5032<sup>b</sup>; -835,6376<sup>c</sup>; -834,6356<sup>d</sup>; -835,4969<sup>e</sup>; -835,6326<sup>f</sup>.

O estado iônico corresponde a uma configuração de camada fechada iônica. Esse estado tem momento de dipolo de 9,86 D (nível MR-CISD) apresentando grande separação de carga, podendo ser descrito como  $\text{CF}_3\text{HCH}^{\delta+} \cdots \text{Cl}^{\delta-}$ , com  $\delta = 0,89$  (população de Mulliken).

**Key-words:** HCFC-133a, fotodissociação, estado iônico.

**Support:** FINEP, CAPES and CNPq.

### References:

- [1] Molina, M. J.; Rowland, F. S. *Nature*, 249, 810–812 (1974).
- [2] Rowland, F. S.; Molina, M. J. *Science*, 190, 1038 (1975).
- [3] G. Rodrigues, E. Ventura, S. Monte, M. Barbatti. Photochemical Deactivation Process of HCFC-133a ( $\text{C}_2\text{H}_2\text{F}_3\text{Cl}$ ): A Nonadiabatic Dynamics Study. *J. Phys. Chem. A*, 118, 12041-12048 (2014).
- [4] V. Medeiros, R. Andrade, E. Leitão, E. Ventura, G. Bauerfeldt, M. Barbatti, S. Monte. Photochemistry of  $\text{CH}_3\text{Cl}$ : Dissociation and  $\text{CH} \cdots \text{Cl}$  Hydrogen Bond Formation. *J. Am. Chem. Soc.* 138, 272-280 (2016).
- [5] H. Lischka, *et al.*, COLUMBUS, an Ab-Initio Electronic Structure Program, release 7.0 (2015).



## Metal–Support Interaction Effect on the Nucleation of Pd<sub>n</sub> particles (n=1-6) on (110C) γ-Al<sub>2</sub>O<sub>3</sub> surface

Thayane P. D. Caldeira<sup>1,IC\*</sup>, Leticia M. Prates<sup>1,PG</sup>, Maurício T. de M. Cruz<sup>1,PQ</sup>

<sup>1</sup>Departamento de Química Geral e Inorgânica, Instituto de Química, Universidade do Estado do Rio de Janeiro (UERJ), Campus Maracanã, Rio de Janeiro (RJ), Brasil.

\*thayanedias94@hotmail.com, cruzmtm@uerj.br

**Introduction:** It is well known that the catalytic efficiency in a heterogeneous catalyst is largely dependent on its specific area, which is related to the size and shape of metal particle.<sup>[1]</sup> The metal–support interactions play an important role in the process of growing of metal particle, since the strength of anchorage can determine the extension of its dispersion or agglomeration over a surface.<sup>[2,3]</sup> It is reported that the effect promoted by strong metal–support interactions (SMSI) can be provided by both morphological and electronic contributions.<sup>[4-6]</sup> Therefore, a better comprehension of the nature of the effects promoted by the metal–support interaction and, how it influences the metal particle nucleation process, is of great importance. In this work, we performed DFT/B3LYP calculations to obtain an ensemble of structural, energetic and electronic parameters in Pd<sub>n</sub>/Al<sub>24</sub>O<sub>41</sub>H<sub>10</sub> (n=1-6) agglomerates, in order to investigate the influence of metal-support interaction on the atom-to-atom growth mechanism of palladium particles on γ-Al<sub>2</sub>O<sub>3</sub> support.

**Key-words:** nucleation, palladium particle, γ-Al<sub>2</sub>O<sub>3</sub>, metal-support interaction, DFT

**Methodology:** A model to represent the structure of γ-Al<sub>2</sub>O<sub>3</sub> (Al<sub>24</sub>O<sub>41</sub>H<sub>10</sub>) was constructed based on experimental parameters.<sup>[7]</sup> In order to construct atom-to-atom a Pd<sub>6</sub> agglomerate on the (110C) γ-Al<sub>2</sub>O<sub>3</sub> surface, a first palladium atom (Pd<sub>(1)</sub>) was optimized in different sites on Al<sub>24</sub>O<sub>41</sub>H<sub>10</sub>. Following, on Pd<sub>(1)</sub> placed at the most stable site, a second palladium atom was approximated. This process was successively repeated until the formation of Pd<sub>6</sub> agglomerate, relaxing only the n<sup>th</sup> palladium in each step (Fig. 1). The individual adsorption energy of each adsorbed palladium atom was estimated in presence (Eq. 1,  $E_{ad} = E_{(Pd_n/Al_{24}O_{41}H_{10})} - [E_{(Pd)} + E_{(Pd_{n-1}/Al_{24}O_{41}H_{10})}]$ ) and absence (Eq. 2,  $E'_{ad} = E_{(Pd/Al_{24}O_{41}H_{10})} - [E_{(Pd)} + E_{(Al_{24}O_{41}H_{10})}]$ ) of the other palladium atoms. The nucleation energy ( $E_{nuc}$ ) for both supported and isolated (in the same geometry obtained on Al<sub>24</sub>O<sub>41</sub>H<sub>10</sub>) Pd<sub>n</sub> (n=2–6) was obtained (Eq. 3,  $E_{nuc} = E_{ad} - E'_{ad}$ ). The DFT/B3LYP methodology was employed using Gaussian 03 program. The electrons of γ-Al<sub>2</sub>O<sub>3</sub> and palladium clusters were described by 6-31G(d,p) and LANL2DZ, respectively. All computed energies were corrected by the basis set superposition error (BSSE), calculated by the counterpoise method. In all calculated structures, the electronic spin state of lowest energy was obtained, and spin contamination higher than 15% was not observed. Additionally, the stability of wave function was tested.

**Results and discussion:** For all calculated Pd<sub>n</sub>/Al<sub>24</sub>O<sub>41</sub>H<sub>10</sub> structures, the electronic spin state of lowest energy is triplet, except for n = 1 (singlet). After the formation of Pd<sub>6</sub> agglomerate on Al<sub>24</sub>O<sub>41</sub>H<sub>10</sub>, the Pd–Al distances assume values from 2.49 to 2.54 Å, in

good agreement with the experimental bond length (2.46 to 2.67 Å).<sup>[8]</sup> The first palladium atom adsorbs preferentially on two octahedral aluminum cations (Al<sub>o</sub>), with energy of  $-60.4 \text{ kcal.mol}^{-1}$  (Fig. 1). The second atom (Pd<sub>(II)</sub>) anchors on Pd<sub>(I)</sub>/Al<sub>24</sub>O<sub>41</sub>H<sub>10</sub> in on-top mode, involving a tetrahedral aluminum cation ( $E_{\text{ad}} = -50.1 \text{ kcal.mol}^{-1}$ ). Removing Pd<sub>(I)</sub>, the adsorption energy for Pd<sub>(II)</sub> on this aluminum (Al<sub>t</sub>) decreases to  $-24.5 \text{ kcal.mol}^{-1}$ . This result points to the existence of a significant Pd–Pd interaction. However, considering an isolated Pd<sub>2</sub> cluster, in the same arrangement on alumina, the Pd–Pd interaction decreases to  $-16.0 \text{ kcal.mol}^{-1}$ . This result suggests that the palladium–alumina interaction is promoting an increase of the Pd–Pd interaction in Pd<sub>2</sub>/Al<sub>24</sub>O<sub>41</sub>H<sub>10</sub>. This fact is in according to the elevation in  $+9.7 \text{ kcal.mol}^{-1}$  in the energy of nucleation for Pd<sub>2</sub> in presence of alumina, comparing with this cluster isolated (Fig. 1). However, this influence of the palladium–alumina interaction in the palladium nucleation is observed only in Pd<sub>2</sub>. From the third palladium atom onwards, a decrease in the Pd–Pd interaction occurs as the size of the metal agglomerate grows. It is important to note that the smallest energy of nucleation is verified when Pd<sub>(III)</sub> agglomerates in supported Pd<sub>2</sub> (Fig. 1). The Pd<sub>(III)</sub> atom adsorbs strongly on alumina in hollow mode, involving two Al<sub>o</sub> and two oxygen ions. Thus, the palladium atoms that adsorb more strongly on the alumina surface (Pd<sub>(III)</sub>) and Pd<sub>(V)</sub>,  $E'_{\text{ad}}(\text{Pd}) = -51.0$  and  $-26.1 \text{ kcal.mol}^{-1}$ , respectively) present the smaller energies of nucleation ( $-2.8$  and  $-15.2 \text{ kcal.mol}^{-1}$ , respectively).

#### Nucleation Energy (kcal.mol<sup>-1</sup>)

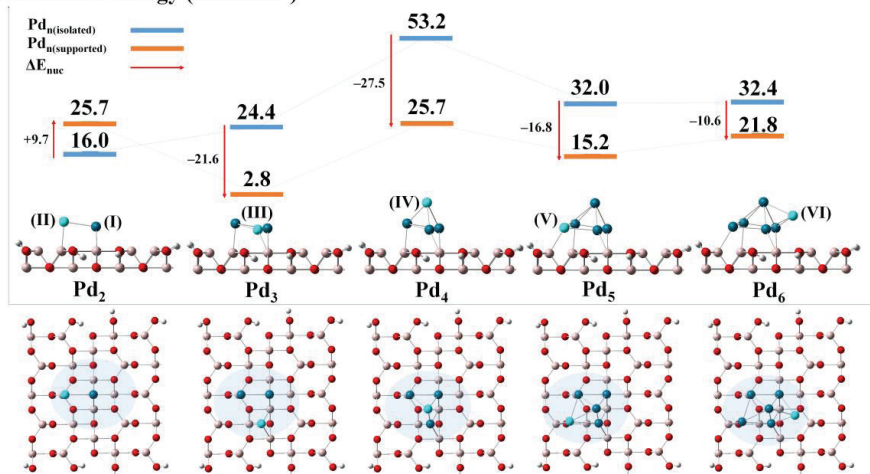


**Figure 1.** Nucleation energy of isolated and supported Pd<sub>n</sub> (n=2–6) and superior and lateral views of Pd<sub>n</sub>/Al<sub>24</sub>O<sub>41</sub>H<sub>10</sub>.

**Conclusion:** Our results suggest that, in general, the effect promoted by the Pd–alumina interaction leads to a weakening of the Pd–Pd nucleation energy. The Pd–Pd interaction is weaker when it involves strongly adsorbed Pd atoms in alumina.

**Support:** The authors would like to thank CAPES and FAPERJ for the financial support.



#### References:

- [1] C. Zhou et al., *J. Phys. Chem. C*, 111, 13786 (2007).
- [2] S.-T. Zhang et al., *J. Phys. Chem. C*, 116, 3514 (2014).
- [3] M. C. Valero, P. Raybaud, P. Sautet, *Phys. Rev. B*, 75, 045427 (2007).
- [4] W. E. Kaden et al., *Surf. Sci.*, 621, 40 (2014).
- [5] C. T. Campbell, *Nat. Chem.*, 4, 597 (2012).
- [6] L. M. Prates et al., *J. Phys. Chem. C*, 121, 14147 (2017).
- [7] O. J. Maresca et al., *Theochem.*, 58, 620 (2003).
- [8] M. Ettenberg, K. L. Komarek, E. Miller, *Metall. Trans. B*, 2, 1173 (1971).





## Painel 306 | PN.306

# Theoretical Study of Interactions between Drugs and Metal-Organic Frameworks

K. R. Coutinho, T. S. Duarte

*Address: Institute of Physics, University of São Paulo*

**Abstract:** In the last two decades a new material class, now called Metal-Organic Framework (MOF), arose and rapidly became eligible for a wide range of applications, especially in fields related to gas selection and storing [1-3]. Beyond its great values of superficial area and pore volume, MOFs might have its chemical functionality modified, which make them a good alternative for drug delivering as well [4]. However there is none theoretical works that explore the reaction details between MOF, drug and the media in which these reactions occur. Thus the objective of the project is to study the interactions between the MOF Zeolitic Imidazolate Framework (ZIF-8), water and the pharmacological agents theophylline, caffeine and dipropylline, through Monte Carlo (MC) and Molecular Dynamics (MD) simulations. Understanding how systems composed by these substances behaves at the microscopic level may bring insights for interpretation of the experimental results already available.

**Key-words:** molecular simulation, metal-organic framework, drug delivery

**Introduction:** Metal-Organic Frameworks constitute a class of materials made by metallic nuclei linked by organic molecules, which forms crystalline structures with permanent porous. MOFs have many desirable features for fields related to porous media: large porous, great superficial areas, low density and thermal stability. Additionally, the uncountable combinations of ionic nucleus and organic ligand makes possible produce MOFs with properties commonly sought for biomedical applications such as high hydrothermal stability and low toxicity [5]. Such features can be used to make MOFs with pores able to store drugs and release them on controlled basis, or even for produce MOFs made of therapeutic compounds, which also can be disassembled in a controlled manner. Regarding the first possibility, MIL-100, MIL-101, MIL-53 and ZIF-8 are examples of MOFs that are stable on environments that simulates human physiology [6, 7].

**Methodology:** In order to develop low-cost processing methodologies for studying MOFs with potential for drug loader, this project has two milestones: first check how suitable the available ZIF-8 force fields are for the systems we intend to study. Since they was originally developed aiming the gas storing properties of ZIF-8 [8, 9], it is necessary to verify what happens on calculations of hydrated environments. At this stage all simulations will be performed by the MC molecular simulation software DICE [10]. Once that is done, the second milestone is to simulate MOF-drug systems in water. Beyond the MC approach, these systems will be simulated by MD as well through





Gromacs. Accompanying this process will be the development of tools able to facilitate the peripheral steps to the simulation, such as the handling of atomic coordinate files which will originate the simulations inputs, and specific data scraping from simulation outputs.

**Perspectives:** This project is being developed in collaboration with the Fundamental Chemistry Department, Federal University of Pernambuco (DQF/UFPE), which already has experimental data collected. Then as soon as all simulations has been finished, it will be possible confront them with the measurements as a means for checking the plausibility of the calculations and, ideally, searching for clues about the prospects of ZIF-8 as a drug carrier . It is also expected that the used methods become reproducible so that other MOFs of biomedical interest can be studied, in particular those which the DQF/UFPE is able to synthesize.

**Support:** This work has been supported by CNPq, CAPES and FAPESP.

#### References:

- [1] O Yaghi, H Li, M Eddaoudi, M O’Keeffe. Design and synthesis of an exceptionally stable and highly porous metal-organic framework. *Nature*, 402(6759):276–279 (1999).
- [2] M Eddaoudi. Systematic Design of Pore Size and Functionality in Isorecticular MOFs and Their Application in Methane Storage. *Science*, 295(5554):469-472 (2002).
- [3] P Silva, S Vilela, J Tomé, F Paz. Multifunctional metal-organic frameworks: from academia to industrial applications. *Chem. Soc. Rev* (2015).
- [4] P Horcajada et al. Metal-Organic Frameworks in Biomedicine. *Chemical Reviews*, 112(2):1232–1268 (2012).
- [5] A McKinlay et al. BioMOFs: Metal-Organic Frameworks for Biological and Medical Applications. *Angewandte Chemie International Edition*, 49(36):6260–6266 (2010).
- [6] P Horcajada et al. Metal-Organic Frameworks in Biomedicine. *Chemical Reviews*, 112(2):1232–1268 (2012).
- [7] C Sun, C Qin, X Wang, Z Su. Metal-organic frameworks as potential drug delivery systems. *Expert Opinion on Drug Delivery*, 10(1):89–101, (2012).
- [8] K Coutinho, S Canuto. DICE: Um programa para simulação computacional de líquidos moleculares, utilizando o método Monte Carlo Metropolis e Teoria de Perturbação Termodinâmica para cálculos de energia livre, Universidade de São Paulo (1997).
- [9] B Zheng, M Sant, P Demontis, G Suffritti. Force Field for Molecular Dynamics Computations in Flexible ZIF-8 Framework. *The Journal of Physical Chemistry C*, 116(1), 933-938 (2012).
- [10] Z Hu, L Zhang, J Jiang. Development of a force field for zeolitic imidazolate framework-8 with structural flexibility. *The Journal of Chemical Physics*, 136(24), 244703 (2012).



## Computational studies on the temperature-induced transition in PNnPAm hydrogels.

Tiago E. de Oliveira<sup>1</sup>, Carlos M. Marques<sup>1</sup>, Paulo A. Netz<sup>2</sup>

<sup>1</sup> Institut Charles Sadron, CNRS, Strasbourg, France.

<sup>2</sup> Universidade Federal do Rio Grande do Sul, Porto Alegre, Brazil.

[tiago.espinosa@ics-cnrs.unistra.fr](mailto:tiago.espinosa@ics-cnrs.unistra.fr)

**Abstract:** *N*-substituted acrylamide-based polymers are widely studied thermoresponsive polymers [1]. In particular, poly(*N*-*n*-propylacrylamide) (PNnPAm) exhibits a unique and sharp volume phase transition in aqueous solution, in contrast to poly(*N*-isopropylacrylamide) [2]. In this work, we carried out all-atom molecular dynamics simulations of single- and multiple-oligomers of PNnPAm with 32 repeating units solutions in water. Systems with one and four oligomers were investigated for two different temperatures, 280 and 340 K, below and above the LCST. Our analysis suggests that systems with multiple-oligomers form aggregates and assemble as a cluster, forming a physical gel at higher temperature [3]. Radius of gyration, inter-chain distances and number of contacts between chains, display all the temperature-dependent signature of the structural changes of PnnPAm.

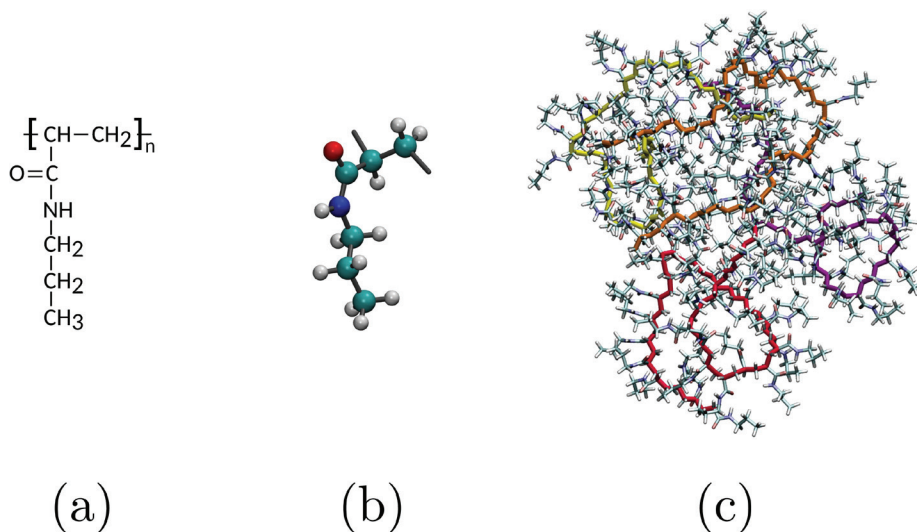


**Figure 1:** (a) A schematic of a NnPAm monomer, (b) a snapshot of a NnPAm monomer and (c) snapshot of four PNnPAm chains at the end of 100 ns above the LCST (340 K).

**Key-words:** poly(*N*-isopropylacrylamide), PNnPAm, LCST, hydrogels.

**References:**

- [1] T. E. de Oliveira, D. Mukherji, K. Kremer, P. A. Netz, *J. Chem. Phys.*, 146, 034904 (2017).
- [2] B. Wedel, Y. Hertle, O. Wrede, J. Bookhold, and T. Hellweg, *Polymers* 8, 162 (2016).
- [3] T. E. de Oliveira *et al. to be submitted*, (2017).



## Computational Study of the Interactions between TiO<sub>2</sub> Anatase Nanoparticles

Uallisson Silva Santos and André Farias de Moura

*Department of Chemistry – Federal University of São Carlos – Rodovia Washington Luís km 235 – CP 676 – CEP 13565-905 – São Carlos – SP*

**Abstract:** Experimental and theoretical studies have shown that the aggregation of TiO<sub>2</sub> anatase nanoparticles (NPs) occurs with preferential crystallographic orientation between the NPs by the so-called oriented attachment (OA) mechanism.<sup>1</sup> TiO<sub>2</sub> anatase NPs exhibit a truncated bipyramid shape with eight (101) faces and two (001) faces. The interaction between TiO<sub>2</sub> anatase NPs was described by a classical forcefield comprising Buckingham and Coulomb potentials.<sup>2</sup> Although the size of the model NPs and the numerical efficiency of the classical force field should allow direct simulation to be accomplished with either molecular dynamics simulations or Monte Carlo methods, preliminary investigations of the potential energy landscape revealed multiple minima with energy differences larger than 10<sup>2</sup> kJ/mol, usually separated by barriers higher than 10<sup>3</sup> kJ/mol, potentially leading to kinetically trapped NPs dimers, with a very restricted sampling of the available phase space. We then devised an alternative approach to perform a thorough and uniform sampling of the phase space of TiO<sub>2</sub> NPs at contact distance, which amounts to the actual calculation of a partition function. The microstates of the system were obtained by placing one NP on previously chosen points of a regular grid around the other NP, then allowing the former NP to rotate and pivot around the latter, with both NPs treated as rigid bodies. The profile of Helmholtz energy obtained for the (101) face of one NP around the other (Figure 1) was computed with a solvent accessible surface grid with 6886 points, allowing the second NP to rotate at 492 different directions and to pivot at 10° intervals, amounting to a partition function with 121 964 832 independent microstates explicitly calculated. Color scheme indicates favorable Helmholtz energies in darker red (lowest value being -875 kJ/mol) whereas darker blue stands for most positive Helmholtz energies (up to 569 kJ/mol). Similar grids have been calculated for other combinations of faces, edges and corners of the NPs and they point out to the interaction between two (001) faces as the most stable thermodynamically. This finding might be considered to be at odds with previous investigations that consider the interaction between two (001) faces as the most probable outcome of an oriented attachment for TiO<sub>2</sub> anatase NPs. This apparent contradiction is most likely due to the small ration between the (001):(101) areas, so we are extending the modeling to include other sizes and shapes of the TiO<sub>2</sub> NPs. But even at the present status of the investigation, the most important conclusion is already sound and clear: the usual picture of a well-defined surface free energy describing the self-assembling in general and the oriented attachment as simple surface area



minimization might be naïve, since there are hot spots separated by thermodynamically unfavorable regions, and thus there are a few preferred positions and orientations. So decreasing the exposed area is no longer an acceptable explanation, since there is a very large number of possible dimers which have a decreased surface area and yet have prohibitively larger free energies.

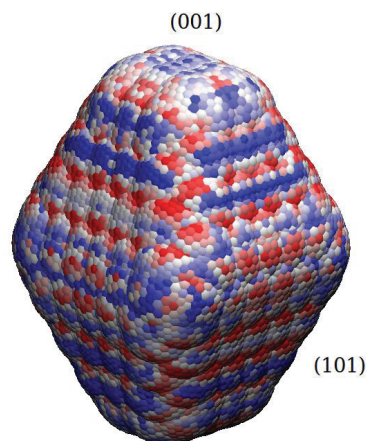


**Figure 1:** Profile of Helmholtz energy for the interaction of one (101) face around the reference TiO<sub>2</sub> NP. Red spots stand for the most negative values whereas blue spots stand for the most positive.

**Key-words:** oriented attachment, nanoparticles, TiO<sub>2</sub> anatase, free energy.

**Support:** The authors are indebted to FAPESP for the financial support (2012/15147-4, 2013/07296-2). USS thanks CNPq for a scholarship. AFM thanks MEC/PET for a fellowship. The authors acknowledge the National Laboratory for Scientific Computing (LNCC/MCTI, Brazil) for providing HPC resources of the SDumont supercomputer, which have contributed to the research results reported within this communication. URL: <http://sdumont.lncc.br>

#### References:

- [1] LV, W.; HE, W.; WANG, X.; NIU, Y.; CAO, H.; DICKERSON, J. H. & WANG, Z. “Understanding the oriented-attachment growth of nanocrystals from an energy point of view: a review”. *Nanoscale*, **6**: 2531, 201.
- [2] MATSUI, M. & AGAKOI, M. “Molecular dynamics simulation of the structural and physical properties of the four polymorphs of TiO<sub>2</sub>”. *Mol. Simul.*, **6**: 239, 1991.



## Multiconfigurational Study of $X^2\Sigma^+$ and $A^2\Pi$ States of BeF, MgF and CaF molecules

Ulisses J. Faria Jr, Luiz F. A. Ferrão, Francisco B. C. Machado

*Instituto Tecnológico da Aeronáutica, São José dos Campos, SP, Brazil*

Alkaline-earth monofluorides have applications in several areas such as industrial chemistry and astrophysics. Recently, the diatomic molecules BeF, MgF and CaF have been used in laser deceleration and cooling processes [1]. These processes allow more accurate measurements of the properties of these systems. The objective of this work is to perform a qualitative and quantitative description of the BeF, MgF and CaF potential energy curves of the two low-lying states  $X^2\Sigma^+$  and  $A^2\Pi$ . The qualitative analysis of the chemical bond between halogens and alkaline-earth metals was carried out from the information of the separated atoms, using a simple model to describe the ionic and covalent character of this bond and predicting the behavior of the potential energy curves. The quantitative analysis of the electronic states was performed employing MRCI and CASPT2 correlation methods assigning dynamic weight to the involved states in the average orbital during the CASSCF method. Calculations were performed using the cc-pV5Z basis set for the metals and aug-cc-pV5Z for the fluorine. Potential energy curves show interaction between states of the same symmetry at the internuclear distance where there is charge transfer. At these distances, avoided crossings arise and the change of ionic character to covalent occurs. Spectroscopic constants of these diatomic molecules were calculated and compared to the experimental data [2]. Analyzing the results was possible to observe that the choice of multiconfiguration methods allows the wave function to correctly describe the change of character of the chemical bond. The obtained molecular constants are in agreement with the experimental data. The calcium monofluoride exhibits the lowest excitation energy among the studied molecules, being the transition  $A^2\Pi \rightarrow X^2\Sigma^+$  more favorable for that molecule.

**Key-words:** Eletronic structure, Diatomics, Qualitative analysis

**Support:** This work has been supported by CAPES

**References:**

- [1] ZHELYAZKOVA, V.; CURNOL, A.; WALL, T. E.; MATSUSHIMA, A.; HUDSON, J. J.; HINDS, E. A.; TARBUTT, M. R.; SAUER, B. E. Laser cooling and slowing of CaF molecules. **Phys. Rev. A - At. Mol. Opt. Phys.**, v. 89, n. 5, p. 2–6, 2014.
- [2] HERZBERG, G. **Molecular Spectra and Molecular Structure**. New York: Van Nostrand Reinhold Company, 1991.

## Molecular properties of N-benzoyl-2-hydroxybenzamide derivatives related to *Plasmodium falciparum* inhibition

Verlucia A. M. Freitas, Karen C. Weber

*Departamento de Química - Universidade Federal da Paraíba*

**Abstract:** The current treatment of choice for malaria, caused by *Plasmodium falciparum*, are artemisinin-based combination therapies (ACTs), which combine an artemisinin derivative with a second antimalarial drug. Unfortunately, artemisinin resistance has been reported in 2014 and is now widespread in southeast Asia. This poses a challenge for the development of new drugs able to tackle the three stages of Plasmodium infection in humans [1]. Molecular modeling tools play an important role in this problem, being a research field of strong potential, as demonstrated by the continuous interest of pharmaceutical industry in computational methods applied to lead optimization [2,3]. In the search for new compounds, Stec and coworkers [4] reported the synthesis and biological evaluation for a set of N-benzoyl-2-hydroxybenzamides and related compounds as potent agents against *P. falciparum*. In the present work, we performed a quantitative structure-activity relationship (QSAR) study on these compounds in order to determine the most relevant molecular properties responsible for antimalarial activity. Molecular structures were modelled in Gaussview 5.0 and optimized with the DFT method using M06-2X functional and 6-311+g(d,p) basis set in Gaussian 09 [5]. At this level of calculation, we have also obtained several electronic descriptors such as frontier orbital energies, dipole moment, polarizability and NBO charges. Thousands of topological, physicochemical and molecular descriptors were obtained with the E-Dragon platform [6]. The whole data set was divided into training and test sets, containing 30 and 7 compounds, respectively. Variable selection was undertaken with Ordered Predictor Selection (OPS) and Genetic Algorithm (GA) techniques, in combination with the use of Partial Least Squares (PLS) and Multiple Linear Regression (MLR) methods for QSAR model building. These analyses were performed with the aid of QSAR-modeling [7], Pirouette 3.11 [8] and Matlab 6.5 [9] software. The best model was achieved with the OPS-PLS combination, with statistical parameters of  $q^2 = 0,69$  and  $r^2 = 0,76$ , and  $r^2_{\text{pred}} = 0,94$  for the test set. This model was submitted to the additional  $y$ -scrambling and leave-N-out validation tests, which indicated that a robust and statistically stable model was achieved. The results obtained reveal that the antimalarial activity of the hydroxybenzamides under study depend on the following descriptors: dipole moment and polarizability, derived from DFT calculations; Mor30v, Mor32p and Mor32p, which reflect the three-dimensional distribution of molecular branching; RDF115e, RDF105e and RDF105u, which are based on radial distribution function of substituents; MATS6p, MATS6m and MATS6e, which are 2D-autocorrelation descriptors calculated from Euclidean distances between atoms or points in the molecular surface; and BIC5, an



information index descriptor calculated from graph theory [6]. These findings are of considerable relevance since the methodology applied was able to provide a QSAR model of good predictive power, which can be used to predict the biological activity against *P. falciparum* for similar molecules, helping so in the decision-making step of new active compound synthesis.

**Key-words:** QSAR, hydroxybenzamides, DFT.

**Support:** This work has been supported by CAPES.

**References:**

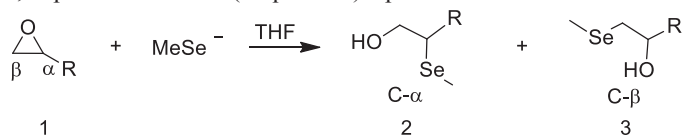
- [1] D. A. Fidock, Nature 538, 323, 2016.
- [2] A. Cherkasov et al., J. Med. Chem. 57, 4977, 2014.
- [3] B. Kuhn et al., J. Med. Chem. 59, 4087, 2016.
- [4] J. Stec et al., J. Med. Chem. 55, 3088, 2012.
- [5] Gaussian 09, Revision D.01, Frisch, M. J. et al. Gaussian, Inc., Wallingford CT, 2009.
- [6] I. V. Tetko et al., J. Comput. Aid. Mol. Des. 19, 453, 2005.
- [7] J. P. A. Martins, M. M. C. Ferreira Quim. Nova 36, 554, 2013.
- [8] Infometrix Inc. Pirouette 4.0. Woodinville, 2008.
- [9] Matlab and Statistics Toolbox, Revision 13, The MathWorks, Inc., Natick, 2002.



## Abertura seletiva de epóxidos com Metil Selenolato de Lítio

Verônica M. Nascimento, Gizele Celante, Alcindo A. dos Santos, Ataulpa A. C. Braga  
 \*veronica@iq.usp.br  
 Instituto de Química –USP. Av. Prof. Lineu Prestes, 748 - Butantã - São Paulo - SP

A regioselectividade em reações de abertura de epóxidos com metil selenolato de lítio, foi estudada, experimentalmente (Esquema 1) e por cálculos teóricos.



R = CO<sub>2</sub>Et (**1a**)

R = Ph (**1b**)

R = C<sub>6</sub>H<sub>11</sub> (**1c**)

**Esquema 1:** Reação entre epóxidos (**1a-1c**) e metil selenolato de lítio.

O álcool **2a** foi obtido majoritariamente quando **1a** foi submetido a reação com MeSeLi. Cálculos teóricos foram realizados e confirmaram os resultados experimentais. Na Figura 1 estão ilustradas as estruturas dos estados de transição (TS) relacionados aos conteúdos de energia obtidos para os ataques do MeSeLi aos C- $\alpha$  e C- $\beta$  do 2,3-epoxipropanoato de etila (**1a**).

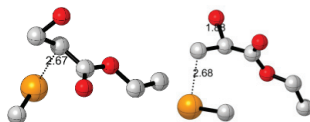


**Figura 1:** TS's obtidos da reação entre **1a** e MeSeLi. Cálculos realizados com GAUSSIAN 09[1], nível B3LYP-D3/6-31+G(d,p)[2], incluindo método de solvente contínuo SMD.[3]

Na Tabela 1 estão compilados os dados obtidos dos cálculos realizados para ambos os processos de abertura da reação de MeSeLi com **1a** via os C- $\alpha$  e C- $\beta$ . Os valores de energia obtidos corroboram os resultados experimentais para a abertura pelo C- $\alpha$  (regioselectividade igual a 98%). A fim de melhor compreender a natureza eletrofílica desses compostos, experimentos com o epóxido **1b** (R = Ph) e estudos teóricos com **1b** e **1c** (R = C<sub>6</sub>H<sub>11</sub>) também foram realizados.



**Tabela 1:** Energia dos TSs obtidos para reação entre metil selenolato e epóxido (**1a**)

	$\Delta E$ /kcalmol <sup>-1</sup>	Barreira /kcalmol <sup>-1</sup>	$\Delta G$ /kcalmol <sup>-1</sup>
<b>TS Ataque no C-<math>\alpha</math></b>	10,6	<b>4,8</b>	20,7
<b>TS Ataque no C-<math>\beta</math></b>	11,5	<b>16,1</b>	21,8

Na Tabela 2 estão apresentados os dados de energia obtidos para os ataques aos C- $\alpha$  e C- $\beta$  de **1b** e **1c**.

**Tabela 2:** Energia dos TS's obtidos para reações de abertura dos epóxidos **1b** e **1c** com MeSeLi

TS/substituintes(posição)	$\Delta E$ /kcalmol <sup>-1</sup>	Barreira /kcalmol <sup>-1</sup>	$\Delta G$ /kcalmol <sup>-1</sup>
<b>1b(C-<math>\alpha</math>)</b>	13,6	16,7	23,4
<b>1b(C-<math>\beta</math>)</b>	13,1	16,3	22,4
<b>1c(C-<math>\alpha</math>)</b>	19,2	22,2	29,6
<b>1c(C-<math>\beta</math>)</b>	14,1	18,8	21,5

Os resultados obtidos (teóricos e experimentais) tanto para a reação de abertura da epóxido **1a** quanto com **1b** com MeSeLi são corroborativos. No caso do epóxido **1a** esperávamos haver abertura por C- $\beta$ , fazendo um paralelo ao perfil eletrofílico de compostos  $\alpha,\beta$ -insaturados. Contudo, os modelos e cálculos teóricos demonstraram maior preferência de aproximação do átomo de selênio por C- $\alpha$  que está de acordo com os experimentos realizados. No caso dos experimentos e cálculos com **1b** observou-se preferência para abertura por  $\beta$ , com um percentual de abertura de 80%. Por fim, os cálculos realizados para **1c**, com efeitos estéricos, a abertura se deu majoritariamente por C- $\beta$ , o que está de acordo com resultados experimentais publicados em literatura[4]. A comparação, entre os dados experimentais e os obtidos por modelos teóricos, demonstra que os cálculos com DFT podem contribuir para a elucidação de mecanismos de reações de abertura de epóxidos.

**Palavras-chave:** regioseletividade, epóxido, selenolato, DFT.

**Agradecimentos:** CNPq, FAPESP, LCCA-USP.

#### Referência:

- [1] M.J. Frisch, et.al. Gaussian 09, revisão D01. Gaussian, Inc. 2009.
- [2] Zhao, Y.; Truhlar, D. G. *Theor. Chem. Acc.* **2008**, *120*, 215–241.
- [3] [2] Zaccaria, F. & Wolters, L. P. (2016).
- [4] Bach RD, Dmitrenko O. *J. Am. Chem. Soc.* 2006;128:4598.



## Solamargine and Solamarine: Why so different?

Victor A. V. Ferreira<sup>a</sup>, Eduardo da Conceição<sup>b</sup>, Julyana R. Machado, Antonio Jorge R. da Silva, Mauro B. de Amorim

<sup>a</sup> [victor.augusto7@yahoo.com.br](mailto:victor.augusto7@yahoo.com.br) / <sup>b</sup> [eduardodcon@gmail.com](mailto:eduardodcon@gmail.com)  
 Walter Mors Institute of Research in Natural Products <sup>c</sup> Federal University of Rio de Janeiro.

### Introduction:

The Solanaceae family is composed of approximately 2500 species, which include some of the most important species for agriculture. However, the co-occurrence of compounds that exert a negative impact on nutritional quality is a very common problem. Most of the compounds of this type are formed by steroidal alkaloids and steroidal glycoalkaloids, which contribute to plant resistance against pathogens and predators.<sup>1,2</sup> Two of these steroidal glycoalkaloids are Solamargine and Solamarine which differs only in the position of methylene (or amine) group in the heterocyclic ring (figure 1).

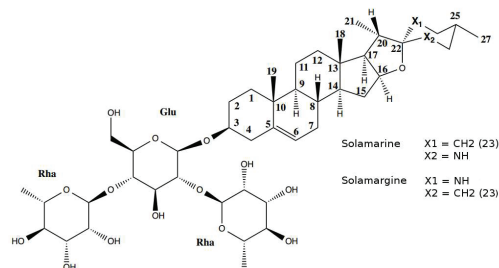


Figure 1: Structures of Solamargine and Solamarine.

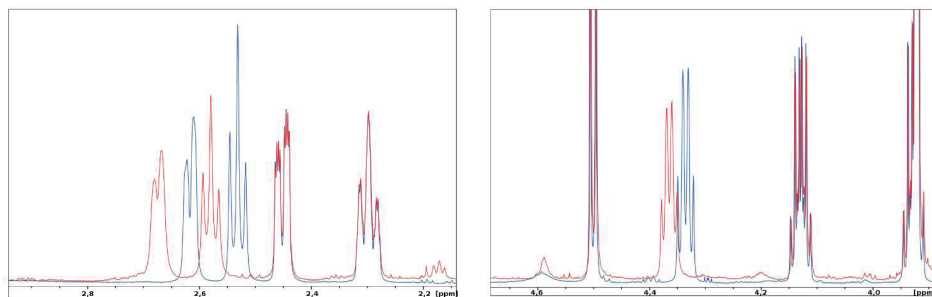


Figure 2: NMR zoomed spectra of Solamargine(blue) and Solamarine (red). On the left the region of H26 (axial and equatorial) chemical shift and on right H16. [800MHz - CD<sub>3</sub>OD]



The Solamargine and Solamarine NMR spectra shows a quick difference between chemical shifts of protons of the heterocyclic rings, H16 and H26a and H26e (figure 2).

In order to identify the reason for these differences, NMR (chemical shifts and coupling constant) and NBO calculations were performed.

### Results and Discussion:

Conformational analysis of three compounds has led to six conformers for Solamargine, where only three of them have more than 24% of the total population. On the other hand, five conformers were found for Solamarine, only three of them with more than 29% of the total population. Calculations were carried out with Gaussian 09 package at the wB97XD/def2-TZVP level of theory.<sup>3</sup> The Boltzmann averaged calculated chemical shifts and coupling constant are in accordance with the experimental data.

We observe that the differences in spectra are mainly in the chemical shifts of the hydrogen atoms with a heteroatom neighbor (oxygen for H16 and N for H26a and H26e). Based on the observation that the nonbonding electron pairs of the O and N atoms could be, through hyperconjugative effects, the cause of these differences, an NBO analysis was performed.<sup>4</sup> The hyperconjugative effect tends to change the molecular geometric (bond lengths) and electronic parameters of the involved atoms and these changes may lead to a change in the NMR data. The effects of hyperconjugation can be inferred from the NBO data shown in the table below.

Table 1: NBO data for Solamargine and Solamarine.

Atoms	Solamargine		Solamarine	
	Interaction	Energy (kcal/mol)	Interaction	Energy (kcal/mol)
16	O(LP) → C-H	13,32	O(LP) → C-H	13,44
26a	N(LP) → C-H	11,70	N(LP) → C-H	11,08
26e	N(LP) → C-H	1,45	N(LP) → C-H	1,82

We notice that the hyperconjugative interactions for C-H16 bonds are very similar on both isomers, with a difference of only 0,12 kcal/mol; an effect not so prominent but sufficient to account for the small difference observed in the chemical shifts (spectral region at the right side of figure 2). On the other hand, for the C-H26, the hyperconjugative transference of electron density is more pronounced (0,62 and 0,39 kcal/mol) and therefore compatible with the greater difference in chemical shifts shown in the spectral region on the left side of figure 2.

**Key words:** Steroidal alkaloids; NMR; NBO.

**Support:** CNPq and CAPES for the financial support.

### References:

- [1] Cárdenas P.D., Sonawane P.D., Heinig U., Bocobza S.E., Burdman S. & Aharoni A.. *Phytochemistry*, 113 (2015) 24-32.
- [2] Dolan L.C., Matulka R.A. and Burdock G.A.. *Toxins*, 2 (2010) 2289-2332.
- [3] M. J. Frisch, et al., Gaussian, Inc., Wallingford CT, (2009).
- [4] J. P. Foster & F. Weinhold, *J. Am. Chem. Soc.*, 102, 7211, (1980)



## Theoretical Study on Electron Collisions with Methylamine

Victor A. S. da Mata<sup>1</sup>, Leonardo M. F. de Oliveira<sup>2</sup>, Manoel G. P. Homem<sup>1</sup>,  
and Gabriel L. C. de Souza<sup>2</sup>

<sup>1</sup>*Departamento de Química, Universidade Federal de São Carlos, 13565-905, São Carlos, Brazil*

<sup>2</sup>*Departamento de Química, Universidade Federal de Mato Grosso, 78060-900, Cuiabá, Brazil*

**Abstract:** In this work, we present a theoretical study on electron collisions with methylamine (CH<sub>3</sub>NH<sub>2</sub>). Elastic differential, integral, and momentum-transfer cross sections, as well as the grand-total and total absorption cross sections were calculated in the 1-500 eV energy range. A complex optical potential derived from a Hartree-Fock molecular wave function was used to represent the collision dynamics and a single-center expansion method combined with the Padé approximant technique was used to solve the scattering equations. For that, the EPolyScat-D package, originally developed by Gianturco *et al.* [1] and further modified by Souza *et al.* [2] to include the absorption potential, was used to perform the calculations. In this framework, the complex optical potential is given by:

$$V_{\text{opt}} = V_{\text{st}} + V_{\text{ex}} + V_{\text{cp}} + iV_{\text{abs}}, \quad (1)$$

where  $V_{\text{st}}$  and  $V_{\text{ex}}$  are the static and exchange components, respectively, derived exactly from the target wave function,  $V_{\text{cp}}$  is the correlation-polarization contribution obtained within the framework of free-electron-gas model [3], and  $V_{\text{abs}}$  is the improved model absorption potential developed by our group [4].

In Fig. 1, we present our calculated results for the in Differential Cross Sections (DCS) for the elastic  $e^-$ -CH<sub>3</sub>NH<sub>2</sub> scattering at 500 eV. Unfortunately, there is no experimental data available in the literature for this molecule. Thus, experimental results for the isoelectronic molecule methanol (CH<sub>3</sub>OH) taken from Sugohara *et al.* [5]



are presented for comparison purposes. The computed results of the elastic  $e^-$ -CH<sub>3</sub>NH<sub>2</sub> scattering present similar trend to that observed for the measured  $e^-$ -CH<sub>3</sub>OH DCS. In addition, the DCS magnitudes are practically the same for all the angular region covered by the measurements. The complete results obtained in the 1-500 eV energy range will be presented at the Conference.

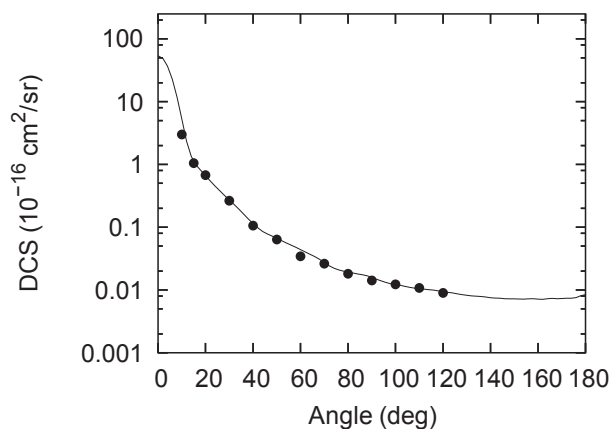


**Figure 1:** Differential cross sections for elastic scattering at 500 eV. Solid line: present results for  $e^-$ -CH<sub>3</sub>NH<sub>2</sub>; Circles: experimental data from Sugohara *et al.* [5] for  $e^-$ -CH<sub>3</sub>OH.

**Key-words:** Electron scattering, methylamine, cross sections.

**Support:** This work has been supported by FAPESP and CNPq. M. G. P. H. acknowledges FAPESP for the financial support under the grant 2015/08258-2.

#### References:

- [1] F. A. Gianturco *et al.*, The Journal of Chemical Physics **102** (14), 5743-5751 (1995).
- [2] G. L. C. Souza *et al.*, Physical Review A **82** (1), 012709 (2010).
- [3] N. T. Padial and D. W. Norcross, Physical Review A **29** (4), 1742-1748 (1984).
- [4] M.-T. Lee *et al.*, Journal of Electron Spectroscopy and Related Phenomena **155** (1-3), 14-20 (2007).
- [5] R. T. Sugohara *et al.*, Physical Review A **83** (3), 032708 (2011).



## DFT Study of the interaction between the $[\text{Zn}(\text{H}_2\text{O})_6]^{+2}$ , $[\text{Cd}(\text{H}_2\text{O})_4]^{+2}$ , $[\text{Hg}(\text{H}_2\text{O})_2]^{+2}$ aquacomplexes and monodentate O-, N- and S-donor ligands

Victor Hugo Malamace da Silva<sup>b</sup>, Daniel Garcez S. Quattrociochi<sup>a</sup>, José Walkimar de M. Carneiro<sup>a</sup>, Leonardo Moreira da Costa<sup>a</sup>, Glauccio Braga Ferreira<sup>a</sup>

Address: <sup>a</sup> Programa de Pós-graduação em Química, Universidade Federal Fluminense Outeiro de São João Batista s/n, 24020-141 Niterói, RJ, Brazil,

<sup>b</sup> Escola de Engenharia Universidade Federal Fluminense Rua Passos da Pátria 156, 24210-253, Niterói, RJ, Brazil.

**Abstract:** In the last decades, the environmental pollution caused by heavy metals has increased principally due to anthropogenic activities. The release of zinc, cadmium and mercury in the biosphere is mostly due to the steel and metallurgical industries, mining, and agricultural activities [1]. These metal cations tend to accumulate in the liver, kidney, thyroid and bones leading to liver dysfunction, renal damages and cancer [2].

The pharmaceutical industry uses chelating agents to enhance the removal of harmful cations from the human body. In these medicines, the active site is usually constituted by polar groups [3] that bind the metal cation. However, the chelating agents have small metal cation specificity, which can also eliminate essential species [4].

The present study identifies the molecular block with the strongest affinity for the  $[\text{Zn}(\text{H}_2\text{O})_6]^{2+}$  aquacation. Additionally, evaluates the influence of the gas and aqueous (CPCM and Vukovic procedure [5]) media in the formation constant, Gibbs free energy, electrostatic and covalent terms (from EDA calculation) of the interaction.

The geometries of the octahedral  $\text{Zn}^{+2}$  aquacomplexes with the carboxylic acid, amide, ester, lactame, ammonia and thioester ligands were fully optimized using the restricted B3LYP method with the 6-311+G(d,p) basis set for the O, N, S, C, H, Zn atoms and the LANL2DZ-ECP for Cd and Hg with CPCM and gas phase. The Gibbs free energy was calculated by the substitution of one water molecule by a ligand (Table 1). The formation constant of the complex in gas phase ( $\log K_{\text{Gas}}$ ) and with water solvent ( $\log K_{\text{Aq}}$  and  $\log K_{\text{Vuk}}$ ) was obtained employing the following equation:

$$\log K = \frac{-\Delta G}{2.303RT}$$

The analysis of Table 1 shows that the O- donor ligands have a stronger interaction with the  $\text{Zn}^{+2}$  cation in gas phase ( $\Delta G_{\text{Gas}}$ ), however for the Vukovic ( $\Delta G_{\text{Vuk}}$ ) and the aqueous solvent ( $\Delta G_{\text{Aq}}$ ) calculations the N- donor ligand shows the strongest interaction. The S- donor ligands have a non-spontaneous interaction in the aqueous solvent and for Vukovic, due to its softness that favors the interaction with large cations.

The EDA results show that the covalent and electrostatic components are sensitive to the media (gas or aqueous). In the gas phase, the results indicate the electrostatic and covalent are stabilizing terms, with larger magnitude for the first one.

In the aqueous and Vukovic methods, the electrostatic component is positive and the covalent component is largely a negative term.

Table 1: Gibbs free energy calculated in gas phase ( $\Delta G_{\text{Gas}}$ ), in aqueous solvent ( $\Delta G_{\text{Aq}}$ ) and with Vukovic procedure ( $\Delta G_{\text{Vuk}}$ ) and electrostatic and covalent component of the metal-ligand interaction obtained from the EDA analysis, in kcal.mol<sup>-1</sup>.

Zn									
Ligand	$\Delta G_{\text{Gas}}$	$E_{\text{elec.}}$	$E_{\text{cov.}}$	$\Delta G_{\text{Vuk}}$	$E_{\text{elec.}}$	$E_{\text{cov.}}$	$\Delta G_{\text{Aq}}$	$E_{\text{elec.}}$	$E_{\text{cov.}}$
-COOH	-16.73	-61.73	-44.58	-2.27	131.31	-199.31	0.25	132.95	-205.13
-CONH <sub>2</sub>	-16.40	-68.85	-55.14	-2.12	123.00	-206.12	-0.64	125.46	-210.33
-COO-	-14.69	-60.75	-44.9	0.26	130.42	-198.03	2.17	134.54	-202.94
Lactame	-23.50	-74.15	-60.34	-3.52	116.44	-205.22	-1.80	122.20	-209.53
NH <sub>3</sub>	-8.41	-81.61	-55.47	-8.03	106.65	-225.57	-7.04	109.94	-233.56
Thioether	-14.76	-67.02	-73.03	1.41	130.26	-223.40	3.05	139.10	-224.10

Table 2 presents the formation constant values in gas phase and in both solvent methods and their absolute errors (in comparison with the experimental data). For the Zn<sup>+2</sup> cation the gas phase result has the smallest absolute error. The Vukovic methodology presents the smallest absolute errors for the Cd<sup>+2</sup> and Hg<sup>+2</sup> complexes. The results from all methods show two correlations between the size of the metal cation and the absolute errors. In gas phase as the size of the metal cation increases, the error also increases, while for the aqueous and Vukovic calculations as the size of the atom increases the error decreases.

Table 2: Experimental formation constant ( $\log K_{\text{Exp}}$ ) for the Zn<sup>+2</sup>, Cd<sup>+2</sup> and Hg<sup>+2</sup> complexes with the ammonia ligand and the formation constants calculated in gas phase ( $\log K_{\text{Gas}}$ ), in aqueous phase ( $\log K_{\text{Aq}}$ ) and with the Vukovic procedure ( $\log K_{\text{Vuk}}$ ) and the respective absolute errors (in comparison with the experimental values).

	$\log K_{\text{Exp}}$	$\log K_{\text{Gas}}$	Abs. Error	$\log K_{\text{Vuk}}$	Abs. Error	$\log K_{\text{Aq}}$	Abs. Error
Zn	2.18	3.36	1.18	5.88	3.70	5.16	2.98
Cd	2.65	5.92	3.74	5.25	2.59	6.65	2.72
Hg	8.8	35.28	33.10	8.28	0.52	6.69	2,11

As a continuing study we will also consider more functional groups for the evaluation of the coordination interactions of ligands with metal cations.

**Key-words:** metal cations, DFT, formation constant, EDA

**Support:** This work has been supported by CNPq, FAPERJ, PROPPi-UFF

**References:**

- [1] J. O. Nriagu, *et al*, Nature 333, 134 (1988)
- [2] S. Tong *et al*, B World Health Organ 78, 1068 (2000)
- [3] C. Wang *et al*, Toxicol. Appl. Pharmacol. 200, 229 (2004)
- [4] R. Rahimi *et al*, J. Braz. Chem. Soc. 27, 1814 (2016)
- [5] S. Vukovic *et al*, Inorg. Chem. 54, 3995 (2015)

## Conformational analysis of molecules with potential antileishmania activity

Vinícius Bonatto (PG)<sup>1</sup>, Juliana Fedoce Lopes (PQ)<sup>1</sup>

<sup>1</sup>Laboratório de Química Computacional □LaQC, IFQ - Instituto de Física e Química

UNIFEI, Itajubá □MG CEP: 37500 903.vi\_bonatto@hotmail.com

**Abstract:** Leishmaniasis are a set of endemic protozooses present in 88 countries, being able to manifest in cutaneous, mucocutaneous and visceral forms[1]. In Brazil, *L. amazonensis* and *L. braziliensis* species are the main cause of leishmaniasis occurrences[2]. Since there is no effective treatment against the different species of *Leishmania* a lot of drugs have been developed to improve the treatment as well as attenuate the side effects of those existing. A possible target for the development for new drugs are the enzymes of topoisomerase family[3]. The overall mechanism of action, however, still not known. In these sense, an experimental group in UNIFEI has synthesized some new compounds with potential antileishmania activity. Thus, the

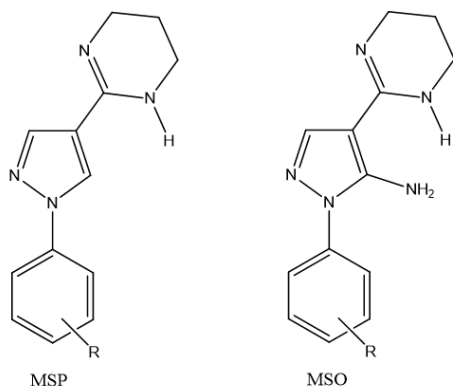


Figure 1: Structural Representation of basic compounds studied in this work. For **MSP**: **01**: R=H; **02**: R=3-Cl; **04**: R=3,5-diCl; **07**: R=4-Cl; **10**: R=4-F; **13**: R=4-Br; **20**: R=4-OCH<sub>3</sub>. For **MSO**: **01**: R=H; **02**: R=3-Cl; **04**: R=3,5-diCl; **05**: R=3,4-diCl; **07**: R=4-Cl; **10**: R=4-F; **13**: R=4-Br; **14**: R=3-Br; **20**: R=4-OCH<sub>3</sub>.

overall aim of the project is to make a structural, electronic, thermodynamics and kinetics analysis of these new molecules and their process involved on mechanism of action through topoisomerase interactions using computational tools. In this work, the conformational analyses of the first compounds which are presented in figure 1, are studied as well as their substituent. The conformational freedom is an important feature to describe key interactions with biomolecular targets. All calculation have been performed using the Gaussian 09 program, through DFT calculations, with M06-2X functional and 6-31g(d,p) basis set for geometry optimization, followed by vibrational analysis which confirm the initial guesses as local minima and also for conformers search, as can by the multiple rotation of two dihedrals angles as represented in Figure 2.

After analyzed the optimized 16 molecules structures, scan calculations were performed. There are centers of free rotation in these molecules, so changing the angles over these centers will make the

energy of the compound changes too. Scan calculation run over 36 steps, varying 10 degrees rotation in each step for both dihedrals  $\theta$  and  $\varphi$  as presented in Figure 2. Since there are two possible dihedrals, 1296 conformations were evaluated. As example, Figure 2 shows the optimized structure of MSP04, with the two dihedrals represented and Table 1 shows the highest energy conformation for the same molecule, indicated at 0 kcal/mol, and also the five most stable conformations from this calculation. The number of conformation is only an arbitrary number as structures identifier over the scan run.

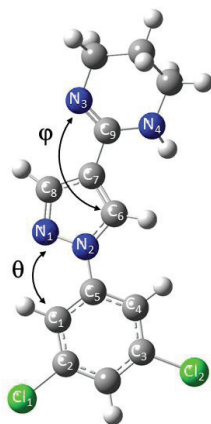


Figure 2: Optimized structure of MSP04.

Table 1: The energy values which vary according the dihedral values of the molecule MSP04.

Conformer	$\theta$ (°)	$\varphi$ (°)	$\Delta E$ (kcal/mol)
948	93,50	99,17	0
36	333,50	199,17	-10,67
684	333,50	19,17	-10,70
2	353,50	199,17	-10,75
649	343,50	19,17	-10,82
1	343,50	199,17	-10,85 (global minimum)

Analyzing the results for MSP04, the minimum of energy for possible conformations was of the initial structure optimized and the maximum of energy occurred when the dihedral  $\theta$  modified  $110^\circ$  from the local minimum and the dihedral  $\varphi$  modified  $260^\circ$ . For the most stable conformations the angles for the dihedral  $\theta$  are closer to each other and for the dihedral  $\varphi$  they stay the same or rotate  $180$  degrees. This behavior suggests that the intramolecular forces between nitrogen ( $N_3$  and  $N_4$ ) and the hydrogens of the middle ring will be practically the same in both angle, increasing the molecule stability.

However, in a general analysis of the scan for this molecule, 95 conformations have energy in average close to 1 kcal/mol from global minimum. It is a too tight variation and these energy values of conformations would also be an energy minimum in solvent effect were included. A perspective for this work is optimize these others conformations to observe if the optimized structure will converge to the global minimum conformation or not. With global minimum defined, atomic charges calculation can be done, followed by docking analysis with the enzymes of topoisomerase family.

**Key-words:** Leishmaniasis, Conformational analysis, DFT

**Support:** This work has been supported by CAPES, CNPQ, PPGMQ-MG, FAPEMIG.

**References:**

- [1] A. Oryan, M. Akbari, Asian Pacific J. of Tropical Medicine, 10, 925-932 (2016)
- [2] M. E. M. C. Dorval, et al, Rev. da Soc. Bras. de Medicina Tropical, 39, 43-46 (2006)
- [3] B. B. Das, et al, Molecular Microbiology, 62, 917-927 (2006)

## Comparative Kinetic Analysis of Hydrogen Abstraction Reactions by OH Radicals: Dimethyl Ether and Diethyl Ether

Vinícius Nunes da Rocha, Glauco Favilla Bauerfeldt

*Universidade Federal Rural do Rio de Janeiro, BR-465, Km 7 Seropédica, RJ*

**Abstract:** Aliphatic ethers have been indicated as possible additives for fuels [1]. In its combustion mechanisms, the initiation is given from the unimolecular and bimolecular reactions, including reactions with OH radicals, which follow a hydrogen abstraction mechanism [2]. Concerning the Atmospheric Chemistry, OH radicals are the most important oxidants in troposphere, responsible for the chemical removal of the majority of the pollutant organic volatile compounds. This study aims at the theoretical description of the reactions of dimethyl ether (DME) and diethyl ether (DEE) with OH radicals, prediction of rate coefficients and kinetic parameters, and the comparative analysis on the results. The calculations have been performed at the M06-2X/aug-cc-pVTZ level, using the Gaussian09 program [3]. Canonical variational rate coefficients have been calculated with the kvct program. These reactions have been previously discussed in the literature. Here, new stationary points have been located, as pre- and post-barrier complexes as well as new saddle points. The geometries of the intermediates and the corresponding saddle points keep some similarities, and their connections have been confirmed by intrinsic reaction coordinate (IRC) calculations. These calculations allowed the proposal of novel reaction channels. For DME, three pre-barrier complexes have been located at 0.76, 4.81 and 5.05 kcal mol<sup>-1</sup> below the isolated reactants and connected to their respective saddle points, lying at 0.29, -0.34 and 1.57 kcal mol<sup>-1</sup>, respectively (the reported relative energy values include vibrational zero point energy corrections). In the DEE mechanism, two pre-barriers were located, stabilized at 1.40 and 6.12 kcal mol<sup>-1</sup> below the isolated reactants. These stationary points are connected to their saddle points, one of them at 2.40 kcal mol<sup>-1</sup> and three remaining at -0.20, -0.99 and -1.58 kcal mol<sup>-1</sup>, respectively (concerning the isolated reagents and including zero point energy corrections). The global reactions are exothermic and products are predicted to lie at -22.44 kcal mol<sup>-1</sup> (CH<sub>3</sub>OCH<sub>2</sub> + H<sub>2</sub>O), -16.72 kcal mol<sup>-1</sup> (CH<sub>3</sub>CH<sub>2</sub>OCH<sub>2</sub>CH<sub>2</sub> + H<sub>2</sub>O) and -24.36 kcal mol<sup>-1</sup> (CH<sub>3</sub>CH<sub>2</sub>OCHCH<sub>3</sub> + H<sub>2</sub>O), in good agreement with thermochemical predictions from literature values. This model is more detailed than the (best and most recent) mechanism proposal found in the literature [4]. Our predicted molecular properties and reaction paths have been used to predict rate coefficients in the range from 250 to 2000 K. Our predictions reveal an increasing behavior of the coefficients with the temperature in the DME mechanism and, in contrast, in the range from 250 to 400 K, a non-Arrhenius behavior is observed for the DEE + OH rate coefficients, confirming previous experimental results. Both respect the experimental values, as well as the chemical nature concerning the function of temperature. For the DME, the most recent expression for the



rate coefficients found in the literature is  $8.45 \times 10^{-18} (T^{2.07}) \exp(0.521/RT)$  [5] and our predicted rate coefficients are fit under the expression  $1.10 \times 10^{-17} (T^{2.02}) \exp(0.596/RT)$ . Small deviation among these values are noted. For DEE, Arrhenius parameters for this reaction are available in the literature only in the range from 250 to 400 K, suggesting a non-Arrhenius behavior in this range of temperatures [6]. This trend has not been observed in the most recent theoretical investigation on the kinetics of this reaction [7]. Our calculated rate coefficient, at 300 K, is  $4.75 \times 10^{-11} \text{ cm}^3 \text{ molecule}^{-1} \text{ s}^{-1}$ , whereas the experimental value, at this temperature, is  $1.24 \times 10^{-11} \text{ cm}^3 \text{ molecule}^{-1} \text{ s}^{-1}$ . As mentioned above, detailed reaction path calculations have been performed with the objectives of mapping the potential energy surface and collecting the required information for the prediction of accurate rate coefficients in a large temperature range. The good agreement between the kinetic parameters obtained from our proposed models and the experimental results allow the conclusion that the present mechanisms are consistent. Moreover, the temperature dependence of the rate coefficients for the OH + DME and DEE reactions have been here, for the first time, explained. Finally, our results represent new contributions to Combustion and Atmospheric Chemistry areas concerning the reactivity of aliphatic ethers.

**Key-words:** Diethyl Ether, Dimethyl Ether, Combustion Chemistry, Atmospheric Chemistry, OH Reactions.

**Support:** This work has been supported by CNPq

**References:**

- [1] LIU, X.; ZHANG, Q.; ITO, S.; WADA, Y. *Fuel* 165, 513 – 525, 2016.
- [2] NASH, J. J.; FRANCISCO, J. S. *J. Phys. Chem. A* 102, 236 – 241, 1998.
- [3] FRISCH, M. J. *et al. Gaussian 09, Revision E.01*, Gaussian, Inc., Wallingford CT, 2009.
- [4] SANDHIYA, L.; PONNUSAMY, S.; SENTHILKUMAR, K. *RSC Adv.*, 6, 81354 - 81363, 2016.
- [5] BÄNSCH, C.; KIECHERER, J.; SZÖRI, M.; OLZMANN, M. *J. Phys. Chem. A* 117, 8343–8351, 2013.
- [6] SEMADENI, M.; STOCKER, D. W.; KERR, J. A. *J. Atmos. Chem.* 16, 79-93, 1993.
- [7] ZAVALA-OSEGUERA, C.; ALVAREZ-IDABOY, J.R.; MERINO, G.; GALANO, A. *J. Phys. Chem. A* 113, 13913 - 13920, 2009.



## Thermochemistry of monoterpene $\beta$ -ocimene

Virginia C. Rufino (PG), Stella M. Resende (PQ)

*Laboratório de Química Atmosférica Teórica (LAQAT)*

*Departamento de Ciências Naturais, Universidade Federal de São João del-Rei (UFSJ)  
São João del-Rei, Minas Gerais, Brazil*

**Abstract:** Monoterpenes are the second group of volatile organic compounds (VOC) most emitted into the atmosphere by biogenic sources.[1,2] The atmospheric decomposition reaction can lead to the formation of O<sub>3</sub>, which in the troposphere is a greenhouse gas. [3] However, there is not much information on the properties of monoterpenes present in the atmosphere, being necessary further investigations. The  $\beta$ -ocimene is a monoterpene having two stereoisomeric forms, *trans*- $\beta$ -ocimene ((E)-3,7-dimethyl-1,3,6-octatriene) and *cis*- $\beta$ -ocimene ((Z)-3,7-dimethyl-1,3,6-octatriene) to whom, according to our knowledge, there are not studies on its structural and thermochemical properties. Thus, in this study, we have characterized structurally and determined the thermochemical properties of the *trans*- $\beta$ -ocimene and *cis*- $\beta$ -ocimene. Conformational analyses were performed to obtain the most stable conformation for the stereoisomers of  $\beta$ -ocimene. Geometric optimization and harmonic vibrational frequency calculations were done at the MP2/6-311G(d,p) level of theory. Single point calculations were also carried at the MP2/cc-pVDZ, MP2/cc-pVTZ e MP2/cc-pVQZ, with the objective of approaching of a complete basis set (CBS) limit. In order to obtain a high level of electronic correlation, were also performed single point calculations at the QCISD(T)/6-311G(d,p) level of theory, from which, through the use additivity approximation, the QCISD(T)/CBS level of theory was obtained. For the determination of the thermodynamics properties, isodesmic reactions were used, in which the values of the standard enthalpy of formation and standard Gibbs free energy of formation for the other species involved in the reaction are known, which allowed to calculate the values for the standard enthalpy of formation and standard Free Gibbs energy of formation of the species under study. The most stable geometries for *trans*- $\beta$ -ocimene and *cis*- $\beta$ -ocimene are presented in the Figure 1.

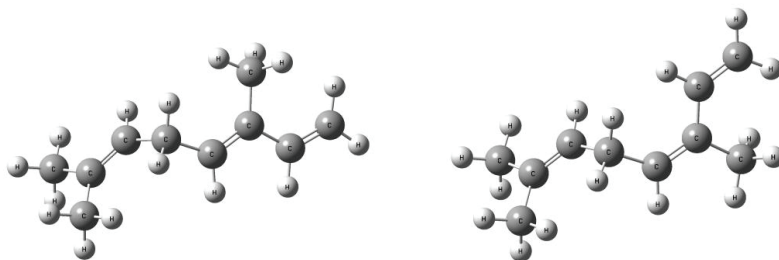


**Figure 1:** Most stable geometries for *trans*- $\beta$ -ocimene and *cis*- $\beta$ -ocimene, respectively.



The values obtained for the standard enthalpy of formation and standard free Gibbs energy of formation of the *trans*- $\beta$ -ocimene and *cis*- $\beta$ -ocimene are presented in Table I. To the best of our knowledge, it is the first determination of these thermochemical data. Of these data, we can conclude that by a difference of 0.342 kcal/mol between standard Gibbs free energies of formation, we can consider that *trans* and *cis* stereoisomers are in equilibrium in the atmosphere.

**Table 1.** Standard Enthalpy and Gibbs free energy of formation in kcal/mol (298 K and 1 atm).

Species	$\Delta H_f^\circ$	$\Delta G_f^\circ$
<i>trans</i> - $\beta$ -ocimene	17.09	63.37
<i>cis</i> - $\beta$ -ocimene	17.43	63.71

The most stable conformer and the standard enthalpy and Gibbs free energy of formation para *trans*- $\beta$ -ocimene and *cis*- $\beta$ -ocimene were determined using a high level of theory. To the best of our knowledge, it is the first determination of these thermochemical data, which may be useful in later studies of atmospheric decomposition.

**Key-words:** *ab initio*, thermochemistry, atmospheric chemistry, VOC, ocimene.

**Support:** This work has been supported by CNPq, FAPEMIG and Rede Mineira de Química (RQ-MG).

#### References:

- [1] K. Sindelarova, C. Granier, I. Bouarar, A. Guenther, S. Tilmes, T. Stavrou, J.-F. Müller, U. Kuhn, P. Stefani, W. Knorr, *Atmos. Chem. Phys.* 14, 9317 (2014).
- [2] R. Atkinson, J. Arey, *Atmos. Environ.* 37, S197, (2003).
- [3] B. J. Finlayson-Pitts, J. N. Pitts Jr, "Chemistry of the Upper and Lower Atmosphere". (2000), Academic Press, San Diego, United States.



## Thermochemistry of the atmospheric decomposition of $\beta$ -ocimene initiated by OH radical

Virginia C. Rufino<sup>a</sup> (PG), Stella M. Resende<sup>a</sup> (PQ), Josefredo R. Pliego Jr.<sup>b</sup> (PQ)

<sup>a</sup>Laboratório de Química Atmosférica Teórica (LAQAT)

<sup>b</sup>Laboratório de Química Teórica e Computacional (LQTC)

Departamento de Ciências Naturais Universidade Federal de São João del-Rei  
São João del-Rei, Minas Gerais, Brasil

**Abstract:** Volatile Organic Compounds (VOCs) are an important class of compounds emitted into the atmosphere, mainly by biogenic sources.[1] Under atmospheric conditions, they may react with OH and NO<sub>3</sub> radicals.[2] Reaction with OH radical occur mainly daytime and may lead to the formation of O<sub>3</sub>, considered a greenhouse in troposphere, and atmospheric aerosols, which affect terrestrial albedo.[3]  $\beta$ -Ocimene is a monoterpene with two stereoisomeric forms: *trans*- $\beta$ -ocimene ((E)-3,7-dimethyl-1,3,6-octatrieno) and *cis*- $\beta$ -ocimene((Z)-3,7-dimethyl-1,3,6-octatrieno), and the presence of three insaturations provides the possibility of multiple reaction paths. The atmospheric decomposition of  $\beta$ -ocimene initiated by OH radical can occur by OH addition or hydrogen abstraction, and Figure 1 shows the different reaction positions (except carbon 3 and 6 for abstraction).

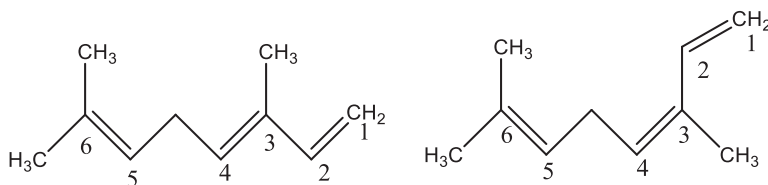


**Figura 1:** *Trans*- $\beta$ -ocimene and *cis*- $\beta$ -ocimene structures, respectively.

In this way, before a kinetic study, an analysis of the thermodynamic viability of these reaction paths is necessary and this is the proposal of this work. Geometry optimizations and harmonic vibrational frequency calculations were done at the MP2/6-311G(d,p) level of theory, in order to obtain the reaction enthalpy and Gibbs free energy for all reaction possibilities. Regarding the hydrogen abstraction, only the reaction path occurring in the carbon 5 is spontaneous, whose enthalpy and Gibbs free energy are, respectively, -6.00 and -5.97 kcal mol<sup>-1</sup> and -7.06 and -7.01 kcal mol<sup>-1</sup> for *trans* and *cis*- $\beta$ -ocimene. On the other hand, all reaction paths for OH addition are spontaneous and exothermic, as can be seen in Table 1.



**Table 1:** Enthalpy and Gibbs free energy for OH addition to  $\beta$ -ocimene, at 298 K and 1 atm (in kcal mol<sup>-1</sup>).

Reaction path	<i>trans</i> - $\beta$ -ocimene		<i>cis</i> - $\beta$ -ocimene	
	$\Delta H_R$	$\Delta G_R$	$\Delta H_R$	$\Delta G_R$
P1	-37.28	-27.46	-35.98	-25.68
P2	-24.32	-14.72	-24.15	-14.48
P3	-19.89	-8.73	-22.62	-11.89
P4	-42.06	-31.77	-40.08	-29.28
P5	-31.27	-21.57	-31.76	-21.52
P6	-33.36	-22.10	-32.96	-21.61

From these results, it can be observed that the addition path will predominate over the hydrogen abstraction, but the thermodynamics of the reactions of the two isomers is similar. Besides, position 3 is the least thermodynamically favorable. Furthermore, the most exothermic and exoergic path is the one through the carbon 4. According to our knowledge, this is the first determination of these values and these results may be useful for future kinetic studies of the atmospheric decomposition.

**Key-words:** *ab initio*, thermochemistry, atmospheric chemistry, OH radical, ocimene

**Support:** This work has been supported by FAPEMIG, CNPq and Rede Mineira de Química (RQ-MG).

#### References:

- [1] J. P. Greenberg, A. Guenther, P. Zimmerman, W. Baugh, C. Geron, K. Davis, D. Helmig, L. F. Klinger, *Atmos. Environ.* 33, 855 (1999).
- [2] R. Atkinson, J. Arey, *Atmos. Environ.* 37, S197, (2003).
- [3] J. A. Coakley, R. L. Bernstein, P. A. Durkee *Science*, 237, 1020 (1987).



## Theoretical Study on Selectivity Trends in (*N*-heterocyclic carbene)-Pd Catalyzed Heck reactions: Exploring Density Functionals Methods and Models

Vitor H. Menezes da Silva (PG)<sup>1</sup>, Ana. P. de Lima Batista (PQ)<sup>1,2</sup>, Oscar Navarro (PQ)<sup>3</sup>,  
Ataualpa A. C. Braga (PQ)<sup>1</sup>

<sup>1</sup>*Departamento de Química Fundamental, Instituto de Química, Universidade de São Paulo, Av. Prof. Lineu Prestes, 748, São Paulo, SP 05508-000, Brazil*

<sup>2</sup>*Departamento de Química, Faculdade de Filosofia, Ciências e Letras de Ribeirão Preto, Universidade de São Paulo, Ribeirão Preto, SP 14040-901, Brazil*

<sup>3</sup>*Division of Biomaterials and Biomechanics, Department of Restorative Dentistry, School of Dentistry, Oregon Health & Science University, 2730 SW Moody Ave, Portland, Oregon 97239*

**Abstract:** In the present work, we investigated the use of different sizes of molecular systems and several DFs in predicting the regioselectivity of the *N*-Heterocyclic carbene (NHC)-Pd catalyzed Heck coupling involving phenyl bromide and styrene.<sup>[1]</sup> The density functional theory (DFT) results were compared to wave-function (WF) methods DLPNO-CCSD(T), MP2-DLPNO, and experimental data. The migratory insertion (MI) step was considered as selectivity-determining step of the overall reaction.<sup>[2,3]</sup> In small model, the transition states (TSs), in which methyl groups were used as substituents in the NHC ligand, all tested density functionals (DFs) were capable to predict the selectivity found in the experimental studies: the linear coupling product. In those systems, the electronic effects of the ligand were prominent compared to the non-covalent interactions (NCI). When crowded NHC ligand was used, in which the methyl groups were replaced by the bulkier 2,6-diisopropylphenyl substituents, dispersion-corrected DFs were required for describing the correct regioselectivity trend.<sup>[4]</sup> TPSS-D3, x B97X-D, M06-L, and BP86-D3 are consistent DF approaches to predict the regioselectivity trend observed in this NHC-Pd catalyzed Heck reaction, independently of the size of the basis set. In addition, the NCI analysis revealed the role of weak interactions in stabilizing the MI TSs.<sup>[5]</sup> The main weak interaction responsible for the stabilization of the TSs was found between the NHC moiety and the phenyl rings. In more realistic systems, the weak interaction between the chlorine auxiliary ligand and the 2,6-diisopropylphenyl substituents was responsible for further stabilization of the **rTS1** (Figure 1). TS. Therefore, the attractive dispersion forces should be correctly described to achieve reliable theoretical predictions of the regioselectivity concerning crowded NHC-based palladium catalysts. The present study validated a simpler and feasible computational protocol able to predict the regioselectivity of the current reaction.

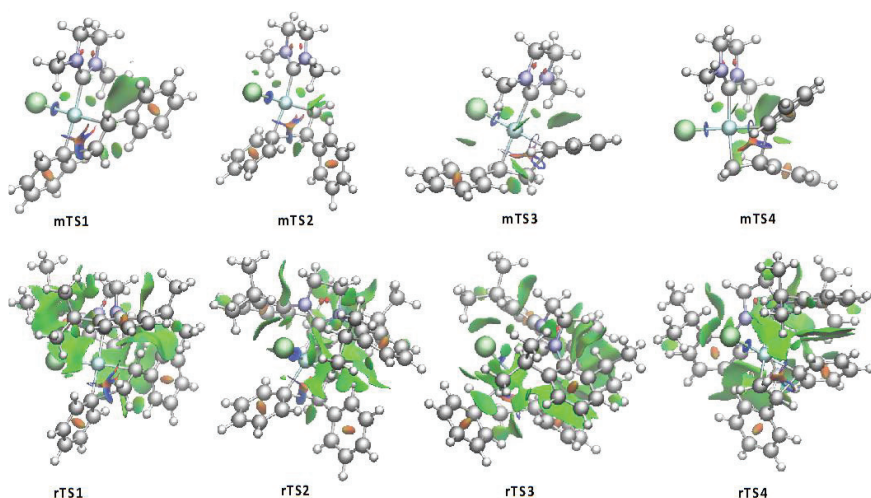


**Figure 1.** The optimized geometry of MI transition states analyzed to predict the regioselectivity of (NHC)-Pd catalyzed Heck coupling reaction. The model (above) and real (below) ligands were used in present work. NCI analysis using its color scale: green area translates into weak non-covalent interactions among atoms or groups of atoms, red regions depict strong nonbonded overlaps, and blue areas represent strong attractive interactions.

**Key-words:** N-heterocyclic carbene ligands, Heck reactions, selectivity, non-covalent interactions, DFT methods.

**Support:** São Paulo Research Foundation (FAPESP; to V.H.M.S. and A.P.d.L.B.); Contract grant number: 2013/04813-6 and 2015/ 22203-6; Contract grant sponsor: Universidade de São Paulo (HPC-USP)/ Rice University (National Science Foundation Grant OCI-0959097); Contract grant sponsor: FAPESP (to A.A.C.B.); Contract grant number: 2015/01491-3 and 2014/25770-6

#### References:

- [1] V. H. Menezes, A. P. de Lima Batista, A. A. C. Braga, O. Navarro, *J. Comp. Chem.*, In Press, DOI: 10.1002/jcc.24867 (2017).
- [2] D. Guest, V. H. Menezes, A. P. de Lima Batista, S. M. Roe, A. A. C. Braga, O. Navarro, *Organometallics*, 24, 2463 (2015).
- [3] V. H. Menezes, A. A. C. Braga, T. R. Cundari, *Organometallics*, 35, 3170 (2016).
- [4] S. Grimme, *WIREs Comput. Mol. Sci.* 1, 211 (2011).
- [5] J. Contreras-García, E. R. Johnson, S. Keinan, R. Chaudret, J.-P. Piquemal, D. N. Beratan, W. Yang, *J. Chem. Theory Comput.*, 7, 625 (2011).





## Painel 324 | PN.324

# On the negative dipole moment derivatives of HNgX molecules

Wagner Eduardo Richter (PQ)

---

Federal Technological University of Paraná, *Campus Ponta Grossa*  
richter@utfpr.edu.br

### Introduction

The HNgX (Ng = Ar, Kr; X = F, Cl) molecules were studied using the CCFDF model about a decade ago[1] because the stretching of this bond leads to a decrease of the molecular dipole moment, while for most molecules the opposite is observed. After that, substantial improvements were achieved to this partition scheme until a new model was proposed, called CCTDP[2]. Although the latter can be viewed as a rearrangement of the CCFDF terms, it provides us deeper and more accurate interpretations of IR intensities. In this work the CCTDP model will be used to analyze the dipole moment derivatives of HNgX (Ng = Ar, Kr; X = F, Cl, Br) and compare them with the derivatives for the respective HX molecules.

### Theory

Both the CCFDF and CCTDP models are based on theories which express the molecular dipole moment as a sum of atomic charges and atomic electric dipoles:

$$\vec{p} = \sum_{\alpha=1}^N q_{\alpha} \vec{r}_{\alpha} + \sum_{\alpha=1}^N \vec{m}_{\alpha} \quad (1)$$

Since the  $j^{th}$  IR intensity is proportional to the squared dipole moment derivative, it turns that:



moment derivative, it turns that:

$$\left(\frac{\partial \vec{p}}{\partial Q_j}\right) = \left(\frac{\partial \vec{p}}{\partial Q_j}\right)_{(C)} + \left(\frac{\partial \vec{p}}{\partial Q_j}\right)_{(CF)} + \left(\frac{\partial \vec{p}}{\partial Q_j}\right)_{(DF)} \quad (2)$$

The second and third terms in this CCFDF model can be summed since most of the times they act together in the IR absorption phenomena:

$$\left(\frac{\partial \vec{p}}{\partial Q_j}\right) = \left(\frac{\partial \vec{p}}{\partial Q_j}\right)_{(C)} + \left(\frac{\partial \vec{p}}{\partial Q_j}\right)_{(CTDP)} \quad (3)$$

Within this context, the “*Charge Flux–Dipole Flux*” label was changed to “*Charge Transfer–Dipolar Polarization*” since the latter describes better the molecular electronic structure behavior during the IR absorption.

## Calculations

Both the geometry optimizations and vibrational analyses were carried out using GAUSSIAN09 at the MP2(full)/aug-cc-pVTZ level of theory. The CCTDP partition was obtained using the PLACZEK program. Unlike the previous reference, which used CHelpG charges, the population analysis chosen here was QTAIM, employing the AIMALL software for the integrations.

## Results and discussion

Even though the CCFDF model can be employed with any population analysis which delivers both atomic charges and atomic dipole moments, the results with these different schemes will not be necessarily equivalent. For example, the derivatives reported for the CHelpG/CCFDF analyses[1] differ considerably from the respective QTAIM/CCFDF derivatives reported here. For instance, while the charge term, C, is much lower for HCl than for HF in the QTAIM/CCFDF model, they are very similar in the CHelpG/CCFDF, against our expectation based on chemi-



cal electronegativities. Moreover, in the CHelpG/CCFDF model the charge flux (CF) derivative for the HArF and HArCl differ by a large amount while they are about equal for HKrF and HKrCl molecules. Since the same model is being used in these two pairs,

**Table 1.** Dipole moment derivatives for the H stretching (in units of  $e.amu^{\frac{1}{2}}$ ).

	<b>C</b>	<b>CF</b>	<b>DF</b>	<b>Total</b>
HF	0.770	-0.308	-0.109	0.353
HCl	0.300	0.370	-0.443	0.226
HBr	0.098	0.927	-0.895	0.130
HArF	0.331	-1.415	0.131	-0.953
HArCl	0.327	-2.710	0.427	-1.955
HArBr	0.282	-3.525	0.629	-2.614
HKrF	0.134	-0.675	-0.186	-0.727
HKrCl	0.150	-1.665	0.104	-1.411
HKrBr	0.135	-2.196	0.265	-1.796

	<b>C</b>	<b>CTDP</b>	<b>Total</b>	<i>ab initio</i>
HF	0.770	-0.418	0.353	0.353
HCl	0.300	-0.073	0.226	0.226
HBr	0.098	0.032	0.130	0.131
HArF	0.331	-1.284	-0.953	-0.954
HArCl	0.327	-2.283	-1.955	-1.958
HArBr	0.282	-2.896	-2.614	-2.618
HKrF	0.134	-0.861	-0.727	-0.727
HKrCl	0.150	-1.561	-1.411	-1.411
HKrBr	0.135	-1.931	-1.796	-1.798

similar trends would be expected. These differences are not observed for the QTAIM/CCFDF results, where nice patterns are found for all the contributions.

The only CCFDF contribution which does not display a singular trend along the  $Ar \rightarrow Kr$  and  $F \rightarrow Br$  series in HNgX is the charge term, C. This is interesting since this term exhibit a nice linear correlation with the electronegativities of the halogen atoms in the HX molecules. The invariance of the charge term in the





HNgX molecules could be described in terms of a shielding character of the noble gas, which makes the charge assigned to the hydrogen atom independent of the halogen bonded to it. This is supported because both CHelpG and QTAIM charges display the same trend, though with different magnitudes for this term.

Finally, for the HX molecules all the CCFDF terms display clear trends related to the size and electronegativity character of the halogen atom. Both the CF and DF derivatives increase in magnitude when passing from fluorine to bromine, but they also tend to cancel each other more effectively in this series. This is summarized in the CCTDP results, for which the CTDTP term is much lower (in magnitude) for HBr than for HF. For the HNgX molecules, however, the magnitude of this term increases rapidly when passing from HNgF to HNgBr. Since the CTDTP term is related to the rearrangements in the electronic density while the molecule is vibrating along that normal coordinate, this is in agreement with the larger polarizability of bromine compared to chlorine and chlorine compared to fluorine.

## Conclusions

The results suggest that the models employing the QTAIM density partition are better suited to the description of infrared intensities because their results follow more closely what is expected from chemical insight, in agreement with similar works in the literature[3]. While the CCFDF model configures a good choice when employed with the QTAIM density partition, it is harmed when the CHelpG charges are used instead.

The CCTDP results also display simpler patterns for their contributions, making the interpretation of the derivatives easier. The CTDTP term is the main responsible for the high IR intensity of the HNgX molecules since the charge term is very small for all of them.

## Acknowledgements

WER thanks UTFPR for financial support to attend this event.





- 
- [1] SAC McDowell. *J. Mol. Struc. THEOCHEM*, 760:109, 2006.
- [2] AF Silva, WE Richter, HGC Meneses, and RE Bruns. *Phys. Chem. Chem. Phys.*, 16:23224, 2014.





## Painel 325 | PN.325

### **Electronic-structural study of the interaction of inhibitors of the protein Abl-Bcr tyrosine kinase in mutated form against the wild-type**

Washington A. Pereira (PG) , João B. L. Martins (PQ)

*Address: Universidade de Brasilia (UnB)*

#### **Abstract**

The proteins kinase are a larger family of proteins in eukaryotes, they are the key central communication for intracellular control, regulation and signal transduction[1]. The regulatory mechanism includes various phenomena ranging from chemical and Structural properties of the protein until transcriptional control[2]. Therefore, the understanding from the mechanism of control of the kinase proteins and focus of many researches. In Chronic Myeloid Leukemia, a tyrosine kinase (TK) is improperly activated by the accidental fusion of the Bcr gene with Intracellular gene encoding tyrosine kinase, that specific protein, using it as a therapeutic target, making a Bcr-Abl tyrosine kinase hitherto the main target for the design of new drugs, not only for the control of the disease, but also for Mechanism of cure. They will be used for molecular calculation, among them, molecular mechanics. *Ab initio* methods and hybrid methods. It was used to measure a protein antenna with drug programs such as Auto-Docking Vina. The study may shed light on an electronic activity of the protein and which residues play crucial roles in interacting with the primers. To better understand the structural and electronic functioning of the protein Tyrosine (DM / MM) and quantum models (*ab initio*, Semi-Empirical among others). With these tools it will be possible to compare the different mutations and different inhibitors and may point out the best possible inhibitor characteristic to achieve complete inhibition. The procedure using is to choose the best protein in the database of Protein Data Bank (PDB) structures, select the molecules of the main drugs, which are deposited in the database Zinc fingerings using the docking program Auto Docking Vina, map the amino acids that are participating Directly or indirectly from the inhibition and type of interaction that each residue makes with the protein, applying methods like ONIOM, determining the energy that these amino acids have with inhibitor. The study of molecular dynamics to understand the structural behavior and conformations that protein assumes the different stimuli, finally the electronic study comprising importance of each amino acid of the active site in inhibition. Finally, a fragment docking was performed, directing the main residues and choosing new molecules. From the mid-1970s, methods known as hybrids appeared. These methods consist of the combination of different types of approximations, *ab initio*, semiempirical and molecular mechanics, thus trying





to take advantage of each one And circumventing some of its limitations. The ONIOM method then appeared [3]. Simulation of Molecular Dynamics (DM) is one of the most versatile computational techniques for the study of biological macromolecules. In rational structure-based drug planning, DM simulations have contributed extensively at various stages of the process [4].

Keywords: tyrosine kinase, Ab initio methods, molecular modeling

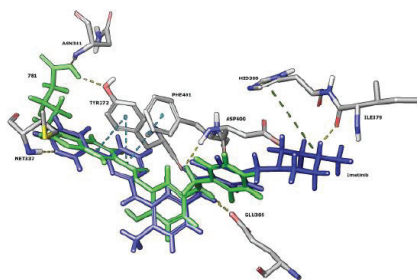


Figure 1. Interaction with TKIs and TK

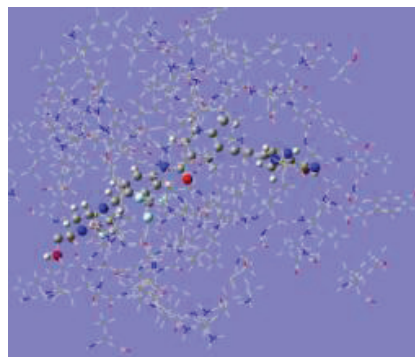


Figure 2. Selected wastes Applying ONIOM method

**Support:** This work has been supported by CNPq, CAPES, FAPDF

#### References:

- [1] BOLUDA, J. C. H.; CERVANTES, F. Prognostic factors in chronic myeloid leukaemia. *Best Practice & Research Clinical Haematology*, v. 22, p. 343–353, 2009.
- [2] BUYUKASIK, Y.; HAZNEDAROGLU, I. C.; ILHAN, O. Chronic myeloid leukemia: Practical issues in diagnosis and treatment and follow-up. *International Journal of Hematology and Oncology*, v. 20, p. 1–12, 2010.
- [3] AM Namba, VB Da Silva, CHTP Da Silva, et al. Dinâmica molecular: teoria e aplicações em planejamento de fármacos. *Eclética Química*, 33(4):13–24, 2008.
- [4] HALPERIN, I. et al. Principles of docking: An overview of search algorithms and a guide to scoring functions. *PROTEINS: Structure and Function and Genetics*, v. 47, p. 409–443, 2002.



## ESTUDO TEÓRICO DA REAÇÃO DE HIDROFORMILAÇÃO UTILIZANDO A MOLÉCULA DE (-)-ISOPULEGOL PARTE (II).

Yago Francisco Lopes<sup>1</sup>, Tarcísio Souza Carvalho<sup>2</sup>

*Grupo de Química Teórica e Estrutural de Anápolis, Ciências Exatas e Tecnológicas.*

*Universidade Estadual de Goiás, CP 459, 75001-970 Anápolis, GO Brasil.*

**Abstract:** A reação de hidroformilação é amplamente utilizada em vários processos de sínteses de alcoois e aldeídos.<sup>1</sup> Aspectos estéricos e eletrônicos da reação de hidroformilação do (-)-isopulegol catalisada por complexo de ródio (I) determinam sua diastereosseletividade.<sup>2</sup> O controle dessa seletividade foi estudado usando diferentes grupos protetores: benzoila e Acetila.<sup>3</sup> A otimização dos sistemas, bem como os estados de transições foram caracterizados no nível DFT/B3LYP usando o conjunto de funções de base 6-31G\* para os átomos de C, H, O e P, e para o Rh foi usado o pseudopotencial LANL2DZ.<sup>4,5</sup> Todo o procedimento computacional foi realizado no Laboratório de Química Teórica e Estrutural de Anápolis utilizando-se dos *softwares* HyperChem® e Gaussian®. Os resultados obtidos permitiram descrever a etapa 3 que é determinante da estereoquímica da reação, bem como julgar as possíveis estruturas do catalisador, e o desenvolvimento da reação frente aos diferentes grupos protetores.

**Key-words:** hidroformilação, (-)-isopulegol, complexo de ródio (I), seletividade.

**Support:** Universidade Estadual de Goiás – Campus de Ciências Exatas e Tecnológicas

### References:

- [1] BHATIA, S. P. *et al.* Fragrance material review on isopulegol. (2008). v. 46.
- [2] SHAHARUN, M. S.; MUKHTAR, H.; DUTTA, B. K. Selectivity of Rhodium-catalyzed Hydroformylation of 1-Octene in a Thermomorphic Solvent System. **Journal of Applied Sciences**, 1 jul. (2011). v. 11, n. 7, p. 1157–1163.
- [3] BRAGA, A. L. *et al.* Catálise assimétrica no Brasil: Desenvolvimento e potencialidades para o avanço da indústria química Brasileira. **Química Nova**, (2013). v. 36, n. 10, p. 1591–1599.
- [4] 46GANKIN, V. Y.; GUREVICK, G. S. Chemical Technology of Oxosynthesis. (1970). v. 62.
- [5] CRAMER, C. J. Essentials of Computational Chemistry. Wiley, New York. (2002).

## Description of multiple pathways on rearrangement the H atom on methylchlorocarbene

Yago de Sousa\*, Ademir João Camargo, Valter Henrique Carvalho-Silva

*Grupo de Química Teórica e Estrutural de Anápolis, Ciências Exatas e Tecnológicas.  
Universidade Estadual de Goiás, CP 459, 75001-970 Anápolis, GO Brazil.*

**Abstract:** The purpose of this paper is to demonstrate the Sub-Arrhenius behavior in the H atom intramolecular rearrangement in the methylchlorocarbene molecule, accounting the temperature dependence of quantum effects. Previous similar works pointed a deep curvature upwards, characteristic of the Sub-Arrhenius behavior [1,2]. The series of hypotheses has been conditioned to this behavior, are specially competitive paths, reaction in the excited state, tunneling and variable transition state, however, these studies were inconclusive [3,4]. We believe that the neglect of certain arguments has boosted the discrepancy among previous theoretical papers and the experimental behavior. To solve this bottleneck, we have performed a set of semi-classical and quantum simulations. Applying Car-Parrinello molecular dynamics (CPMD), coupled with a quantum treatment using Path Integral molecular dynamics (PIMD) [5,6]. This allowed us to identify five distinct reaction pathways, including the conventional rearrangement. It was evaluated the formation of intermediates and products using electronic structures methods at several level of calculation.

**Key-words:** branching ratios, deep tunneling, Feynman integrals, small mass.

**Support:** Yago de Sousa thanks PrP/UEG and CAPES.

### References:

- [1] Meana-Pañeda, R.; Truhlar, D. G.; Fernández-Ramos, A. J. Chem. Phys. 2011, 134.
- [2] Dix, E. J.; Herman, M. S.; Goodman, J. L. J. Am. Chem. Soc 1993, 115, 10424.
- [3] Albu, T. V.; Lynch, B. J.; Truhlar, D. G.; Goren, A. C.; Hrovat, D. A.; Borden, W. T.; Moss, R. A. J. Phys. Chem. A 2002, 106, 5323.
- [4] Dix, E. J.; Goodman, J. L. Res. Chem. Intermed. 1994, 20 (2), 149
- [5] Car, R.; Parrinello, M. Phys. Rev. Lett. 1985, 55 (22), 2471.
- [6] Cao, J.; Voth, G. A. J. Chem. Phys. 1994, 100 (7), 5106.

## Computational Simulations of POPG Aggregates in presence of the Antimicrobial Peptide LL37

Yeny Y. P. Valencia (PG), Gabriel C. A. da Hora (PQ), Thereza A. Soares (PQ)

<sup>1</sup>*Department of Fundamental Chemistry. Federal University of Pernambuco. Cidade Universitária, Recife - PE, 50740-540*

**Abstract:** The antimicrobial peptide LL37 is the first amphipathic alpha-helical peptide isolated from human cells. It is part of the first line of defense against local infection and systemic invasion of pathogens at sites of inflammation. LL37 has antibacterial and anti-biofilm activities, being also significantly resistant to proteolytic degradation in solution. Preliminary SAXS data suggest that LL37 destabilizes 1-palmitoyl-2-oleoyl-sn-glycero-3-phosphoglycerol (POPG) bilayers and induce the formation of a different aggregate structure. We have performed MD simulations at the coarse-grained level of the antimicrobial of LL37 in POPG bilayers and vesicles to investigate potential POPG aggregate arrangements. These data are further mapped back into atomistic models and compared the SAXS measurements. The MARTINI force-field [1,2] was used in conjunction with the GROMACS v4.6.7 software package.[3] The CG membrane bilayer was built with the INSANE script [4] and the CG vesicle with the PACKMOL software.[5] The systems were energy-minimized and solvated with CG water molecules and 150 mM of NaCl, followed by a second round of energy minimization and equilibration for 2  $\mu$ s under *NpT* conditions. We analyze and discuss structural properties derived from these simulations to argue in support of one given aggregate arrangement.

**Key-words:** phase transition, membrane hydration, diffusion coefficients

**Support:** This work has been supported by FACEPE, BioMol Project/CAPES, STINT, CNPq.

### References:

- [1] S.J. Marrink, H.J. Risselada, S. Yefimov, D.P. Tieleman, A.H. de Vries, *J. Phys. Chem. B.* 111 (2007) 7812–7824.
- [2] S.J. Marrink, A.H. de Vries, A.E. Mark, *J. Phys. Chem. B.* 108 (2004) 750–760.
- [3] B. Hess, C. Kutzner, D. van der Spoel, E. Lindahl, *J. Chem. Theory Comput.* 4 (2008) 435–447.
- [4] T.A. Wassenaar, H.I. Ingólfsson, R.A. Böckmann, D.P. Tieleman, S.J. Marrink, *J. Chem. Theory Comput.* 11 (2015) 2144–2155.
- [5] L. Martinez, R. Andrade, E.G. Birgin, J.M. Martínez, *J. Comput. Chem.* 30 (2009) 2157–2164.



# Lista dos Participantes



# A

Nome	Email	Instituição	Apresentador do trabalho
Acassio Rocha Santos	acassioroch@hotmail.com	UFPB	PN.001
Adalberto Araújo	adalberto.araujo@usp.br	USP	CO.01
Alberto dos Santos Marques	marquesalbertods@gmail.com	UFAM	PN.004
Alejandro Lopez-Castillo	alcastil@gmail.com	UFSCar	PN.005
Aleksey Kuznetsov	aleksey73kuznets@gmail.com	USP	PA.23
Alessandra Albernaz	albernazalessandra@gmail.com	UnB	PN.006
Alexandre Bertoli	bertolialexandre@yahoo.com.br	UFMG	PN.008
Alexandre Carauta	ancarauta@gmail.com	FTESM	PN.011
Alexandre Coelho R. Gomes	alexandrecregomes@yahoo.com.br	CEFET/MG	PN.009
Alexandre Costa	alexandre_ufma@yahoo.com.br	UFSCar	PN.010
Alexandre Leitão	alexandre.leitao@ufjf.edu.br	UFJF	
Alexandre Osmar Ortolan	ortolan.ao@gmail.com	UFSC	PN.012
Alexandre Rocha	rocha@iq.ufjf.br	UFRJ	PN.007
Alexsander Carvalho Vendite	alexsander.vendite@usp.br	USP	PN.013
Alfredo Mayall Simas	simas@ufpe.br	UFPE	
Aline de Oliveira	alinetgui@yahoo.com.br	UFMG	PN.014
Alyson Medeiros	alyson.medeiros54@gmail.com	UFPE	PN.015
Amanda Fernandes Gouveia	amandafernandes.gouveia@gmail.com	UFSCar	PN.016
Amanda Ziviani de Oliveira	amanda_ziviani@outlook.com	UFES	PN.017
Amauri Francisco Francisco	amauriquimica@gmail.com	UFPB	PN.018
Ana Claudia P. da Silva Cruz	anaclaudia.ps.cruz@gmail.com	INPE	PN.019
Ana Débora Porto Silveira	aninha1912@hotmail.com	CEFET/MG	PN.020
Ana Paula de Lima Batista	aplma@iq.usp.br	USP	PN.021
Anderson José Lopes Catão	anderson.catao@hotmail.com	UFSCar	PN.023
André Farias de Moura	moura@ufscar.br	UFSCar	PN.024
André Formiga	formiga@g.unicamp.br	UNICAMP	PA.09
André Gustavo Horta Barbosa	andre@vm.uff.br	UFF	
André Pacheco de Oliveira	apacheolive@gmail.com	UFRJ	PN.025
Andres Reyes	areyesv@unal.edu.co	Bogotá/Colombia	PA.18
Andresa Messias da Silva	andresamessias4@gmail.com	UFPE	PN.026
Angelita Nepel	angelnoppel@gmail.com	UNICAMP	PN.027
Angelo Giussani	angelo.giussani@ucl.ac.uk	London/Inglaterra	PA.10
Antônio Barbosa	antonioepb@ime.eb.br	IME	
Antônio Carlos A. de Faria Jr	atoni.carlos@gmail.com	IEAv-UTFPR	PN.028

Nome	Email	Instituição	Apresentador do trabalho
Antonio Carlos Borin	ancborin@iq.usp.br	USP	PL.09
Antônio Francisco C. Arapiraca	arapiraca@deii.cefetmg.br	CEFET/MG	PA.14
Antonio G. S. Oliveira Filho	antoniogsof@gmail.com	FFCLRP/USP	CO.02
Antonio Ricardo Belinassi	arbelinassi@usp.br	USP	PN.031
Antonio Rodrigues da Cunha	cunha.antonio@ufma.br	UFMA	CO.03
Antonio Silva	antonio.sjf@gmail.com	UFPB	PN.030
Arnaldo F. da Silva Filho	arnsilho@gmail.com	UNICAMP	PN.32
Augusto Batagin-Neto	abatagin@itapeva.unesp.br	UNESP	PN.35
Bárbara M. T. Costa Peluzo	barbarapeluzo@gmail.com	CEFET/MG	PN.37
Benedito J. C. Cabral	bjcabral@fc.ul.pt	Listoa/Portugal	PL.06
Bernardo de Souza	bernardo.souza@ufsc.br	UFSC	PA.21
Brenda S. D. Frachoni	frachonibrenda@gmail.com	UFU	PN.038
Bruna Luana Marcial	bruna.marcial@ifgoiano.edu.br	IFGoiano	PN.039
Bruna Thalita de Lima Pereira	brulimaquimica@yahoo.com.br	UFLA	PN.040
Bruno Edson de Freitas	bruno.edson.freitas@usp.br	USP	PN.041
Bruno Henrique de M. Mendes	bruno.hmm@hotmail.com	UFRRJ	PN.042
Bruno Moraes Servilha	moraesservilha@hotmail.com	USP	PN.043
Bruno Vilella de Faria	brunovf96@gmail.com	UNESP	PN.044
Caio César Ferreira Florindo	ccffjc@gmail.com	UNICAMP	PN.045
Calisa Carolina Dias	calisaksudias@gmail.com	UFPE	PN.046
Camila M. Benevides Machado	ppgcamila@gmail.com	UFPE	PN.049
Camila Rocha de A. Neves	cr.andradeneves@gmail.com	UFF	PN.050
Carla Grijó Fonseca	carla.grijo@ice.ufjf.br	UFJF	PN.051
Carlos Cruz	carlos.quimica.ufpe@gmail.com	FIOCRUZ/PE	PN.052
Carlos Eduardo da Silva	carlos.eduardo@iqm.unicamp.br	UNICAMP	PN.053
Carmen Domene	m.c.domene.nunez@bath.ac.uk	Bath/Inglaterra	PA.02
Chiara Valsecchi	cvalsecc@gmail.com	UFRGS	PN.055
Clebio Nascimento Jr.	clebio@ufsj.edu.br	UFSJ	
Cleiton Maciel	cleiton.maciell@gmail.com	IFSP	PN.056
Cleuton Silva	cleutonsouza@yahoo.com.br	UFAM	PN.057
Daiana Mancini	daianateixeira60@yahoo.com.br	UFLA	PN.059
Daniel Garcez S. Quattrociochi	daniel_garcez@yahoo.com.br	UFF	PN.062
Daniel Mungo	danielmungo_@hotmail.com	UFMS	PN.063
Daniel Polisel	dpolisel@yahoo.com.br	UFLA	PN.060

# D/F

Nome	Email	Instituição	Apresentador do trabalho
Danillo Valverde	dvalverd@if.usp.br	USP	PN.064
David Wilian Oliveira de Sousa	david.sousarj@yahoo.com.br	UFRJ	PN.065
Dayse Alessandra A. S. Bispo	dayse.aasilva@hotmail.com	UEFS	PN.066
Denys Santos	ewerton.denys@gmail.com	UFPE	PN.067
Diego José Raposo da Silva	sherlockmang@yahoo.com.br	UFPE	PN.068
Diego Nascimento de Jesus	diego.n.jesus@gmail.com	UFRRJ	PN.069
Douglas Gonçalves	douglas.ufam@gmail.com	USP	PN.071
Éderson DMartin Costa	edm_quimica@yahoo.com.br	UNIFAL	PN.073
Ednilsom Orestes	eorestes@gmail.com	UFF	
Eduardo Campos Vaz	edu2vaz@gmail.com	UEG	PN.075
Eduardo da Conceição	eduardodcon@gmail.com	UFRJ	PN.076
Eduardo Dias Vicentini	edudiasvicentini@hotmail.com	FFCLRP/USP	PN.077
Eduardo Franca	eduardofranca@ufu.br	UFU	
Elaine Cesar do C. A. de Souza	elainecesar.ufrj@gmail.com	UFRJ	PN.079
Elder Taciano Romão da Silva	romaoquimica@gmail.com	UnB	PN.080
Elizete Ventura do Monte	elizete@quimica.ufpb.br	UFPB	
Eliziane da Silva Santos	eliziane2silva@yahoo.com.br	UFSJ	PN.081
Ellen Vasconcelos	ellencefet13@gmail.com	UFSJ	PN.082
Elsó Drigo Filho	elso@ibilce.unesp.br	UNESP	
Erica Prates	ericatprates@gmail.com	UNICAMP	PN.084
Erick Guimarães França	erickfranca@gmail.com	IFG	PN.085
Ericson Hamissés Nunes Souza Thaines	hamissesufmt@gmail.com	UFMT	PN.086
Eufrasia Sousa	efrsousa@gmail.com	UFMG	CO.04
Evanildo Gomes Lacerda Jr	evanildo@if.usp.br	USP	PN.087
Ewerton F. da Silva Souza	ewertonsouza-13@hotmail.com	UFRRJ	PN.088
F. Javier Torres	jtortes@usfq.edu.ec	Quito/Equador	PA.16
Fabio Luiz Paranhos Costa	fabbioquimica@gmail.com	UFG	PN.090
Fabício Bracht	fabracht@gmail.com	UNICAMP	PN.091
Fátima Maria P. de Rezende	fp.rezende@bol.com.br	UFLA	PN.092
Felipe A. La Porta	felipelaporta@utfpr.edu.br	UTFPR	PN.205
Felipe Cesar Torres Antonio	fcesarta@gmail.com	UFABC	CO.05
Felipe Curtolo	felipe.curtolo@usp.br	USP	PN.093
Felipe Fantuzzi	felipe.fantuzzi@gmail.com	UFRJ	PN.094
Felipe Oliveira Ventura	felipeventura19@hotmail.com	UFBA	PN.095

# F/G

Nome	Email	Instituição	Apresentador do trabalho
Felipe Silveira S. Schneider	dudektria@gmail.com	UFSC	PN.096
Felippe Mariano Colombari	colombarifm@hotmail.com	UFSCar	PN.097
Fernando Marques Lisboa	fermlisboa@gmail.com	UFSJ	PN.100
Fernando Rei Ornellas	frornell@usp.br	USP	PN.101
Fernando Silva	fernando.silva@usp.br	USP	PN.099
Fernando Steffler	fernando.steffler@gmail.com	UFMG	PN.102
Fernando Wypych	wypych@ufpr.br	UFPB	
Filipe Belarmino	filipebelima52@hotmail.com	UFPB	PN.103
Filipe C. D. Alves Lima	fdlima@ifsp.edu.br	IFSP	PN.104
Flávia Cristina Assis Silva	flavia.assis.silva@gmail.com	UFF	CO.06
Flavio Manoel Barros Oliveira	flaviopalmares@oi.com.br	UFPE	PN.105
Flávio Olimpio Sanches Neto	flavio_olimpio@outlook.com	UEG	CO.07
Francisco Antonio Martins	francisco.qui.martins@gmail.com	UFLA	PN.106
Francisco Machado	fmachado@ita.br	ITA	PN.107
Frederico de Sousa	fredbsousa@gmail.com	UNIFEI	
Frederico Pontes	pontesfrederico@gmail.com	UFPE	PN.108
Frederico Teixeira Silva	frederico.teixeira@ufpe.br	UFPE	PN.109
Gabriel Aguiar de Souza	ga_aguiar@id.uff.br	UFF	PN.110
Gabriel Costa A. da Hora	gabriel.costa.hora@gmail.com	UFPE	CO.08
Gabriel Freire S. Fernandes	gabriel sanzovo@hotmail.com	ITA	PN.112
Gabriel Heerdt	gheerdt@hotmail.com	UNICAMP	PN.113
Gabriel Jara	gabriel.fcq.unc.ar@gmail.com	UNICAMP	PN.111
Gabriel Jordy Cascardo Araujo	gabriel_jordi@hotmail.com	UFF	PN.114
Gabriel Libânio Silva Rodrigues	glibaniosr@gmail.com	UFMG	PN.115
Gabriel Luiz Cruz de Souza	gabrielquim02@yahoo.com.br	UFMT	CO.09
Gabriel Merino	gmerino@cinvestav.mx	Guanajuato/Mexico	PA.03
Gabriel Modernell Zanotto	gabriel.zanotto@ufrgs.br	UFRGS	PN.116
Gabriel Sobral Silva Brites	gabriel.brites@gmail.com	UFRRJ	PN.117
Gabriela Nascimento Pereira	gabi_nape@hotmail.com	UFRRJ	
Gabriela Volpini Soffiati	gabisoffiati@gmail.com	UNICAMP	PN.119
Gerd Bruno Rocha	gbr@quimica.ufpb.br	UFPB	PN.120
Gerlane Bezerra da Silva	gerlanebezerra17@live.com	IFRN	PN.121
Giovanni Finoto Caramori	giovanni.caramori@ufsc.br	UFSC	
Gisele Franco de Castro	francogisele@gmail.com	UFAM	PN.123

Nome	Email	Instituição	Apresentador do trabalho
Giseli Maria Moreira	gmm08@fisica.ufpr.br	UFPR	PN.124
Giuliano Cordeiro	giulianomc07@gmail.com	UFRRJ	PN.125
Gladson de Souza Machado	gladsonsm@hotmail.com	UFRRJ	PN.126
Glauco Bauerfeldt	bauerfeldt@ufrj.br	UFRRJ	PN.127
Glauco Fonseca Silva	glaucofonsec@hotmail.com	UFRRJ	PN.128
Guedmiller Souza de Oliveira	guedmiller@gmail.com	UFSCar	PN.129
Guilherme Arantes Canella	guycanella@gmail.com	UNESP	PN.130
Guilherme Augusto B. Soares	guilhermepudin@uol.com.br	UNIFEI	PN.131
Guilherme de Souza Tavares de Morais	gui_tmorais@hotmail.com	UNICAMP	PN.133
Guilherme Ferreira de Lima	guilhermeferreira2@gmail.com	UFMG	
Guilherme Luiz Chinini	guilherme_chem@yahoo.com.br	UNICAMP	PN.134
Gustavo A. Aucar	gaa@unne.edu.ar	Corrientes/Argentina	PL.04
Gustavo Gomes de Sousa	gustavo.gds.873@gmail.com	UEG	PN.135
Gustavo Juliani Costa	gustavojuli@hotmail.com	UTFPR	PN.137
Gustavo Seabra	gustavo.seabra@ufpe.br	UFPE	PA.07
Heibbe Cristhian Oliveira	heibbe@unb.br	UnB	
Heitor Avelino de Abreu	heitorabreu@ufmg.br	UFMG	
Helene Lopes Lima	helenellima@hotmail.com	UFAM	
Helio Anderson Duarte	helioaduarte@gmail.com	UFMG	
Henrique B. C. de Azevedo	henrique.cerqueira94@gmail.com	UFRJ	CO.10
Henrique de Oliveira Euclides	henriqueuclides@gmail.com	INPE	PN.139
Henrique Musseli Cezar	henrique.musseli@gmail.com	USP	PN.140
Hubert Stassen	gullit@iq.ufrgs.br	UFRGS	
Hugo de Oliveira Batael	hugobatell@gmail.com	IBILCE/UNESP	PN.141
Hugo Gontijo Machado	hugogontijomachado@gmail.com	UEG	PN.142
Igo Tôrres Lima	igo.torres@ufma.br	UFMA	PN.143
Igor Araujo Lins	igoralins@gmail.com	UFBA	PN.144
Igor Badke Ferreira	ibadke_hc@hotmail.com	UFES	PN.089
Igor Barden Grillo	barden.igor@gmail.com	UFPB	PN.145
Isabella de Melo S. Rosado	isabella.msrosado2@ufpe.br	UFPE	PN.146
Isadora Aurora Guerra	i.auroraguerra@gmail.com	IFES	PN.147
Italo Curvelo dos Anjos	italocurvelo@gmail.com	UFPB	PN.148
Itamar Borges Jr.	itamar.borges.jr@gmail.com	IME	PN.149
Iuri Neves Soares	iurinsv@gmail.com	UFMT	PN.150

Nome	Email	Instituição	Apresentador do trabalho
Janay Stefany C. Araújo	janay@hotmail.com.br	UEFS	PN.153
Javier Oller	ollerjavier@gmail.com	UDEC/Chile	PN.154
Jéssica Boreli dos Reis Lino	jessicaboreli@outlook.com	UFLA	PA.13
João Batista Lopes Martins	lopes@unb.br	UnB	PN.280
João Carlos Oliveira Guerra	jcog@ufu.br	UFU	PN.151
João Cláudio Avila Fonseca	joaoclaudioufrj@gmail.com	UFRRJ	
João Gabriel Farias Romeu	joao.romeu@usp.br	USP	PN.155
João Guilherme S. Monteiro	joao_guilherme@id.uff.br	UFF	CO.11
João Paulo Ataide Martins	joaopauloam@ufmg.br	UFMG	PN.157
Joao Paulo Cascudo Rodrigues	jpccrfis@gmail.com	UnB	PN.158
João Vitor Afonso Borges	jalaborges@gmail.com	UFU	PN.161
Jorge Leonardo Oliveira Santos	jdiogolisboa@gmail.com.br	UFS	PN.162
José Diogo Lisboa Dutra	diogobios@hotmail.com	UFS	PN.163
José Roberto Politi	politi@unb.br	UnB	PA.22
José Walkimar M. Carneiro	jose_walkimar@id.uff.br	UFF	
Josefredo Pliego	pliego@ufsj.edu.br	UFSJ	PN.164
Josene Toldo	josene.toldo@ufrgs.br	UFRGS	PN.165
Josimar Silva	josimarfisilva@sjrp.unesp.br	IBILCE/UNESP	PN.166
Joyce Karoline Daré	joy.vga@gmail.com	UFLA	PN.167
Julia Contreras-García	julia.contreras@lct.jussieu.fr	Paris/França	PL.03
Juliana C. de Carvalho Gallo	julianaccgallo@gmail.com	UEFS	PN.168
Juliana de Oliveira Mendes	mendesjuliana.juli@gmail.com	UFRJ	PN.169
Juliana Fedoce Lopes	jfedoce@unifei.edu.br	UNIFEI	
Juliana Silva	juangeiras@yahoo.com.br	UFPE	
Julio Cesar Guedes Correia	jguedes@cetem.gov.br	CETEM/MCTIC	PN.171
Júlio da Silva	juliodcsasilva@gmail.com	UFAL	PN.170
Kahlil Salome	kahlil.salome@gmail.com	UNICAMP	PN.172
Kaline Coutinho	kaline@if.usp.br	USP	
Karen Weber	kac.weber@gmail.com	UFPB	
Kurt Mikkelsen	kmi@chem.ku.dk	Copenhagen/Dinamarca	PL.02
Larissa de Mattos Oliveira	lare_oliveira@yahoo.com.br	UEFS	PN.174
Larissa Ferreira Vasconcelos	lferreiravas@hotmail.com	UFF	PN.175
Larissa Lavorato Lima	larissa.lavorato@ice.ufff.br	UFJF	PN.176
Lars G.M. Pettersson	lgm@fysik.su.se	Stockholm/Suécia	PA.01

Nome	Email	Instituição	Apresentador do trabalho
Laurent Dardenne	le.dardenne@gmail.com	LNCC	PN.177
Leandro Rezende Franco	leofrancofisica@gmail.com	USP	PN.178
Leonardo A. de Souza	desouza.leonardo.chem@gmail.com	UFF	PN.179
Leonardo Baptista	leobap@gmail.com	UERJ	PN.180
Leonardo dos Anjos Cunha	leonardonorge@gmail.com	ITA	PN.182
Leonardo Duarte	leo.j.duarte@hotmail.com.br	UNICAMP	PN.185
Leonardo Gois Lascane	leogoiscva@hotmail.com	UNESP	PN.183
Leonardo Morais	leonardohenrique.demoraes@gmail.com	UFMT	PN.184
Leonardo Silva Dias	leonardosdyas@gmail.com	UFSCar	CO.12
Leticia Assis	leticiaassisquimica@hotmail.com	UFLA	PN.186
Leticia Maia Prates	leticiamaiapr@gmail.com	UERJ	PN.187
Leticia Rodrigues C. Corrêa	leticiaacorrea@gmail.com	UFRJ	PN.188
Lilian Camargo	lilianthaty@yahoo.com.br	IFG-UEG	PN.047
Lisandra Paulino dos Santos	lisandrapaulinosantos@gmail.com	UERJ	PN.189
Ljiljana Stojanovic	stojanovicmljljana@gmail.com	ICR/CNRS/França	PN.190
Lourival R. de Sousa Neto	lorosone@hotmail.com	UFU	PN.191
Lucas Chuman Santana	lucas_chumansantana@hotmail.com	UNIFEI	CO.13
Lucas Colucci Ducati	ducati@iq.usp.br	USP	PN.192
Lucas Modesto da Costa	lucmod@gmail.com	IME	PN.193
Lucas Nascimento Trentin	lucas.trentin@hotmail.com	UNICAMP	PN.194
Lucas Pereira Mendes	lucaspml17.lm@gmail.com	UNESP	PN.195
Luciana Guimarães	lucianaguimaraes@ufsj.edu.br	UFSJ	
Luciano Ribeiro	lribeiro@ueg.br	UEG	PN.197
Luciano Nassif Vidal	lnvidal@utfpr.edu.br	UTFPR	PN.196
Luciano T. Costa	lcosta@id.uff.br	UFF	PA.20
Luis Mauricio da Silva Soares	luismauriciosoares@gmail.com	UFRGS	PN.199
Luís Pedro Viegas	lviegas@aiaa.au.dk	AIAS/Dinamarca	CO.20
Luiz Antonio Costa	luiz.costa@ufjf.edu.br	UFJF	
Luiz Felipe Guain Teixeira	lfguaint@iq.usp.br	USP	PN.201
Luiz Fernando Ferrão	ferrao@ita.br	ITA	PN.202
Luiz Henrique M. da Costa	medeiroslhc@hotmail.com	UFRN	PN.203
Lyzette Gonçalves M. de Moura	lgmdemoura@gmail.com	UFMA	PN.204
Maiara Oliveira Passos	maipassos05@gmail.com	UFBA	PN.206

# M

Nome	Email	Instituição	Apresentador do trabalho
Maicon Faria	maiconsaulfaria@gmail.com	Abax HPC	
Maira dos Santos Pires	mairapires15@hotmail.com	UFLA	PN.207
Majed Chergui	majed.chergui@epfl.ch	Lausanne/Suíça	PL.01
Malucia Marques Soeiro	maluciasoeiro@hotmail.com	UFF	PN.208
Marcelo Andrade Chagas	andrade.mchagas@gmail.com	UFMG	PN.211
Marcelo André Petry Pontes	marceloappontes@gmail.com	ITA	PN.210
Marcelo Hidalgo Cardenuto	mhidalgo@if.usp.br	USP	CO.14
Marcelo Mota Reginato	marcelo@iq.usp.br	USP	PN.213
Márcia K. da Luz Belarmino	marciakarine23@hotmail.com	UFPE	PN.214
Márcio Oliveira Alves	marcio28oa@yahoo.com.br	CEFET/MG	PN.215
Marcio Varella	mvarella@if.usp.br	USP	PA.19
Marco A. Chaer Nascimento	chaer01@gmail.com	UFRJ	
Marco A. de Mecenas Filho	marcomecenasfilho@gmail.com	UFLA	PN.216
Marco Aurelio Euflauzino Maria	marcomaria@ufscar.br	UFSCar	PN.217
Marcos Paulo de Oliveira	marcos.oliveiravr@yahoo.com.br	UFRRJ	PN.218
Marcos Serrou do Amaral	marcos.amaral@ufms.br	UFMS	PA.12
Marcus Vinícius Juliaci Rocha	mvjrocha@hotmail.com	UFF	PN.220
Maria Carolina N. B. Muniz	carolmuniz60@gmail.com	IME	PN.221
Mariana Toretta Caldeira	marytoretta@gmail.com	UNICAMP	PN.222
Marina Dourado	dourado.marina@hotmail.com	UnB	PN.224
Marina Pelegrini	marinapelegrini101@gmail.com	AFA	PN.223
Marina Purri	marina.purri@hotmail.com	UFMG	PN.225
Mateus Gonçalves	mateus.a.g@hotmail.com	UFLA	PN.227
Mateus Augusto M. de Paiva	mts381@gmail.com	CEFET/MG	PN.226
Mateus Ribeiro Lage	mateus.lage@ufma.br	UFMA	PN.229
Mateus Xavier Silva	xaviersmateus@gmail.com	UFMG	PN.230
Mateus Zanotto	m.zanotto@live.com	UFABC	PN.231
Matheus Lazarotto	matheus_jean_l@hotmail.com	USP	PN.232
Matheus R. Miranda Signorelli	math.signorelli@gmail.com	UFF	PN.233
Mauricio A. Vega-Tejjido	mauryvg@fq.edu.uy	UdelaR/Uruguai	PN.234
Mauricio D. Coutinho Neto	mdcoutinho@gmail.com	UFABC	PN.236
Maurício Portiol Franco	mpf@iq.usp.br	USP	PN.237
Maurício T. de Macedo Cruz	cruzmtmr@gmail.com	UERJ	
Mauro Barbosa de Amorim	mbamorim@nppn.ufjf.br	UFRJ	

# M/R

Nome	Email	Instituição	Apresentador do trabalho
Max Nunes Pereira	maxnunes-ifrj@hotmail.com	UERJ	PN.238
Max Pinheiro Jr	maxjr82@gmail.com	ITA	PA.06
Maximiliano Segala	maximiliano.segala@ufrgs.br	UFRGS	PN.048
Michele Aparecida Salvador	michelesalvador@gmail.com	UFABC	PN.239
Michell de Oliveira Almeida	michelloliveira02@gmail.com	UFABC	PN.240
Milene Aparecida R. de Oliveira	milene@ifsc.usp.br	USP	PN.241
Milton Massumi Fujimoto	milton@fisica.ufpr.br	UFPR	PN.242
Mirele B. Pinto	mirele.quimica@gmail.com	UFMG	PN.243
Mirian Chaves Costa Silva	mirian.chaves3@gmail.com	UFU	PN.244
Monica Pickholz	mpickholz@gmail.com	IFIBA	PA.17
Munique Rodrigues Pereira	muniqerper@gmail.com	UFRGS	PN.245
Munir Skaf	skaf@g.unicamp.br	UNICAMP	PL.07
Naiara Leticia Marana	namarana@fc.unesp.br	UNESP	PN.246
Natália Aparecida Rocha Pinto	nataliarochaqm@yahoo.com	UFSJ	PN.247
Natalie M. Colodette	nm.colodette@gmail.com	UFRJ	PN.248
Natieli Da Silva	natieli.iqsc@usp.br	USP	PN.249
Nelson H. Morgon	nhmorgon@gmail.com	UNICAMP	PN.251
Neubi Xavier	neubi@live.com	UFRRJ	PN.252
Orlando Roberto Neto	landorobertoneto@gmail.com	IEAv	PN.253
Osmair Vital de Oliveira	osmair@ifsp.edu.br	IFSP	PN.254
Otávio Santana	otavio.quimica@gmail.com	UFPB	
Patricia Barreto	patricia.barreto@inpe.br	INPE	PN.255
Paúl Pozo	jppozo@estud.usfq.edu.ec	USFQ	PN.256
Paula do Nascimento Goulart	nas.goulart@gmail.com	UFRRJ	PN.257
Paula Homem-de-Mello	paula.mello@ufabc.edu.br	UFABC	PN.258
Paulo A. Netz	netz@iq.ufrgs.br	UFRGS	PA.05
Paulo Fernando G. Velloso	paulo.fgo@gmail.com	UFMG	CO.15
Paulo Henrique Amaral	phramaral@gmail.com	UFMG	PN.260
Paulo Roberto G. Gonçalves Jr	pgarcs@gmail.com	UFMG	PN.261
Pedro Henrique Naves Binda	binda766@hotmail.com	UFU	
Pedro Ivo Rodrigues Moraes	pedroivo@ice.ufjf.br	UFJF	PN.264
Pedro Oliveira M. de Carvalho	pomc.ecc@gmail.com	UNICAMP	PN.265
Pollyanna Pinto Maia	pollypmaia@hotmail.com	UFSJ	PN.266
Puspitapallab Chaudhuri	puspito@ufam.edu.br	UFAM	PA.11
Rafael de Oliveira Lima	rafael_oliveira.lima@live.com	ITA	PN.267
Raphael da Silva Alvim	qralvim@gmail.com	USP	PN.269

Nome	Email	Instituição	Apresentador do trabalho
Raquel Costabile Bezerra	racosbez@gmail.com	UFAM	PN.270
Regis Casimiro Leal	regis.casimiro@ifrn.edu.br	IFRN	PN.272
Regis Tadeu Santiago	registsantiago@gmail.com	USP	PN.273
Renan Vidal Viesser	renan.viesser@gmail.com	UNICAMP	
Renato Cesar da Silva	natocezar@gmail.com	UFPE	PN.274
Renato Luis Tame Parreira	renato.parreira@unifran.edu.br	UNIFRAN	
Renato Miceli	renatomiceli@gmail.com	Laniaq	
Rênica Alves de Moraes Rocha	renicamorais@hotmail.com	UFG	PN.275
Rhuiago Mendes de Oliveira	rhuiago@gmail.com	IFMA-UnB	PN.276
Ricardo de Almeida	rialmeida1975@gmail.com	UERJ	PN.277
Ricardo Fagundes da Rocha	ricardorocha.biochemistry@gmail.com	UFRGS	PN.279
Ricardo Lima	ricardo2.lima@usp.br	USP	PN.278
Ricardo Longo	longo@ufpe.br	UFPE	PA.15
Ricardo Oliveira	rrodrigues.iq@gmail.com	UFRJ	CO.16
Ricardo Oliveira Freire	rfreire@ufs.br	UFS	
Roberta Dias	rdiasufpe@gmail.com	UFPE	PN.281
Roberto Lins	linsrd@gmail.com	FIOCRUZ/PE	
Roberto Ribeiro Faria	robertoribeiro90@gmail.com	UFU	
Rodolfo Goetze Fiorot	fiorot.rodolfo@gmail.com	IFRJ	CO.17
Rodrigo A. L. Silva	silvarodrigo021@gmail.com	UnB	PN.282
Rodrigo Araújo Mendes	rodrigoaramendes@gmail.com	USP	PN.283
Rodrigo Fraga de Almeida	fraga@ice.ufjf.br	UFJF	PN.284
Rogério Custodio	rogerct@g.unicamp.br	UNICAMP	
Rogério José da Costa	rogerquim@gmail.com	UnB	PN.285
Rogério Vaz	rogeriovaz_quimica@hotmail.com	UFPE	PN.286
Roiney Beal	nei_beal@hotmail.com	UFRGS	PN.287
Rosemberg Fortes	rosembergnunes@yahoo.com.br	UEG	PN.288
Roy Bruns	bruns@iqm.unicamp.br	UNICAMP	PA.08
Sarah Arvelos	sarvelos@gmail.com	UFU	PN.291
Sebastian Fernandez-Alberti	seba@unq.edu.ar	Quilmes/Argentina	PL.08
Selma Fabiana Bazan	sfbazan@hotmail.com	UFMG	CO.18
Sérgio Galembeck	segalemb@usp.br	USP	PA.24
Shawan Almeida	shawalmeida@gmail.com	UFMT	PN.292
Silmar Andrade do Monte	silmar@quimica.ufpb.br	UFPB	
Silviana Corrêa	silvianacorrea123@yahoo.com.br	UFLA	PN.293
Sinkler Eduardo T. Gonzalez	sinklereduardo@gmail.com	UNICAMP	PN.294
Stella Maris Resende	stella@ufsj.edu.br	UFSJ	PN.320

Nome	Email	Instituição	Apresentador do trabalho
Stephan Sauer	sauer@chem.ku.dk	Copenhagen/Dinamarca	PL.05
Sylvio Canuto	canuto@if.usp.br	USP	
Tais Christofani	taiskc@gmail.com	UFMG	PN.295
Tamires Lima Pereira	thammyresz@hotmail.com	UnB	PN.296
Tárcius Nascimento Ramos	tarcius@if.usp.br	USP	PN.297
Tatiane Nicola Tejero	tatiane.nicola@hotmail.com	UFRRJ	PN.298
Taylane da Silva Araújo	araujotaylane@gmail.com	UEFS	PN.299
Telles Cardoso Silva	tellescardoso@hotmail.com	UFLA	PN.300
Teodorico Ramalho	teodorico.ramalho@gmail.com	UFLA	PN.301
Thais Forest Giacomello	thaisgiaco@gmail.com	UFG	PN.302
Thais Karine de Lima	thaislimaufu@gmail.com	UFU	
Thayana Maria L. de Lima	thayana_jp@hotmail.com	UFPB	PN.303
Thayane Paula Dias Caldeira	thayanedias94@hotmail.com	UERJ	PN.304
Thereza Soares	tizza.soares@gmail.com	UFPE	PA.04
Thiago Duarte	thiago.duarte@usp.br	USP	PN.306
Tiago Espinosa de Oliveira	tiago.espinosa@ics-cnrs.unistra.fr	ICS/CNRS/França	PN.308
Tuanan Lourenço	lourenco.tuanan@gmail.com	UFF	
Uallisson Silva Santos	uallisson2.718@gmail.com	UFSCar	PN.310
Ulisses José de Faria Jr	ulissesfjr@gmail.com	ITA	PN.312
Verlucia Amanda M. de Freitas	verluciamanda@hotmail.com	UFPB	PN.313
Veronica Maria do Nascimento	veronica@iq.usp.br	USP	PM.314
Victor Augusto S. da Mata	victorssantana.93@hotmail.com	UFSCar	PN.316
Victor Augusto V. Ferreira	victor.augusto7@yahoo.com.br	UFRJ	PN.315
Victor Hugo M. da Silva	victormala22@yahoo.com.br	UFF	PN.317
Vinícius Bonatto	vi_bonatto0@hotmail.com	UNIFEI	PN.318
Vinícius Manzoni Vieira	vmanzoni@fis.ufal.br	UFAL	CO.19
Vinícius Nunes da Rocha	viniciusnunes.qi@gmail.com	UFRRJ	PN.319
Virginia Camila Rufino	virginiacamila12@gmail.com	UFSJ	PN.321
Vitor Hugo Menezes da Silva	vhugomenezes@gmail.com	USP	PN.322
Wagner De Almeida	wbdealmeida@gmail.com	UFF	
Wagner Eduardo Richter	richter@utfpr.edu.br	UTFPR	PN.324
Washington Pereira	was.a.pra@gmail.com	Unb	PN.325
William Oliveira Sote	wsote83802@gmail.com	UFU	
Willian R. Rocha	wrochauufmg@gmail.com	UFMG	



# Y

<b>Nome</b>	<b>Email</b>	<b>Instituição</b>	<b>Apresentador do trabalho</b>
Yago de Sousa	yssousa078@gmail.com	UEG	PN.327
Yago Lopes	yago_4tri@hotmail.com	UEG	PN.326
Yeny Yaneth P. Valencia	yaneth.uq@gmail.com	UFPE	PN.328



